TELECOM PARIS
école nationale supérieure des télécommunications

École Doctorale d'Informatique, Télécommunications et Électronique de Paris

Thèse

présentée pour obtenir le grade de docteur de l'Ecole Nationale Supérieure des Télécommunications

Spécialité: **Electronique et Communications**

Fatma KHARRAT-KAMMOUN

Adaptive techniques and classification for MIMO systems

ENST Paris-Motorola Labs Saclay

Ezio Biglieri	Président
Raymond Knopp	Rapporteurs
Emre Telatar	
Jean Claude Belfiore	Examinateurs
Hugues Randriambololona	
Joseph Boutros	Directeurs de Thèse
Stephanie Rouquette	

A mes parents
Pour l'amour, l'encouragement et l'éducation qu'ils ont su me donner

A mon mari
Pour les sacrifices, pour l'amour, le soutien, l'encouragement, l'aide qu'il a su m'apporter

A mon bébé
Pour tout le bonheur qu'il m'a offert.

Remerciements

Je tiens à exprimer toute ma reconnaissance aux personnes qui m'ont aidée, encouragée, soutenue, tout au long des années de ma thèse.

Je tiens tout d'abord à remercier Monsieur Ezio Biglieri, Professeur à l'université Pompeu Fabra de Barcelone, pour m'avoir fait l'honneur de présider le jury de ma thèse.

Mes plus vifs remerciements s'adressent à Monsieur Emre TELATAR, Professeur à l'Ecole Polytechnique Fédérale de Lausanne pour le temps précieux qu'il m'a accordé en acceptant d'être rapporteur de cette thèse. La qualité de ce rapport s'est vue remarquablement améliorée par sa relecture attentive et pointilleuse, et ses nombreuses corrections.

Je tiens également à exprimer ma profonde gratitude envers Monsieur Raymond Knopp, Professeur à l' Institut EURECOM à Sophia Antipolis, pour avoir lui aussi accepté d'être rapporteur de cette thèse. Ses commentaires élogieux m'ont touché. Qu'il trouve ici l'expression de ma sincère reconnaissance.

Ma gratitude va également à Monsieur Jean-Claude Belfiore, professeur à l'ENST pour avoir cordialement accepté d'être membre de mon jury, et pour lequel j'éprouve le plus grand respect.

Mes plus vifs remerciements vont tout particulièrement à Monsieur Hugues RANDRIAMBOLOLONA, Maître de conférences à l'ENST, qui a bien voulu participer à mon jury de thèse. Hugues, merci pour le temps que tu m'as consacré, et les précieux conseils que tu m'as donnés concernant la classification des canaux MIMO. Travailler avec toi était vraiment très enrichissant pour moi.

Un grand merci à mon directeur de thèse, Joseph Boutros, sans lequel ce travail n'aurait jamais vu le jour. Ses compétences techniques, sa rigueur, son dynamisme ont été déterminants dans la réalisation de mes travaux. Joseph, je te remercie pour ton écoute, tes conseils, ton encadrement et surtout pour la confiance que tu as su m'accorder.

Je n'oublie pas le centre de recherche de Motorola à Saclay et en particulier Sandrine Fontenelle et Didier Bourse. C'est grâce à eux que mon contrat CIFRE avec le département COMELEC a pu voir le jour. Je remercie aussi Sandrine pour son encadrement, pour sa rigueur, pour son soutien et son encouragement. Sandrine, j'étais très touchée par ta volonté de relire mon rapport thèse après ton départ de Motorola. Je remercie également Stéphanie Rouquette-Léveil pour son encadrement pendant la dernière année de ma thèse, pour son écoute et pour sa disponibilité.

Mes plus sincères remerciements vont également aux enseignants du département Comelec, et plus particulièrement, Ghaya Rekaya, Cedric Ware, Philippe Ciblat pour leurs aides et pour leurs conseils. Un très grand merci aux secrétaires Chantal Cadiat, Danielle Childz et Marie Baquero pour leur aide efficace.

Merci à tous amis thésards. Et surtout merci à mes collègues de bureau, avec lesquels j'ai passé des moments inoubliables: Ghaya, Souheil, Nicolas, Ghassan et Sheng.

Résumé

Ce mémoire se focalise sur les systèmes de communication sans fil ayant plusieurs antennes en réception et en émission. D'abord, on étudie les performances de ces systèmes en se basant sur un schéma de multiplexage spatial en transmission et sur un détecteur ML en réception. On en déduit une bonne approximation de la probabilité d'erreur conditionnelle pour un canal quasi statique. Cette approximation est obtenue dans le cas où différentes modulations sont appliquées sur les antennes de transmission et pour toute configuration de canal MIMO.

Ensuite, on met en avant des techniques adaptatives pour les systèmes MIMO : modulation adaptative et sélection d'antennes. La première adapte les modulations en émission en fonction des conditions radio afin de maximiser l'efficacité spectrale tout en respectant une contrainte sur la probabilité d'erreur. Alors que la deuxième, sélectionne un sous ensemble d'antennes actives pour optimiser le critère de sélection (par exemple : maximiser la capacité, etc.) étant donnée une estimation de canal. Les deux techniques adaptatives ont besoin d'une métrique pour évaluer les performances du système MIMO. On propose donc un nouveau schéma de modulation adaptative et un nouvel algorithme de sélection d'antennes où l'approximation de la probabilité d'erreur obtenue précédemment est utilisée comme métrique.

Finalement, on considère la quantification des canaux MIMO. Cette quantification, ou dans notre terminologie classification, permet de faire une partition de l'ensemble des canaux MIMO en des classes différentes, où chaque classe est identifiée par un représentant. Cette méthode peut être utilisée pour les techniques adaptatives afin de trouver le meilleur jeu de paramètre. Dans ce chapitre, on décrit l' algorithme de classification et on illustre son application pour les systèmes MIMO à boucle fermée comme le " beamforming ".

Thesis abstract

This thesis report focuses on wireless communication systems with multiple transmit and multiple receive antennas. At first, we study the performance of such systems assuming a spatial multiplexing scheme at the transmitter and an ML detection at the receiver. We derive an accurate approximation for the conditional error probability on a quasi static channel. This approximation is computed when distinct modulations are applied on the transmit antennas and for any MIMO channel configuration.

Then, we outline some adaptive techniques for MIMO systems: adaptive modulation and antenna selection. The first one adjusts the modulations on transmit antennas according to the channel conditions in order to maximize the spectral efficiency while satisfying a constraint on error probability. The second technique selects the set of active antennas to optimize the chosen selection criterion (e.g. maximize the capacity, etc) providing a channel estimation. Both adaptive techniques need a relevant matric to evaluate the MIMO system performance. We propose a new adaptive modulation scheme and antenna selection algorithm where the derived error probability approximation is used as a selection metric.

Finally, we consider the quantization of MIMO channels. This quantization, in our terminology classification, allows the partitioning of MIMO channels set into different classes, where each class is identified by a representative. This method could be used for adaptive techniques to find the best adjustable parameters. We describe our MIMO classification algorithm and we illustrate its application for closed-loop MIMO systems, e.g beamforming.

Contents

List of Figures

List of Tables

List of acronyms

AWGN	Additive White Gaussian Noise
BER	Bit Error Rate
CDF	Cumulative Density Function
CSI	Channel State Information
FER	Frame Error Rate
HSDPA	High Speed Downlink Packet Access
HSUPA	High Speed Uplink Packet Access
ICI	Inter-Channel Interference
iid	independent identical distribution
WLAN	Wireless Local Area Network
WMAN	Wireless Metropolitan Area Network
MIMO	Multiple Input Multiple Output
MISO	Multiple Input Single Output
ML	Maximum Likelihood
MMSE	Minimum Mean Square Error
OFDM	Orthogonal Frequency Division Multiplexing
OSuIC	Ordered Successive Interference Cancellation
PAM	Pulse Amplitude Modulation
PDF	Probability Density Function
PER	Point Error Rate
PSK	Phase Shift Keying
QAM	Quadrature Amplitude Modulation
QoS	Quality of Service
QPSK	Quadrature Phase Shift Keying
RF	Radio Frequency
SIMO	Single Input Multiple Output
SISO	Single Input Single Output
SNR	Signal to Noise Ratio
SVD	Singular Value Decomposition
wrt	with respect to
ZF	Zero Forcing

List of notations

$\lfloor . \rfloor$	Floor function
$\lceil . \rceil$	Ceil function
$[.]$	Nearest integer function
$\binom{n}{k}$	Binomial coefficients, "n choose k"
$\|a\|$	Module of the scalar a
$\mathbf{A}^T$	Transpose of $\mathbf{A}$
$\overline{\mathbf{A}}$	Conjugate of $\mathbf{A}$
$\mathbf{A}^\dagger$	Transpose conjugate of $\mathbf{A}$
$\|\|\mathbf{A}\|\|$	Euclidean norm of $\mathbf{A}$
$\mathbb{Z}$	Set of integers
$\mathbb{R}$	Set of reals
$\mathbb{C}$	Set of complex numbers
$card(X)$	Number of elements belonging to the set X
$\det(\mathbf{A})$	Determinant of $\mathbf{A}$
$diag(a_1,a_2,\ldots,a_n)$	$n \times n$ diagonal matrix with $[diag(a_1,a_2,\ldots,a_n)]_{i,i} = a_i$
$E_x()$	Expectation operator over x
$tr(\mathbf{A})$	Trace of $\mathbf{A}$
$\mathbf{I}_n$	$n \times n$ identity matrix
$n_t \times n_r$	Dimension of a MIMO channel matrix with n_t transmit and n_r receive antennas
$\mathrm{Q}(x)$	Q-function, defined as $\mathrm{Q}(x) = (1/\sqrt{2\pi}) \int_x^\infty e^{-t^2/2} dt$
$\Re(\mathbf{A}),\Im(\mathbf{A})$	Real and imaginary parts of $\mathbf{A}$, respectively
$\langle \mathbf{x},\mathbf{y} \rangle$	Scalar inner product between the real vectors $\mathbf{x} = (x_1,x_2,\ldots,x_n)$ and $\mathbf{y} = (y_1,y_2,\ldots,y_n) : \langle x,y \rangle = \sum_{i=1}^n x_i y_i$
$\langle \mathbf{x},\mathbf{y} \rangle$	Hermitian inner product between the complex vectors $\mathbf{x} = (x_1,x_2,\ldots,x_n)$ and $\mathbf{y} = (y_1,y_2,\ldots,y_n) : \langle x,y \rangle = \sum_{i=1}^n x_i \overline{y_i}$
$S(\mathbf{y},R)$	Sphere of radius R and centered at $\mathbf{y}$
$P(\mathbf{x} \rightarrow \mathbf{y})$	Classical notation for the pairwise error probability = P(the decoder chooses y when x is transmitted)
$\max(a,b)$	$= a$ if $a \geq b$ and b otherwise
$\min(a,b)$	$= a$ if $a \leq b$ and b otherwise
$\mathbb{Z}[i]$	Ring of Gaussian integers $= \{a + ib \mid a,b \in \mathbb{Z}\}$ where $i = \sqrt{-1}$

Introduction

Next generation wireless systems require considerably high data rates and transmission reliability. In a conventional communication system using one antenna at the transmitter and the receiver (Single Input Single Output (SISO)), the achievable capacity is directly limited by the transmitted power and the available spectrum bandwidth. Therefore, the use of SISO architecture for future wireless systems requires large modulation sizes and higher power devices. In order to cope with these limitations, the use of multiple antennas at each side (Multiple Input Multiple Output (MIMO)) was suggested. In fact, the channel capacity achieved by MIMO systems was shown to increase proportionally to the minimum number of antennas at the transmitter and at the receiver. That's why, the integration of MIMO technology into 3GPP for mobile wireless communications is currently under way with HSDPA/HSUPA standards. MIMO technique can also be used in conjunction with OFDM, and is part of the broadband WMAN standard IEEE 802.16 and will also be part of the high-throughput WLAN standard IEEE 802.11n.

However, MIMO systems are sensitive to fading radio conditions. So, they need robust and spectrally efficient communication mechanisms, e.g. the adaptive techniques. Most current systems do not assume any channel knowledge at the transmitter and hence could not adapt the data rate or the modulation of the transmission. These non-adaptive methods necessitate a fixed link margin to maintain acceptable performance when the channel quality is poor, and are thus designed for the worst case channel conditions, resulting in insufficient utilization of the full channel capacity. When channel knowledge is available at the transmitter (e.g. in TDD systems or more generally, when channel reciprocity can be assumed), it may be used in order to improve the overall throughput of the system. Adapting transmit characteristics to the signal fading allows the channel to be used more efficiently since power and rate can be adjusted to take advantage of favorable channel conditions. The basic idea behind adaptive transmission is to maintain a target quality of service (QoS) (e.g. error rate) by varying the transmitted power level, symbol transmission rate, constellation size, coding rate/scheme or any combination of these parameters. Without sacrificing the Bit Error Rate (BER) or Frame Error Rate (FER), these schemes provide high average spectral efficiency by transmitting at high data rates under favorable channel conditions and reducing the throughput as channel degrades. Adaptive modulation and coding (AMC) concept was specified for HSDPA by using computed look-up tables for different modulation and coding schemes.

The application of multiple antennas in wireless systems provide significant gains in both channel capacity and transmission reliability without any additional bandwidth. Nevertheless, increasing the number of antennas leads to an elevated hardware cost and signal processing

complexity. Antenna selection technique reduces these impacts by using less radio frequency (RF) chains (transmit amplifiers, digital-to-analog converters, etc.) while keeping the diversity gain. This technique adapts the subset of active transmit and/or receive antennas according to the channel conditions. Therefore, it is proposed for IEEE 802.11n standard.

The adaptive techniques allow to improve the MIMO system performance. But, they imply the search of the appropriate adaptive parameter(s) for each given channel. This fact increases the computation complexity of such systems especially when several possibilities for adaptive parameter(s) are available. To reduce this complexity, we propose to quantize the set of all MIMO channels and consequently to generate a discrete set of representatives. Then, we associate for each representative the optimal adaptive parameters that can be stored in look-up tables. Thus, it is possible to determine the best parameters for a given channel by considering its nearest representative. This MIMO classification concept could be also used in other applications that need some knowledge about channels at the transmitter, e.g. beamforming. In this case, the channel can be estimated by its representative.

Thesis outline

In chapter 1, we start with a brief summary of wireless channel characteristics. Then, we focus on the wireless system which uses multiple antennas at the transmitter and at the receiver. First, we illustrate the conventional model for a such system. Second, we point out the advantages of using multiple antennas in terms of channel capacity and transmission reliability. Finally, we present for these systems a transmission scheme that will be adopted in our studies. Some assumptions and notations, used in the sequel, are also illustrated in this chapter.

In chapter 2, we present some mathematical tools (from lattices and number theory) that will be used in next chapters to study the performance of MIMO systems, in terms of error probability, and to design a classification algorithm for these systems. At first, we deal with the main lattice parameters. Then, we illustrate some mathematical concepts from the number theory allowing to study lattices, e.g. quadratic forms and lattice reduction. The notion of lattice codes is introduced and it will be considered to represent MIMO channels in next chapters. Finally, we expose two lattice decoder algorithms, using the ML criterion: sphere decoder based on Pohst enumeration and sphere decoder based on Schnorr-Euchner enumeration. The adaptation of both algorithms to lattice codes is also given. The representation of MIMO channels with lattice codes makes it possible to use lattice decoders in our transmission scheme.

In chapter 3, we study thanks to lattice theory, the performance (in terms of error probability) of a quasi-static uncoded multiple antenna system. The system model described in the first chapter is assumed. At first, we show how a MIMO channel, described by its channel matrix, can be associated to a lattice code (or lattice constellation). After that, we present our accurate approximation of the conditional error probability for MIMO channels with more receive than transmit antennas. This approximation is derived in the general case where distinct modulations are applied on transmit antennas. The proposed bound is validated by comparing its analytical expression to Monte-Carlo simulation results for different modulation and antenna configurations. Next, we give a generalization of this approximation for any number of transmit/receieve antennas and we present an existing generalized sphere decoder algorithm. This decoder is then used in the transmission scheme to validate our approximation by comparison

to Monte-Carlo simulation results.

In chapter 4, we propose a new adaptive modulation scheme as well as a new antenna selection algorithm. Both techniques use the accurate approximation of the conditional error probability in a MIMO system, derived in chapter 3, as a metric to select the best parameters, namely modulation size and antenna set for transmission. We start by detailing our adaptive modulation scheme for MIMO systems. Next, we compare by simulations the performance of the proposed adaptive modulation technique to that of the non-adaptive systems in terms of spectral efficiency. Our adaptive scheme is compared also to another one based on a simple bound for the lattice associated to the MIMO channel. Then, we focus on the antenna selection technique. We study the impact of this technique on the diversity order for SIMO systems. Next, we introduce our proposed selection criterion and other existing selection criteria. Finally, we point out the advantage of the antenna selection (with different selection criteria) while comparing the achieved performance to that without selection, assuming the same number of active antennas. We also compare the performance obtained with our proposed selection criterion to other existing criteria for different receiver schemes (optimal and sub-optimal receivers).

In chapter 5, we focus on the classification of MIMO channels by considering their associated Hermitian forms. First, we introduce the MIMO system model on which the classification will be based. Second, we illustrate some basic notions from algebra and differential geometry that will be used in our classification algorithm. Third, we detail our classification algorithm that is proposed firstly for MIMO channels and is extended, then, to lattices. To design this algorithm, we propose a new metric to compute the distance between Hermitian forms. This metric is compared to the natural one based on the Euclidean distance by illustrating the behavior of classification parameters (e.g. centroids, classes population, etc). After that, we validate our classification by measuring the resemblance between the channels and their representatives (e.g using Voronoi regions, error probabilities). Finally, we consider this classification for closed-loop MIMO systems. We focus on beamforming technique where each channel is estimated by its representative at the transmitter. The classification approach for beamforming is compared in performance with the case where a perfect estimation is assumed at the transmitter. In addition, an application of the classification to coded MIMO systems is outlined.

Chapter 1

An overview of MIMO wireless systems

Introduction

In recent years, wireless communication devices have become more and more popular since they allow users to communicate with each other independently from their locations. At the same time, the demand for high data rate and reliable radio systems has grown. Unfortunately, the design of systems satisfying these requirements is difficult in traditional wireless channel using one antenna at the transmitter and at the receiver. Indeed, due to the fading caused by multiple reflections of the transmitted signal, the reliability of these systems is not guaranteed during the communication. In addition, the capacity of such systems is limited. To cope with these limitations, the use of multiple antennas at both sides is a promising solution. In fact, increasing the number of antennas leads to important benefits regarding the reliability and the transmission throughput.
This chapter gives an overview for multiple antenna systems. It also introduces their important parameters which are necessary for the next chapters.

Section 1.1 deals with wireless channels. At first, we briefly discuss the main known problem for such channels which is fading. Then, we present a basic model for the fading in traditional wireless channel. Finally, we point out different types of time-variation wireless channel.
Section 1.2 focuses on a particular example of wireless channel: multiple antenna channel. The conventional model for such system is introduced at the beginning of this section. Then, the advantages of using multiple antennas in terms of channel capacity and reliability are discussed. At the end, different transmission schemes were proposed in the literature for MIMO systems. Section 1.3 describes the scheme that is adopted in our studies.

1.1 The wireless channel

The wireless channel is the channel that uses radio waves to transmit data between two devices, namely the transmitter and the receiver. It is characterized by its random time-variation variable, called *fading*. At the receiver, the channel fading is seen as a multiplicative process that affects the transmitted signal. In practice, the radio signal reaches the receiver via different

paths (multi-path) that experience differences in attenuation, delay and phase shift. The superposition of these paths results in fading. Due to propagation delay, the fading is presented as a complex number with a phase and a magnitude that represents the channel distortion. Different statistical models are associated to the fading, depending on the propagation environment. In this section, we present a statistical model for the channel fading, which will be used later in our studies.

1.1.1 Statistical model for fading

Assume that there are many objects in the environment that scatter the radio signal before it arrives at the receiver. By the *Central Limit Theorem*, each component of the fading channel (real and imaginary parts) will be well-modelled as a Gaussian random variable. If there is no line-of-sight (LOS) between the transmitter and the receiver, then fading will have zero mean and phase evenly distributed between 0 and 2π. The magnitude of the channel fading will therefore be Rayleigh distributed. Calling this random variable r, it will have a probability density function (PDF)

$$p(r) = \frac{r}{\sigma_r^2} \exp\left(\frac{-r^2}{2\sigma_r^2}\right), \quad r \geq 0 \tag{1.1}$$

where $\sigma_r^2 = E(r^2)$ is the mean received power.

In the presence of LOS, the fading channel has a non zero mean. Its magnitude follows a Rician distribution with a PDF expressed as

$$p(r) = \frac{r(K+1)}{\sigma_r^2} \exp\left(-K - \frac{(K+1)r^2}{2\sigma_r^2}\right) I_0\left(r\sqrt{\frac{K(K+1)}{\sigma_r^2}}\right), \quad r \geq 0, K \geq 0 \tag{1.2}$$

where $I_0(x)$ is the zeroth-order modified Bessel function defined as

$$I_0(x) = \frac{1}{2\pi} \int_0^{2\pi} \exp(-x \cdot cos(\theta)) d\theta,$$

and the parameter K is the ratio of the power received via the LOS path to the power contribution of the non-LOS paths. When $K = 0$, the Rician distribution (1.2) is reduced to the Rayleigh distribution (1.1).

1.1.2 Time selective fading, Frequency selective fading

As indicated before, the fading is a time varying effect. This variation is characterized by the channel coherence time, T_c, that serves as a measure of how fast the channel changes in time. In fact, the coherence time corresponds to the longest interval during which the channel is assumed to be constant.
Let's denote by T_s (respectively T_f) the time needed to transmit a symbol (respectively a frame). Using these parameters, different channel models could be distinguished:

- **Ergodic** : When $T_c = T_s$, the channel is said to be ergodic. In this case, each transmitted symbol is associated with a new realization of the channel.

- **Quasi-static** : If the channel remains constant during one frame, i.e. $T_c = T_f$, the channel is called quasi-static.
- **Block fading** : When fading does not change during N frame transmissions, the channel is said to be block fading. In this case, $T_c = N.T_f$. It is noted that a quasi static channel is also a block fading channel with $N = 1$.

In the wireless channel, the multi-path propagation leads to a time delay spread to receive the different paths. This spread is characterized in the frequency domain by the coherence bandwidth, B_c. Indeed, B_c is a measure of the range of frequencies over which the channel has approximately equal gain.

- When the signal bandwidth is comparable or less than B_c, all the frequency components of the transmitted signal undergo the same attenuation, the channel is said to be **flat** or **non-frequency selective** fading.
- When the radio channel has different gains within the signal bandwidth, a **frequency selective** fading is experienced.

As mentioned in section 1.1, fading causes attenuations and distortions for the transmitted signal. To combat this phenomenon and improve the reception of the transmitted signal, diversity techniques are used. These techniques consist in receiving and transmitting multiple versions of the same transmitted signal in a gainful manner. Diversity is obtained by different means [48]: frequency, time, code or space. One promising technique is spatial diversity, which is produced by the use of multiple antennas at the transmitter or/and at the receiver. The resulting wireless system is called MIMO channel. Next section provides some assumptions on MIMO channel and describes the multiple antenna channel model that will be used in our studies.

1.2 Multiple antenna channel

A multiple antenna channel, known also as MIMO channel, is a wireless channel with multiple transmit and receive antennas. The use of multiple antennas provides two types of gain: *diversity gain* and *channel capacity gain*. The first one will be further examined in section 1.2.2. The second gain will be illustrated in section 1.2.3.

1.2.1 General model for multiple antenna channel

Let n_t and n_r be the number of transmit and receive antennas, respectively. A MIMO channel, as given in Fig. 1.1, can be represented mathematically by an $n_r \times n_t$ complex matrix $\mathbf{H} = [h_{ij}]$.

$$\mathbf{H} = \begin{bmatrix} h_{11} & h_{12} & \cdots & h_{1n_t} \\ h_{21} & h_{22} & \cdots & h_{2n_t} \\ \vdots & \vdots & \ddots & \vdots \\ h_{n_r1} & h_{n_r2} & \cdots & h_{n_rn_t} \end{bmatrix} \leftarrow 1^{rst} \text{ receive antenna}$$

$$\uparrow 2^{nd} \text{ transmit antenna}$$

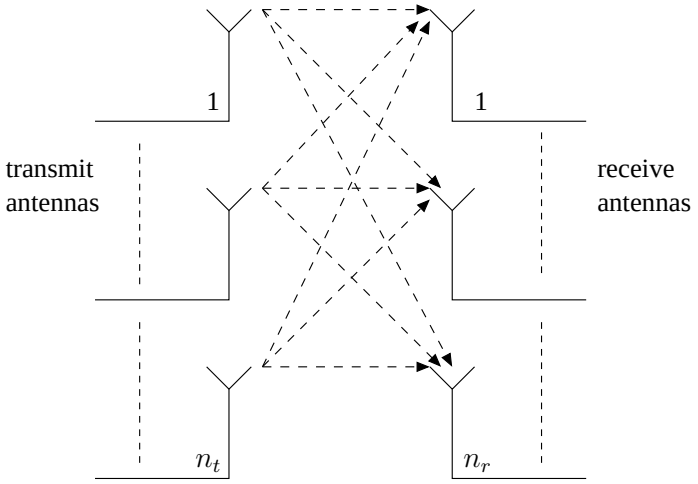

Figure 1.1: MIMO channel model with n_t transmit and n_r receive antennas.

The coefficient h_{ij} denotes the single-input single-output (SISO) channel fading between the j^{th} ($j = 1,2,\ldots,n_t$) transmit antenna and the i^{th} ($i = 1,2,\ldots,n_r$) receive antenna. The column vector $\mathbf{h}_j = [h_{1j},h_{2j},\ldots,h_{n_rj}]^T$ is the single-input multiple-output (SIMO) channel produced by the j^{th} transmit antenna through the n_r receive antennas. The row vector $\mathbf{h}_i^T = [h_{i1},h_{i2},\ldots,h_{in_t}]$ is the multiple-input single-output (MISO) channel that represents the different n_t paths arriving to the i^{th} receive antenna.

The **rank** of the MIMO channel corresponds to the number of independent signals that one may safely transmit through the MIMO system. It is determined by the algebraic rank of the $n_r \times n_t$ channel matrix, which is lower than $\min(n_t,n_r)$. A MIMO channel is said *rank-deficient* if $n_t > n_r$ and *full rank* otherwise.

1.2.2 Multiple antenna channel diversity

As mentioned before, the use of multiple antennas, sufficiently spaced to ensure independent fading between antennas, produces spatial diversity. This diversity is characterized by the number of independently fading branches, known as **diversity order**. Diversity order can be observed as the slope of the BER versus signal-to-noise ratio curve.

Two types of diversity are potentially provided by MIMO channels :

- **Receive Diversity** : The use of multiple antennas at the receiver produces a receive spatial diversity. The diversity order is equal to the number of receive antennas.
- **Transmit diversity** : It consists in sending the same information over different transmit antennas. The diversity order in this case is equal to the number of transmit antennas.

Thus, the diversity order in MIMO channels is equal to the product of both transmit and receive antenna numbers, if the channel between each transmit/receive antenna pair fades independently.

1.2.3 MIMO Information theory

Some performance limits of MIMO systems are given in this section in terms of spectral efficiency with reliability. These limits are derived thanks to the classical information theory initiated by Shannon in 1948 [53].

Let the random variables $\mathbf{x}$ and $\mathbf{y}$ be the input and the output of a memoryless wireless channel. The observation of the channel output $\mathbf{y}$ gives us an information about the variable $\mathbf{x}$. The mutual information $I(\mathbf{x};\mathbf{y})$ is defined by the information theory to measure the amount of information that $\mathbf{y}$ contains about $\mathbf{x}$. The maximization of the mutual information over all possible input distributions $p(\mathbf{x})$ determines the maximum data rate that a channel can support without error, also known as channel capacity. The channel capacity is then measured in bits per channel use. Commonly, it is represented within a unit bandwidth of the channel and it is measured in bits/s/Hz.

For a discrete memoryless channel, the channel capacity is defined by [16]

$$C^{inst} = \max_{p(\mathbf{x})} I(\mathbf{x};\mathbf{y}) \tag{1.3}$$

When constraining the available power at the transmitter to P_T, the channel capacity becomes

$$C^{inst} = \max_{p(\mathbf{x}),E(\mathbf{x}^\dagger\mathbf{x})\leq P_T} I(\mathbf{x};\mathbf{y}) \tag{1.4}$$

In [21] and [59], the capacity of MIMO channel were evaluated for different channel time-variations (ergodic and non-ergodic). Next sections present the MIMO capacity and illustrate simulation results that outline the benefit of multiple antenna systems.

1.2.3.1 Ergodic capacity

To show the gain offered by the use of multiple antennas at both sides in terms of capacity, we begin with fundamental results derived for single antenna (SISO) or multiple antennas at one side (SIMO or MISO) wireless systems.

In the following, we assume that the channel is ergodic and flat fading. Perfect CSI (Channel State Information) is available only at the receiver and the transmitter is constrained in its total power to P_T, i.e. $E(\mathbf{x}^\dagger\mathbf{x}) \leq P_T$. The ergodic capacity is defined as the expectation of the instantaneous channel capacity (1.4) over the distribution of the elements of the channel matrix $\mathbf{H}$

$$C^{erg} = E_{\mathbf{H}}\left\{\max_{p(\mathbf{x}),E(\mathbf{x}^\dagger\mathbf{x})\leq P_T} I(\mathbf{x};\mathbf{y})\right\} \tag{1.5}$$

Capacity of SISO channel

For a memoryless SISO system ($n_t = n_r = 1$), the channel matrix $\mathbf{H}$ is reduced to a scalar complex variable h. The ergodic capacity is given by

$$C^{erg}_{SISO} = E_h\left\{\max_{p(x),E(|x|^2)\leq P_T} I(x;y)\right\} \tag{1.6}$$

For a SISO channel, the ergodic capacity (1.6) can be written as [21]

$$C_{SISO}^{erg} = E_h \left\{ \log_2(1 + \rho |h|^2) \right\}, \tag{1.7}$$

where ρ denotes the average Signal-to-Noise Ratio (SNR) per receive antenna.

If we assume $|h|^2 = 1$, the instantaneous capacity equals $C_{SISO}^{inst} = \log_2(1 + \rho)$. It increases slowly with respect to the SNR, according to the logarithm of $(1 + \rho)$. For high SNR, it is noticed that a gain of 3 dB on ρ will provide only one bit increase in capacity.

When the channel gain amplitude $|h|$ is Rayleigh distributed, $|h|^2$ follows a chi-squared distribution with two degrees of freedom [48] which leads to an exponential distribution. Equation (1.7) can then be written as [21]

$$C_{SISO}^{erg} = E_h \left\{ \log_2 \left(1 + \rho \chi_2^2 \right) \right\}, \tag{1.8}$$

where χ_2^2 is a chi-square distributed random variable with two degrees of freedom.

Capacity of SIMO and MISO channels

Consider a SIMO channel $\mathbf{h} = [h_1, h_2, \ldots, h_{n_r}]$, with a single transmit and n_r receive antennas. The capacity under ergodicity assumption is given by [21], [45]

$$C_{SIMO}^{erg} = E_{\mathbf{h}} \left\{ \log_2 \left(1 + \rho \sum_{i=1}^{n_r} |h_i|^2 \right) \right\} \tag{1.9}$$

Like in the SISO case, if we assume that $\mathbf{h}$ satisfies $|h_i| = 1$, $i = 1, \cdots, n_t$, then the instantaneous capacity becomes $C_{SIMO}^{inst} = \log_2(1 + \rho n_r)$. Thus, the addition of receive antennas only results in a logarithmic increase of the capacity with the SNR.

With optimal combining at the receiver, the capacity of a Rayleigh fading SIMO channel can be expressed as [21]

$$C_{SIMO}^{erg} = E_{\mathbf{h}} \left\{ \log_2 \left(1 + \rho \chi_{2n_r}^2 \right) \right\} \tag{1.10}$$

where $\chi_{2n_r}^2$ is a chi-squared distributed random variable with $2n_r$ degrees of freedom.

When multiple antennas are employed only at the transmitter, the capacity of the MISO channel is given by [21], [45]

$$C_{MISO}^{erg} = E_{\mathbf{h}} \left\{ \log_2 \left(1 + \frac{\rho}{n_t} \sum_{i=1}^{n_t} |h_i|^2 \right) \right\} \tag{1.11}$$

If $|h_i| = 1$, $i = 1, \cdots, n_t$, then the instantaneous capacity is equal to $C_{MISO}^{inst} = \log_2(1 + \rho)$. There is no gain in capacity over a SISO channel. By comparing equations (1.11) and (1.9) and assuming the same total number of antennas, it is clear that C_{MISO} is lower than C_{SIMO} when CSI is not available at the transmitter.

Capacity of MIMO channel

The average capacity of a random ergodic MIMO channel is given by [59]

$$C_{MIMO}^{erg} = E_{\mathbf{H}} \left\{ \max_{p(\mathbf{x});\ tr(\mathbf{Q}) \leq P_T} I(\mathbf{x};\mathbf{y}) \right\}, \tag{1.12}$$

where $\mathbf{Q} = E(\mathbf{x}\mathbf{x}^{\dagger})$ is the transmit signal covariance matrix, and $tr(\mathbf{Q}) = E(\mathbf{x}^{\dagger}\mathbf{x})$ denotes the trace of $\mathbf{Q}$.

The mutual information is maximized for a zero mean circularly symmetric complex Gaussian distributed input [59]. The capacity is then given by

$$C_{MIMO}^{erg} = E_{\mathbf{H}} \left\{ \log_2 \left(\det \left(\mathbf{I}_{n_r} + \frac{1}{2N_0} \mathbf{H}\mathbf{Q}\mathbf{H}^{\dagger} \right) \right) \right\} \tag{1.13}$$

When **no CSI is available at the transmitter**, the available power P_T can be uniformly distributed among the transmit antennas. For uncorrelated channel, the transmit covariance matrix is equal to $\mathbf{Q} = \frac{P_T}{n_t}\mathbf{I}_{n_t}$ and the corresponding channel capacity becomes

$$C_{MIMO}^{erg} = E_{\mathbf{H}} \left\{ \log_2 \left(\det \left(\mathbf{I}_{n_r} + \frac{P_T}{2N_0 n_t} \mathbf{H}\mathbf{H}^{\dagger} \right) \right) \right\} \tag{1.14}$$

Let $\rho = \frac{P_T}{2N_0}$ be the average SNR per receive antenna. For optimal combining between n_r antennas at the receiver, the capacity can be written as [21], [59]

$$C_{MIMO}^{erg} = E_{\mathbf{H}} \left\{ n_t \log_2 \left(1 + \frac{\rho}{n_t} \chi^2_{2n_r} \right) \right\} \tag{1.15}$$

By the law of large numbers, the term $\frac{1}{n_t}\mathbf{H}\mathbf{H}^{\dagger} \rightarrow I_{n_r}$ as n_t gets larger and n_r remains fixed [44], [35]. Thus, the ergodic capacity in this case is :

$$C_{MIMO}^{erg} = E_{\mathbf{H}} \left\{ n_r \log_2(1+\rho) \right\}$$

Hence, the capacity reaches an asymptotic value for a fixed n_r. It is then unadvantageous to increase indefinitely the number of transmit antennas.

Further analysis of the MIMO channel capacity could be conducted by applying the singular value decomposition (SVD) to the channel matrix $\mathbf{H}$ [59], that is

$$\mathbf{H} = \mathbf{U}\mathbf{D}\mathbf{V}^{\dagger}.$$

The $n_r \times n_r$ and $n_t \times n_t$ complex matrices $\mathbf{U}$ and $\mathbf{V}$ are unitary and the $n_r \times n_t$ non-negative diagonal matrix $\mathbf{D}$ contains the singular values of the matrix $\mathbf{H}$. Substituting $\mathbf{H}$ by its decomposition in (1.14) leads to the following capacity expression:

$$\begin{aligned} C_{MIMO}^{erg} &= E_{\mathbf{H}} \left\{ \sum_{i=1}^{m} \log \left(1 + \frac{\rho}{n_t} \lambda_i \right) \right\} \\ &= \sum_{i=1}^{m} E_{\lambda_i} \left\{ \log \left(1 + \frac{\rho}{n_t} \lambda_i \right) \right\} \end{aligned} \tag{1.16}$$

where $(\lambda_i)_{1\leq i\leq m}$ are the square of the non-zero entries of the diagonal matrix

$$\mathbf{D} = diag(\sqrt{\lambda_1}, \sqrt{\lambda_2}, \ldots, \sqrt{\lambda_m}, 0, \ldots, 0)$$

and $m = \min(n_t, n_r)$ is equal to the channel rank. We can deduce that the total capacity of a given MIMO channel $\mathbf{H}$ is made up by the sum of m parallel independent AWGN SISO sub-channels, whose channel gain equals respectively $\sqrt{\lambda_i}$, $i = 1, \ldots, m$. Consequently, the MIMO capacity grows linearly with $m = \min(n_t, n_r)$ rather than logarithmically [21], [59].

In case of **perfect CSI at the transmitter**, the optimal transmitted power is not uniformly distributed but is optimized according to the water-filling algorithm [12], [21], [59]. The resulting capacity is then given by

$$C_{MIMO}^{erg} = E_{\mathbf{H}} \left\{ \sum_{i=1}^{m} \log_2(\mu \lambda_i)^+ \right\} \tag{1.17}$$

where μ is chosen to satisfy

$$\rho = \sum_{i=1}^{m} (\mu - \lambda_i^{-1})^+ \tag{1.18}$$

for each given channel $\mathbf{H}$. The notation x^+ is defined as $\max(x, 0)$.

The impact of the channel knowledge at the transmitter is studied in the literature, e.g. [11], [12], [54]. Authors notice that the water-filling gains over equal power are significant at low SNR but converge to zero as the SNR increases.

Simulation results are depicted on Figs. 1.2 and 1.3 for i.i.d. Rayleigh fading ergodic channels for different scenarios of (n_t, n_r) and different power allocation. The input variable $\mathbf{x}$ is supposed to be Gaussian distributed. When uniform power allocation is considered (1.14)), Fig. 1.2 shows the channel capacity as a function of the average SNR per receive antenna, ρ. Clearly, the use of multiple antennas increases the achievable rates on fading channels. At moderate to high SNRs, the capacity of a $n_t = n_r = 4$ MIMO channel is about twice the capacity of a 2×2 system and 4 times the capacity of a 1×1 system. The slope of the capacity versus SNR is proportional to $\min(n_t, n_r)$.
As indicated above, the capacity of SIMO system is higher than MISO system for both cases $n = 5$ and $n = 3$, where $n = n_t + n_r$. The capacity gain achieved by the following MISO systems : 2×1 and 4×1, over SISO system (1×1) is not significant.

Figure 1.3 compares the capacity observed with two power allocation strategies: uniform power allocation and optimal power allocation based on water-filling algorithm. Both power allocations maintain the capacity proportional to the channel rank which is equal to $\min(n_t, n_r)$. However, an SNR gain is noticed while applying the optimal strategy. This gain is more significant at low SNR, especially for 4×4 system.

For slow-varying or block fading channel, the ergodicity property is not respected and the classical capacity definition is no longer appropriate. A new capacity definition for non ergodic

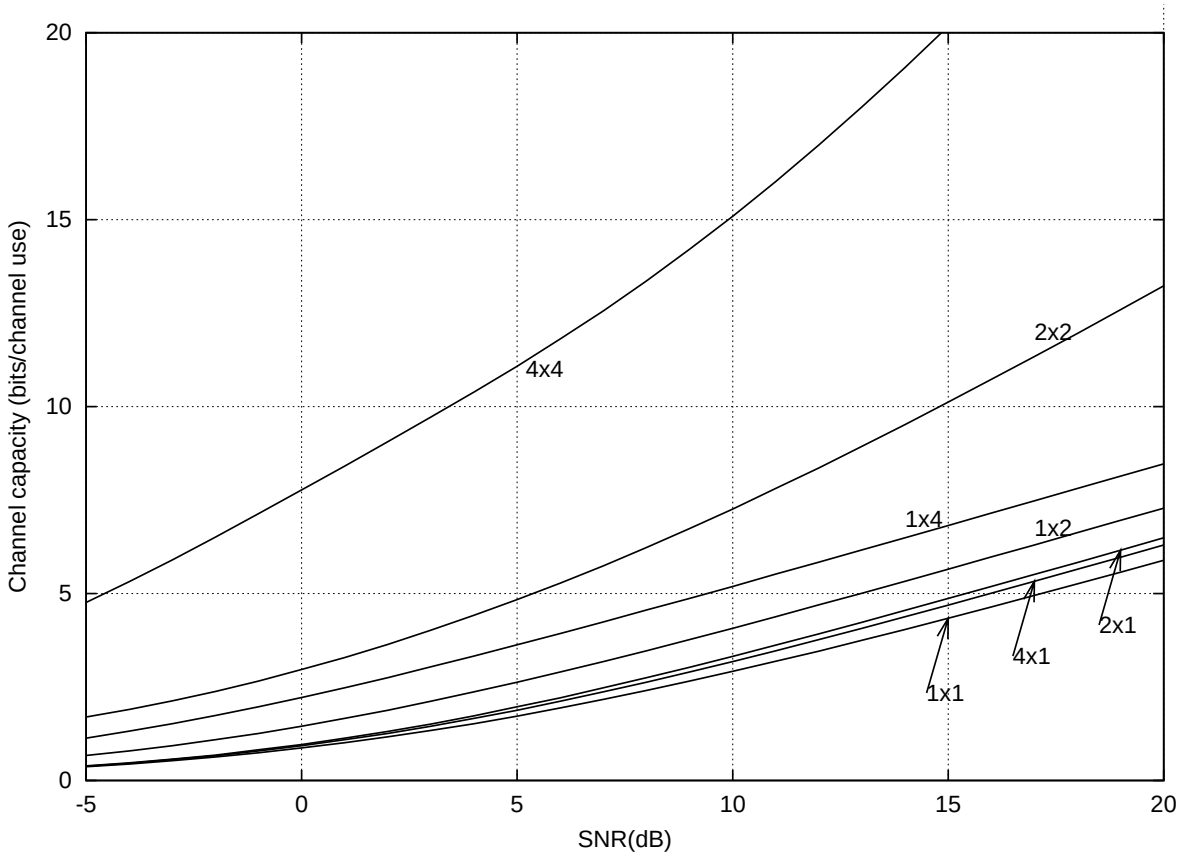

Figure 1.2: Capacity on an i.i.d Rayleigh fading ergodic channel (Gaussian input and uniform power allocation).

channel is introduced in [6], [4], [21], [59]: capacity is associated to outage probability. Capacity becomes a random variable which depends on the channel instantaneous response. Next section focuses on the capacity for non ergodic channel.

1.2.3.2 Outage capacity/outage probability

The capacity under channel ergodicity is defined as the average of the maximal value of the mutual information between the transmitted and the received signal. A closed-form expression for the capacity assuming a perfect CSI at the receiver is given by equation (1.14). However, real communication systems transmit blocks of information within a limited time duration. This duration is not long enough to contain a statistically representative set of propagation conditions and the channel is non ergodic. In this case, another definition of channel capacity is frequently used that is outage capacity. With this definition, the channel is characterized by an outage probability [21], [59]. The capacity is treated as a random variable which depends on the channel instantaneous response. The outage probability is the probability that the channel capacity falls below the effective bit rate R that the system is trying to transmit[59].

$$P_{out}(R) = \inf_{\mathbf{Q},tr(\mathbf{Q})\leq P_T} P(C(\mathbf{Q},\mathbf{H}) < R),$$

where

$$C(\mathbf{Q},\mathbf{H}) = \log_2 \det(I_{n_r} + \mathbf{H}\mathbf{Q}\mathbf{H}^{\dagger})$$

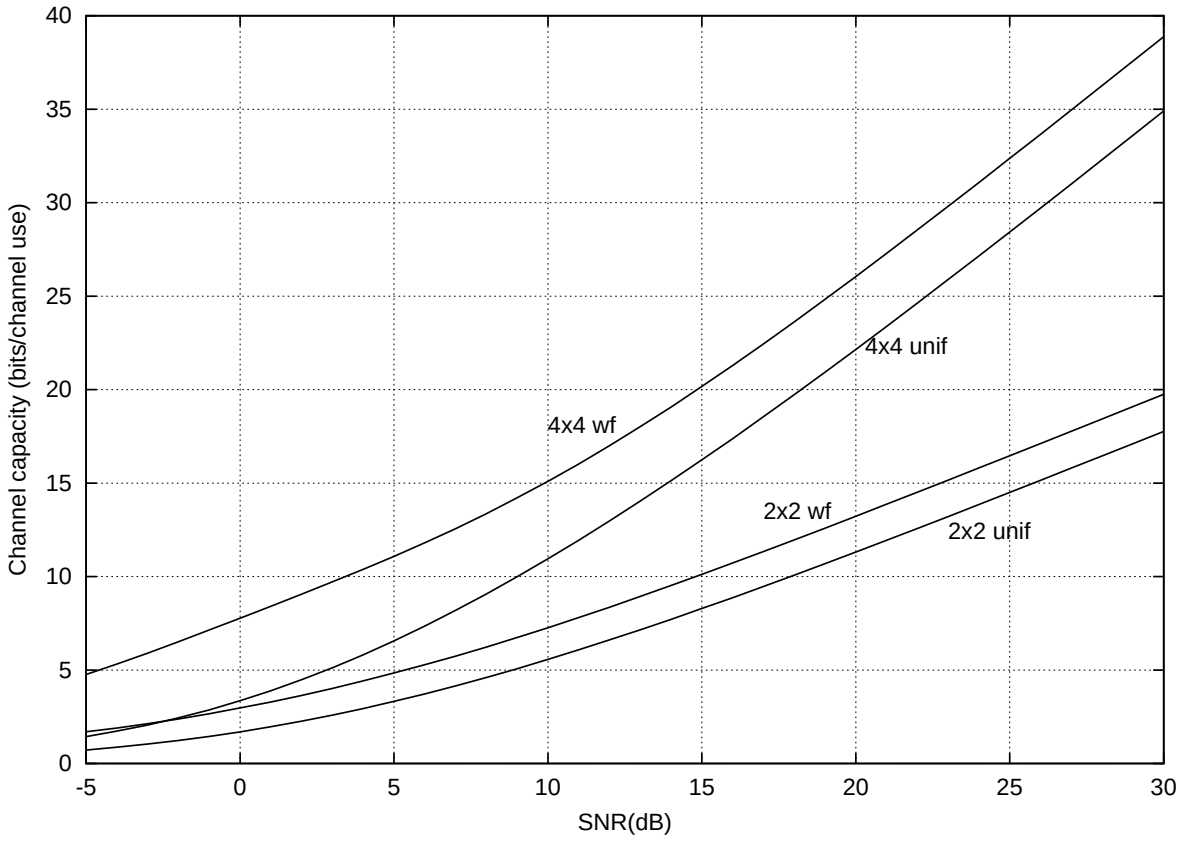

Figure 1.3: Capacity on an i.i.d Rayleigh fading ergodic channel, Gaussian input. Uniform power allocation (unif), optimal power allocation (wf).

Thus, the outage probability is the probability that a certain rate can be supported. Alternatively, the outage capacity is defined as the rate for which the error probability of a frame (or codeword) is below a certain level.

In Fig. 1.4, the outage capacity is plotted for 2×2 and 4×4 MIMO systems as a function of the average received SNR per bit, E_b/N_0, where $E_b/N_0 = n_r\rho/R$ and E_b is the bit energy. The outage probability corresponding to the outage capacity for both cases is fixed to 5.10^{-2}. For a given SNR, the transmit rate at which the error probability is below to 5.10^{-2} increases with the number of antennas.

The next section describes our MIMO transmission scheme and gives some assumptions and notations that will be adopted in the sequel.

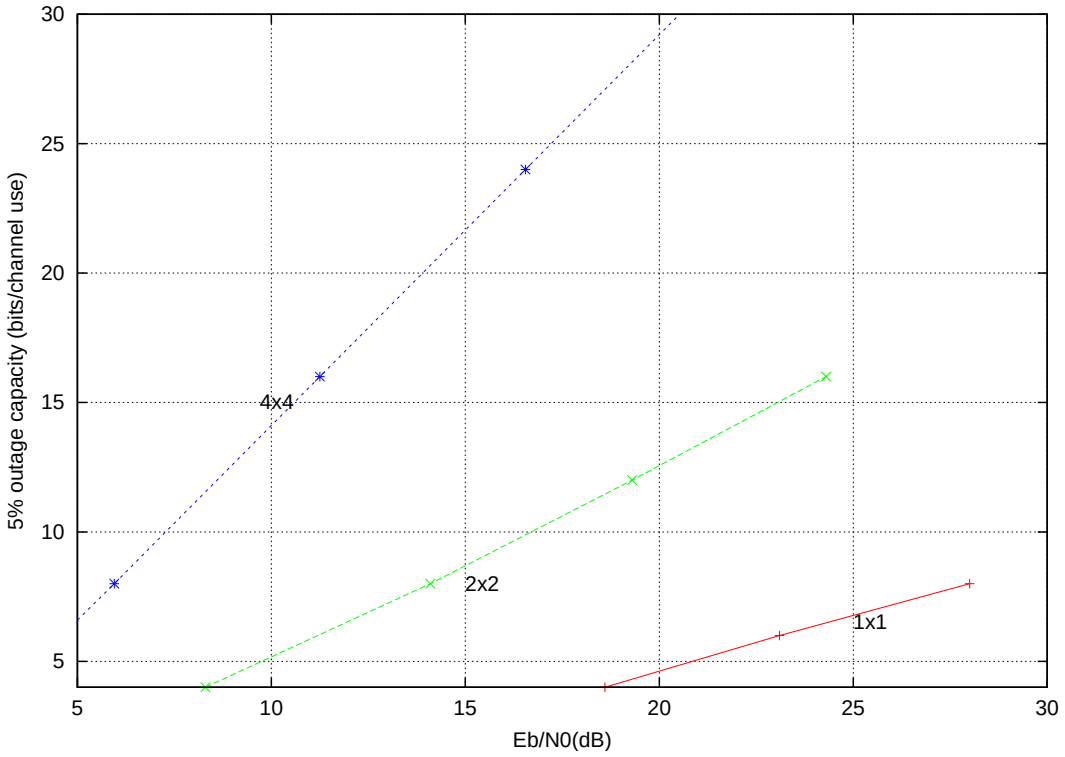

Figure 1.4: Outage capacity in an i.i.d Rayleigh fading channel. Gaussian input and uniform power allocation. Outage probability = 5.10^{-2}.

1.3 Description of our multiple antenna transmission scheme

In this section, we describe the transmission model that we considered in our studies. This model is depicted in Fig. 1.5 which shows an uncoded digital transmission system with n_t transmit antennas and n_r receive antennas. This model consists of a transmitter, a MIMO channel and a receiver. In chapters 3 and 4, the MIMO channel is assumed to be in row convention with a channel matrix of dimension $n_t \times n_r$.

For each channel use, the relationship between the receive and the transmit vectors is given by

$$\mathbf{r} = \mathbf{sH} + \boldsymbol{\nu}, \tag{1.19}$$

where $\mathbf{r}$ is the n_r length receive complex vector, $\mathbf{s}$ is the n_t length transmit vector, and $\boldsymbol{\nu}$ is the n_r length additive white Gaussian noise vector.

The following subsections present the different blocks of the MIMO transmission model.

1.3.1 The transmitter: scheme and assumptions

The incoming binary data stream is mapped to n_t complex modulation symbols s_k, $k = 1, \ldots, n_t$ (e.g. quadrature amplitude modulation (QAM), phase shift keying (PSK)). In this mapping same or distinct modulations can be applied for the different s_k. The resulted symbols are demultiplexed to be sent independently and simultaneously on the n_t transmit antennas. Such

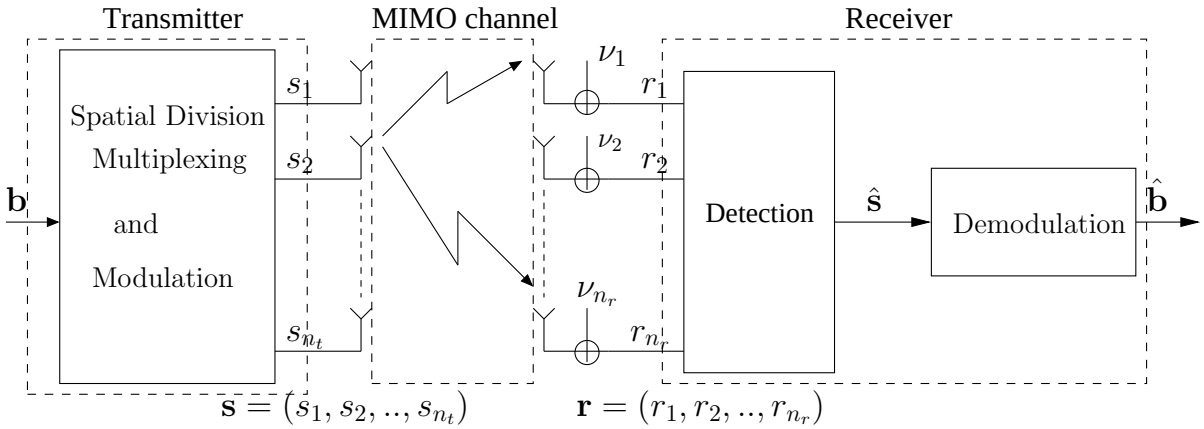

Figure 1.5: MIMO system model with spatial multiplexing.

a transmission algorithm is referred in the literature as *spatial multiplexing*.
This scheme over MIMO channels increases the transmission rate linearly in the number of transmit-receive antenna pairs or min(n_t,n_r). In the sequel, square QAM modulation with Gray mapping is selected. The transmitted symbol s_k belonging to a M_k-QAM modulation [48], $k = 1 \dots n_t$, is written as

$$s_k = \Re(s_k) + \sqrt{-1}\Im(s_k) \in \mathbb{C}, \ \Re(s_k),\Im(s_k) \in \{\pm 1, \pm 3, \cdots, \pm(\sqrt{M_k} - 1)\}$$

The average energy per transmit symbol is equal to

$$E_s = \frac{2}{3} \cdot (M - 1), \tag{1.20}$$

where M stands for the modulation size. Figure 1.6 illustrates some examples of square QAM constellations, with Gray mapping. The average symbol energy, per complex dimension, for 4-QAM, 16-QAM and 64-QAM are respectively 2, 10 and 42.

The n_t QAM constellations are not necessarily identical. Let C_{QAM} be their Cartesian product. The projection of the multidimensional constellation C_{QAM} onto a plane could lead to a rectangular constellation. For example, if we assume the modulation combination (16-QAM,4-QAM) for a 2×2 MIMO system,

$$C_{\text{QAM}} = \{\mathbf{s} = (s_1,s_2), \ s_1 \in \text{16-QAM}, \ s_2 \in \text{4-QAM}\}$$

The observation of C_{QAM} on the plane corresponding to $\Im(s_1)$ and $\Re(s_2)$ leads to the set of symbols illustrated by the rectangular constellation in Fig. 1.7.

1.3.2 The channel: model and assumptions

The MIMO channel is assumed to be uncorrelated frequency non-selective and quasi-static. The $n_t \times n_r$ MIMO channel matrix $\mathbf{H} = [h_{ij}]$ is constant during T_c channel uses, where the integer T_c is the channel coherence time and one time unit is equal to one transmission period. The coefficients h_{ij} are independent zero-mean unit-variance complex Gaussian variables that take independent values each T_c periods. The channel gains $|h_{ij}|$ are then Rayleigh distributed random variables with PDF given by (1.1).

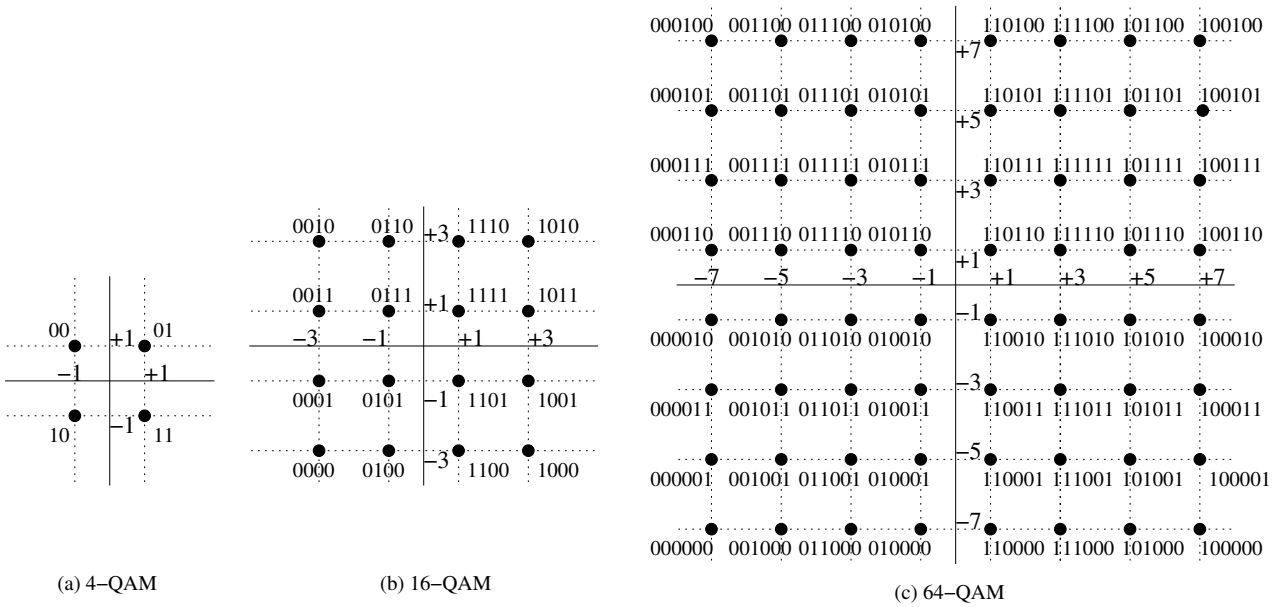

(a) 4–QAM (b) 16–QAM (c) 64–QAM

Figure 1.6: Examples of square QAM constellation: 4-QAM, 16-QAM, and 64-QAM with Gray labelling.

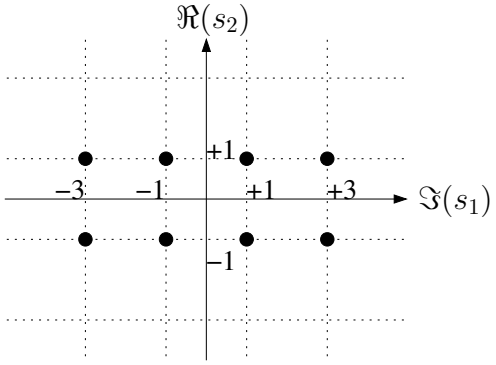

Figure 1.7: Projection of multidimensional constellation (16-QAM,4-QAM) onto a plane.

1.3.3 The receiver: scheme and assumptions

At the receiver, additive thermal noise corrupts the received signal on the n_r receive antennas. Detection and demapping operations are then performed to recover the transmit message. Different detection schemes were proposed in the literature for spatial multiplexing systems. Most of them are linear equalization followed by quantization, nulling and cancelling (or decision feedback), and ML detection [61], [1]. The first two detectors are suboptimal but with lower complexity computation than the ML detector. Next subsections briefly describe the principles of such detectors that will be used in the sequel.

1.3.3.1 Sub-optimal receivers

Linear equalization

In this case, the detection consists in applying at first an $n_r \times n_t$ equalizer matrix $\mathbf{G}$ to the received vector $\mathbf{r}$. Then an estimate of the transmitted vector $\mathbf{s}$ is obtained using the quantization operation, that is

$$\hat{\mathbf{s}} = Q(\mathbf{rG})$$

where $Q(.)$ denotes the quantization operator.

For *zero-forcing* (ZF) receiver, the equalization aims to null the inter-symbol interference. The equalizer matrix is given by the pseudo-inverse of the channel matrix $\mathbf{H}$ [32], [60] as

$$\mathbf{G}_{ZF} = \mathbf{H}^{\dagger}(\mathbf{H}\mathbf{H}^{\dagger})^{-1}$$

Therefore, the equalization results in

$$\mathbf{r}_{ZF} = \mathbf{r}\mathbf{G}_{ZF} = \mathbf{s} + \boldsymbol{\nu}\mathbf{G}_{ZF}$$

which is the transmitted vector $\mathbf{s}$ corrupted by the modified noise $\boldsymbol{\nu}\mathbf{G}_{ZF}$.

The *minimum mean-square error* (MMSE) receiver searches to minimize the mean-square error given by

$$E\left(\|\mathbf{rG} - \mathbf{s}\|^2\right).$$

The equalizer matrix is then given by [60]

$$\mathbf{G}_{MMSE} = \mathbf{H}^{\dagger}\left(\mathbf{H}\mathbf{H}^{\dagger} + \frac{2N_0}{E_s/n_t} I_{n_t}\right)^{-1},$$

and the result of the MMSE equalization is

$$\mathbf{r}_{MMSE} = \mathbf{r}\mathbf{H}^{\dagger}\left(\mathbf{H}\mathbf{H}^{\dagger} + \frac{2N_0}{E_s/n_t} I_{n_t}\right)^{-1}$$

Nulling and cancelling

Unlike the linear receiver, where detection is performed simultaneously for all vector symbols, nulling and cancelling (NC) approach, called also successive interference cancelling (SIC), is based on the decision-feedback method to detect each symbol separately (e.g V-BLAST [66], [22]). When a symbol is estimated, it is subtracted from the received vector $\mathbf{r}$ and the result is used to detect the next symbol, etc. To detect a particular symbol, the symbols that have not been detected yet are nulled via ZF or MMSE equalizer.
The presence of error detection could increase the interference when detecting the next symbols. That is why, the order in which the symbols are detected strongly impacts the performance of NC detector. In the case when symbols are detected in the order of decreasing SNR, the receiver is called Ordered Successive Interference Cancellation (OSuIC). In chapter 4, we consider the OSuIC, where the nulling operation is performed with MMSE equalizer. This detector is denoted MMSE-OSuIC.

1.3.3.2 ML detection

The optimal receiver, in terms of minimum error probability, is based on *maximum likelihood* (ML) detection. The detection looks for the vector $\hat{\mathbf{s}}$ that solves

$$\hat{\mathbf{s}} = arg \min_{\mathbf{s}} \|\mathbf{r} - \mathbf{sH}\|$$

The search is performed exhaustively over all $\prod_{i=1}^{n_t} M_i$ candidate vectors $\mathbf{s}$, where M_i is the modulation size applied on the i^{th} transmit antenna.
The decoding complexity of the exhaustive ML receiver is exponential in n_t. Several algorithms were proposed in the literature to decrease this complexity. For example, the sphere decoder algorithm which finds the ML solution with a polynomial complexity with respect to the rank of the channel [1], [63].

1.3.3.3 Simulation results

Figures 1.8 and 1.9 compare the performance achieved with the different detection schemes for an uncoded 2×2 and 4×4 MIMO system with QPSK modulation applied on all transmit antennas. The performance are illustrated in terms of Bit Error Rate (BER) versus the average received SNR per bit, E_b/N_0. For both cases, it is clear that the best performance is obtained with the optimal receiver, i.e. ML, that provides a receive diversity equal to n_r. The system diversity is minimized with the Zero-Forcing linear receiver, that equals $n_r - n_t + 1 = 1$ (when $n_t = n_r$) [65]. Finally, the MMSE-OSuIC receiver provides more than $n_r - n_t + 1$ and lower than n_r order diversity thanks to an ordering process.

In next chapters, the performance of wireless systems are evaluated with respect to the variation of the average received SNR per bit. Under the assumption mentioned in this section, the SNR is computed as follows

$$SNR = \frac{n_r \sum_{i=1}^{n_t} E_{s_i}}{2 \sum_{i=1}^{n_t} \log_2(M_i) N_0} \tag{1.21}$$

where E_{s_i} is the average energy per complex dimension of a symbol belonging to a QAM constellation of size M_i.

Conclusions

This chapter introduced the MIMO system model that will be used in the sequel. To show the advantages of this system, it was compared to a SISO system. When employing a single antenna at the transmitter and at the receiver, the reliability is not guaranteed due to channel fading. To combat fading, we saw that using multiple antennas at both sides is beneficial, by creating a spatial diversity. Moreover, we outlined that multiple antennas do not only improve the reliability of wireless channel; but also, increase the channel capacity. We illustrated the performance of spatial multiplexing MIMO systems, in terms of error probability, with different receiver schemes (ZF, MMSE, OSuIC, and ML). We showed that the optimal one (ML receiver) achieves the full receive diversity. Finally, we provided the MIMO transmission scheme and some assumptions/notations adopted in our studies in the last section.

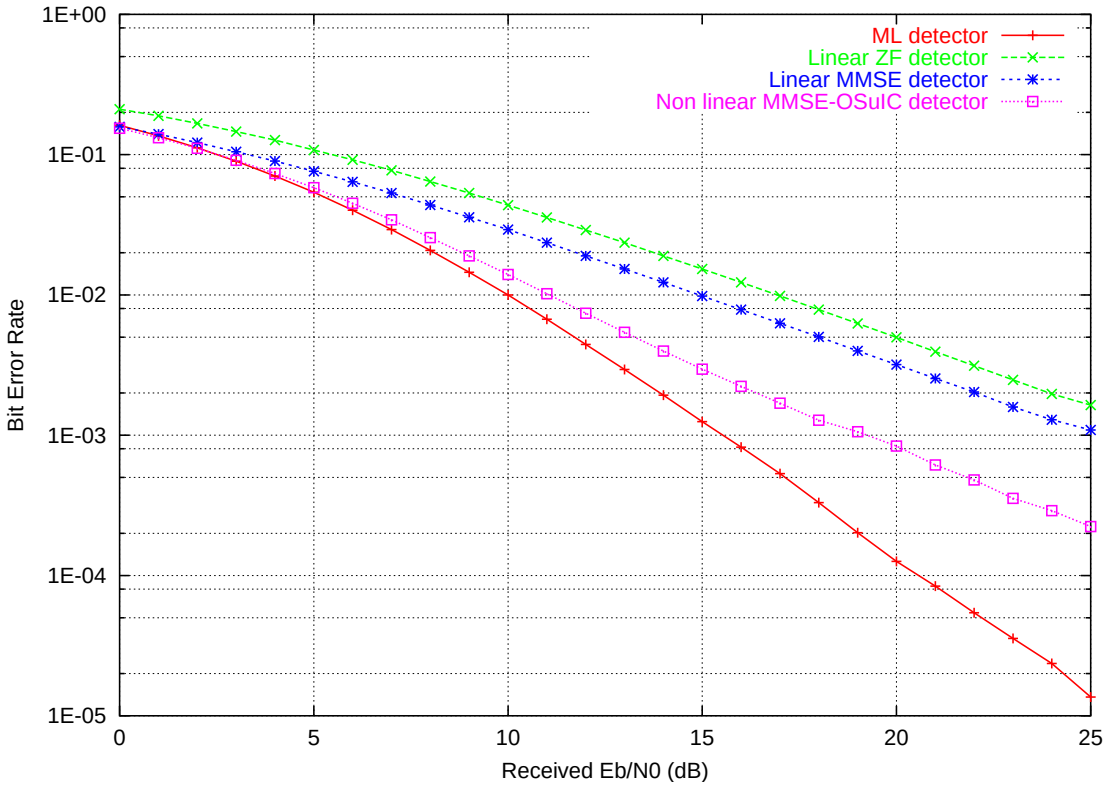

Figure 1.8: Average bit Error Rate of a 2×2 quasi-static MIMO Rayleigh channel. QPSK modulation on transmit antennas.

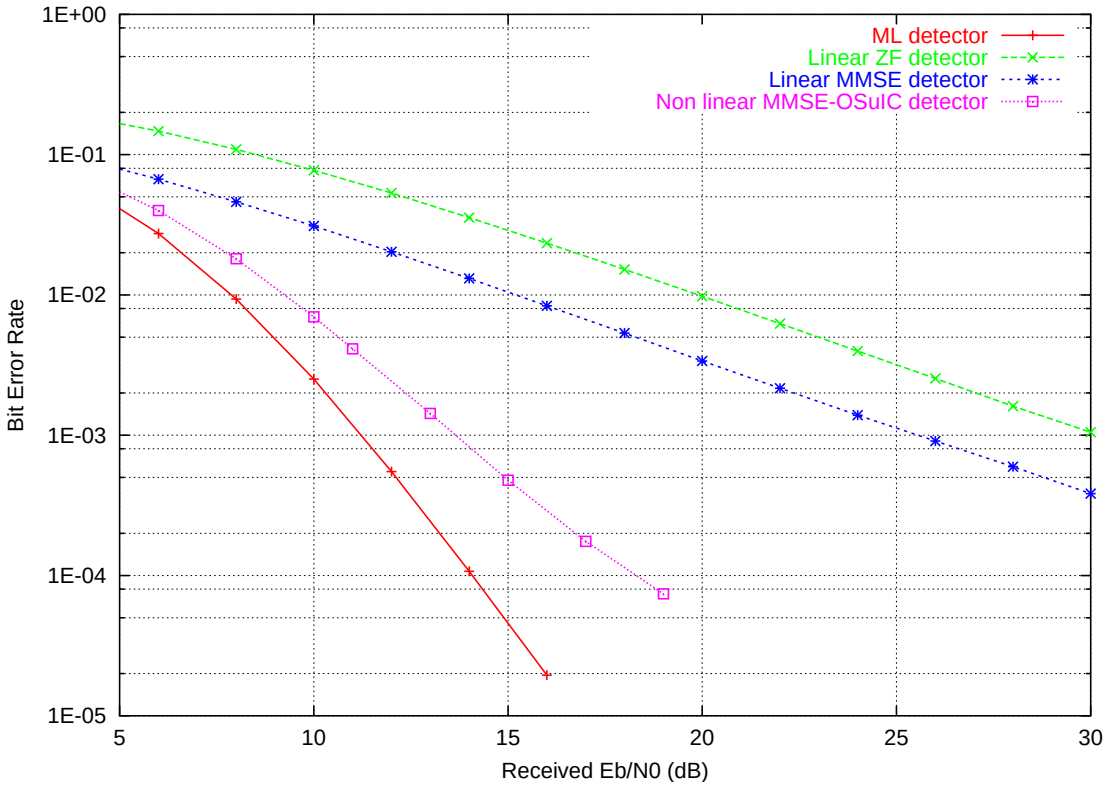

Figure 1.9: Average bit Error Rate of a 4×4 quasi-static MIMO Rayleigh channel. QPSK modulation on transmit antennas.

Chapter 2

Lattices and MIMO systems

Introduction

Lattices and number theory provide powerful means to study MIMO channel properties and to deal with the performance of MIMO systems, their transmission schemes, etc. In particular, by exploiting lattice theory, many detectors are recently proposed for MIMO systems [23], [68], [67]. Like linear receivers, these detectors are designed with low complexity, but they approaches the performance of ML receiver. In this thesis report, lattice theory and number theory allow not only to study the performance of MIMO systems but also to design a MIMO classification algorithm.

This chapter provides the important parameters and concepts from lattices and number theory, which are necessary to understand the next chapters.
The first section focuses on lattices. Main lattice parameters are presented as well as some mathematical concepts from number theory allowing to deal with lattices, namely quadratic forms and lattice reduction. These concepts will be used in the next chapters.
Next, we present the definition and some properties of lattice codes (or lattice constellations). The notion of lattice code will be considered in next chapters to represent MIMO system and then to study their performance. Finally, section 2.2 describes two lattice decoder algorithms based on the ML criterion. In the next chapters, the representation of MIMO systems as lattice codes justifies the use of these decoders in our transmission scheme for the detection.

2.1 Generalities on lattices

This section introduces first the main lattice parameters. Then, we outline the relationship between quadratic forms and lattices. Next, some lattice reduction algorithms are presented. A finite set of a lattice, called lattice code, is after that focused. Finally, the last part gives a bound for the performance of n-dimensional lattices on an AWGN channel, assuming a ML detection.

2.1.1 Main lattice parameters

Let K be a field, e.g. $K = \mathbb{R}$ the field of real numbers, or $K = \mathbb{C}$ the field of complex numbers. Let $A \subset K$ be a ring, e.g. $A = \mathbb{Z}$ the ring of integers, or $A = \mathbb{Z}[i] = \{a + ib | \ a,b \in \mathbb{Z}\}$ the ring of

Gaussian integers.

Definition 1 *(Lattice):*
A lattice $\Lambda \subset K^n$, also called a point lattice, is a free A-module in K^n. An element belonging to Λ is called a point or equivalently a vector. Any point $\mathbf{x} = (x_1, x_2, \ldots, x_n) \in \Lambda$ can be written as a linear combination of m vectors ($m \leq n$)

$$\mathbf{x} = \sum_{i=1}^{m} z_i \mathbf{v}_i,$$

where $(\mathbf{v}_i)_{1 \leq i \leq m}$ is an A-basis of Λ, and $(z_i)_{1 \leq i \leq m} \in A$. The components $\{v_{ij}\}_{j=1,\ldots,n}$ of the vector $\mathbf{v}_i$, $i = 1, \ldots, m$, belong to the field K. The rank of the lattice is equal to m which is the cardinality of the basis $(\mathbf{v}_i)_{1 \leq i \leq m}$. If $m = n$, the lattice is said to be of full-rank.

In the following, we assume that $m = n$. The lattice is viewed also as an infinite discrete additive group in K^n. The sum of two lattice vectors produces a new vector in Λ, both vectors $\mathbf{x}$ and $-\mathbf{x}$ belong to Λ and the null vector $\mathbf{0}$ is a lattice point.

The minimum Euclidean distance between two lattice points $\mathbf{x} = (x_1, \ldots, x_n)$ and $\mathbf{x}' = (x'_1, \ldots, x'_n)$ is equal to

$$d_{Emin} \stackrel{\text{def}}{=} \min_{\mathbf{x} \neq \mathbf{x}' \in \Lambda} \sqrt{\sum_{i=1}^{n} |x_i - x'_i|^2}$$

If $\mathbf{x}' = \mathbf{0}$, d_{Emin} is the minimum Euclidean norm of the non zero lattice points.

The canonical basis of the real Euclidean space $\mathbb{R}^n$ generates the so called integer lattice $\mathbb{Z}^n$, with $d_{Emin} = 1$.

Definition 2 *(Generator matrix):*
The $n \times n$ matrix built from a basis of Λ is called a generator matrix for Λ. In line convention, let $\mathbf{M} = [v_{ij}]_{1 \leq i \leq n, 1 \leq j \leq n}$, then the lattice is defined by

$$\Lambda = \{\mathbf{x} = \mathbf{z}\mathbf{M}, \ \mathbf{z} \in A^n\} \tag{2.1}$$

Therefore, we can see the lattice Λ as a transformed version of the lattice A^n by the linear transformation defined by the matrix $\mathbf{M}$. When column convention is assumed, i.e. the basis vectors form the columns of the generator matrix, a lattice point is defined by $\mathbf{x}^\dagger = \mathbf{M}\mathbf{z}^\dagger$, where $\dagger$ denotes transpose conjugation operation. Throughout this chapter, the lattice is defined as in equation (2.1) and row convention is used.

For a given generator matrix $\mathbf{M}$, the lattice Λ can be generated by any matrix $\mathbf{M'} = \mathbf{U}\mathbf{M}$, where $\mathbf{U}$ is a unimodular matrix with elements in A and determinant satisfying $|\det(\mathbf{U})| = 1$. The matrix $\mathbf{M'}$ is then another generator matrix of Λ obtained simply by the rotation of the ring A^n via the transformation $\mathbf{U}$. The matrix $\mathbf{U}$ can be also viewed as the basis change from $\mathbf{M}$ to $\mathbf{M'}$.

Definition 3 *(Gram matrix) :*
The product $\mathbf{G} = \mathbf{M}\mathbf{M}^\dagger$ is called a Gram matrix. Its elements $g_{ij}{}_{1 \leq i \leq n, 1 \leq j \leq n}$ are the inner product of pairs of vectors of the lattice basis, that is $g_{ij} = \langle \mathbf{v}_i, \mathbf{v}_j \rangle = \sum_{k=1}^{n} v_{ik} \overline{v_{jk}}$, where $\overline{x}$ denotes the conjugate of x. Therefore, $\mathbf{G}$ is Hermitian when $K = \mathbb{C}$ and symmetric when $K = \mathbb{R}$.

Geometrically, the diagonal elements of $\mathbf{G}$ ($g_{ii} = \langle \mathbf{v}_i, \mathbf{v}_i \rangle = \|\mathbf{v}_i\|^2$) are equal to the square norm of the basis vectors, whereas the other non diagonal elements ($g_{ij\ i\neq j} = \langle \mathbf{v}_i, \mathbf{v}_j \rangle$) correspond to the inter-vector angles.

If Λ is a full rank lattice, then a generator matrix $\mathbf{M}$ of rank n determines uniquely a positive definite Gram matrix $\mathbf{G}$. However, a Gram matrix determines an infinite number of generator matrices which are, in fact, the rotated versions of the same lattice. Thus, two generator matrices $\mathbf{M}$ and $\mathbf{M'}$ associated to the same Gram matrix are related by

$$\mathbf{M'} = \mathbf{MB}$$

where $\mathbf{B}$ is a unitary matrix. In the real case, $\mathbf{B}$ is said to be an orthogonal matrix.

Definition 4 *(**Fundamental parallelotope** and **fundamental volume**):*
Let $(\mathbf{v}_i)_{1\leq i\leq n}$ be a basis for the lattice. The parallelotope surrounded by the basis vectors

$$\mathcal{P}(\Lambda) = \{\mathbf{x} \in K^n \mid \mathbf{x} = \sum_{i=1}^{n} \alpha_i \mathbf{v}_i,\ 0 \leq \alpha_i < 1\}.$$

is a fundamental parallelotope. It is an example of a fundamental region for the lattice, such that one repetition of this region leads to the generation of a lattice point. Since different bases are possible for the lattice, the fundamental parallelotope is not unique. Its volume given by

$$vol(\Lambda) \stackrel{def}{=} |\det(\mathbf{M})| = \sqrt{\det(\mathbf{G})}$$

and it is independent from the basis choice. It is called fundamental volume and is the determinant of the lattice. When $|\det(\mathbf{M})| = 1$, the lattice is said unimodular.

Definition 5 *(**Voronoi cell**s) :*
Consider a point $\mathbf{x} \in \Lambda$ and delimit its neighborhood by mediating hyperplanes between $\mathbf{x}$ and all other lattice points. The obtained region is called Voronoi cell or Dirichlet region of $\mathbf{x}$ and is defined as

$$\mathcal{V}(\mathbf{x}) = \{\mathbf{y} \in K^n \mid |\mathbf{y} - \mathbf{x}| < |\mathbf{y} - \mathbf{x'}|,\ \forall \mathbf{x'} \in \Lambda\}.$$

The shape of Voronoi region does not depend on the lattice point $\mathbf{x}$. It depends only on the lattice structure and its volume equals $vol(\Lambda)$.

Definition 6 *(**Lattice density** and **center density**):*
*In lattice , the density Δ determines the fraction of the space covered by spheres of radius $\rho = \frac{1}{2} d_{Emin}$ and centered at lattice points, where d_{Emin} denotes the **minimum Euclidean distance** of the lattice. The density Δ of a lattice is then defined by*

$$\Delta = \frac{volume\ of\ a\ packing\ sphere\ of\ radius\ \rho}{volume\ of\ a\ Voronoi\ cell} = \frac{V_n \rho^n}{vol(\Lambda)} \leq 1, \tag{2.2}$$

where V_n is the volume of unit sphere in $\mathbb{R}^n$, given by

$$V_n = \pi^{n/2}/\Gamma(n/2+1) = \begin{cases} \frac{\pi^{n/2}}{(n/2)!} & , n\ even \\ \frac{2^n \pi^{(n-1)/2}((n-1)/2)!}{n!} & , n\ odd \end{cases}$$

*The **center density** δ is defined by normalizing Δ, that is*

$$\delta = \frac{\Delta}{V_n} = \frac{\rho^n}{vol(\Lambda)}$$

The center density determines the number of sphere centers, i.e. lattice points, per unit volume and it is used generally to compare lattices density in different dimensions.

The possible densest lattice packings are known in dimension ≤ 8 [15]. For example, the densest lattice in dimension 1 is the integer lattice $\mathbb{Z}$ with $\Delta(\mathbb{Z}) = 1$. In 2 dimensions, the hexagonal lattice A_2 is the densest lattice with $\Delta(A_2) = \pi/\sqrt{12}$.

Definition 7 *(**Fundamental gain**) :*
The density of Λ and its error rate performance in presence of additive noise are also related to its fundamental gain (also known as Hermite constant) defined by the energetic ratio [15][20]

$$\gamma(\Lambda) \stackrel{def}{=} \frac{d^2_{Emin}(\Lambda)}{\sqrt[n/2]{vol(\Lambda)}} = 4\sqrt[n/2]{\delta}. \tag{2.3}$$

The fundamental gain of the integer lattice $\mathbb{Z}^n$ is equal to $\gamma(\mathbb{Z}^n) = 1$.

Definition 8 *(**Kissing number**):*
For a lattice sphere packing, the kissing number is defined by the number of spheres tangent to one sphere. The kissing number is the same for all spheres in the case of lattice packing. It determines the number of points τ located at minimum distance from any lattice point.

For example, the kissing number for the integer lattice $\mathbb{Z}$ is 1. It is equal to 240 for the densest lattice packing in dimension 8, called E_8.

Definition 9 *(**Theta series**) :*
Since a lattice is a discrete subgroup of K^n, the distribution of the Euclidean distances around a lattice point $\mathbf{x}$ does not depend on $\mathbf{x}$. It is uniquely determined by its lattice.
A lattice shell is defined as the set of lattice points lying at a distance r, called shell radius, from a lattice point x. Then , the Euclidean distance distribution is given by the radius of lattice shells and their population (number of points in a shell). Similar to the Hamming weight distribution of an error-correcting code defined over a finite field, the theta series $\Theta_\Lambda(z)$ of Λ describes its Euclidean distance distribution

$$\Theta_\Lambda(z) \stackrel{def}{=} \sum_{\mathbf{x}\in\Lambda} q^{\|\mathbf{x}\|^2} = 1 + \tau q^{4\rho^2} + \ldots, \tag{2.4}$$

where $q = e^{i\pi z}$, $i = \sqrt{-1}$ and z is a complex variable. The theta series of highly structured lattices (e.g. integral lattices) is known for low dimensions [15].

Some simple examples are :

1. $\Lambda = \mathbb{Z}$

$$\Theta_{\mathbb{Z}}(z) = \sum_{m=-\infty}^{+\infty} q^{m^2} = 1 + 2q + 2q^4 + 2q^9 + 2q^{16} + \ldots = \theta_3(z),$$

where $\theta_3(z)$ is a Jacobi theta function. It is trivial to show that $\Theta_{\mathbb{Z}^n}(z) = \Theta_{\mathbb{Z}}(z)^n = \theta_3(z)^n$.

2. $\Lambda = \mathbb{Z} + 1/2$ The theta series of the translated lattice $\mathbb{Z} + 1/2$ is

$$\Theta_{\mathbb{Z}+1/2}(z) = \sum_{m=-\infty}^{+\infty} q^{(m+1/2)^2} = 2q^{1/4} + 2q^{9/4} + 2q^{25/4} + \ldots = \theta_2(z),$$

where $\theta_2(z)$ is also a Jacobi theta function.

3. $\Lambda = A_2$ the theta function of the hexagonal lattice is given by

$$\Theta_{A_2}(z) = \sum_{\mathbf{x}\in\Lambda} q^{\|\mathbf{x}\|} = \theta_3(z)\theta_3(3z) + \theta_2(z)\theta_2(3z) = 1 + 6q + 6q^3 + 6q^4 + 12q^7 + \ldots,$$

where $Q(\mathbf{x})$ is the quadratic form associated to A_2.

The reader can check that the theta series exactly describes A_2 shells population and radius as illustrated in Fig. 2.2. If Λ is a random lattice, then $\Theta_\Lambda(z)$ or at least all its terms up to q^C can be determined using the *Short vectors* algorithm that solves $\|\mathbf{x}\| \leq C$ [46][47][14].

Definition 10 ***(Equivalent lattices)**:*
Two lattices Λ_1 and Λ_2 are said equivalent, if one lattice can be obtained from the other by a rotation or a reflection or a change of scale without changing the shape of the Voronoi region. Two generator matrices $\mathbf{M}_1$ and $\mathbf{M}_2$ of equivalent lattices are related by

$$\mathbf{M}_2 = c\mathbf{U}\mathbf{M}_1\mathbf{B}$$

where $c = \left(\frac{|\det(\mathbf{M}_2)|}{|\det(\mathbf{M}_1)|}\right)^{1/n}$ is a constant corresponding to the scaling factor, $\mathbf{U}$ is an unimodular matrix that contains the coordinates of the basis given by $\mathbf{M}_2$ according to the basis $\mathbf{M}_1$ and $\mathbf{B}$ is a unitary matrix. For real case, $\mathbf{B}$ is associated to an isometry transformation, e.g. reflection, rotation, translation, ...

The Gram matrices of two equivalent lattices are related simply by

$$\mathbf{G}_2 = c^2\mathbf{U}\mathbf{G}_1\mathbf{U}^\dagger$$

If the scaling factor $c = 1$, equivalent lattices Λ_1 and Λ_2 are called congruent. When $\mathbf{B}$ is the identity matrix and $c \neq 1$, Λ_2 is a scaled version of Λ_1. If $\mathbf{U}$ is the identity matrix and $c = 1$, Λ_2 is a rotated version of Λ_1.

Figure 2.1 illustrates the integer lattice $\mathbb{Z}^2$ generated by the basis ($\mathbf{v}_1$,$\mathbf{v}_2$). Two equivalent lattices for $\mathbb{Z}^2$ could be obtained as follows

1. A simple rotation of the basis ($\mathbf{v}_1$,$\mathbf{v}_2$) using the orthogonal matrix

$$\mathbf{B} = \begin{bmatrix} cos(\phi) & -sin(\phi) \\ sin(\phi) & cos(\phi) \end{bmatrix}$$

with $\phi = 30$, generates a new basis ($\mathbf{w}_1$,$\mathbf{w}_2$) for the rotated version of $\mathbb{Z}^2$.

2. A scaled version of the lattice $\mathbb{Z}^2$ constructed via the basis ($\boldsymbol{\omega}_1$,$\boldsymbol{\omega}_2$) is also depicted. The latter basis is obtained through the multiplication of the basis ($\mathbf{v}_1$,$\mathbf{v}_2$) by the scalar $c = 1/2$.

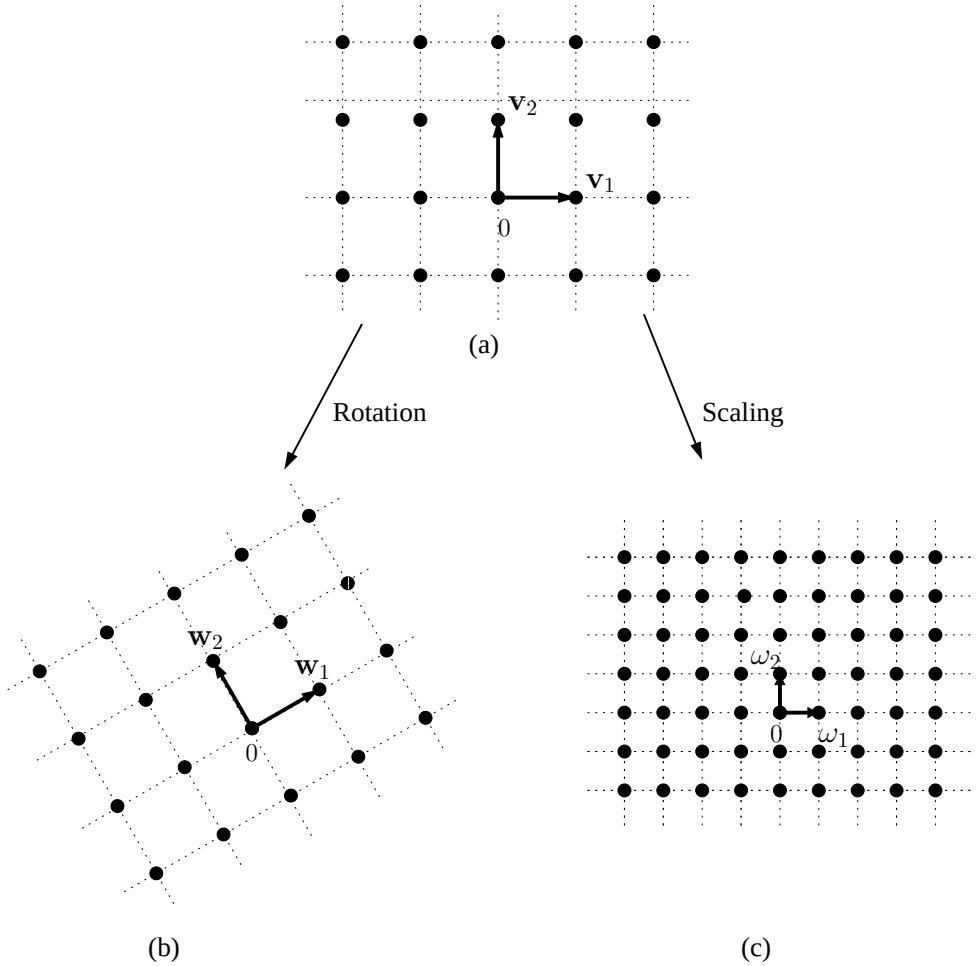

Figure 2.1: (a) The integer lattice $\mathbb{Z}^2$. (b) A rotated version of the lattice $\mathbb{Z}^2$. (c) A scaled version of the lattice $\mathbb{Z}^2$.

- **Example of a lattice in** $\mathbb{R}^2$: hexagonal lattice A_2

As an illustrative example for deterministic highly structured lattices, Fig. 2.2 shows the structure of the famous hexagonal lattice A_2. A generator matrix for A_2 is given by

$$\mathbf{M}(A_2) = \begin{bmatrix} 1 & 0 \\ 1/2 & \sqrt{3}/2 \end{bmatrix}.$$

Some of the important lattice parameters are also depicted in Fig. 2.2. The *minimum Euclidean distance* between distinct lattice points is $d_{Emin}(\Lambda) = 2\rho$, where ρ is the sphere packing radius associated to Λ as shown in the upper left part of Fig. 2.2. According to the generator matrix $\mathbf{M}(A_2)$, we deduce that $d_{Emin} = 2\rho = 1$ and $vol(A_2) = |\det(\mathbf{M}(A_2))| = \sqrt{3}/2$.

Each lattice point has τ neighboring points located at minimum distance. For A_2, we have $\tau = 6$. The Voronoi region $\mathcal{V}(\mathbf{x})$ of the lattice A_2 has six facets obtained by the six mediating segments with the nearest points. For higher order shells, let τ_i, $i \geq 1$, be the number of points belonging to the i^{th} shell and d_i their Euclidean distance from the origin.
For A_2, we observe in Fig. 2.2 the (τ_i, d_i) first values illustrated in the table 2.1.

Shell i	τ_i	d_i
1	6	2ρ
2	6	$2\sqrt{3}\rho$
3	6	4ρ
4	12	$2\sqrt{7}\rho$

Table 2.1: Number of neighboring points and distances of the first shells for the lattice A_2.

Thus, the theta series for A_2 could be written as

$$\begin{aligned}\Theta_{A_2}(z) &= \sum_{\mathbf{x}\in\Lambda} q^{\|\mathbf{x}\|^2} \\ &= 1 + \tau_1 q^{d_1^2} + \tau_2 q^{d_2^2} + \tau_3 q^{d_3^2} + \tau_4 q^{d_4^2} + \dots\end{aligned}$$

Replacing ρ by its value, the first terms of the theta series for this example can be written as

$$\Theta_{A_2}(z) = 1 + 6q + 6q^3 + 6q^4 + 12q^7 + \dots$$

which corresponds to the expression given in Definition 9.

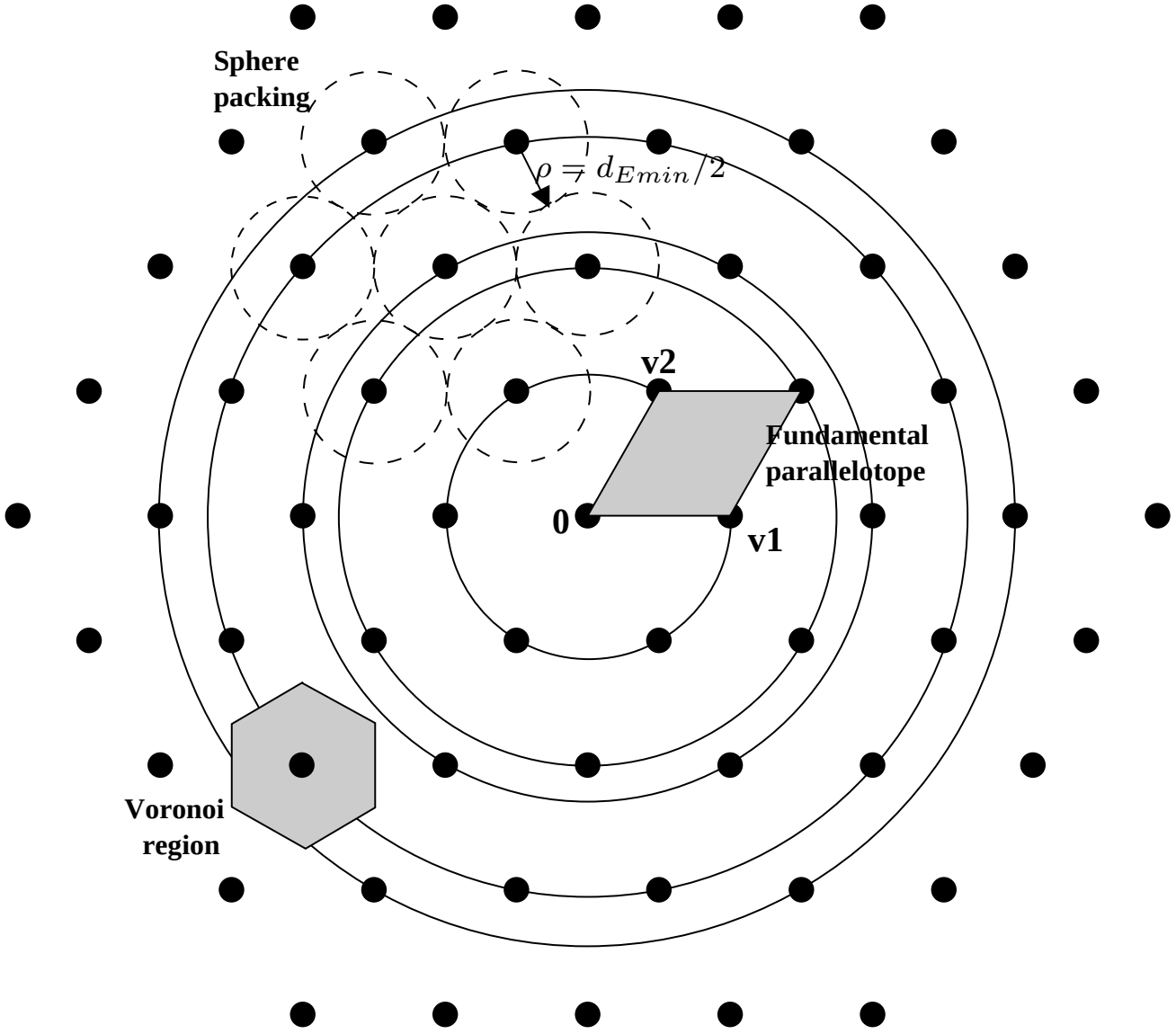

Figure 2.2: Structure of the hexagonal lattice A_2 in the real bidimensional space.

2.1.2 Lattices and quadratic forms

Quadratic form theory is a useful tool to study arithmetical properties of lattices in the Euclidean space. This theory will be used in the last chapter for MIMO channel classification.
This section gives at first the definition of the quadratic forms in real and complex spaces. Then, it describes the relationship between lattices and quadratic forms.

2.1.2.1 Definitions

Let V be a vector space over a field K, mainly $K = \mathbb{R}$ or $\mathbb{C}$. An Hermitian form on a vector space V over the field K is a function $h : V \times V \to K$ such that for all $\mathbf{u}$, $\mathbf{v}$, $\mathbf{w} \in V$ and for all ρ, $\lambda \in K$, we have

1. $h(\lambda\mathbf{u} + \rho\mathbf{v},\mathbf{w}) = \lambda h(\mathbf{u},\mathbf{w}) + \rho h(\mathbf{v},\mathbf{w})$
2. $h(\mathbf{u},\mathbf{v}) = \overline{h(\mathbf{v},\mathbf{u})}$

If K is the real field, the function h is considered as a symmetric bilinear form.

A map Q from V to K is called a quadratic form if the following conditions are satisfied:

1. $Q(\lambda\mathbf{u}) = |\lambda|^2 Q(\mathbf{u}),\ \forall\ \lambda \in K$ and $\forall\ \mathbf{u} \in V$
2. $h(\mathbf{u},\mathbf{v}) = \frac{1}{2}\left(Q(\mathbf{u} + \mathbf{v}) - Q(\mathbf{u}) - Q(\mathbf{v})\right)$ is an Hermitian or a symmetric bilinear form on V

If V is of rank n over the complex (respectively real) field and $(\mathbf{v}_i)_{1\leq i\leq n}$ is a basis for V, the Hermitian form (respectively bilinear form) relative to this basis can be represented by an Hermitian (respectively symmetric) matrix B with coefficients $b_{ij} = h(\mathbf{v}_i,\mathbf{v}_j)$. For $\mathbf{u} = (u_1,u_2,\ldots,u_n) \in V$, the associated quadratic form is given by

$$Q(\mathbf{u}) = \sum_{1\leq i,j\leq n} b_{ij} u_i \overline{u_j} = \mathbf{u}\mathbf{B}\mathbf{u}^\dagger$$

2.1.2.2 Lattices as quadratic forms

In the following, we show how lattices and quadratic forms are related. Let us consider a free A module lattice Λ generated by the basis vectors $(\mathbf{v}_i)_{1\leq i\leq n}$ (forming the rows of a generator matrix $\mathbf{M}$). A is the ring of integers or Gaussian integers. The squared norm of a lattice point $\mathbf{x} = \mathbf{z}\mathbf{M}$ is defined as

$$\|\mathbf{x}\|^2 = \mathbf{x}\mathbf{x}^\dagger = \sum_{i=1}^{n} z_i\overline{z_j}\langle\mathbf{v}_i,\mathbf{v}_j\rangle = \mathbf{z}\mathbf{G}\mathbf{z}^\dagger \tag{2.5}$$

The reader could notice that equation (2.5) defines a quadratic form, of the vector $\mathbf{z}$ associated with the Gram matrix $\mathbf{G} = \mathbf{M}\mathbf{M}^\dagger$ of the lattice. Therefore, an alternative approach to study a lattice Λ consists in dealing with its corresponding quadratic form Q_Λ defined by:

$$Q_\Lambda : A^n \to K\ :\ \mathbf{z} \mapsto \mathbf{z}\mathbf{G}\mathbf{z}^\dagger, \tag{2.6}$$

where $\mathbf{G}$ is a Gram matrix for Λ.

For any lattice, Q_Λ is a positive quadratic form, in particular, for all $\mathbf{z} \in A^n$,$Q_\Lambda(\mathbf{z})$ is positive.

Given the relationship between lattices and quadratic forms, it is possible to carry out computations on a lattice knowing only a Gram matrix and not necessarily a generator matrix. For example, the minimum squared Euclidean distance between any two points of Λ is equivalent to the minimum of Q_Λ in $A^n - \{\mathbf{0}\}$, where $\mathbf{0}$ is the null vector of A^n.

Examples :

- $\Lambda = A_2$: a quadratic form of the hexagonal lattice A_2 shown in Fig. 2.2 is

$$Q_{A_2}(\mathbf{z}) = z_1^2 + z_1 z_2 + z_2^2.$$

  The Gram matrix relative to $Q_{A_2}$is

$$G_{A_2} = \begin{bmatrix} 1 & 1/2 \\ 1/2 & 1 \end{bmatrix}.$$

- $\Lambda = \mathbb{Z}^n$: The n-dimensional cubic lattice $\mathbb{Z}^n$ generated by the identity matrix $\mathbf{I}_n$ can be represented by its associated quadratic form as

$$Q_{\mathbb{Z}^n}(\mathbf{z}) = z_1^2 + z_2^2 + \ldots + z_n^2$$

The following section describes a useful tool which will be recalled in the last chapter.

2.1.3 Lattice reduction algorithms

Any lattice can be described by different bases. Given a lattice basis $\mathbf{M}_1$ and any unimodular matrix $\mathbf{U}$ ($\mathbf{U}$ with entries in A and $|\det(\mathbf{U})| = 1$) the product $\mathbf{M}_2 = \mathbf{U}\mathbf{M}_1$ generates a new basis for the lattice Λ. Then, $\mathbf{U}$ is a basis change matrix. So, it is easy to verify that

$$|\det(\mathbf{M}_2)| = |\det(\mathbf{U}\mathbf{M}_1)| = |\det(\mathbf{M}_1)| = vol(\Lambda)$$

Among all lattice bases, some are better than others. The best bases are those whose elements are the shortest (i.e. having the lowest norm) and the most orthogonal (to each other). The lattice reduction is a old notion which consists in searching the best lattice basis, called reduced basis.

Figure 2.3 illustrates two bases for the 2-dimensional integer lattice $\mathbb{Z}^2$, ($\mathbf{w}_1$,$\mathbf{w}_2$) and ($\mathbf{v}_1$,$\mathbf{v}_2$). Their corresponding generator matrices are respectively

$$\mathbf{M}_1 = \begin{bmatrix} 3 & 2 \\ 2 & 1 \end{bmatrix} \quad \mathbf{M}_2 = \begin{bmatrix} 1 & 0 \\ 0 & 1 \end{bmatrix} \tag{2.7}$$

The basis $\mathbf{M}_2$ is obtained by multiplying the basis $\mathbf{M}_1$ by the matrix $\mathbf{U}$, $\mathbf{M}_2 = \mathbf{M}_1\mathbf{U}$ where :

$$\mathbf{U} = \begin{bmatrix} -1 & 2 \\ 2 & -3 \end{bmatrix} \tag{2.8}$$

It is clear that the entries of $\mathbf{U}$ are in $\mathbb{Z}$ and $|\det(\mathbf{U})| = 1$. The basis $\mathbf{M}_2$ is obtained by the

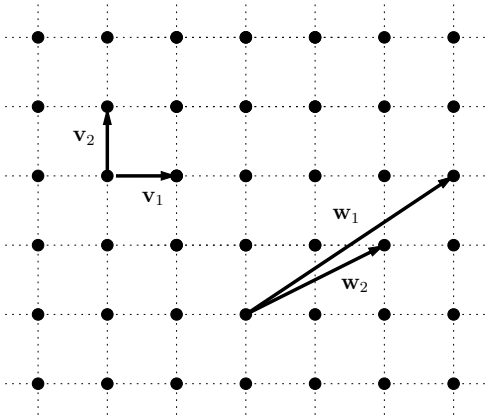

Figure 2.3: Integer lattice $\mathbb{Z}_2$. ($\mathbf{v}_1$,$\mathbf{v}_2$): reduced basis, ($\mathbf{w}_1$,$\mathbf{w}_2$): non reduced basis.

reduction of the basis $\mathbf{M}_1$.

The lattice reduction is used in conjunction with detector structures to improve performance. In [8], the authors show that the lattice decoder (VB and AEVZ) may be accelerated if the generator matrix is reduced. Conventional detection methods based on zero-forcing and minimum square error criterions have very low complexity but does not give the full diversity order. However, the application of lattice reduction with such detection schemes achieves the maximum receive diversity [68]. In our study, the lattice reduction will be used in chapter 5 to represent lattices with their reduced bases in order to classify them.

The main known reduction algorithms are illustrated in the following sub-sections.

2.1.3.1 Minkowski reduction

Let $(\mathbf{b}_i)_{1\leq i\leq n}$ be a basis of a lattice Λ. This basis is said *Minkowski reduced* if the following holds:

1. $\mathbf{b}_1$ is a shortest vector in Λ
2. For $i \in \{2,\ldots,n\}$, $\mathbf{b}_i$ is a shortest vector in Λ independent from $(\mathbf{b}_j)_{1\leq j\leq i-1}$ such that $(\mathbf{b}_j)_{1\leq j\leq i}$ can be extended to a basis of Λ.

Such a reduced form has found an application in the theory of numbers, but it is not useful computationally, and other classes of reduction were developed.

2.1.3.2 KZ reduction

Korkine-Zolotareff (KZ) reduction is a variant of Minkowski reduction that is more useful algorithmically. Consider a lattice Λ with a basis $(\mathbf{b}_i)_{1\leq i\leq n}$. This basis is *KZ reduced*, if

1. $\mathbf{b}_1$ is a shortest vector of Λ
2. Let Λ_i be the lattice obtained by the projection of Λ_{i-1} into the subspace of $\mathbb{R}^{n-i+1}$ orthogonal to $\mathbf{b}_{i-1}$, where $\Lambda = \Lambda_1$. The vector $\mathbf{b}_i$ should be a shortest vector of Λ_i.

2.1.3.3 LLL reduction

In 1982, Lenstra, Lenstra, and Lovasz succeeded in defining a new notion of reduction with a polynomial-time consuming algorithm. The LLL reduction is often used in situations where the KZ reduction would be too time-consuming.

Let $(\mathbf{b}_i)_{1\leq i\leq n}$ be a basis of a lattice Λ. For LLL reduction, the basis vectors are considered pairwise, and each vector $\mathbf{b}_i$ is required to be the shortest in the two-dimensional projected lattice generated by $\mathbf{b}_i$ and $\mathbf{b}_{i+1}$. Since LLL reduction is local in nature, so the basis found does not necessarily include a shortest vector, but only an approximation of one.

For a two-dimensional real lattice Λ, the basis $(\mathbf{b}_1,\mathbf{b}_2)$ is LLL reduced iff

$$\begin{cases} \frac{\langle \mathbf{b}_1,\mathbf{b}_2\rangle}{|\mathbf{b}_1|^2} & \leq & \frac{1}{2} \\ |\mathbf{b}_1|^2 & \leq & |\mathbf{b}_2|^2 \end{cases} \tag{2.9}$$

where $\langle \mathbf{b}_1,\mathbf{b}_2\rangle$ is the scalar inner product between the vectors $\mathbf{b}_1$ and $\mathbf{b}_2$.

To guarantee a polynomial-time completion, (2.9) is relaxed to

$$\delta|\mathbf{b}_1|^2 \leq |\mathbf{b}_2|^2 \tag{2.10}$$

where $0.5 \leq \delta \leq 1$. Often, $\delta = \frac{3}{4}$.

When Λ is a complex lattice, $(\mathbf{b}_1,\mathbf{b}_2)$ is LLL reduced iff

$$\begin{cases} \Re\left(\frac{\langle \mathbf{b}_1,\mathbf{b}_2\rangle}{\|\mathbf{b}_1\|^2}\right) & \leq & \frac{1}{2} \\ \Im\left(\frac{\langle \mathbf{b}_1,\mathbf{b}_2\rangle}{\|\mathbf{b}_1\|^2}\right) & \leq & \frac{1}{2} \\ \|\mathbf{b}_1\|^2 & \leq & \|\mathbf{b}_2\|^2 \end{cases} \tag{2.11}$$

where $\langle \mathbf{b}_1,\mathbf{b}_2\rangle$ is the Hermitian inner product between the vectors $\mathbf{b}_1$ and $\mathbf{b}_2$.

Now, let us generalize the conditions given in (2.9) to a basis $\mathbf{B} = (\mathbf{b}_i)_{1\leq i\leq n}$ of dimension n. To do this, we need an orthogonalization of the basis $\mathbf{B}$ [14], for example the Gram-Schmidt orthogonalization of a basis $\mathbf{B}$ in an Euclidean space vector E. This process leads to an orthogonal basis $(\mathbf{b}_i^*)_{1\leq i\leq n}$, such that

$$\mathbf{b}_i^* = \mathbf{b}_i - \sum_{j=1}^{i-1} \mu_{ij}\mathbf{b}_j^*,\ 1 \leq i \leq n \tag{2.12}$$

where $\mu_{ij} = \frac{\langle \mathbf{b}_i,\mathbf{b}_j^*\rangle}{|\mathbf{b}_j^*|^2}$. The vector $\mathbf{b}_i^*$ is the projection of $\mathbf{b}_i$ on the space spanned by $(\mathbf{b}_j)_{1\leq j\leq i-1}$.

Let Λ_i be the lattice defined by a pair of vectors $\mathbf{b}_i$ and $\mathbf{b}_{i+1}$. The orthogonal projection of Λ_i into $(\mathbf{b}_j)_{1\leq j\leq i-1}$ produces a lattice generated by the basis $b_i(i)$,$b_{i+1}(i)$, such that $b_i(i) = b_i^*$ and

$b_{i+1}(i) = b^*_{i+1} + \mu_{i+1,i} b^*_i$. The application of the conditions (2.9) and (2.10) for the pair of adjacent vectors $(\mathbf{b}_i, \mathbf{b}_{i+1})$ gives the LLL basis reduction conditions

$$\begin{cases} |\mu_{ij}| \leq \frac{1}{2}, \text{ for } 1 \leq i < j \leq n \\ \delta |b^*_i|^2 \leq |b^*_{i+1} + \mu_{i+1,i} b^*_i|^2, \text{ for } 1 \leq i < n \end{cases} \tag{2.13}$$

A basis $\mathbf{B} = (\mathbf{b}_i)_{1 \leq i \leq n}$ satisfying (2.13) is said to be LLL size-reduced.

Both Minkowski and KZ reduction algorithms may find the reduced basis but with an exponential complexity on lattice dimension. The last one, i.e. LLL reduction, does not guarantee to find the shortest lattice vectors. It generates in polynomial time a basis whose vectors are relatively short and orthogonal.

2.1.4 Lattice codes

A lattice code $C(\Lambda)$ is defined as a set of lattice points that are contained in a bounded support region of the field K^n [58]. A support region is defined as a convex, measurable, nonempty bounded region of K^n (e.g. a cube, a sphere, etc). In digital communication, this finite set is called as a signal constellation, or a multi-dimensional constellation ($n \geq 2$) for real space.

Some lattice parameters can no longer be used when considering only a finite subset of the lattice. This fact is observed essentially by points which are located close to the borders of the constellation. It is more significantly experienced for small lattice codes (i.e. small cardinal) where a high number of points are lying in the borders. An example of a lattice parameter that depends on the position of the point within the constellation is the Voronoi region. If the point $\mathbf{x}$ lies close to the boundary of the support region, the Voronoi region of $\mathbf{x}$ may be larger than that of any lattice point [58] (see also Fig. 2.4). This implies that the minimum Euclidean distance of lattice code $d_{Emin}(C(\Lambda))$ is bigger than that of the lattice

$$d_{Emin}(\Lambda) \leq d_{Emin}(C(\Lambda))$$

Also, the distribution of the Euclidean distance around a point depends on its position (within the constellation) and on the constellation shape.
Figure 2.4 illustrates two examples of lattice codes C_1 and C_2 carved from the hexagonal lattice A_2. Their support regions are given respectively by the bases $(\mathbf{v}_1, \mathbf{v}_2)$ and $(\mathbf{w}_1, \mathbf{w}_2)$. For both examples, we plot the Voronoi regions of points $\mathbf{x}_1 \in C_1$ and $\mathbf{x}_2 \in C_2$, that are located at the border of the constellations. Clearly, both cells are larger than the one which is around any point in the lattice A_2 (see Fig. 2.2). The distribution of the Euclidean distance around the points $\mathbf{x}_1$ and $\mathbf{x}_2$ depends on the support region shape. Indeed, the kissing number $\tau(\mathbf{x}_1)$ is equal to 3, whereas $\tau(\mathbf{x}_2) = 4$.
Hence, the performance of a lattice code on a Gaussian channel depends not only on the underlying lattice Λ but also on the shape of the support region.

2.1.5 Lattice performance

This section presents a known bound on the error probability of n-dimensional lattices on an AWGN channel assuming ML detection.

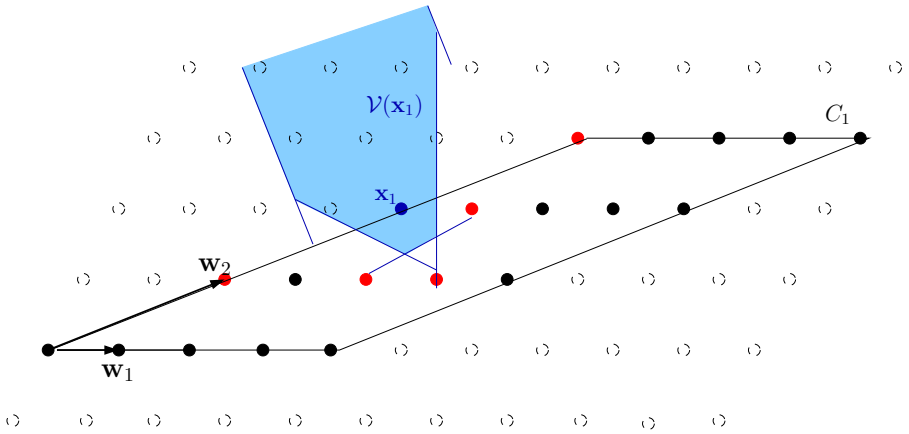

(a) lattice codes carved from the lattice A_2 with support region is given by the basis $(\mathbf{w}_1, \mathbf{w}_2)$

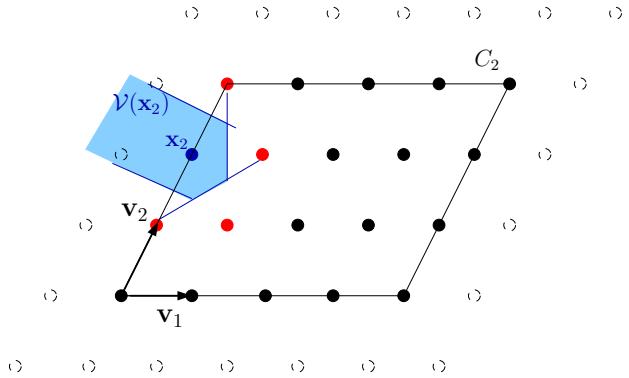

(b) lattice codes carved from the lattice A_2 with support region is given by the basis $(\mathbf{w}_1, \mathbf{w}_2)$

Figure 2.4: Voronoi cells around points in lattice constellations carved from the hexagonal lattice A_2.

Due to the geometrical uniformity of Λ, the error probability $Pe(\Lambda)$ does not depend on the transmitted point, e.g. $Pe(\Lambda) = Pe_{|\mathbf{0}} \leq \sum_{\mathbf{x}\neq\mathbf{0}} P(\mathbf{0} \to \mathbf{x})$, where $P(\mathbf{x} \to \mathbf{y})$ is the classical notation for the pairwise error probabilities (the probability that the received point is closer to the point $\mathbf{y}$ than to the transmitted point $\mathbf{x}$) and $Pe_{|\mathbf{x}}$ is the error probability conditioned on the transmission of $\mathbf{x}$. The exact expression of the error probability is obtained by computing

$$Pe(\Lambda) = Pe_{|\mathbf{0}} = 1 - \frac{1}{(\sigma\sqrt{2\pi})^n} \int_{\mathcal{V}(0)} e^{-\|x\|^2/2\sigma^2} dx$$

where $\mathcal{V}(0)$ is the Voronoi region around the origin $\mathbf{0}$. To evaluate the above expression, one should integrate over the Voronoi region.
It is well known in lattice theory [15] that integrating over any Voronoi region is an extremely difficult task. If integration is to be done numerically and if a random lattice is considered, one can imagine to determine a complete description of the Voronoi region via the Diamond Cutting Algorithm [62] and then integrate using the Gaussian distribution. Unfortunately, the task is still extremely complex. The integration must be done for all points in the case of a finite

constellation, or at least a large number of points if symmetry exists.
Hence, error rate $P_e(\Lambda)$ cannot be exactly computed by numerical integration that avoids Monte Carlo simulation. Under the assumption that all facets of the Voronoi region are created by lattice points lying on the first lattice shell, we have

$$Pe(\Lambda) \leq \tau(\Lambda) \times \mathrm{Q}\left(\frac{d_{Emin}(\Lambda)}{2\sigma}\right). \tag{2.14}$$

In the next chapters, we will consider lattice codes to represent MIMO channels. Therefore, it is possible to use the known lattice decoders in our transmission scheme to perform an ML detection with low complexity. The next section describes the most known lattice decoder algorithms and shows how they could be adapted to lattice codes.

2.2 Lattice decoder algorithms

Given an n-dimensional lattice Λ and any vector $\mathbf{y}$ in the real Euclidean space $\mathbb{R}^n$, decoding consists in finding the closest lattice point to the vector $\mathbf{y}$. An exhaustive search of the closest point is an intractable solution having an exponential complexity on the dimension n.
An efficient decoding algorithm for any lattice is then required with low complexity. In [15], several decoding algorithms, depending on the lattice structure, are described for the well-known lattices, namely the integer lattices $A_n(n \geq 1)$, root lattices $D_n(n \geq 2)$, E_6, E_7, E_8 and their duals. The problem here is how to find the closest point to $\mathbf{y}$ in a random lattice. The first step to solve this problem is to find a bounded region B in $\mathbb{R}^n$ surrounding the optimal lattice point. Then all the lattice points belonging to B will be checked. It is noticed that the size of B could be reduced during the search using the distance between any lattice point in B and the vector $\mathbf{y}$.

Two approaches are mainly used when searching the closest point. On the one hand, Pohst proposed in [46] to limit the search in an hypersphere. On the other hand, Kannan recommends to restrict the search in a rectangular parallelepiped [33]. Pohst method is considered to be more practical and easier to be implemented, while Kannan's strategy remains mostly used in a theoretical context.

The Pohst method was first used in digital communications by Viterbo and Biglieri [61], and then by Viterbo and Boutros [63] to find the closest point for a single antenna fading channels. Lately, Agrell et al [1] introduced the Schnorr-Euchner strategy [51], which represents an improvement of Pohst method, for the closest point search.
Both search strategies will be described in the following subsections for lattice decoder. We will also outline how both strategies could be adapted to lattice codes.

2.2.1 Lattice decoder based on Pohst enumeration

A lattice decoding algorithm searches the closest lattice point in a sphere of radius R and centered at the vector $\mathbf{y}$, $S(\mathbf{y},R)$. The search in the real space is conducted within a spherical region, while in the integer space it is made inside an ellipsoid. This idea was proposed at first for the search of the shortest nonzero vector in a lattice by exploring the ellipsoid centered at the origin [46][47][14]. Viterbo and Boutros detailed in [63] the decoding algorithm of any point in $\mathbb{R}^n$ and gave a flowchart for a specific implementation of this algorithm. The decoder

searches for a vector $\mathbf{y}$ the lattice point which is associated to the minimum of the set

$$\{\|\mathbf{y}-\mathbf{x}\|, \mathbf{x}\in\Lambda\} = \{\|\mathbf{w}\|, \mathbf{w}\in\mathbf{y}-\Lambda\}$$

That is, the search in the lattice Λ is equivalent to a search among the points of the translated lattice $\mathbf{y}-\Lambda$.
Let the real vectors $\mathbf{x}$, $\mathbf{y}$ and $\mathbf{w}$ be defined as

$$\begin{aligned}\mathbf{x} &= \mathbf{z}\mathbf{M},\ \mathbf{z}\in\mathbb{Z}^n\\ \mathbf{y} &= \boldsymbol{\rho}\,\mathbf{M},\ \boldsymbol{\rho}=(\rho_1,\rho_2,\ldots,\rho_n)\in\mathbb{R}^n\\ \mathbf{w} &= \mathbf{y}-\mathbf{x}=\boldsymbol{\xi}\,\mathbf{M},\ \boldsymbol{\xi}=(\xi_1,\xi_2,\ldots,\xi_n)\in\mathbb{R}^n\end{aligned}$$

The matrix $\mathbf{M}$ is invertible so $\rho = \mathbf{y}\mathbf{M}^{-1}$ is the Zero-Forcing point. Moreover, $\xi_i = \rho_i - z_i$, $i = 1,\ldots,n$ define the coordinates of the point $\mathbf{x}$ in the new coordinate system obtained with the translation.

As pointed out previously, the search according to Pohst strategy is performed inside a sphere of radius R. The checked lattice points should satisfy the inequality:

$$\|\mathbf{y}-\mathbf{x}\|^2 = \|\mathbf{w}\|^2 = \boldsymbol{\xi}\,\mathbf{G}\boldsymbol{\xi}^{\,T} = Q(\boldsymbol{\xi}) = \sum_{i=1}^{n}\sum_{j=1}^{n} m_{ij}\xi_i\xi_j \le R^2 \tag{2.15}$$

where $\mathbf{G} = \mathbf{M}\mathbf{M}^T$ denotes a Gram matrix for the lattice Λ and Q is the quadratic form on $\mathbb{R}^n$ associated to $\mathbf{G}$.

By diagonalizing the matrix $\mathbf{G}$ as $\mathbf{G} = \mathbf{P}\mathbf{D}\mathbf{P}^T$, where $\mathbf{P}$ is unitary, equation (2.15) becomes

$$Q(\boldsymbol{\xi}') = \sum_{i=1}^{n} d_i|\xi_i'|^2 \le R^2 \tag{2.16}$$

where $\boldsymbol{\xi}' = (\xi_1',\ldots,\xi_n') = \boldsymbol{\xi}\,\mathbf{P}$ and d_i is the i^{th} eigenvalue of $\mathbf{M}$.

Equation (2.16) illustrates the equation of an ellipsoid, whose semi-axe lengths are equal to $\frac{1}{\sqrt{d_i}}$, and direction are carried by the basis rotated from the Euclidean basis using the matrix $\mathbf{P}$.

As a consequence, the search inside a sphere of radius R is equivalent to a search into an ellipsoid centered at the origin of the new coordinate system, whose axis are defined by the transformed basis (Fig. 2.5).

Now, to find the bounds for the unknown components $(z_i)_{1\le i\le n}$ corresponding to the sphere $S(\mathbf{y},R)$, we proceed as follows. The Cholesky factorization of the Gram matrix yields to $\mathbf{G} = \mathbf{R}^T\mathbf{R}$, where $\mathbf{R} = [r_{ij}]_{i,j=1,..,n}$ is an upper triangular matrix. Substituting this result in the inequality (2.15) leads to:

$$Q(\boldsymbol{\xi}) = \boldsymbol{\xi}\,\mathbf{R}^T\mathbf{R}\boldsymbol{\xi}^{\,T} = \|\mathbf{R}\boldsymbol{\xi}^{\,T}\|^2 = \sum_{i=1}^{n}\left(r_{ii}\xi_i + \sum_{j=i+1}^{n} r_{ij}\xi_j\right)^2 \le R^2 \tag{2.17}$$

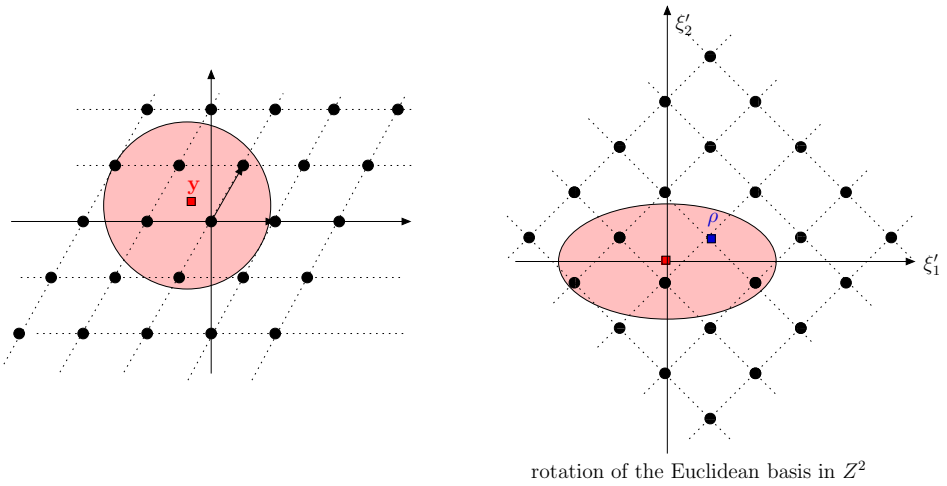

Figure 2.5: Example of sphere decoder search in bidimensional lattice.

If $q_{ii} = r_{ii}^2$ for $i = 1,..,n$ and $q_{ij} = \frac{r_{ij}}{r_{ii}}$ for $i = 1,..,n$, $j = i+1,..,n$, we can write:

$$Q(\boldsymbol{\xi}) = \sum_{i=1}^{n} q_{ii} \left(\xi_i + \sum_{j=i+1}^{n} q_{ij} \xi_j \right)^2 \leq R^2 \tag{2.18}$$

Substituting ξ_i by $\rho_i - z_i$ in (2.18), the reader could notice that the search in the real space can be carried on more easily in the integer space. The search algorithm consists in spanning at each level i the possible values of z_i, starting from level $i = n$ and going down to levels $i = n-1, n-2, \ldots, 1$. The borders of the coordinate z_n are given by

$$\left\lceil -\sqrt{\frac{R^2}{q_{n,n}}} + \rho_n \right\rceil \leq z_n \leq \left\lfloor \sqrt{\frac{R^2}{q_{n,n}}} + \rho_n \right\rfloor \tag{2.19}$$

The bounds of the component z_i are determined by the current values of the components $(z_j)_{j=n\ldots i+1}$ as follows:

$$\begin{gathered} \left\lceil -\sqrt{\frac{1}{q_{ii}} \left(R^2 - \sum_{l=i+1}^{n} q_{il} \left(\xi_l + \sum_{j=l+1}^{n} q_{lj} \xi_j \right)^2 \right)} + \rho_i + \sum_{j=i+1}^{n} q_{ji} \xi_j \right\rceil \\ \leq z_i \leq \\ \left\lfloor \sqrt{\frac{1}{q_{ii}} \left(R^2 - \sum_{l=i+1}^{n} q_{il} \left(\xi_l + \sum_{j=l+1}^{n} q_{lj} \xi_j \right)^2 \right)} + \rho_i + \sum_{j=i+1}^{n} q_{ji} a_j \right\rfloor \end{gathered} \tag{2.20}$$

where $\lceil x \rceil$ is the smallest integer greater than x and $\lfloor x \rfloor$ is the greatest integer smaller than x.

When a vector inside the search region is found, its squared distance from $\mathbf{y}$, denoted $\hat{d}^2$, is compared to the minimum distance, which is initialized at R. If it is smaller, this point is considered as a candidate lattice point and the enumeration is restricted to the lattice points belonging to a sphere $S(\mathbf{y},\hat{d})$. The bounds of the integer components z_i (2.20) are then updated. If no integer component z_n is found in the sphere, the initial radius R is increased and the search is restarted with the new squared radius.

Since the bounds considered in the equation (2.20) depend on the sphere radius R, a suitable choice of its initial value is recommended. Note that if R is too large, many points are obtained and the search remains exponential in size, whereas if R is very small, no point is obtained in the sphere. The initial sphere radius can be chosen based on noise statistics as suggested by Hassibi and Vikalo in [28]. In this case, the radius can be adjusted such that the probability to find a lattice point inside the corresponding sphere is high.

Notice that the described algorithm is proposed for the infinite lattice. Since, in digital communications, finite lattice constellations are often used, it is necessary to adapt the decoding algorithm to this kind of structures. To solve this problem, one trivial idea consists in applying the lattice decoder and then checking the position of the selected point in the constellation. In this case, the probability to find a point within the constellation is lower than the case of the infinite lattice. Then the search complexity is increased.

To reduce this complexity, a solution proposed in [8], [49] consists in exploring only the lattice points inside the finite constellation. This limitation is made simply by taking into account the borders of the constellation when evaluating the bounds of the components z_i, $i = 1, \ldots, n$.
Let $z_{\max}$ and $z_{\min}$ be the higher and the lower value respectively, of the coordinates of the points belonging to the constellation. Thus, the components z_i, $i = 1, \ldots, n$ lie on the following set

$$I_i^c = \{z \in \mathbb{Z}, \max(z_{\min}, I_{\min,i}) \leq z \leq \min(z_{\max}, I_{\max,i})\}$$

where $I_{\min,i}$ and $I_{\max,i}$ are the lower and the higher bound respectively for the component z_i in (2.20).

When a non square constellation is considered, the bounds $z_{\max}$ and $z_{\min}$ may vary with the dimension i. The decoder must take into account this variation while computing the bounds of the components z_i, $i = 1, \ldots, n$.
Figure 2.6 illustrates an example of a lattice code in the 2-dimensional real space. The corresponding constellation in the integer lattice $\mathbb{Z}^2$ is a rectangular constellation with $z_{\max} = -z_{min} = 2$ for the first dimension, and $z_{\max} = -z_{min} = 1$ for the second dimension.

2.2.2 Lattice decoder based on Schnorr-Euchner enumeration

Agrell, Eriksson, Vardy and Zeger proposed in [1] a lattice decoder based on the Schnorr-Euchner strategy. The proposed algorithm requires to represent the lattice by a triangular generator matrix. Such representation can be obtained by a QR decomposition of any generator matrix $\mathbf{M}$. In row convention, we have

$$\mathbf{M} = \mathbf{RQ}$$

where $\mathbf{R}$ is a lower triangular matrix with positive diagonal elements and $\mathbf{Q}$ is an orthogonal matrix satisfying $\mathbf{QQ}^T = \mathbf{I}$.

The decoder tries to find the closest point $\mathbf{x} = \mathbf{zM}$ to the vector $\mathbf{y}$, that can be written as $\mathbf{y} = \mathbf{x} + \mathbf{w}$, where $\mathbf{w} \in \mathbb{R}^n$. Using the QR decomposition for the matrix $\mathbf{G}$, the preimage of $\mathbf{y}$ by the orthogonal matrix $\mathbf{Q}$ is

$$\tilde{\mathbf{y}} = \mathbf{yQ}^T = \mathbf{zR} + \mathbf{wQ}^T$$

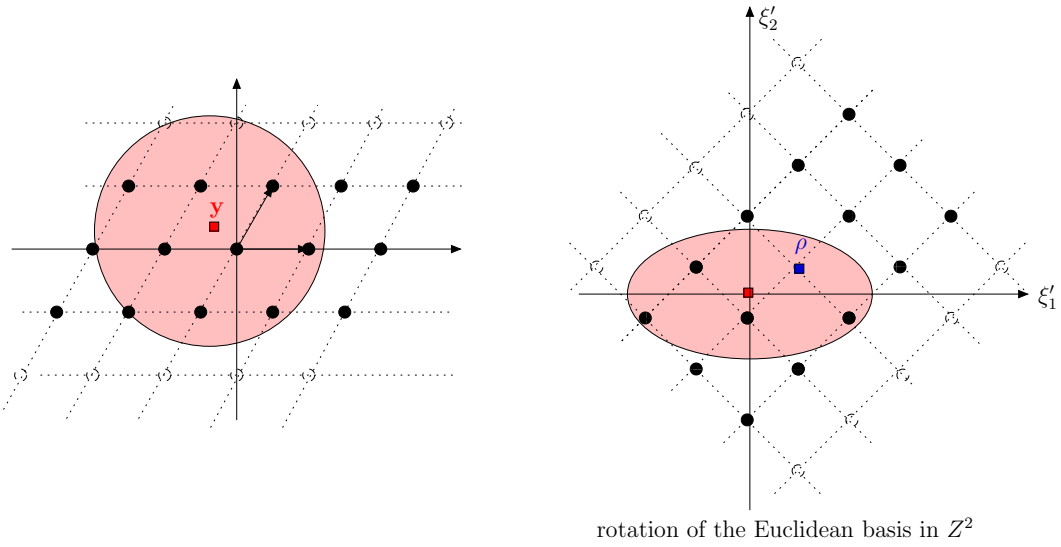

Figure 2.6: An example of a sphere decoder search in a 2-dimensional lattice code.

The matrix $\mathbf{R}$ could be written as

$$\mathbf{R} = \begin{bmatrix} \mathbf{R}_n \\ \mathbf{r}_n \end{bmatrix}$$

where $\mathbf{r}_i$, $i = 1, \ldots, n$, equals the i^{th} row of the matrix $\mathbf{R}$, and the $n-1 \times n$ matrix $\mathbf{R}_n$ is made up by $\{\mathbf{r}_i\}_{1 \leq i \leq n-1}$.

The rank of the matrix $\mathbf{R}_n$ is $n-1$ since the rank of $\mathbf{R}$ equals n (the vectors $\{\mathbf{r}_i\}_{1 \leq i \leq n-1}$ are linearly independent). Let H_n be the hyperplane generated by the vectors $\{\mathbf{r}_i\}_{1 \leq i \leq n-1}$ and $(\mathbf{e}_i)_{1 \leq i \leq n}$ be the canonical basis of $\mathbb{R}^n$. Therefore, it is easy to note that $\mathbf{e}_n$ is orthogonal to H_n (as $\mathbf{R}$ is lower triangular).
Then, the vector $\mathbf{r}_n$ could be written as

$$\mathbf{r}_n = \underbrace{\langle \mathbf{r}_n, \mathbf{e}_n \rangle . \mathbf{e}_n}_{\mathbf{r}_{n_\perp}} + \underbrace{(\mathbf{r}_n - \langle \mathbf{r}_n, \mathbf{e}_n \rangle . \mathbf{e}_n)}_{\mathbf{r}_{n_\parallel}}$$

where the vector $\mathbf{r}_{n_\perp}$ is orthogonal to H_n and the vector $\mathbf{r}_{n_\parallel}$ is in H_n.
Let $\mathbf{v}$ be a vector in $\mathbb{R}^n$. Then,

$$\begin{aligned} \mathbf{v} \in \Lambda_{\mathbf{R}} \Leftrightarrow \exists\, \mathbf{z} = (z_1, \ldots, z_n) \in \mathbb{Z}^n \\ \text{such that} \\ \mathbf{v} = \mathbf{z}\mathbf{R} &= \begin{bmatrix} [z_1 \ldots z_{n-1}] & z_n \end{bmatrix} \cdot \begin{bmatrix} \mathbf{R}_n \\ \mathbf{r}_n \end{bmatrix} \\ &= \underbrace{[z_1 \ldots z_{n-1}].\mathbf{R}_n}_{\mathbf{w}} + z_n.\mathbf{r}_n \end{aligned}$$

where $\mathbf{w}$ belongs to the lattice $\Lambda_{\mathbf{R_n}}$. Consequently, a lattice point $\mathbf{v}$ in $\Lambda_{\mathbf{R}}$ can be decomposed in

$$\mathbf{v} = \mathbf{w} + z_n \cdot \mathbf{r}_{n_\perp} + z_n \cdot \mathbf{r}_{n_\parallel},\ z_n \in \mathbb{Z} \text{ and } \mathbf{w} \in \Lambda_{\mathbf{R_n}}$$

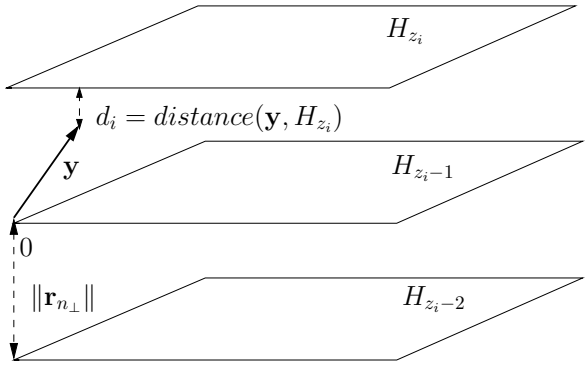

Figure 2.7: Projection of the received vector $\mathbf{y}$ on the different layers carrying the lattice.

Therefore, the lattice $\Lambda_\mathbf{R}$ can be viewed as

$$\Lambda_\mathbf{R} = \bigcup_{z_n \in \mathbb{Z}} \{\mathbf{w} + z_n \cdot \mathbf{r}_{n_\perp} + z_n \cdot \mathbf{r}_{n_\parallel}, \mathbf{w} \in \Lambda_{\mathbf{R_n}}\}$$

With this representation, the n-dimensional lattice $\Lambda_\mathbf{R}$ can be seen as the superposition of $(n-1)$-dimensional translated sublattices associated to $\Lambda_{\mathbf{R_n}}$.

Let $\mathbf{v} \in \Lambda_\mathbf{R}$, $\mathbf{v}$ could be written also as

$$\mathbf{v} = \tilde{\mathbf{w}} + z_n \cdot \mathbf{r}_{n_\perp}$$

where $\tilde{\mathbf{w}} = \mathbf{w} + z_n \cdot \mathbf{r}_{n_\parallel}$ belongs to the hyperplane H_n. Therefore

$$\Lambda_\mathbf{R} \subset \bigcup_{z_n \in \mathbb{Z}} \{\tilde{\mathbf{w}} + z_n \cdot \mathbf{r}_{n_\perp}, \tilde{\mathbf{w}} \in H_n\}$$

As a consequence, the lattice $\Lambda_\mathbf{R}$ is included in a stack of hyperplanes or layers L_{z_n} indexed by $z_n \in \mathbb{Z}$ and separated by at least $\|\mathbf{r}_{n_\perp}\|$ (Fig. 2.7). The search of the closest point will be based on this observation.

Let denote $\hat{\mathbf{y}}$ the orthogonal projection of $\mathbf{y}$ onto the vector $\mathbf{r}_{n_\perp}$. Thus,

$$\hat{\mathbf{y}} = \underbrace{\frac{\langle \mathbf{y}, \mathbf{r}_{n_\perp} \rangle}{\|\mathbf{r}_{n_\perp}\|^2}}_{\tilde{z}_n} \cdot \mathbf{r}_{n_\perp}$$

The distance between the vector $\mathbf{y}$ and the layer L_{z_n} is given by

$$d_n = \|\hat{\mathbf{y}} - z_n \cdot \mathbf{r}_{n_\perp}\| = |\tilde{z}_n - z_n| \cdot \|\mathbf{r}_{n_\perp}\|$$

The nearest layer to $\mathbf{y}$ is $L_{\hat{z}_n}$, where $\hat{z}_n = [\tilde{z}_n]$ and $[x]$ denotes the closest integer to x.

Let us consider the real vector $\boldsymbol{\rho} = (\rho_1, \ldots, \rho_n)$ such that $\boldsymbol{\rho} = \mathbf{y}\mathbf{R}^{-1}$: $\boldsymbol{\rho}$ is the ZF vector. Therefore,

$$\begin{cases} \mathbf{y} & = \boldsymbol{\rho}\, \mathbf{R} \\ y_n & = \rho_n \cdot \langle \mathbf{e}_n, \mathbf{r}_n \rangle = \quad \rho_n \cdot \langle \mathbf{e}_n, \mathbf{r}_{n_\perp} \rangle \end{cases}$$

Since

$$\langle \mathbf{y}, \mathbf{r}_{n_\perp} \rangle = \sum_{i=1}^{n} y_i \cdot \langle \mathbf{e}_i, \mathbf{r}_{n_\perp} \rangle = y_n \cdot \langle \mathbf{e}_n, \mathbf{r}_{n_\perp} \rangle,$$

we have

$$\begin{cases} \tilde{z}_n & = \frac{\langle \mathbf{y}, \mathbf{r}_{n_\perp} \rangle}{\|\mathbf{r}_{n_\perp}\|^2} = \rho_n \\ d_n & = |\rho_n - [\rho_n]| \cdot \|\mathbf{r}_{n_\perp}\|, \quad (\hat{z}_n = [\rho_n]) \end{cases}$$

Knowing that $\mathbf{y} = \boldsymbol{\rho}\, \mathbf{R}$,

$$y_{n-1} = \rho_{n-1} \cdot r_{n-1,n-1} + \rho_n \cdot r_{n-1,n}.$$

Using the decision on ρ_n ($\rho_n = \hat{z}_n$),

$$\rho_{n-1} = \frac{1}{r_{n-1,n-1}}(y_{n-1} - \hat{z}_n r_{n-1,n}) \text{ and } \hat{z}_{n-1} = [\rho_{n-1}]$$

More generally, for $i = n-1, \ldots, 1$, ρ_i could be written as

$$\rho_i = \frac{1}{r_{ii}} \cdot (y_i - \sum_{j=i+1}^{n} \hat{z}_j r_{ij})$$

and the distance d_i is

$$d_i = |\rho_i - [\rho_i]| \cdot \|\mathbf{r}_{i_\perp}\|$$

The evaluation of the integer vector $\hat{z} = (\hat{z}, \ldots, \hat{z}_n)$, $\hat{z}_i = [\rho_i]$ recursively, as described in the previous, yields to the Babai point [1]. The squared distance between the Babai point and the vector $\mathbf{y}$ equals

$$d^2 = \sum_{i=1}^{n} d_i^2$$

The described strategy to find the Babai point represents the first step of this algorithm. The Babai point is a first estimation of the closest point, but is not necessarily the closest point. Nevertheless, finding the Babai point gives us a bound on the search region.

Once the Babai point is found, the second step of this decoding algorithm consists in going through the lattice points whose components are obtained by oscillating around the Babai point components. Thus, the i^{th} integer component z_i of the tested point belongs to the (ordered) sequence of values:

$$z_i \in \{\hat{z}_i, \hat{z}_i - 1, \hat{z}_i + 1, \hat{z}_i - 2, \hat{z}_i + 2, \ldots\}$$

As for the Babai point computation, the component z_i at the i^{th} level is computed using the values of the components $z_n, \ldots, z_{i+1}$.

A lattice point $\hat{\mathbf{x}}$ is considered as a candidate to be the closest point if $\|\hat{\mathbf{x}} - \mathbf{y}\|^2 \leq \hat{d}^2$ where $\hat{d}^2$ is initialized at d^2. The distance $\hat{d}^2$ is then updated to $\|\hat{\mathbf{x}} - \mathbf{y}\|^2$ and the search will continue until all points within $S(\mathbf{y}, \hat{d}^2)$ are checked.

When a finite set of the lattice is considered, we should take into account the borders of the constellation [8], [49]. At first, we choose the components of the Babai point $(\tilde{z}_i)_{1\leq i\leq n}$ such that:

$$\begin{cases} \tilde{z}_i = [\rho_i] \\ \tilde{z}_i = z_{\min}, \text{ if } \tilde{z}_i < z_{\min} \\ \tilde{z}_i = z_{\max}, \text{ if } \tilde{z}_i > z_{\max} \end{cases}$$

where $z_{\max}$ and $z_{\min}$ are the higher and the lower value respectively, of the constellation point coordinates.
Then, at each level i $1 \leq i \leq n$, we compare the component z_i to the constellation borders. If the condition $z_{\min} \leq z_i \leq z_{\max}$ is not respected, we restart the search from the level $i+1$.

Conclusions

In this chapter, we introduced some lattice parameters that will be used in the sequel to study the MIMO system performance. Moreover, quadratic forms associated to lattices are pointed out. Indeed, this mathematical tool will be used to classify MIMO channels in the last chapter. Finally, we described two lattice decoder algorithms, namely sphere decoder based on Pohst strategy and sphere decoder based on Schnorr-Euchner strategy. It was shown that sphere decoder with both strategies has a reduced complexity, since it is able to find the ML point in polynomial time. In the next chapters, the ML detector used in conjunction with MIMO channel will be based on Schnorr-Euchner strategy as it is not affected from complexity point of view by the choice of the initial search radius.

Chapter 3

Accurate approximation of the MIMO error probability

Introduction

In this chapter, we propose an accurate approximation of the conditional error probability in a MIMO system. This approximation will be used in the next chapter for adaptive systems (e.g. adaptive modulation, antenna selection).
In the literature, Taricco and Biglieri gave the exact pairwise error probability in [55][56] for frequency non-selective multiple antenna systems. The pairwise error probability considered in their paper is defined as the mathematical expectation over all channel realizations. Thus, their closed form expression cannot be used for adaptive techniques. Besides, Tarokh et al proposed in [58] a lower bound of the error probability for a Gaussian channel. This bound is a valid approximation for high rate lattice codes. Since it is a lower bound, the approximation given in [58] cannot provide good performance for adaptive techniques.
The tight error probability approximation described in this chapter is conditioned on a fixed channel realization. The proposed method does not require an intractable evaluation of all pairwise error probabilities. This is achieved thanks to a judicious choice via Pohst/Schnorr-Euchner enumeration of dominant neighbors inside a sphere centered around a constellation point.

This chapter is organized as follows. Section 3.1 shows how a MIMO channel, described by its channel matrix, can be represented by a finite set of a lattice. Based on the lattice theory, section 3.2 presents first an accurate approximation of the conditional error probability for MIMO channels with more receive than transmit antennas. Next, the validation of this approximation is made by comparing the proposed analytical expression to Monte-Carlo simulation results for different antenna and modulation configurations. The last section 3.3 provides a generalization of the approximation to any number of receive and transmit antennas. We present in this section the generalized sphere decoder algorithm given in [17] for any MIMO channel configuration. This decoder is used to compare the error probability approximation and the Monte-Carlo simulation results.

3.1 Lattice representation of MIMO channel

We consider a digital transmission system with n_t transmit antennas and n_r receive antennas. The notations and the assumptions made in section 1.3 are valid through this chapter. For one channel use, the input-output model is

$$\mathbf{r} = \mathbf{sH} + \boldsymbol{\nu}, \tag{3.1}$$

where $\mathbf{r}$ is the length n_r receive complex vector, $\mathbf{s}$ is the length n_t transmit vector and $\boldsymbol{\nu}$ is an n_r length additive white Gaussian noise vector. The transmitted symbol s_k, for the k^{th} antenna, belongs to a M_k-QAM modulation [48], $k = 1 \dots n_t$, where M_k is the size of the QAM modulation applied on antenna k. The n_t QAM constellations are not necessary identical, their Cartesian product is denoted $\mathcal{C}_{\text{QAM}}$.
At the receiver side, it is assumed that perfect Channel State Information (perfect CSI) is available. CSI is not required at the transmitter side.
Finally, a maximum-likelihood detector based on a sphere decoder is applied [63][1][8] to accomplish a low complexity detection (as described in section 2.2).

For the sake of simplicity, we assume at first that $n_t = n_r$. The study is similar in the asymmetric channel case when $n_r \geq n_t$. The generalization of the proposed bound to the case when $n_r < n_t$ will be provided in the last section of this chapter.

The performance study of the quasi-static multiple antenna model in (3.1) is carried out in this chapter thanks to lattices and sphere packings theory [15]. The reader who is not familiar with group/lattice representation can find in chapter 2 a summary of the main lattice parameters that are used in this chapter.

In equation (3.1), the product $\mathbf{x} = \mathbf{sH}$ is interpreted as a point in the Euclidean space $\mathbb{R}^n$, $n = 2n_t = 2n_r$. The point $\mathbf{x}$ belongs to a real lattice Λ of rank n, whose $n \times n$ generator matrix $\mathbf{M} = [m_{ij}]$ is the real version of $\mathbf{H}$ defined by

$$\begin{cases} m_{2i,2j} & = \Re(h_{i,j}) \\ m_{2i+1,2j} & = -\Im(h_{i,j}) \\ m_{2i,2j+1} & = \Im(h_{i,j}) \\ m_{2i+1,2j+1} & = \Re(h_{i,j}) \end{cases} \tag{3.2}$$

where $\Re(x)$ and $\Im(x)$ denote the real and imaginary parts of the complex x respectively.

Since the transmit vector $\mathbf{s}$ is limited to the Cartesian product $\mathcal{C}_{\text{QAM}} \subset \mathbb{Z}^n$, then $\mathbf{x}$ belongs to a finite set $C^{\mathbf{H}}$ of Λ, $C^{\mathbf{H}}$ is called a lattice constellation or lattice code. When $\mathcal{C}_{\text{QAM}}$ is square, the shape of $C^{\mathbf{H}}$ is given by the parallelotope $\mathcal{P}$, i.e. $C^{\mathbf{H}}$ and $\mathcal{P}$ are homothetic. The reader should notice that a M_k-QAM modulation is defined as a rectangular subset of $\mathbb{Z}^2$ and that any scaling factor or any translation generates an equivalent set.
The cardinal of the lattice constellation $C^{\mathbf{H}}$ is equal to $\prod_{k=1}^{n_t} M_k$. The spectral efficiency of the uncoded QAM system is $\sum_{k=1}^{n_t} \log_2(M_k)$ bits per channel use.

3.2 Accurate Approximation of a MIMO channel error probability

The lattice representation of a multiple antenna channel converts the MIMO model given in equation (3.1) into a simple additive white Gaussian noise (AWGN) channel model

$$\mathbf{r} = \mathbf{x} + \boldsymbol{\nu}$$

For a given random lattice Λ generated by a fixed channel matrix $\mathbf{H}$, let $Pe(\Lambda)$ denote the point error probability associated to the infinite set Λ and let $Pe(C^{\mathbf{H}})$ denote the average point error probability associated to the finite constellation $C^{\mathbf{H}}$. Trivial geometrical properties leads to the inequality

$$Pe(C^{\mathbf{H}}) \leq Pe(\Lambda).$$

As indicated in section 2.1.5, due to the geometrical uniformity of Λ, the error probability $Pe(\Lambda)$ does not depend on the transmitted point, e.g. $Pe(\Lambda) = Pe_{|\mathbf{0}} \leq \sum_{\mathbf{x}\neq\mathbf{0}} P(\mathbf{0} \to \mathbf{x})$, where $P(\mathbf{x} \to \mathbf{y})$ is the classical notation for the pairwise error probability and $Pe_{|\mathbf{x}}$ is the error probability conditioned on the transmission of $\mathbf{x}$.
On the contrary, $C^{\mathbf{H}}$ is not geometrically uniform. To find its exact error probability, the conditional error probability $Pe_{|\mathbf{x}}$ can be evaluated for all $\mathbf{x} \in C^{\mathbf{H}}$, and then averaged:

$$Pe(C^{\mathbf{H}}) = \frac{1}{card(C^{\mathbf{H}})} \sum_{\mathbf{x}\in C^{\mathbf{H}}} Pe_{|\mathbf{x}}.$$

For example, when $n_t = 4$ and $M_k = 16$ for all k, a classical Union bound would cost $2^{\sum_{k=1}^{n_t} \log_2(M_k)} \times (2^{\sum_{k=1}^{n_t} \log_2(M_k)} - 1)$, i.e. 65536×65535, Euclidean distance evaluations. To reduce the complexity, we propose in the following a method which yields to an accurate approximation of the $C^{\mathbf{H}}$ error rate at a low complexity cost.

As shown in section 2.1.5, under the assumption that all facets of the Voronoi region are created by the first lattice shell, we have

$$Pe(C^{\mathbf{H}}) \leq Pe(\Lambda) \leq \tau(\Lambda) \times \mathrm{Q}\left(\frac{d_{Emin}(\Lambda)}{2\sigma}\right). \tag{3.3}$$

where $\tau(\Lambda)$ is the kissing number, $d_{Emin}(\Lambda)$ is the minimum Euclidean distance, and σ^2 is the one-dimensional real noise variance.
The situation in which the right inequality of (3.3) is valid corresponds to dense lattice packings, i.e. the fundamental gain $\gamma(\Lambda)$ given in (2.3) is greater than 1 [15], [20].

When square QAM modulations are applied on the transmit antennas, the noise variance σ^2 is equal to

$$\sigma^2 = \frac{E_s}{2\sum_{i=1}^{n_t} \log_2 M_i} \frac{1}{E_b/N_0}$$

where E_b/N_0 denotes the average received SNR per bit, and E_s is the received signal energy equal to

$$E_s = \frac{n_r}{4} \sum_{i=1}^{n_t} \frac{2(M_i - 1)}{3}$$

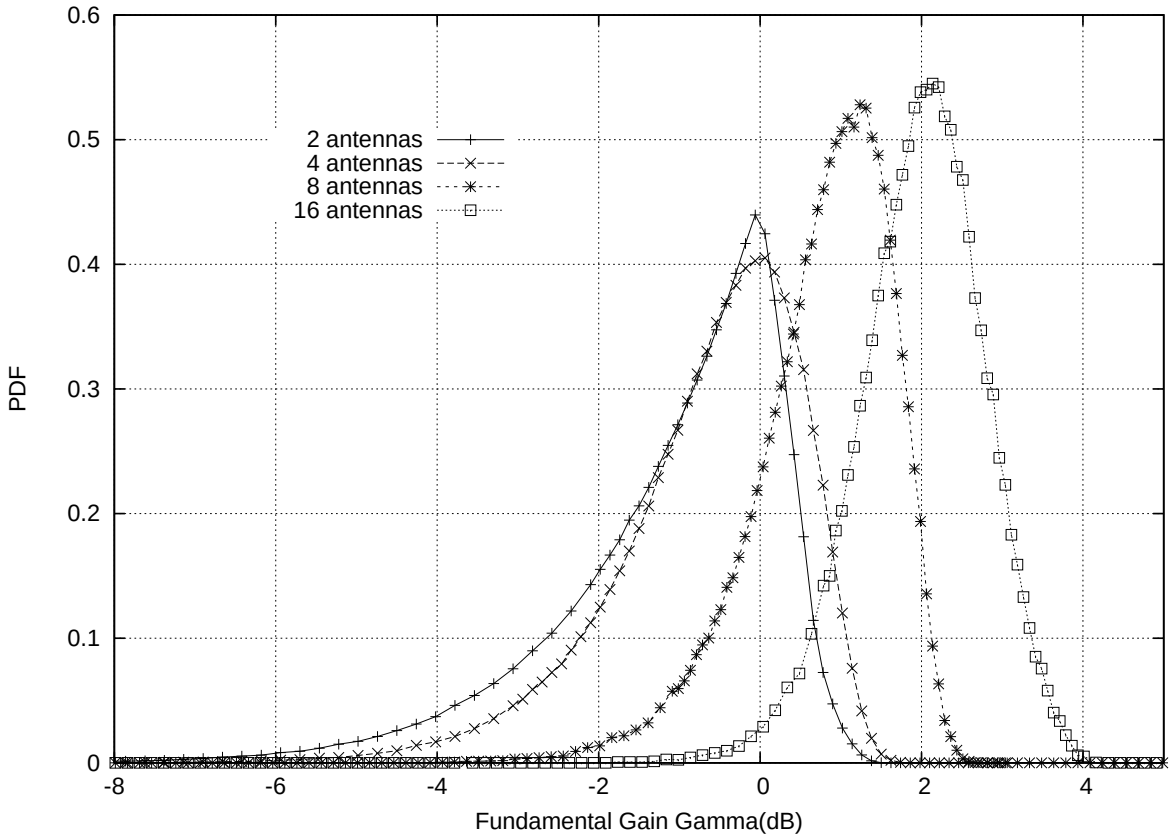

Figure 3.1: Distribution of the lattice fundamental gain $\gamma(dB)$ (Hermite constant) in a symmetric MIMO channel $n_t = n_r$.

Substituting the noise variance and the signal energy expressions in (3.3) leads to the following [9]

$$Pe(\Lambda) \leq \tau(\Lambda) \times \mathrm{Q}\left(\sqrt{\frac{3 \times \sum_{i=1}^{n_t} \log_2 M_i}{n_r \times \sum_{i=1}^{n_t} (M_i - 1)} \times \frac{E_b}{N_0} \times d^2_{Emin}(\Lambda)} \right). \tag{3.4}$$

Unfortunately, random lattices generated by $\mathbf{H}$ are not necessarily dense, especially for $n_t \leq 4$ as illustrated in Fig. 3.1. Thus, in the general case, the theta series of Λ is needed to derive an upper bound for $Pe(\Lambda)$. In practice, the theta series defined in (2.4) will be truncated to a limited number of shells around the transmitted point. This truncation yields to precise numerical results because the lattice is transmitted on a Gaussian channel where pairwise error probability decreases exponentially with respect to Euclidean distance.

Let us now describe how the non geometrically uniform set $C^{\mathbf{H}}$ is handled in order to reduce the computational complexity with respect to the Union bound. With this method, we aim at finding a precise approximation for the point error rate (point refers to a lattice point that corresponds to the transmitted vector $\mathbf{s}$), not an exact evaluation, neither a closed-form expression. Before illustrating the proposed method, we introduce a simple example that highlights our idea for error probability computation.

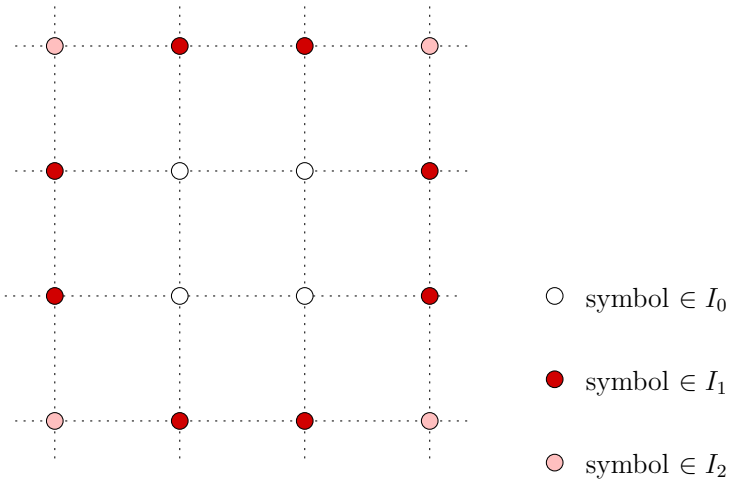

Figure 3.2: An example of a 16-QAM constellation in $\mathbb{R}^2$. Points are distinguished according to the number of crossing facets.

3.2.1 Example of error probability computation strategy

Consider a 16-QAM constellation transmitted on a Gaussian channel (Fig. 3.2). It can be partitioned into 3 subsets: 4 points in the middle (I_0), 8 non-corner points on the facets (I_1), and 4 points on the corners (I_2). There are 3 different error rates, one for each subset. The total point error rate is obtained by

$$Pe = \frac{4}{16}Pe(I_0) + \frac{8}{16}Pe(I_1) + \frac{4}{16}Pe(I_2)$$

Therefore, there is no need to compute 16 error rates corresponding to 16×15 distance evaluations.

3.2.2 Error probability computation for $n \geq 2$

Now, generalize the previous idea to a dimension $n \geq 2$, where the constellation $C^{\mathbf{H}}$ is not cubic shaped since $\mathbf{H}$ is random.

For a given constellation point $\mathbf{x} = \mathbf{sH} = \mathbf{zM}$ ($\mathbf{z} = (z_1, \ldots, z_n) \in \mathbb{Z}^n$ such that $z_{2i-1} = \Re(s_i)$ and $z_{2i} = \Im(s_i)$ for $1 \leq i \leq n$), the local theta series, i.e. the distance distribution of points surrounding $\mathbf{x}$ and belonging to $C^{\mathbf{H}}$, depends on $\mathbf{x}$.
This observation can be noticed in Fig. 3.3 that represents points of a lattice constellation carved from a lattice $\Lambda \subset \mathbb{R}^2$. Consider the points $\mathbf{x}_0$, $\mathbf{x}_1$, $\mathbf{x}_2$. The local theta series of these points, e.g. up to a square radius R, are not identical. Indeed, six neighbors surround the point $\mathbf{x}_0$ inside the constellation, whereas four points surround the point $\mathbf{x}_1$ belonging to one facet, and only two points surround the point $\mathbf{x}_2$ belonging to two facets.

More precisely, the distribution of the Euclidean distances around $\mathbf{x}$ depends on the position of $\mathbf{x}$ in $C^{\mathbf{H}}$. If $\mathbf{x}$ does not belong to the boundary of $C^{\mathbf{H}}$ (the point belongs to the interior of the constellation) then boundary effects can be neglected and the local theta series is well approximated by the theta series of Λ. Otherwise, if the point $\mathbf{x}$ is located on the boundary of $C^{\mathbf{H}}$, then the local theta series is derived by translating the original one (given for the lattice Λ)

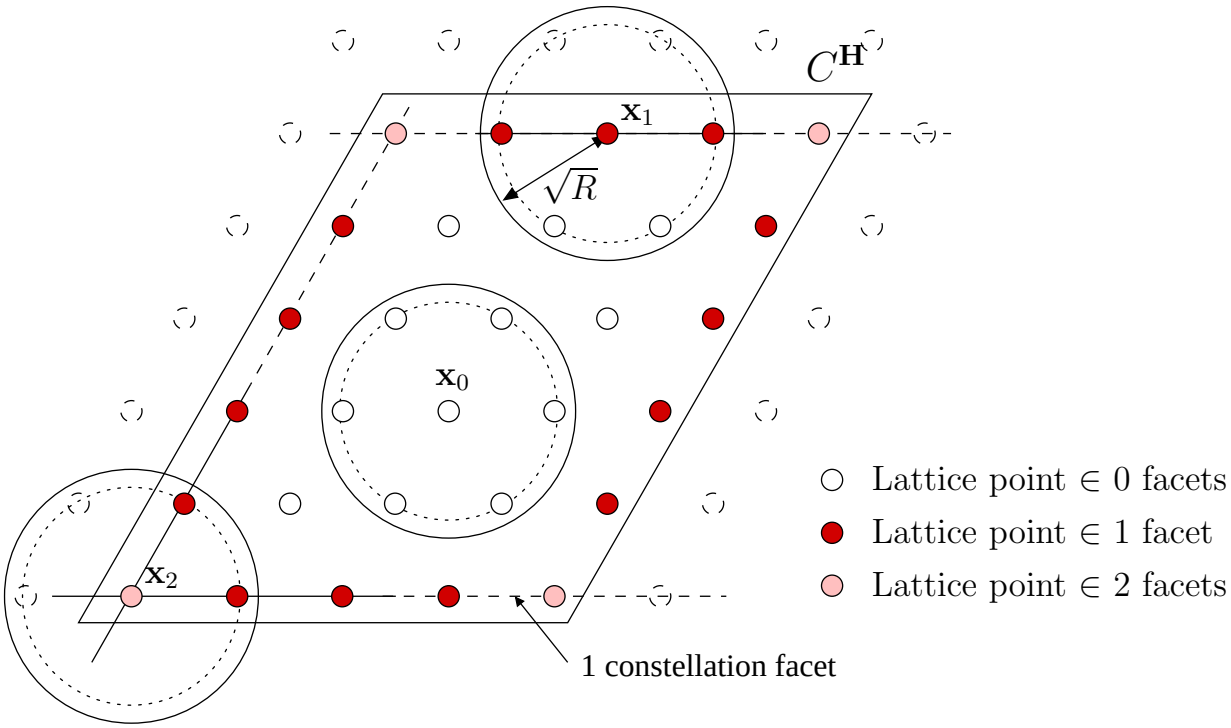

Figure 3.3: An example of lattice constellation in $\mathbb{R}^2$. Points are distinguished according to the number of crossing facets.

around $\mathbf{x}$ and subtracting all lattice points that do not belong to $C^{\mathbf{H}}$.
Consequently, we partition the constellation into $n+1$ subsets

$$C^{\mathbf{H}} = \bigcup_{\ell=0}^{n} I_\ell, \tag{3.5}$$

where I_ℓ contains lattice points located on the intersection of ℓ facets in $C^{\mathbf{H}}$. The subset I_0 is the interior of the constellation. Notice that $\mathbf{x} = \mathbf{zM} \in I_\ell$ is equivalent to $\mathbf{z}$ belonging to the intersection of ℓ facets in $C_{\text{QAM}} \subset \mathbb{Z}^n$.
Following (3.5), the error probability of the constellation becomes

$$Pe(C^{\mathbf{H}}) = \sum_{\ell=0}^{n} p_\ell Pe(I_\ell). \tag{3.6}$$

The weighting factor p_ℓ is the probability that a point of $C^{\mathbf{H}}$ belongs to the subset I_ℓ, and $Pe(I_\ell)$ is the error probability associated to I_ℓ. The probability $Pe(I_\ell)$ is obtained by averaging over all points $\mathbf{x} \in I_\ell$, since the conditional probability $Pe_{|\mathbf{x}}$ depends on the local position of $\mathbf{x}$. In the sequel, we describe how an accurate approximation of (3.6) can be obtained.

3.2.3 Evaluation of the probability p_ℓ

For simplicity reasons, only square QAM constellations are considered in this section. In this case, each M-QAM can be written as the Cartesian product of Pulse Amplitude Modulations : M-QAM = $\sqrt{M}$-PAM $\times$ $\sqrt{M}$-PAM. The generalization to rectangular and cross bi-dimensional

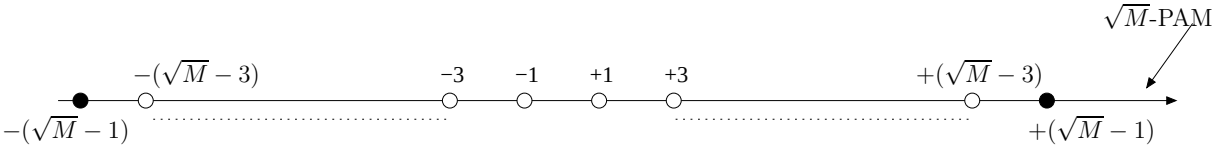

Figure 3.4: Pulse Amplitude Modulation constellation of cardinal M. Points black filled are on the edge of the PAM. Those that are in the interior of the PAM are white filled.

constellations is straightforward. It is also assumed that QAM symbols transmitted through the MIMO channel have the same a priori probability.

Two cases are distinguished:

- **1- All antennas transmit the same QAM set**

Let $\mathbf{x} = \mathbf{zM}$ be a point of the constellation $C^{\mathbf{H}}$ with $\mathbf{z} = (z_1,z_2,..,z_n) \in \mathbb{Z}^n$. The components z_i belong to the $\sqrt{M}$-PAM constellation that is composed of $\sqrt{M}$ symbols as depicted on Fig. 3.4. Only two among the symbols belonging to the PAM are on the edges of the constellation. The probability, p, that a symbol is on the edges of the PAM is equal to:

$$p = \frac{2}{\sqrt{M}} \tag{3.7}$$

Supposing that $\mathbf{x}$ belongs to I_ℓ means that ℓ components of $\mathbf{z}$ are on the edges of the PAM. Let E_i be a discrete random variable having two possible values:

$$\begin{aligned} E_i &= 1 \text{ if } z_i \text{ is on the edge with the probability } p \\ E_i &= 0 \text{ otherwise with the probability } 1-p \end{aligned}$$

Since the components z_i are independent, the variables $(E_i)_{i=1,..,n}$ are iid. Let $F = \sum_{i=1}^{n} E_i$ denote the number of components z_i of the vector $\mathbf{z}$ on the edge of the constellation. Therefore F defines a random binomial variable with parameter p, given by equation (3.7), and the probability p_ℓ is given by:

$$\begin{aligned} p_\ell = \text{Prob}(F=\ell) &= \binom{n}{\ell} p^\ell (1-p)^{n-\ell} \\ &= \binom{n}{\ell} \left(\frac{2}{\sqrt{M}}\right)^\ell \left(\frac{\sqrt{M}-2}{\sqrt{M}}\right)^{n-\ell} \end{aligned} \tag{3.8}$$

- **2- Antennas transmit general QAM sets (not necessarily identical)**

To derive the expression of the probability p_ℓ when distinct QAMs are applied on the transmit antennas, two methods are proposed in the following.

Method 1

Let $\{M_1,M_2,..,M_{N_q}\}$ be the set of available QAM modulation sizes at the transmitter. There are $(N_q)^{n_t}$ potential combinations of modulations that can be applied on the n_t transmit antennas.

Let $n_{t_i} \in \{0,..,n_t\}$ be the number of transmit antennas using the same M_i-QAM modulation and $0 \leq n_i = 2n_{t_i} \leq n$.
For a given value of ℓ, $0 \leq \ell \leq n$, let ℓ_i be the number of the components of the transmitted vector $\mathbf{s}$, that belong to the edges of the M_i-QAM constellation. The variables $\{\ell_i\}$ satisfy the following sum condition:

$$\sum_{i=1}^{N_q} \ell_i = \ell \ , \ 0 \leq \ell_i \leq \ell \tag{3.9}$$

Example :

Assume that four QAM modulations are available at the transmitter: QPSK, 16-QAM, 64-QAM and 256-QAM, i.e. $N_q = 4$. Let $n_t = 8$ and (QPSK, 64-QAM, 16-QAM, 16-QAM, 16-QAM, 64-QAM, 256-QAM, QPSK) be the combination applied on transmit antennas. Let $\mathbf{z} = (z_1,z_2 \dots z_{15},z_{16}) \in \mathbb{Z}^{16}$ be the transmitted vector. According to the chosen modulation, we have

$$\begin{cases} (z_1,z_2), (z_{15},z_{16}) \in \text{4-QAM} \\ (z_5,z_6), (z_7,z_8), (z_9,z_{10}) \in \text{16-QAM} \\ (z_3,z_4), (z_{11},z_{12}) \in \text{64-QAM} \\ (z_{13},z_{14}) \in \text{256-QAM} \end{cases}$$

As indicated before, the pairwise $(z_i,z_{i+1}) \in$ M-QAM belongs to at least one facet of the constellation if z_i or $z_{i+1} = \sqrt{M}-1$. Let $\ell_1, \ell_2, \ell_3, \ell_4$ denote the number of edge components corresponding to QPSK, 16-QAM, 64-QAM and 256-QAM respectively. For example, we give in the following the value of ℓ_i, $i = 1,\dots,4$, when $\mathbf{z} = (-1,1,-5,3,-1,3,-1,-3,1,-1,-7,-1,15,-5,1,1)$.

- $(z_1,z_2,z_{15},z_{16}) = (-1,1,1,1) \rightarrow \ell_1 = 4$
- $(z_5,z_6,z_7,z_8,z_9,z_{10}) = (-1,3,-1,-3,1,-1) \rightarrow \ell_2 = 2$
- $(z_3,z_4,z_{11},z_{12}) = (-5,3,-7,-1) \rightarrow \ell_3 = 1$
- $(z_{13},z_{14}) = (15,-5) \rightarrow \ell_4 = 1$

To find the number of facets ℓ that cross the lattice point $\mathbf{x} = \mathbf{zM}$, it is sufficient to compute the sum $\sum_{i=1}^{4} \ell_i = \ell = 8$. The lattice point $\mathbf{x}$ corresponding to the integer vector $\mathbf{z}$ belongs then to the subset I_8. The components belonging to the edge of the lattice constellation are illustrated in red in Fig. 3.5.

Note that for a given value of ℓ, we can find

$$J_{N_q,\ell} = \begin{pmatrix} \ell + N_q - 1 \\ \ell \end{pmatrix}$$

combinations of ℓ_i that satisfy the condition illustrated by equation (3.9). Let $L_{\ell,j} = (\ell_i^j)_{1 \leq i \leq N_q; 1 \leq j \leq J_{N_q,\ell}}$ be one of these combinations. The probability p_ℓ can be expressed as:

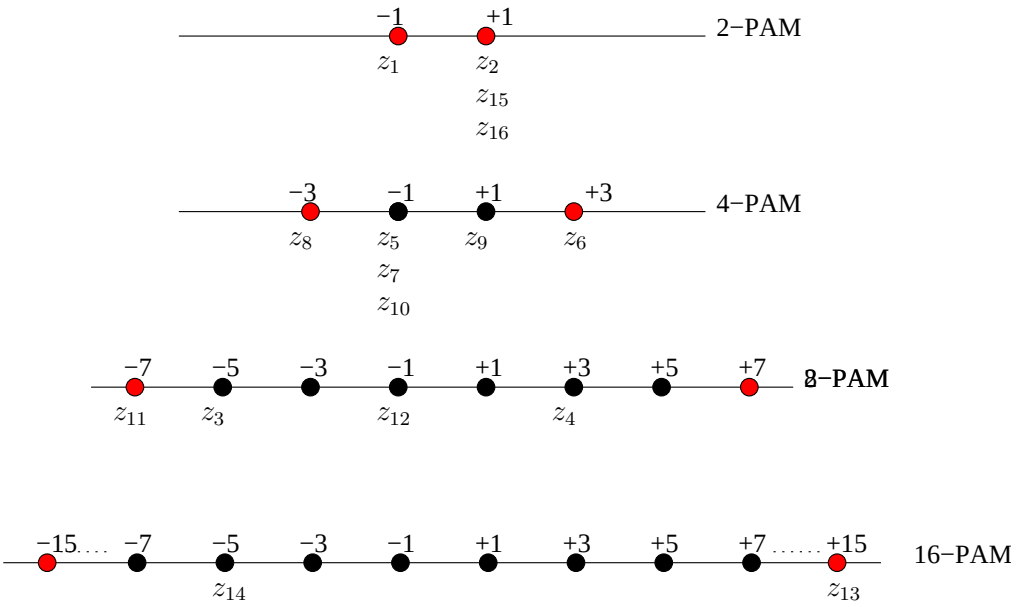

Figure 3.5: An example to compute the number of facets belonging a constellation point in $\mathbb{R}^8$.

$$\begin{aligned} p_\ell = P(\mathbf{x} \in I_\ell) &= P\left(\mathbf{x} \in \bigcup_{1 \le j \le J_{N_q,\ell}} I_\ell^j\right) \\ &= \sum_{j=1}^{J_{N_q,\ell}} P(\mathbf{x} \in I_\ell^j) \end{aligned} \tag{3.10}$$

where I_ℓ^j is a subset of I_ℓ corresponding to the combination $L_{\ell,j}$.

Since the components of the vector $\mathbf{x}$ are independent, the probability $P(\mathbf{x} \in I_\ell^j)$ can be written as:

$$P(\mathbf{x} \in I_\ell^j) = \prod_{i=1}^{N_q} P(\mathbf{x}_i \in I_{\ell,i}^j) \tag{3.11}$$

where $(\mathbf{x}_i)$ is the n_i-uplet that is composed of the components of $\mathbf{x}$ belonging to the $\sqrt{M_i}$-PAM, $1 \le i \le N_q$, and $I_{\ell,i}^j \subset \mathbb{Z}^{n_i}$ contains the vectors $\mathbf{x}_i$ having ℓ_i components on the edge of the $\sqrt{M_i}$-PAM constellation. Note that if $n_i = 0$, $I_{\ell,i}^j = \emptyset$ and the probability $P(\mathbf{x}_i \in I_{\ell,i}^j)$ is equal to 1 $\forall j$.
The probability $P(\mathbf{x}_i \in I_{\ell,i}^j)$ is obtained by substituting the variables ℓ_i^j, n_i and M_i in equation (3.8), that is:

$$P(\mathbf{x}_i \in I_{\ell,i}^j) = \binom{n_i}{\ell_i^j} \left(\frac{2}{\sqrt{M_i}}\right)^{\ell_i^j} \left(\frac{\sqrt{M_i}-2}{\sqrt{M_i}}\right)^{n_i-\ell_i^j} \tag{3.12}$$

Combining equations (3.10), (3.12) and (3.12) leads to

$$p_\ell = \sum_{j=1}^{J_{N_q,\ell}} \prod_{i=1}^{N_q} \binom{n_i}{\ell_i^j} \left(\frac{2}{\sqrt{M_i}}\right)^{\ell_i^j} \left(1 - \frac{2}{\sqrt{M_i}}\right)^{n_i - \ell_i^j} \tag{3.13}$$

When all Tx antennas transmit the same modulation so $N_q = 1$ and one combination $L_{\ell,j}$ is available. The variable n_i is equal to n and ℓ_i^j equals ℓ since one modulation is considered. Thus, the probability p_ℓ given by (3.13) is equivalent to that given by (3.8).

Method 2

The number ℓ of constellation facets to which a point $\mathbf{x} = \mathbf{zM}$ belongs in $\mathbb{R}^n$ is written as

$$\ell = \sum_{i=1}^{n} \ell_i, \tag{3.14}$$

$\ell \in [0...n]$ and $\ell_i \in \{0,1\}$. The integer ℓ_i is set to 1 if z_i is on the PAM boundary . Notice that z_i, $i = 1 \dots n$, belongs to a PAM real constellation of size $\sqrt{M_{[(i+1)/2]}}$, where M_k is the size of the k^{th} bi-dimensional QAM set, $1 \le k \le n_t = n/2$. For a given value of ℓ, let $L_{\ell,j} = (\ell_1^j \dots \ell_i^j \dots \ell_n^j)$ denote a length n binary vector whose components satisfy the sum condition (3.14), $1 \le j \le \binom{n}{\ell}$. It is easy to show that

$$p_\ell = \sum_{L_{\ell,j}} \prod_{i=1}^{n} \left(\frac{2}{\sqrt{M_{[(i+1)/2]}}}\right)^{\ell_i^j} \left(1 - \frac{2}{\sqrt{M_{[(i+1)/2]}}}\right)^{1-\ell_i^j}. \tag{3.15}$$

The above expression reduces to (3.8) when identical QAM sets are used on the MIMO channel.

3.2.4 A bound for the subset error probability $Pe(I_\ell)$

We establish an upper union bound for $Pe(I_\ell)$ using the local theta series. Computer simulations given below show the tightness of this bound based on the simple AWGN model defined by $\mathbf{r} = \mathbf{x} + \boldsymbol{\nu}$.

The error probability $Pe(I_\ell)$ considered in equation (3.6) can be written as:

$$\begin{aligned} Pe(I_\ell) &= \sum_{\mathbf{x} \in I_\ell} Pe(I_\ell, \mathbf{x}) \\ &= \sum_{\mathbf{x} \in I_\ell} Pe(I_\ell / \mathbf{x}) p(\mathbf{x}) \\ &= \frac{1}{card(I_\ell)} \sum_{\mathbf{x} \in I_\ell} Pe(I_\ell / \mathbf{x}) \end{aligned} \tag{3.16}$$

where $card(I_\ell)$ denotes the cardinal of I_ℓ and $Pe(I_\ell/\mathbf{x})$ is the error probability for I_ℓ conditioned on $\mathbf{x}$.

The union bound applied to $Pe(I_\ell/\mathbf{x})$ in equation (3.16) leads to the following inequality:

$$Pe(I_\ell / \mathbf{x}) \le \sum_{\mathbf{y} \in C^{(\mathbf{H})} - \{\mathbf{x}\}} P(\mathbf{x} \to \mathbf{y}) \tag{3.17}$$

Let $S_{\mathbf{x},i} = \{\mathbf{y} \in C^{\mathbf{H}} | d_E(\mathbf{x},\mathbf{y}) = d_i\}$ be the set of points belonging to $C^{\mathbf{H}}$ and surrounding $\mathbf{x}$ at a Euclidean distance d_i. The shape of $S_{\mathbf{x},i}$ is not necessarily spherical due to the cutting boundaries of the constellation. Equation (3.17) can be written as:

$$Pe(I_\ell/\mathbf{x}) \leq \sum_i \sum_{\mathbf{y} \in S_{\mathbf{x},i}} P_i(\mathbf{x} \to \mathbf{y}) \tag{3.18}$$

with

$$P_i(\mathbf{x} \to \mathbf{y}) = \mathrm{Q}\left(\frac{d_i}{2\sigma}\right)$$

Combining equation (3.16) and inequality (3.18), the upper bound for $Pe(I_\ell)$ becomes:

$$Pe(I_\ell) \leq \frac{1}{card(I_\ell)} \sum_{\mathbf{x} \in I_\ell} \sum_i \tau_{\mathbf{x},\ell,i} \times \mathrm{Q}\left(\frac{d_i}{2\sigma}\right) \tag{3.19}$$

with $\tau_{\mathbf{x},\ell,i} = card(S_{\mathbf{x},i})$ and $\mathbf{x} \in I_\ell$. The shells at distance d_i in the local theta series $S_{\mathbf{x},i}$ are indexed by i in the subscript of τ.

Finally, for a fixed channel matrix $\mathbf{H}$, an accurate approximation of the point error probability for a multi-dimensional QAM modulation transmitted on a MIMO channel is obtained by combining equations (3.19) and (3.6),

$$Pe(C^{\mathbf{H}}) \leq \sum_{\ell=0}^{n} \frac{p_\ell}{card(I_\ell)} \sum_{x \in I_\ell} \sum_i \tau_{\mathbf{x},\ell,i} \times \mathrm{Q}\left(\frac{d_i}{2\sigma}\right) \tag{3.20}$$

where p_ℓ is given by equation (3.8) or (3.15). In the following, the bound given in (3.20) is referred by *MEPA* (MIMO Error Probability Approximation).

The next subsection gives our proposed strategy to compute the coefficients $\tau_{\mathbf{x},\ell,i}$ in (3.20).

3.2.5 Numerical implementation of *MEPA*

In this section, the computation of the coefficient $\tau_{\mathbf{x},\ell,i}$ is detailed in the first subsection. Then, the *Short vectors* algorithm used for this computation is presented. The assumptions considered in the evaluation of the error probability $Pe(C^{\mathbf{H}})$ are given in the last subsection as well as the flowchart of the error probability computation. Finally, simulation results are illustrated to show the accuracy of our approximation.

3.2.5.1 Evaluation of $\tau_{\mathbf{x},\ell,i}$ strategy

The coefficients $\tau_{\mathbf{x},\ell,i}$ of the local theta series are easily determined from the original theta series of the random lattice Λ as follows:

- Step 1: Generate lattice points $\mathbf{y} \in \Lambda$ located at a distance d_i from the origin. These points are found using the *Short vectors* algorithm, which is detailed later, based on a Pohst enumeration inside a sphere [46][14].
- Step 2: For each $\mathbf{y}$ found in the previous step, check if the translate $\mathbf{y} + \mathbf{x}$ belongs to the constellation $C^{\mathbf{H}}$ and increment $\tau_{\mathbf{x},\ell,i}$ accordingly.

The *Short vectors* algorithm used in Step 1 to compute the coefficient $\tau_{\mathbf{x},\ell,i}$ is detailed in the following paragraph.

Short vectors algorithm

The *Short vectors* algorithm searches all the points $\mathbf{x} \in \Lambda$ subject to $\|\mathbf{x}\|^2 \leq C$ or equivalently if $\mathbf{x} = \mathbf{zM}$,

$$\|\mathbf{x}\|^2 = \mathbf{zGz}^T = Q(\mathbf{z}) \leq C, \tag{3.21}$$

where C is a positive constant value and $\mathbf{G} = \mathbf{MM}^T$ is the Gram matrix of the lattice Λ. It is noticed that the enumeration of the points $\mathbf{x}$ is equivalent to that illustrated in section 2.2 while assuming the sphere is centered at the lattice origin.
Thanks to Cholesky factorization, the Gram matrix $\mathbf{G}$ can be written as $\mathbf{G} = \mathbf{R}^T\mathbf{R}$, where $\mathbf{R} = [r_{ij}]$ is a real upper triangular matrix. Assuming $q_{ii} = r_{ii}^2$, $i = 1 \ldots n$ and $q_{ij} = \frac{r_{ij}}{r_{ii}}$, $i = 1 \ldots n$ and $j = i + 1 \ldots n$, we can write:

$$Q(\mathbf{z}) = \sum_{i=1}^{n} q_{ii} \left(z_i + \sum_{j=i+1}^{n} q_{ij} z_j \right)^2 \leq C \tag{3.22}$$

The *Short vectors* algorithm used to solve $Q(\mathbf{z}) \leq C$ is given by the following steps, extracted from [46]:

In Step 1 to Step 6, T_i, U_i and Z are operation variables.

Example of computing $\tau_{\mathbf{x},\ell,i}$

Figure 3.6 illustrates an example of lattice constellation in the 2-dimensional real space. This example shows how the parameter $\tau_{\mathbf{x},\ell,i}$ is computed for four different points of the constellation, namely 0, $\mathbf{x}_1$, $\mathbf{x}_2$, $\mathbf{x}_3$. The *Short vectors* algorithm is applied to obtain the neighbors of the origin in the lattice located on different shells. Then translations of the different neighbors around the points $\mathbf{x}_1$, $\mathbf{x}_2$, $\mathbf{x}_3$ are illustrated for cases (a), (b), and (c) respectively in Fig. 3.6. It is clear that the parameter $\tau_{\mathbf{x},\ell,i}$, given by the intersection of the constellation and the translated shells (Step 2), depends on the position of the point $\mathbf{x}$ in the constellation. Notice that the two points $\mathbf{0}$ and $\mathbf{x}_1$ that belong to the subset I_2 do not necessarily have the same parameter $\tau_{\mathbf{x},\ell,i}$.

3.2.5.2 Numerical implementation of *MEPA* assumptions

For the derivation of numerical results, we limited the total number of considered points $\mathbf{x}$ in (3.20) to $N_x = \min(1000, \prod_{k=1}^{n_t} M_k)$. The number of points selected from the subset I_ℓ (points lying on the intersection of ℓ facets) is weighted by p_ℓ, i.e. we consider $p_\ell N_x$ such points. This method accurately approximates the distribution of constellation points according to their position. The number of shells in the considered local theta series is limited to i_{max}, where the most distant shell is at $2d^2_{Emin}(\Lambda)$. The conventional factor 2 is fully justified by its corresponding 3dB signal-to-noise ratio margin on a Gaussian channel. If the local theta series (around $\mathbf{x}$) is empty, then the new search radius can be increased up to $4d^2_{Emin}(\Lambda)$ (6dB SNR margin).

Another heuristic for controlling i_{max} is to select the first squared radius greater than $\min_i g_{ii}$, where $[g_{ij}] = \mathbf{MM}^T$ is the Gram matrix for Λ. It can be shown that the minimum Euclidean distance in $C^{\mathbf{H}}$ satisfies

input : The matrix $[q_{ij}]$ used in (3.22) and $C > 0$
output: All $\mathbf{z} \in \mathbb{Z}^n$, $\mathbf{z} \neq \mathbf{0}$, satisfying (3.21) and additionally each corresponding value $Q(\mathbf{z})$

Step 1 : *(Initialization)*
Set $i \leftarrow n$, $T_i \leftarrow C$, $U_i \leftarrow 0$

Step 2 : *(Bounds for* z_i*)*
Set $Z \leftarrow \sqrt{T_i/q_{ii}}$, $UB(z_i) \leftarrow \lfloor Z - U_i \rfloor$, $z_i \leftarrow \lceil -Z - U_i \rceil$-1,
where $UB(z_i)$ *is an upper bound of* z_i

Step 3 : *(Increase* z_i*)*
if $z_i > UB(z_i)$ **then**
  set $z_i \leftarrow z_i + 1$
end
else
  go to Step 5
end

Step 4 : *(Increase i)*
Set $i \leftarrow i + 1$
Go to Step 3

Step 5 : *(Decrease i)*
if $i = 1$ **then**
  go to 6
end
else
  set $i \leftarrow i - 1$, $U_i \leftarrow \sum_{j=i+1}^{n} q_{ij} z_j$, $T_i \leftarrow T_{i+1} - q_{i+1i+1}(z_{i+1} + U_{i+1})^2$
  go to Step 2
end

Step 6 : *(Solution)*
if $\mathbf{z} = \mathbf{0}$ **then**
  terminate
end
else
  print $\mathbf{z}$, $-\mathbf{z}$ *and* $Q(\mathbf{z}) = C - T_1 + q_{11}(z_1 + U_1)^2$
  go back to Step 3
end

Algorithm 1: Short vectors algorithm.

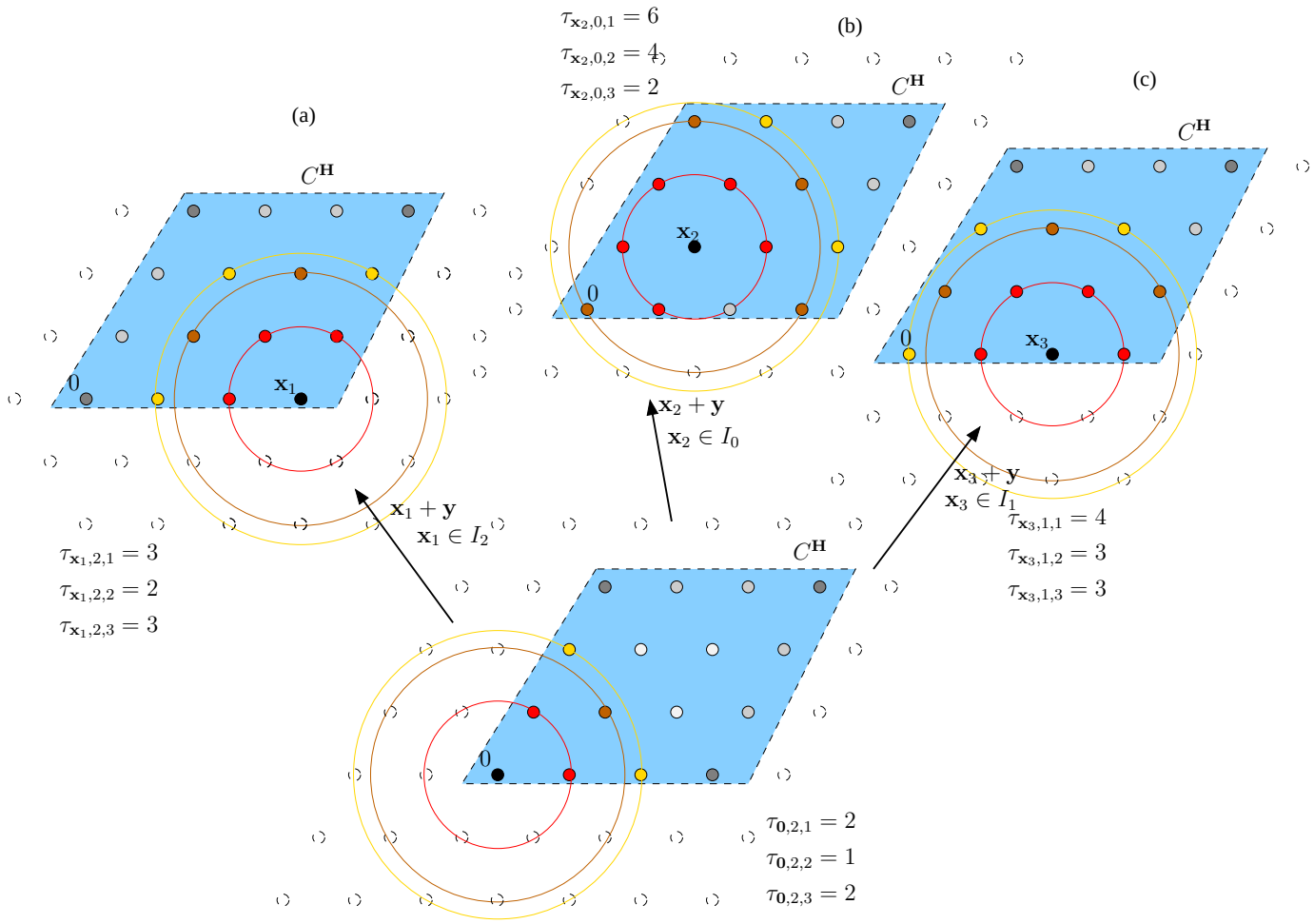

Figure 3.6: Example for computing the parameter $\tau_{\mathbf{x},\ell,i}$ for different points in the bidimensional constellation.

$$d_{Emin}(\Lambda) \leq d_{Emin}(C^{\mathbf{H}})$$
$$d_{Emin}(\Lambda) \leq \sqrt{\min_{i=1\ldots n} g_{ii}} \tag{3.23}$$

For $1 \leq \ell \leq n$, the algorithm proposed to compute Pe_{I_ℓ} is depicted on Fig. 3.7. The notations used in the flowchart are the following:

- K is the current number of points, belonging to ℓ hyperplane facets, actually tested;
- $K_{\mathbf{x}}^{d_i}$ is the number of points located at a distance d_i from the constellation point $\mathbf{x}$;
- $\tau_i(\Lambda)$ is the number of points located at a distance d_i from the constellation point $\mathbf{x}$ in the lattice Λ (results from the theta series of the lattice Λ);
- $S_{\mathbf{0},i}^{\Lambda} = \{\mathbf{y} \in \Lambda, d(\mathbf{0},\mathbf{y}) = d_i\}$ is the i^{th} shell around the lattice origin $\mathbf{0}$;
- z_{min_j} and z_{max_j} denotes respectively the minimum and maximum values of the j^{th} component in the constellation $C^{\mathbf{H}}$;
- $\mathbf{z_x}$ is a n-dimensional vector such as $\mathbf{x} = \mathbf{z_x}\mathbf{G}$ and $\mathbf{z_y}$ is a n-dimensional vector such as $\mathbf{y} = \mathbf{z_y}\mathbf{G}$;

- $(\mathbf{z_x} + \mathbf{z_y})_j$ denotes the j^{th} component of the vector $\mathbf{z_x} + \mathbf{z_y}$;

- The error probability Pe_i is equal to $Pe_i = \mathrm{Q}\left(\frac{d_i}{2\sigma}\right)$

Note that the error probability $Pe(I_\ell)$ computed by the algorithm described in Fig. 3.7 is proportional to the upper bound on the error probability given by the equation (3.19). This proportionality coefficient will be compensated in the evaluation of the overall error probability $Pe(C^{\mathbf{H}})$, presented in Fig. 3.7. Moreover in order to reduce the complexity of the algorithm, the vectors $\mathbf{x}$ belonging to I_ℓ can be stored in a table to avoid generating them for each $i = 1,...,i_{max}$. The same remark may be applied to the lattice points $\mathbf{y}$, which are generated around the constellation origin thanks to *Short vectors* algorithm, i.e. for a given shell i, the same vectors $\mathbf{y}$ can be used for different points $\mathbf{x}$ (only a translation is required). Furthermore, as the lattice is the same for all constellations considered in the set $\mathbb{R}$, the same vector $\mathbf{y}$ can be used for all the constellations to be tested.

3.2.6 Simulation results

Figure 3.8 illustrates the accuracy of the upper bound (3.20) in the case of a fixed 4×4 MIMO channel. The point error rate is plotted versus the average signal-to-noise ratio. The matrix $\mathbf{H}$ is selected at random and kept unchanged ($T_c = \infty$) for all results shown in Fig. 3.8. Four different QAM combinations are tested. The notation 4*M-QAM means that 4 transmit antennas are using the same M-QAM. When transmitted constellations are not identical, a notation as 16-16-64-64-QAM means that $M_1 = M_2 = 16$ and $M_3 = M_4 = 64$. In all cases, simulation results below 10^{-1} are very close to the proposed analytical approximation.

Figure 3.9 illustrates the average error probability of a quasi-static 4×4 MIMO channel with a finite coherence time ($T_c = 10$ instead of $+\infty$). Expectation is made over the distribution of $\mathbf{H}$ in Fig. 3.9. The proposed approximation maps almost exactly with simulation results below 10^{-1}.

The Fig. 3.10 compares the simple upper bound (3.4) to our bound (3.20) that is based on the local theta series. It is shown that the simple bound (3.4) is less accurate than (3.20). For low SNR, (3.4) is not necessarily an upper bound because some Voronoi facets are due to more distant points than those located on the first lattice shell (see the 4*16-QAM case). At high SNR, the influence of those facets is negligible. The gap between the simple bound and the exact error rate decreases with the constellation size at high SNR. For example, at $E_b/N_0 = 16$ dB, a factor of 8 is noticed between both bounds when 4-QAM is applied on transmit antennas, whereas this factor is equal to 3 when 16-QAM is used.

The previous study to evaluate the error probability for a quasi-static MIMO system is valid when $n_t \leq n_r$. Indeed, the upper triangular factorization (e.g. based on Cholesky factorization) of the Gram matrix $\mathbf{G} = \mathbf{M}\mathbf{M}^T$ that is considered in the *Short vectors* algorithm (see section 3.2.5), can be used only for definite positive Gram matrix, e.g. case $n_t \leq n_r$. The next section shows how to generalize this study for any (n_t,n_r).

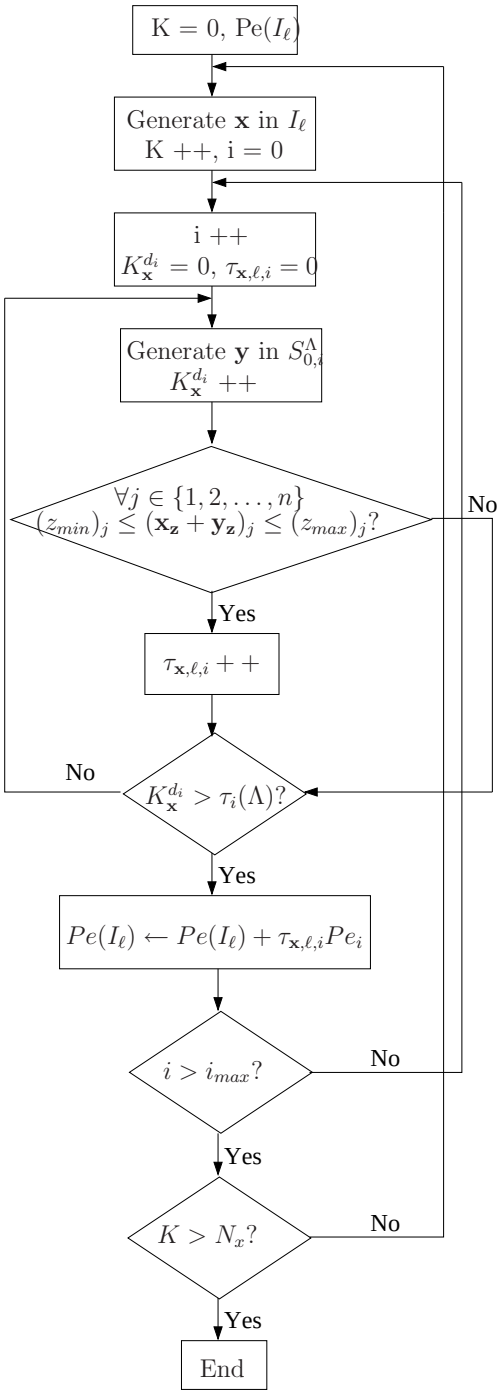

Figure 3.7: Flowchart of the algorithm used to compute the error probability $Pe(I_\ell)$.

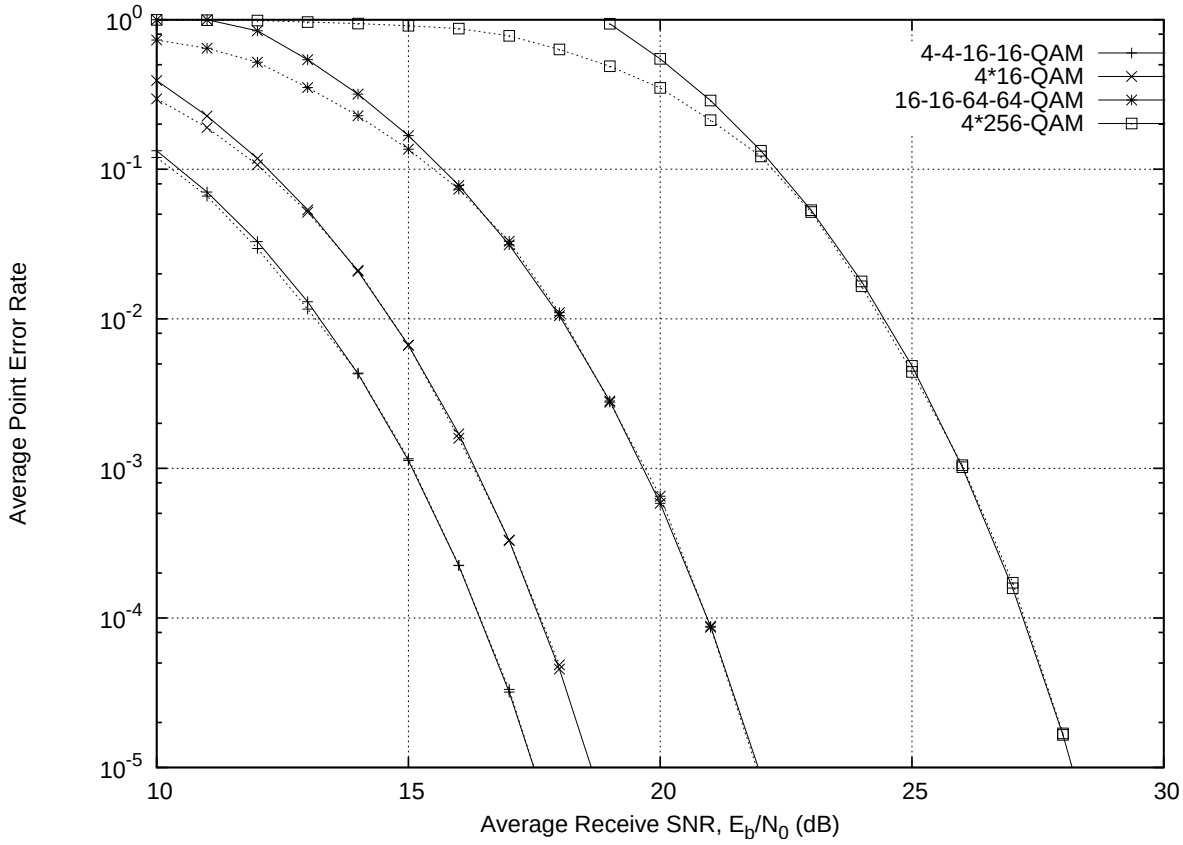

Figure 3.8: Error probability of a 4×4 static MIMO channel ($T_c = +\infty$). Analytic approximation (continuous lines) and Monte Carlo simulation (dotted lines).

3.3 Generalization of the error probability approximation for any MIMO channel

The generalization of the Cholesky factorization for a non definite Gram matrix $\mathbf{G} = \mathbf{R}\mathbf{R}^T$ (when the rank of $\mathbf{G}$ is equal to $2n_r < 2n_t$) yields to an upper triangular matrix $\mathbf{R}$ of rank equal to $2n_r$ with diagonal elements satisfying

$$r_{ii} = \begin{cases} 0 & \text{for } i > n_r \\ \neq 0 & \text{for } 1 \leq i \leq n_r \end{cases} \tag{3.24}$$

Recall that the *Short vectors* algorithm searches the lattice points $\mathbf{x} = \mathbf{z}\mathbf{M}$ located around the lattice origin. Let $\mathbf{z}^{Up}$ and $\mathbf{z}^{Dw}$ refer to the first m and the last $n-m$ elements of the integer vector $\mathbf{z}$, where $m = 2n_r$ and $n = 2n_t$. For a given value of $\mathbf{z}^{Up}$, the *Short vectors* algorithm is applied to search the elements of $\mathbf{z}^{Dw}$. This should be repeated for each possible value of $\mathbf{z}^{Up}$. Note that the components of $\mathbf{z}^{Up}$ are integers belonging to the interval $z_{\min_i} \leq \mathbf{z}_i^{Up} \leq z_{\max_i}$, where $z_{\min_i}$ and $z_{\max_i}$ denote the lower and the higher values of the components belonging to the QAM applied on the $\lceil i/2 \rceil^{th}$ antenna, $1 \leq i \leq n$. However, this approach to generalize the *Short vectors* algorithm has an exponential complexity in $(n - m)$, when the same M-QAM modulation is applied on all transmit antennas. Thus, the search complexity increases with the modulation

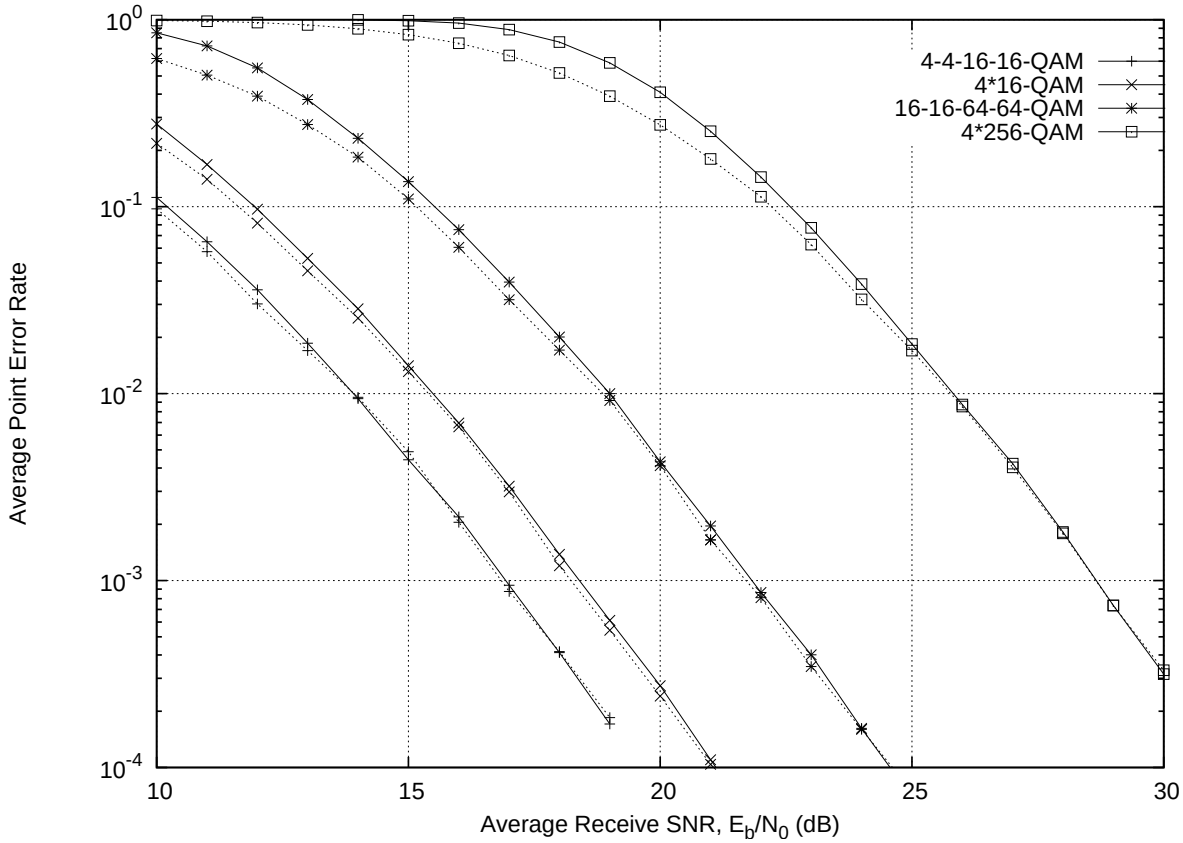

Figure 3.9: Average error probability of a 4×4 quasi-static MIMO channel ($T_c = 10$). Analytic approximation (continuous lines) and Monte Carlo simulation (dotted lines).

size and is higher for large constellations (e.g. 64-QAM, 256-QAM).

In [17], the authors proposed a method to generalize the sphere decoder algorithm with lower complexity than the previous approach. The proposed algorithm aims to find an upper bound for the minimum Euclidean lattice constellation and to search the neighbors surrounding a lattice constellation point at a distance d_i.

In this section, we present first the generalized sphere decoder algorithm proposed in [17] and considered in our simulations. Then, we describe the generalization of the error probability (3.20) for the case when $n_t > n_r$. Finally, we give some simulation results for this case.

3.3.1 Generalization of the sphere decoder algorithm for the case when $n_t > n_r$

Let us write the relationship between the transmit and the receive signal of a $n_t \times n_r$ MIMO system, as

$$\mathbf{r} = \mathbf{sH} + \boldsymbol{\nu} \tag{3.25}$$

Let $\mathbf{x} = \mathbf{zM}$ be equivalent to $\mathbf{sH}$ in the real space $\mathbb{R}^n$, where $\mathbf{M}$ is a $n \times m$ real matrix related to $\mathbf{H}$ as given in equation (3.2). The lattice constellation corresponding to the channel $\mathbf{H}$ is denoted

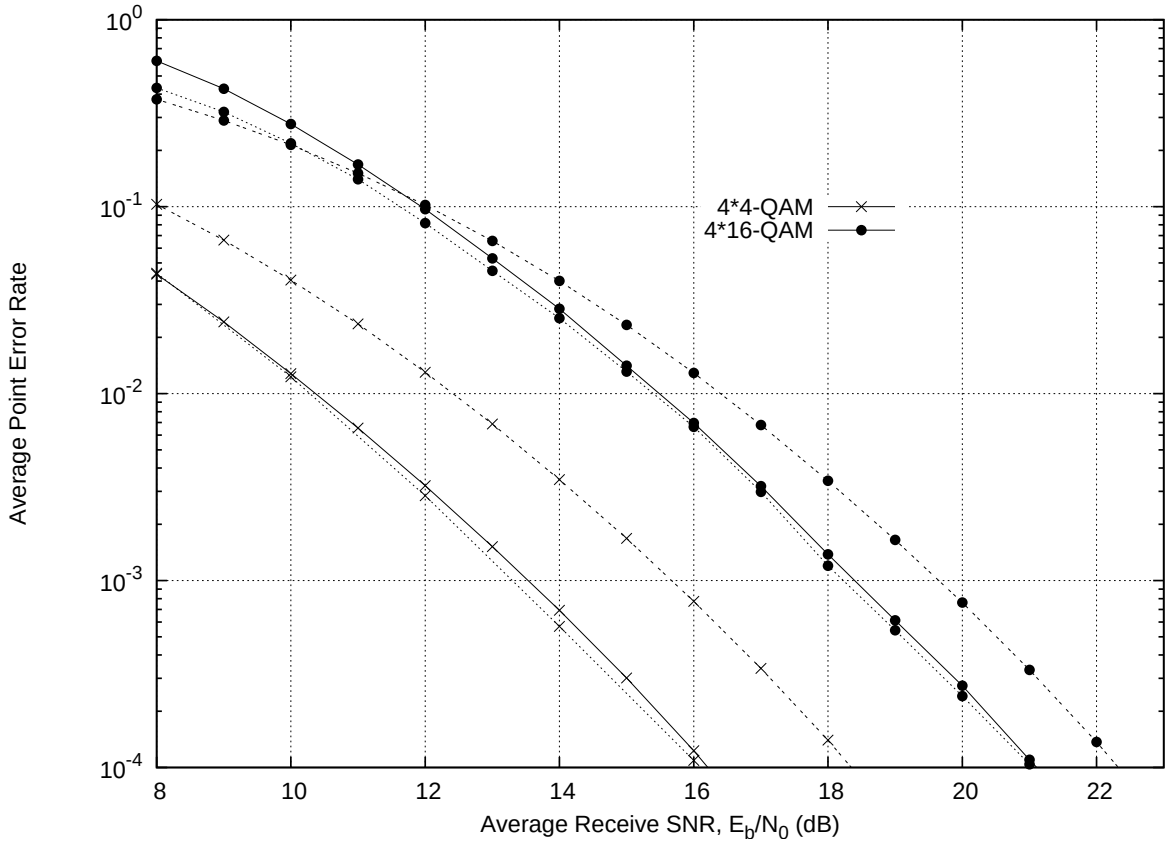

Figure 3.10: Average error probability of a 4×4 quasi-static MIMO channel ($T_c = 10$). Analytic approximation given in (3.20) based on local theta series (continuous lines), bound given in (3.4) based on minimum Euclidean distance (dashed lines), and Monte Carlo simulation (dotted lines).

$C^{\mathbf{H}}$.

As previously seen, the sphere decoder algorithm is based on the maximum-likelihood criterion (see section 2.2). It consists in enumerating all the lattice points $\mathbf{x} = \mathbf{zM} \in C^{\mathbf{H}}$ located within a certain region, denoted $S \subset \mathbb{R}^n$, around the received point $\mathbf{r}$ and selecting the closest point $\hat{\mathbf{x}}$, as follows:

$$\|\mathbf{r} - \hat{\mathbf{x}}\|^2 = \min_{\mathbf{x} \in C^{\mathbf{H}} \cap S} \|\mathbf{r} - \mathbf{x}\|^2 \tag{3.26}$$

The Euclidean distance $\|\mathbf{r} - \mathbf{x}\|^2$ can be expressed as

$$\begin{aligned} \|\mathbf{r} - \mathbf{x}\|^2 &= \|\mathbf{r} - \mathbf{zM}\|^2 + \alpha \mathbf{z}\mathbf{z}^T - \alpha \mathbf{z}\mathbf{z}^T \quad \alpha > 0 \\ &= \|\mathbf{r}\|^2 + \mathbf{z}(\mathbf{M}\mathbf{M}^T + \alpha \mathbf{I}_n)\mathbf{z}^T - \alpha \mathbf{z}\mathbf{z}^T - \mathbf{r}\mathbf{M}^T\mathbf{z}^T - \mathbf{z}\mathbf{M}\mathbf{r}^T, \end{aligned} \tag{3.27}$$

Let consider the positive definite matrix $\tilde{\mathbf{G}} = \mathbf{M}\mathbf{M}^T + \alpha \mathbf{I}_n$. This matrix can be Cholesky factorized as $\tilde{\mathbf{G}} = \tilde{\mathbf{R}}^T \tilde{\mathbf{R}}$, where $\tilde{\mathbf{R}}$ is an upper triangular matrix. Let us define $\boldsymbol{\rho}$ and $\tilde{\mathbf{M}}$ such as $\boldsymbol{\rho} = \mathbf{r}\mathbf{M}^T \tilde{\mathbf{G}}^{-1}$ and $\tilde{\mathbf{M}} = \tilde{\mathbf{R}}\tilde{\mathbf{R}}^T$. The equality (3.27) can be written as

$$\begin{aligned} \|\mathbf{r}-\mathbf{zM}\|^2 &= \|\mathbf{r}\|^2+\mathbf{z}\tilde{\mathbf{R}}\tilde{\mathbf{R}}^T\mathbf{z}^T+\boldsymbol{\rho}\,\tilde{\mathbf{R}}\tilde{\mathbf{R}}^T\boldsymbol{\rho}^{\,T}-\boldsymbol{\rho}\,\tilde{\mathbf{M}}\boldsymbol{\rho}^{\,T}-\alpha\mathbf{z}\mathbf{z}^T-\mathbf{r}\mathbf{M}^T\mathbf{z}^T-\mathbf{z}\mathbf{M}\mathbf{r}^T \\ &= \|(\boldsymbol{\rho}-\mathbf{z})\mathbf{R}\|^2+\|\mathbf{r}\|^2-\boldsymbol{\rho}\,\tilde{\mathbf{M}}\boldsymbol{\rho}^{\,T}-\alpha\mathbf{z}\mathbf{z}^T \end{aligned} \tag{3.28}$$

Thus, the new radius for (3.26) is equal to

$$r_1^2 = r^2-\|\mathbf{r}\|^2+\boldsymbol{\rho}\,\tilde{\mathbf{M}}\boldsymbol{\rho}^{\,T}+\alpha\mathbf{z}\mathbf{z}^T \tag{3.29}$$

In [17], the algorithm is proposed at first in the case of QPSK modulation and then is generalized to any M-QAM modulation. Indeed, if the elements of $\mathbf{z}$ are of constant modulus the QPSK case, the product $\alpha\mathbf{z}\mathbf{z}^T$ remains constant. Thus, the minimization of the Euclidean norm $\|(\boldsymbol{\rho}-\mathbf{z})\mathbf{R}\|^2$ is equivalent to the minimization of $\|\mathbf{r}-\mathbf{zM}\|^2$ on $\mathbf{z}$. Note that the complexity of this proposed algorithm depends on the choice of α. There exists an optimal α that leads to the lowest complexity but it is impossible to derive a closed-form expression for the optimal α, which depends on the variance of the additive noise and $n-m$ [17]. For simulations, we test the value of $\alpha=\frac{0.5}{n-m}$. We apply the Schnorr Euchner strategy [1] to the generalized sphere decoder. This choice is done to avoid searching the closest point into the sphere of radius r_1^2, especially when $r_1 \gg 1$.

To generalize this algorithm to any M-QAM modulation, it is observed that any M-QAM ($M=2^n$) constellation can be represented as a weighted sum of $n/2$ QPSK constellations when n is an even number [17]. Thus,

$$\forall s \in \text{M-QAM}, \exists\, s_i \in \text{QPSK}, 0 \le i \le n/2 \text{ such that } s=\sum_{i=0}^{\frac{n}{2}-1} 2^i s_i \tag{3.30}$$

For example, if we consider a 16-QAM modulation, any symbol $s \in$ 16-QAM can be expressed as:

$$\mathbf{s}=2\mathbf{s}_1+\mathbf{s}_0$$

where $\mathbf{s}_0, \mathbf{s}_1 \in$ QPSK.

The received signal $\mathbf{r}=\mathbf{sH}+\boldsymbol{\nu}$ can be written as

$$\mathbf{r}=\begin{bmatrix}\mathbf{s}_1 & \mathbf{s}_0\end{bmatrix}\begin{bmatrix}2\mathbf{H}\\ \mathbf{H}\end{bmatrix}+\boldsymbol{\nu} \tag{3.31}$$

A MIMO system with n_t transmit, n_r receive antennas, and 16-QAM modulation could be transformed into another MIMO system with $2n_t$ transmit, n_r receive antennas, and QPSK modulation.

In the following, we consider the algorithm described above to generalize the proposed MIMO error probability approximation to any (n_t,n_r).

3.3.2 Generalization of the error probability computation when $n_t > n_r$

We adapt the approximation given in (3.20) to the asymmetric case, $n_t > n_r$. For a fixed channel matrix $\mathbf{H}$, it is shown (see section 3.2) that an accurate approximation of the point error

probability for a multi-dimensional QAM modulation transmitted on a MIMO channel is upper bounded by

$$Pe(C^{\mathbf{H}}) \leq \sum_{\ell=0}^{n} \frac{p_\ell}{card(I_\ell)} \sum_{\mathbf{x}\in I_\ell} \sum_{i} \tau_{\mathbf{x},\ell,i} \times \mathrm{Q}\left(\frac{d_i}{2\sigma}\right) \tag{3.32}$$

where $Pe(C^{\mathbf{H}})$ denotes the average point error probability associated to the finite constellation $C^{\mathbf{H}}$ and I_ℓ is a subset of $C^{\mathbf{H}}$ that contains lattice points located on the intersection of ℓ facets in $C^{\mathbf{H}}$. The subset I_0 represents the interior of the constellation. The factor p_ℓ is the probability that a point of the constellation $C^{\mathbf{H}}$ belongs to the subset I_ℓ. The expressions of p_ℓ given in (3.8) and (3.15) remain valid in the studied case. The coefficients $\tau_{\mathbf{x},\ell,i}$ represents the number of points belonging to ℓ facets and surrounding the point $\mathbf{x}$ at a distance d_i within the constellation. Since the coefficients $\tau_{\mathbf{x},\ell,i}$ is evaluated thanks to the *Short vectors* algorithm, it is necessary to generalize this algorithm for the studied case, $n_t > n_r$.

3.3.2.1 Generalization of the *Short vectors* algorithm

As indicated in section 3.2.5, the *Short vectors* algorithm searches all the points $\mathbf{x} = \mathbf{zM} \in \Lambda$ subject to $\|\mathbf{x}\|^2 \leq C$, where $\mathbf{z} \in \mathbb{Z}^n$.

Considering the approach detailed in section 3.3.1, the Euclidean norm $\|\mathbf{x}\|^2$ can be written as

$$\|\mathbf{x}\|^2 = \mathbf{zMz}^T = \mathbf{z\tilde{G}z}^T - \alpha\mathbf{zz}^T \leq C \tag{3.33}$$

Thus, inequality (3.33) is equivalent to

$$\mathbf{z\tilde{M}z}^T = \|\mathbf{z\tilde{R}}\|^2 \leq C + \alpha\mathbf{zz}^T \leq C + \alpha \sum_{i=1}^{n} z_{\max_i}^2, \ \alpha > 0 \tag{3.34}$$

where $\tilde{\mathbf{M}} = \mathbf{M} + \alpha\mathbf{I}_n$ is a definite positive matrix and $\tilde{\mathbf{R}}$ is an upper triangular matrix resulting from the Cholesky factorization of $\tilde{\mathbf{M}}$ as indicated in section 3.3.1. Since $\tilde{\mathbf{M}}$ is definite and positive, it is possible to apply the *Short vectors* algorithm (detailed in section 3.2.5) to search the points $\tilde{\mathbf{x}} = \mathbf{z\tilde{R}}$ belonging to the sphere centered at the origin of a square radius, equal to $\tilde{C} = C + \alpha \sum_{i=1}^{n} z_{\max_i}^2$. Note that this algorithm outputs all the integer components $\mathbf{z}$ satisfying (3.34) and also the Euclidean distance $\|\tilde{\mathbf{x}}\|^2$. Thus, to determine the components $\mathbf{z}$ which satisfy (3.33), we should compute $\|\mathbf{x}\|^2 = \|\tilde{\mathbf{x}}\|^2 - \alpha\mathbf{zz}^t$ and compare it to the radius C. Note that the minimum Euclidean distance of the constellation $d_{E_{\min}}^2$ is upper bounded by

$$d_{E_{\min}}^2 \leq \min_i g_{ii}$$

where $\mathbf{G} = [g_{ij}]$ is the Gram matrix.

Therefore, it is more efficient to limit the search of the short vectors algorithm to the sphere of square radius $C = \min_i g_{ii}$.
To evaluate the coefficients $\tau_{\mathbf{x},\ell,i}$ corresponding to the different points $\mathbf{x}$ of the constellation, we proceed as in the previous study:

- Step 1: Generate lattice points $\mathbf{v} \in \Lambda$ located at a distance d_i from the origin as described just before.

- Step 2: For each $\mathbf{v}$ found in the previous step, check if the translate $\mathbf{v} + \mathbf{x}$ belongs to the constellation $C^{\mathbf{H}}$ and increment $\tau_{\mathbf{x},\ell,i}$ accordingly.

It is noticed that the complexity of the proposed method to generalize the *Short vectors* algorithm depends on the new radius $\tilde{C}$. Indeed, the value of $\tilde{C}$ increases with the number of transmit antennas and especially with the constellation size (e.g. 64-QAM, 256-QAM). To decrease this complexity, it is possible to limit the search of the vector $\mathbf{z}$ within a region such that the different translations over the lattice points (Step 2) should be taken into account. Thus, it is sufficient to consider only the z_i belonging to the interval [-$z_{\max_i}$,$z_{\max_i}$], where $z_{\max_i}$ denotes the maximum value of the corresponding M-PAM. In simulation results, the coefficient α is fixed to 0.5.

3.3.2.2 Numerical implementation

For the derivation of the numerical results, we limited the number of points $\mathbf{x}$ considered in (3.32) to $N_x = \min(1000, \prod_{k=1}^{n_t} M_k)$, where M_k denotes the size of the modulation applied on the antenna k. The size of a subset I_ℓ is approximated by $card(I_\ell) \approx p_\ell \times N_x$. The number of shells considered in the local theta series is limited to a number i_{max} where the most distant shell is at $\lambda d^{up}_{Emin}(C^{\mathbf{H}})$, with $\lambda \in \{2, 4, 8\}$, and where $d^{up}_{Emin}(C^{\mathbf{H}})$ denotes an upper bound of the constellation minimum Euclidean distance. Starting the computation of the coefficient $\tau_{\mathbf{x},\ell,i}$ for $\lambda = 2$, if the local theta series (around $\mathbf{x}$) is empty, then the new search radius can be increased up to $4d^2_{Emin}(\Lambda)$ or $8d^2_{Emin}(\Lambda)$. The evaluation of $d^{up}_{Emin}(C^{\mathbf{H}})$ is determined by applying the generalized sphere decoder algorithm around a randomly chosen lattice constellation and then searching the closest constellation point.

3.3.3 Simulation results

We consider a quasi-static $n_t \times n_r$ MIMO system. In Figs. 3.11 and 3.12, we plot the point error probability (PER) as a function of the average received E_b/N_0 for both scenarios (n_t,n_r) = (3,2) and ($n_t = n_r$) = (4,2) when applying QPSK and 16-QAM on the transmit antennas. The analytical results map almost exactly with the simulation results for both scenarios and both modulation sizes.

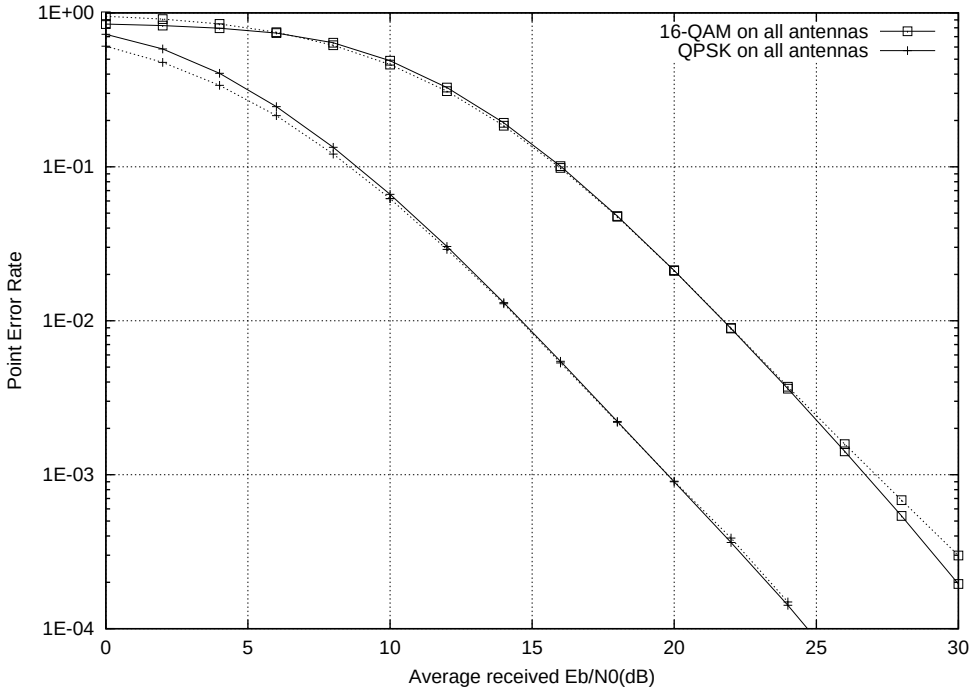

Figure 3.11: Average error probability of a 3×2 quasi-static MIMO channel ($T_c = 100$). Analytic approximation (continuous lines) and Monte Carlo simulation (dotted lines).

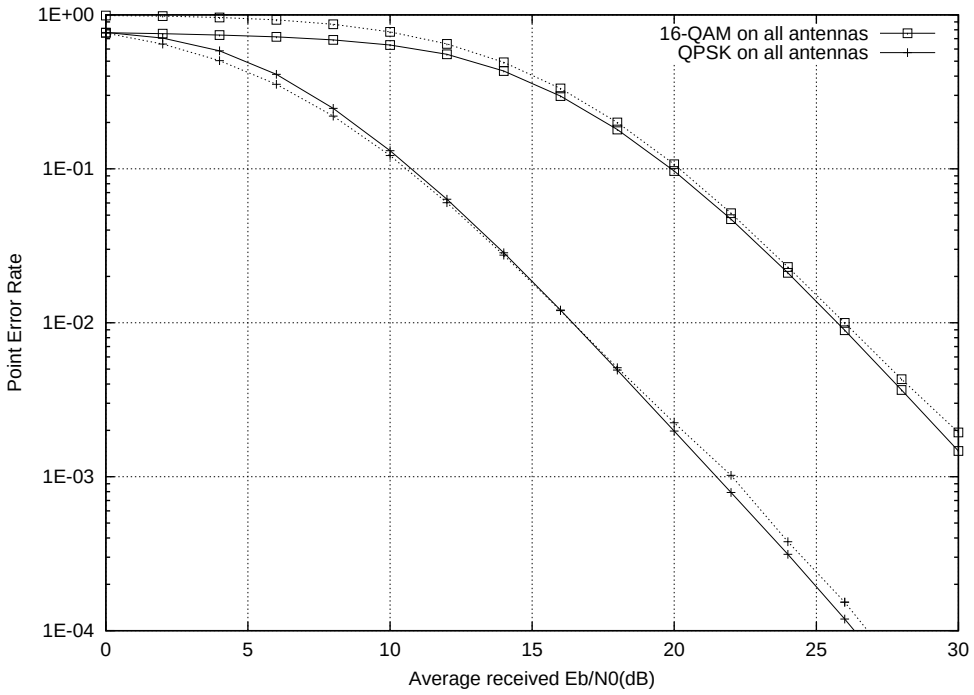

Figure 3.12: Average error probability of a 4×2 quasi-static MIMO channel ($T_c = 100$). Analytic approximation (continuous lines) and Monte Carlo simulation (dotted lines).

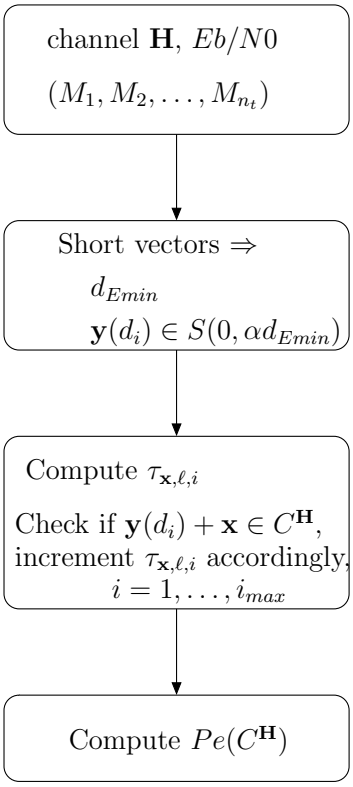

Figure 3.13: Main steps for the error probability computation.

3.4 Complexity of the error probability approximation

As indicated in Fig. 3.13, the evaluation of the conditional error probability approximation (3.20) is based on two main steps that are responsible for the computational complexity:

- Application of *Short vectors* algorithm : It is known that this algorithm has a polynomial complexity with respect to lattice dimension. It is of order n_s^4, where $n_s = \min(2n_t, 2n_r)$.
- Evaluation of the parameter $\tau_{\mathbf{x},\ell,i}$ for different points of the constellation : The complexity study of the approximation (3.20) shows that the evaluation of the factor $\tau_{\mathbf{x},\ell,i}$ is the most time consuming. Indeed, this factor must be computed for $K_c \times i_{max}$ times for each channel realization $\mathbf{H}$, where $K_c = \min(1000, 2^{\sum_{i=1}^{n_t} \log_2(M_i)})$ and i_{max} depends on the number of transmit antennas n_t. Typically, on average, i_{max} equals 2 for $n_t = 2$ and to 10 for $n_t = 4$. For example, when $n_t = n_r = 4$ and 16-QAM modulation applied on all transmit antennas, $\tau_{\mathbf{x},\ell,i}$ is computed 104 times on average for each MIMO channel.

Conclusions

This chapter focused on the performance of uncoded MIMO systems with spatial multiplexing scheme at the transmitter. In this scheme, same or distinct modulations could be applied on transmit antennas. Then, by considering the lattice code associated to the MIMO channel and using lattice theory, we derived an accurate approximation for the conditional error probability. This approximation was derived at first for the case when there are more antennas at the

receiver side. Then, we generalized this approximation without any constraint on the number of antennas. Finally, Monte-Carlo simulation results given for both cases showed the tightness of our analytical approximation for different antenna and modulation configurations. The error probability approximation was compared to another one proposed for the whole lattice associated to the MIMO channel. It was noticed that this bound is less accurate than our approximation (e.g. a loss in SNR higher than 2dB at PER=10^{-3} with 4-QAM on all antennas), but has a lower computation complexity.
Our error probability approximation is used in the next chapter for adaptive techniques in MIMO systems: adaptive modulation and antenna selection.

Chapter 4

Adaptive techniques for MIMO systems

Introduction

MIMO systems can offer significant capacity and diversity gains over traditional SISO systems [59], [21], [57]. That is why, multiple antenna technique is integrated in future wireless systems to provide more reliability and high data rates. Unfortunately, the performance of MIMO systems depend on the radio channel conditions. To maintain a target QoS in conventional multiple antenna systems, transmission parameters (e.g. data rate, modulation and coding, transmit power, etc) should be adjusted to the worst case. This leads to insufficient use of the channel bandwidth under favorable channels. Moreover, the use of multiple antennas demands additive devices (e.g. RF chains) which increases the cost and the complexity of these systems. Several techniques have been proposed to cope with these limitations, for example adaptive modulation [52], [69], [70], [50], [64] and antenna selection [29], [30], [27]. On the one hand, adaptive modulation technique aims to guarantee a target QoS while maximizing the data rate [69], [70], [50], or minimizing the transmit power [64], etc. according to channel conditions. On the other hand, antenna selection is proposed to reduce the cost of MIMO systems by reducing the number of active antennas, while keeping the advantage of using all the available antennas.

In both adaptive techniques, the selection of the appropriate modulation or antenna set at the transmission needs a relevant metric. This metric must be defined to precisely assess the MIMO system performance.

In this chapter, we propose a new adaptive modulation scheme as well as a new antenna selection algorithm. Both techniques use the accurate approximation of the conditional error probability in a MIMO system, given in chapter 3, as a metric to select the best parameters, namely modulation size and antenna set for transmission. The transmission scheme depicted in chapter 1 is assumed in this chapter.
Section 4.1 focuses on the designed adaptive modulation scheme. First, we introduce this technique and we illustrate some existing schemes in the literature. Then, we describe our algorithm to adapt modulations on transmit antennas for spatial multiplexing MIMO systems. A refinement of this algorithm is made to reduce the search complexity of the optimal modulations. Finally, our adaptive modulation scheme is compared to another one using the error

probability bound (3.4), and also to non-adaptive systems.
Section 4.2 deals with the antenna selection technique. First, the principle of this technique as well as some exiting selection schemes are given. Second, we illustrate the general model for MIMO systems with antenna selection and we indicate our assumptions. Third, we study the performance of SIMO systems while activating the best receive antennas in terms of the instantaneous received SNR. After that, our proposed selection criterion and some existing selection criteria are introduced. Finally, we compare the performance achieved with the different criteria for many receiver schemes.

4.1 Adaptive modulation

4.1.1 Adaptive modulation concept

Adaptive modulation is a promising technique to maximize the transmission rate while guaranteeing a target quality of service (QoS). This justifies its popularity for future high-rate wireless systems (e.g. HSDPA, IEEE 802.11). The fundamental concept of adaptive modulation consists in adjusting the transmission parameters (modulation size, transmit power, coding parameters, etc), according to the current channel state. This adaptation aims to guarantee a target QoS and to achieve the highest possible spectral efficiency. In this chapter, QoS will be characterized by a target error rate. Therefore, the adaptive modulation aims to

$$\begin{gathered} \textit{maximize the spectral efficiency} \\ \textit{subject to} \\ Pe(C^{\mathbf{H}}) \leq PER_{target} \end{gathered}$$

where $Pe(C^{\mathbf{H}})$ is the error probability and PER_{target} is the target error rate.

In the literature, adaptive modulation schemes have been studied at first for SISO systems. One of the most famous algorithm for such systems is the one given in [26], [13]. The corresponding adaptive modulation technique selects the maximum information rate subject to a double constraint on the error rate and the average transmitted power. In [26] and [13], the proposed adaptive approach is based on an approximation of the conditional error probability for an AWGN channel. The adaptation is studied for two categories, namely continuous rate and discrete rate. Analytical expressions for transmit power and rate are derived for the continuous rate case, whereas in the discrete rate case, numerical search is undertaken to determine the optimal adaptation parameters. The latter case, when the set of available constellations is discrete, is more interesting from a practical point of view.

Figure 4.1 depicts a general model for an adaptive modulation scheme in a MIMO context. Note that this model is also valid for a SISO context when one antenna is assumed at both sides. Any adaptive modulation algorithm for both MIMO and SISO systems is based on three major input parameters that depend on the adaptation strategy:

1. **Channel State Information (CSI)** : It characterizes the knowledge of the radio channel at one or both (receiver and transmitter) sides of the system. Perfect CSI means that the channel is estimated without error. Systems with perfect CSI available at both sides are referred as ideally designed adaptive modulation systems.

2. **Link quality of the transmission** : It depends on the instantaneous channel state information within the current frame. Based on the link quality of the transmission, the appropriate modulations at the transmitter are selected.

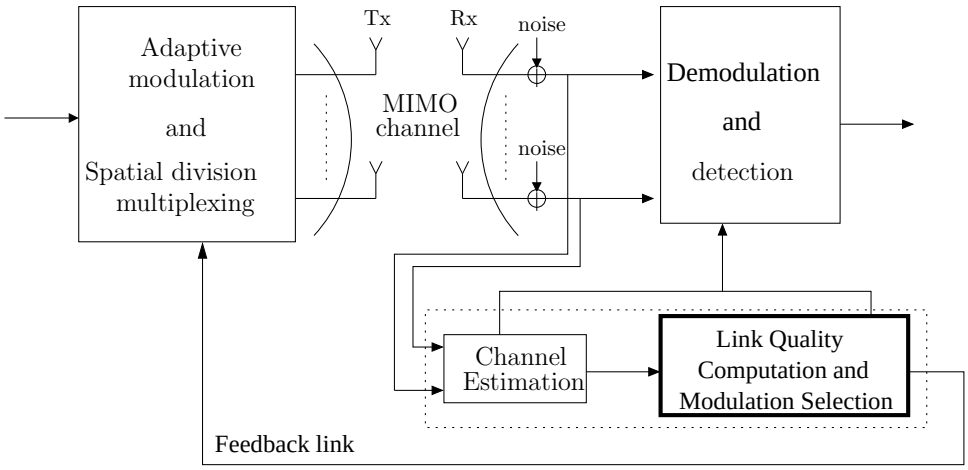

Figure 4.1: Adaptive modulation issue in a MIMO context.

3. **Feedback link** : Once the optimal modulation is selected according to the current channel, this selection should be fed back to the transmitter to adjust the modulations applied on the different transmit antennas. When this information is returned to the transmitter without error, a perfect feedback is assumed.

Different strategies have been proposed based on the system model depicted on Fig. 4.1. The focus of these different schemes is how to determine the link quality of the transmission and then select the appropriate transmission parameters. In [69] and [70], the authors founded their strategy on a singular value decomposition of the MIMO channels to obtain parallel eigen sub-channels. Then, they applied the adaptive scheme for a SISO system [13] on each eigen sub-channel. This method requires a perfect CSI at the transmitter and at the receiver in order to apply the precoding required by the SVD and the related adaptive policy. Such method presents the following drawbacks:

1. Sensitivity to channel estimation errors.

2. Need of a reliable feedback allowing to send a high number of bits (especially for high dimension) to inform the transmitter about the precoding matrix.

In the following, we propose a new adaptive modulation scheme. This scheme requires a few bits to inform the transmitter about the optimal modulation combination to be applied while satisfying the system constraints.

4.1.2 A new adaptive modulation scheme

We restrict our scheme to the adaptation of modulation size for each transmit antenna for uncoded MIMO channels. Power adaptation and channel coding rate variations are not considered. Square QAM modulations are assumed in this work. However, this study is valid for any rectangular QAM that can be implemented with two independent PAMs. Perfect CSI is available at the receiver side only. The transmitter is informed via the feedback link about the selected QAMs that satisfy the system constraints. The link quality of the transmission is evaluated by computing the error probability conditioned on the channel $\mathbf{H}$, $Pe(C^{\mathbf{H}})$. The objective of our adaptive modulation scheme is the following:

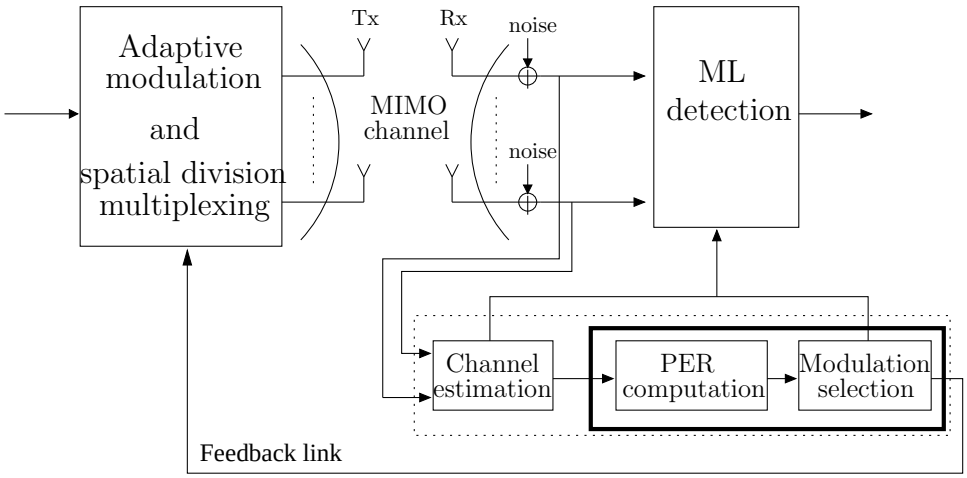

Figure 4.2: Adaptive QAM modulation receiver/transmitter pair for quasi-static MIMO channels.

Given an average signal-to-noise ratio per bit, find modulation sizes $M_1,M_2,\ldots,M_{n_t}$ *for the* n_t *transmit antennas in order to maximize the spectral efficiency* $\sum_{k=1}^{n_t} \log_2(M_k)$ *under the constraint* $Pe(\mathbf{C^H}) \leq PER_{target}$*, where* PER_{target} *is the target point error rate.*

Notice that when $Pe(\mathbf{C^H}) \geq PER_{target}$, no data is transmitted and the conditional error probability $Pe(\mathbf{C^H})$ is equal to 0. In the latter case, an outage is declared.

In practice, if the quality of service depends on the frame error rate (FER) and if a frame has length N_F transmit periods, $N_F \leq T_c$, then $FER = 1-(1-PER)^{N_F} \approx N_F \times PER$. Hence, PER_{target} can be easily linked to FER_{target} and can be used for the adaptation QoS constraint.

Figure 4.2 depicts our adaptive modulation scheme for uncoded MIMO channels. Assume that the n_t-antenna transmitter selects the modulation among N_q distinct QAM modulations. For example, $N_q = 4$ if square constellations 4-QAM, 16-QAM, 64-QAM and 256-QAM are used. If all transmit antennas use the same M-QAM constellation, then the adaptation scheme should select an optimal solution $(M,M,\ldots,M)_{opt}$ among N_q possibilities. If transmit antennas use different QAM constellations, then the adaptation scheme should select an optimal solution $(M_1,M_2,\ldots,M_{n_t})_{opt}$ among $N_q^{n_t}$ possibilities.

At the receiver side, the channel estimation block provides a perfect estimate of the channel $\mathbf{H}$ and the noise variance σ^2 to the adaptation block. The PER computation function uses the approximation (3.20) to compute $PER = Pe(\mathbf{C^H})$, where $\mathbf{C^H} = \mathbf{C^H}(M_1,M_2,\ldots,M_{n_t})$. The final block selects the optimal solution $(M_1,M_2,\ldots,M_{n_t})_{opt}$ that maximizes the total spectral efficiency $\sum_{k=1}^{n_t} \log_2(M_k)$ under the constraint $PER \leq PER_{target}$. Finally, the feedback link conveys $n_t \times \lceil \log_2(N_q) \rceil$ bits to the transmitter, e.g. 8 feedback bits if $n_t = 4$ and $N_q = 4$.

The complexity of the adaptive scheme depends on the number of available modulations. The easiest adaptive modulation scheme when all QAMs are identical, $M_1 = M_2 = \ldots = M_{n_t}$, has a low adaptation complexity proportional to N_q. On the contrary, the most efficient adaptive modulation scheme (when QAM constellations may be distinct per transmit antenna) has an adaptation complexity proportional to the number of possibilities, that is equal to $N_q^{n_t}$, e.g.

$4^4 = 256$ possibilities if 4 types of QAM are authorized ($N_q = 4$ and $M \in \{4,16,64,256\}$) and $n_t = 4$ transmit antennas. Hence, an adaptation with a brute force (exhaustive search means that all combinations are tested) will cost $N_q^{n_t}$ numerical evaluations of (3.20).

Since the spectral efficiency varies when from $n_t \times 2$ to $n_t \times 2 \times N_q$ bits per channel use, it can have exactly $\frac{8n_t - 2n_t}{2} + 1 = (N_q - 1) \times n_t + 1$ possible values. In order to avoid considering all ($N_q^{n_t} = 256$ for $n_t = 4$ and $N_q = 4$) the possibilities, a key idea is to select a reduced number of combinations. This could be achieved by partitioning the set of all the possibilities into subsets (classes) of combinations having the same spectral efficiency (13 for $n_t = 4$ and $N_q = 4$). The following paragraph describes the proposed strategy to generate a representative for each class.

Strategy to reduce the modulation combination list

- **Step 1**: The objective of this step is to select a representative for each spectral efficiency value between $n_t \times 2$ and $n_t \times 8$. For example, if $n_t = 4$, the first step consists in choosing $13 = 3n_t + 1$ representatives as in Table 4.1. So, we start with the lowest modulation combination $(4, \ldots, 4)$. Then, to move upward from the row k to the row $k+1$, we increase the spectral efficiency of the lowest QAM corresponding to the highest antenna index. For example, to generate the next combination starting from (4, 4, 16, 16) (row 3 from the bottom in Table 4.1), we use for the second antenna the modulation 16-QAM instead of 4-QAM which leads to (4, 16, 16, 16) combination.
- **Step 2**: In the second step, each transmit antenna must be assigned to a column as in Table 4.1, i.e. we must properly permute the n_t integers M_k given by the row of Table 4.1 selected in the first step. We proposed to assign the M_k's according to the order of $\|\mathbf{h}_i\|$, where $\mathbf{h}_i$ is the i^{th} row of $\mathbf{H}$. This is inspired by coded systems. Indeed, if an error-correcting code is used in combination with a soft output decoder, then under the genie condition (perfect feedback of *a priori* information), the capacities of the n_t independent channels are sorted according to $\|\mathbf{h}_i\|^2$.

In our case, QAM modulations are uncoded. Nevertheless, simulation results show that the loss in spectral efficiency with our strategy compared to the brute-force is negligible. The adaptation based on 13 possibilities performs almost as well as with 256 possibilities. This strategy reduces the number of QAM combinations from $N_q^{n_t}$ down to $(N_q - 1)n_t + 1$. Moreover, the application of the dichotomy on this list allows to further reduce the complexity of the algorithm to $0(\log_2((N_q - 1)n_t + 1))$. This is made possible thanks to the monotony of the error probability $Pe(C^{\mathbf{H}})$. At the end of this section, we recall the dichotomy method.

For $n_t = N_q = 4$, we sort the transmit antennas such that $\|\mathbf{h}_1\|^2 \leq \|\mathbf{h}_2\|^2 \leq \|\mathbf{h}_3\|^2 \leq \|\mathbf{h}_4\|^2$. Then, we start from the most robust combination (4*4-QAM) upward to the most efficient combination (4*256-QAM) as shown in Table 4.1. Only one integer is changed from one row to another according to a decreasing order of transmit antennas power. Consequently, thanks to the dichotomy method applied on the reduced list, a maximum of $4 = \lceil \log_2(13) \rceil$ evaluations of $Pe(C^{\mathbf{H}})$ are required instead of $N_q^{n_t} = 256$. Considering a large number of antennas, e.g. $n_t = 8$ and $n_q = 4$, the associated reduced list is illustrated in Table 4.2. It consists of 25 QAM combinations among the overall, i.e., $4^8 = 65536$ combinations. When applying the dichotomy on this list, a maximum of $5 = \lceil \log_2(25) \rceil$ computations of $Pe(C^{\mathbf{H}})$ are needed to select the appropriate combination.

Spectral efficiency	Tx 1	Tx 2	Tx 3	Tx 4	Comment
32	256	256	256	256	highest spectral efficiency and worst error rate performance
30	64	256	256	256	
28	64	64	256	256	
26	64	64	64	256	
24	64	64	64	64	
22	16	64	64	64	
20	16	16	64	64	
18	16	16	16	64	
16	16	16	16	16	
14	4	16	16	16	
12	4	4	16	16	
10	4	4	4	16	
8	4	4	4	4	lowest spectral efficiency and best error rate performance

Table 4.1: Reduced list for adaptive modulation, $N_q = 4$ distinct QAM sets and $n_t = 4$ transmit antennas.

Tx 1	Tx 2	Tx 3	Tx 4	Tx 5	Tx 6	Tx 7	Tx 8
256	256	256	256	256	256	256	256
64	256	256	256	256	256	256	256
64	64	256	256	256	256	256	256
64	64	64	256	256	256	256	256
64	64	64	64	256	256	256	256
64	64	64	64	64	256	256	256
64	64	64	64	64	64	256	256
64	64	64	64	64	64	64	256
64	64	64	64	64	64	64	64
16	64	64	64	64	64	64	64
16	16	64	64	64	64	64	64
16	16	16	64	64	64	64	64
16	16	16	16	64	64	64	64
16	16	16	16	16	64	64	64
16	16	16	16	16	16	64	64
16	16	16	16	16	16	16	64
16	16	16	16	16	16	16	16
4	16	16	16	16	16	16	16
4	4	16	16	16	16	16	16
4	4	4	16	16	16	16	16
4	4	4	4	16	16	16	16
4	4	4	4	4	16	16	16
4	4	4	4	4	4	16	16
4	4	4	4	4	4	4	16
4	4	4	4	4	4	4	4

Table 4.2: Reduced list for adaptive modulation, $N_q = 4$ distinct QAM and $n_t = 8$ Tx antennas.

Note that the number of iterations (the number of combinations tested) can be further reduced, by taking into account the frequency of the channel variations. Indeed, when Doppler is low, the channel response variations from one block to another are small and the appropriate QAM modulation will probably be the same on both blocks. In this case it is worth testing first the QAM modulation used on the previous block (instead of starting from the beginning of the modulation combination list). According to the result of the comparison with the target PER, the receiver notifies the transmitter to decrease or to increase the modulation size w.r.t. the previous block modulation.

Dichotomy method

It is a method for numerically solving equations having a single unknown. Consider the equation $f(x) = 0$ with a continuous function f on the interval $[a,b]$, such that $f(a) \cdot f(b) < 0$. Therefore, it exists at least one solution $\hat{x}$ within $[a,b]$. To find $\hat{x}$ approximately, we proceed as shown in algorithm 2.

input : a, b, f, ϵ
output: $\hat{x}$, such that $|f(\hat{x})| \leq \epsilon$

2.1 $a_0 = a$;
2.2 $b_0 = b$;
2.3 $k = 0$;
2.4 $x_0 = \frac{a_0+b_0}{2}$;
2.5 **while** $|f(x_k)| > \epsilon$ **do**
2.6 **if** $f(x_k) \cdot f(a_k) < 0$ **then**
2.7 $a_{k+1} = a_k$;
2.8 $b_{k+1} = x_k$;
2.9 **end**
2.10 **else**
2.11 $a_{k+1} = x_k$;
2.12 $b_{k+1} = b_k$;
2.13 **end**
2.14 $k = k + 1$;
2.15 $x_k = \frac{a_{k+1}+b_{k+1}}{2}$;
2.16 **end**
2.17 *return* $\hat{x} = x_k$;

Algorithm 2: Dichotomy method to solve $f(x) = 0$ in [a,b].

Figure 4.3 illustrates an example to search $\hat{x}$ that satisfies $f(\hat{x}) = 0$ with the dichotomy method.

4.1.3 Computer simulation of the adaptive modulation scheme

The considered target point error rate is $PER_{target} = 10^{-3}$. The QAM selection is made within the reduced list given in Table 4.1. Figure 4.4 presents the performance of a 4×4 antenna system satisfying the constraint on the error probability for each channel $\mathbf{H}$ and each noise variance, *i.e.* $Pe(C^{\mathbf{H}}) \leq PER_{target}$.

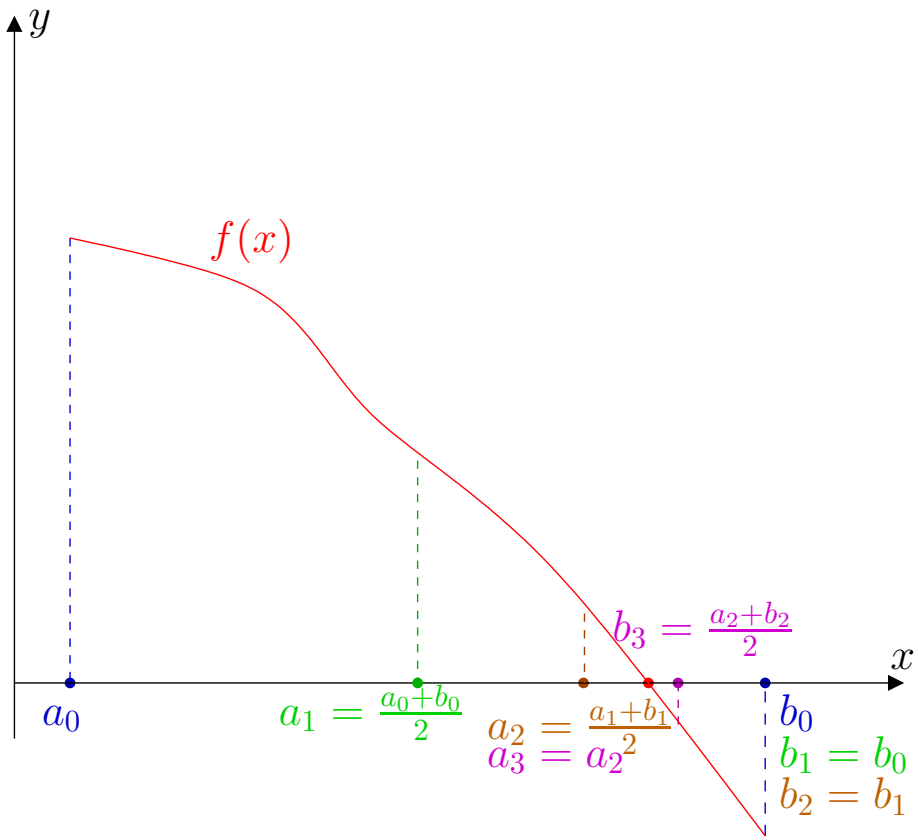

Figure 4.3: First steps in the dichotomy method for a given function f.

Clearly, the curves corresponding to both non adaptive and adaptive schemes are below the target. The upper curve corresponding to adaptive modulation is close but remains below the 10^{-3} target. It also shows a good stability (low variation of PER) within a 10 dB signal-to-noise ratio range. For high noise variance, the selected combination corresponds to the lowest one (*i.e.* 4*4-QAM) for the majority of channels. On the other hand, PER of the adaptive scheme tends to that of 4*256-QAM at high SNR.

Figure 4.5 represents the probability of no transmission (known as *outage probability*), *i.e.* $Pe(C^{\mathbf{H}}) > PER_{target}$. The outage probability of the adaptive modulation is superimposed with the outage of a fixed 4*4-QAM modulation. Therefore, the proposed adaptive modulation is as robust as the 4-QAM but it guarantees a higher spectral efficiency. It leads to a maximization of the spectral efficiency while keeping the error probability close to the target.

In Fig. 4.6, the total spectral efficiency achieved by a 4×4 antenna system is presented versus the average received SNR while satisfying the PER constraint. This figure also emphasizes the advantage of adaptive modulation. The stair including 4 soft steps corresponds to the non adaptive scheme when all Tx antennas are using the same QAM constellation. Albeit the looseness of (3.4) shown in Fig. 3.10, the adaptive modulation based on minimum Euclidean distance exhibits a small spectral efficiency loss at low SNR with respect to adaptation based on local theta series.
The next section introduces the second adaptive technique for MIMO channels : antenna

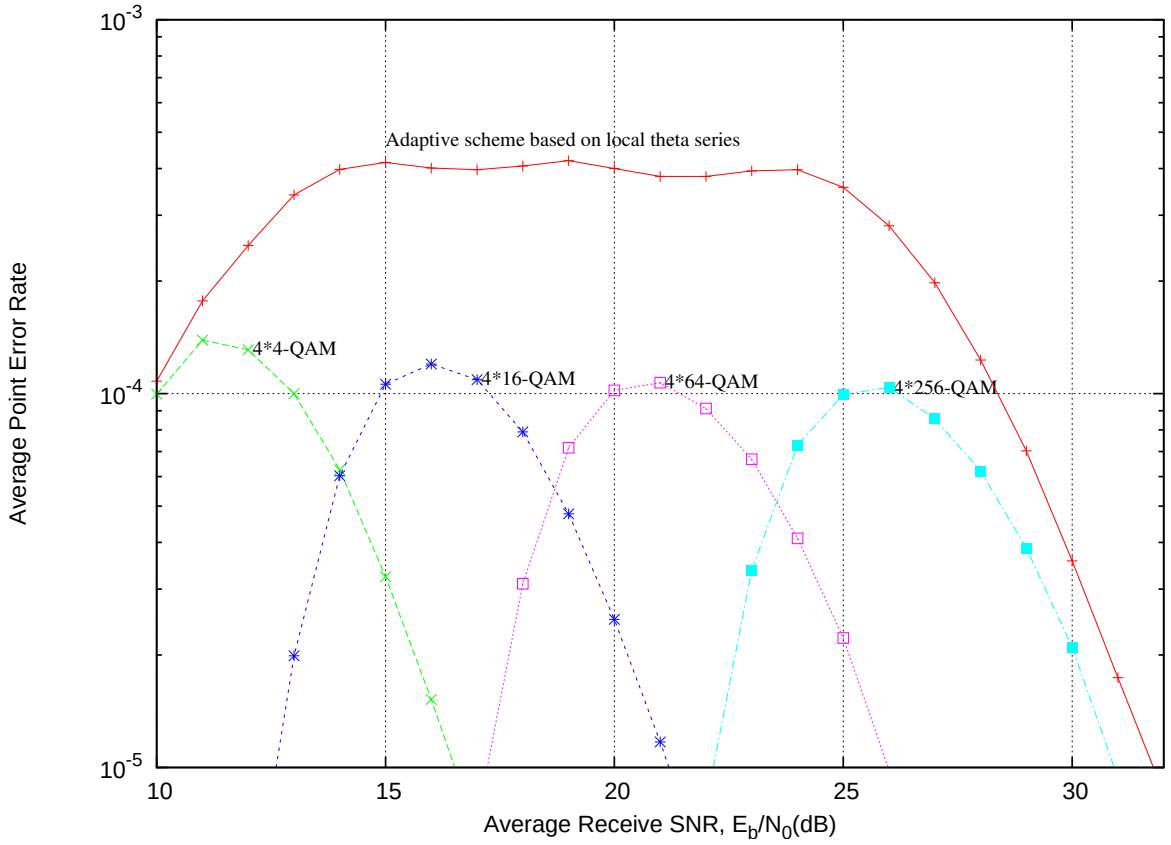

Figure 4.4: Average point error rate function of average signal-to-noise ratio, adaptive versus non-adaptive modulation policy , 4×4 quasi-static MIMO channel.

selection.

4.2 Antenna selection

Multiple antenna systems can offer significant capacity gains over traditional mono-antenna systems [59],[21]. However, the use of multiple antennas requires multiple RF chains consisting of amplifiers, analog to digital converters, mixers, etc. This fact increases the cost of MIMO systems as well as the complexity of both the transmitter and the receiver. Antenna selection is a promising technique that reduces the complexity and the cost of MIMO systems while keeping the diversity benefits of all antennas [27], [25]. That's why, it is proposed for future wireless systems, e.g. IEEE 802.11n. The basic idea behind the antenna selection is to choose the best set of antennas at the transmitter and/or the receiver that achieves the highest system performance according to a selection criterion (e.g error probability, capacity, signal-to-noise ratio,...). Therefore, a reduced number of RF chains is needed at the transmitter and/or the receiver and each RF chain is tried to be optimally assigned to one of the large number of available transmit or receive antennas.

Different selection criteria, according to channel conditions, have been proposed in the literature. In [29], Heath et al proposed the maximization of the post-processing SNR as a selection

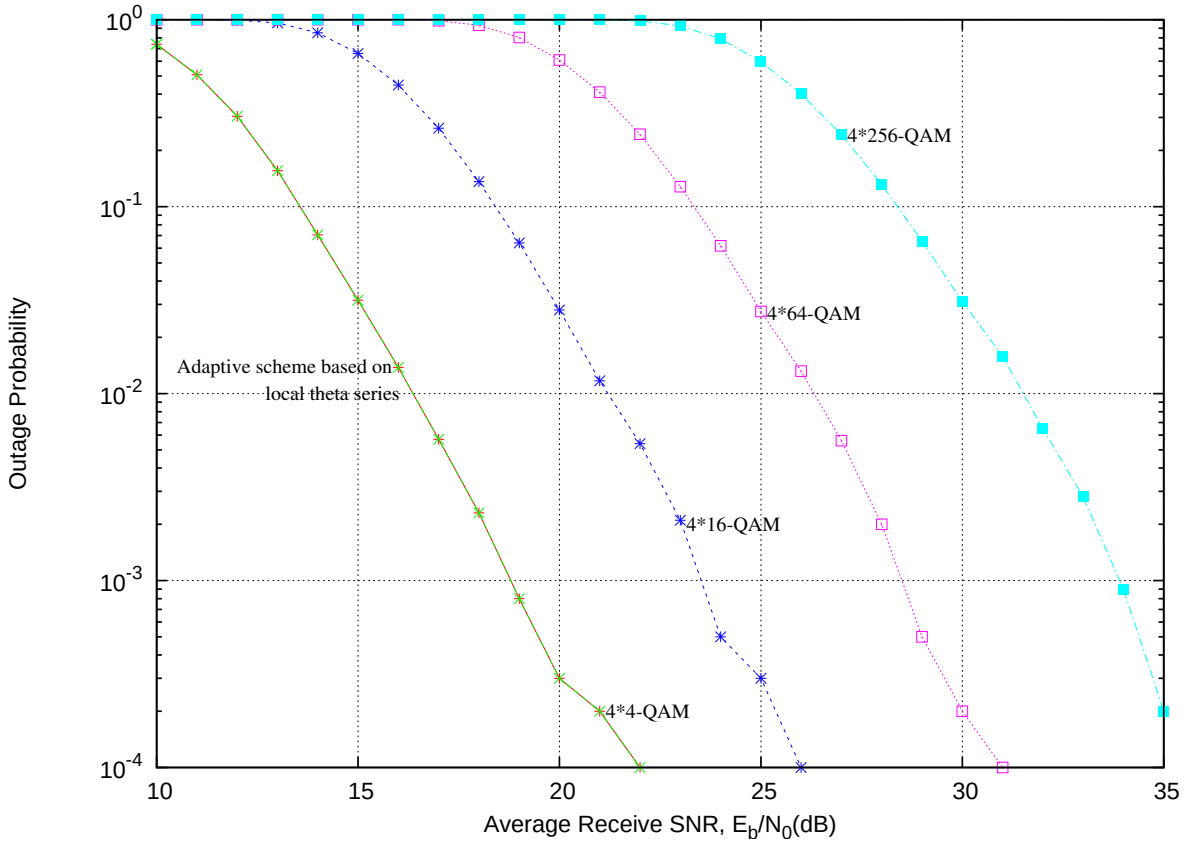

Figure 4.5: Outage probability versus average signal-to-noise ratio, 4×4 quasi-static MIMO channel. No transmission if $Pe(C^H) > Pe_{target}$.

criterion for linear receivers (ZF or MMSE). For the maximum likelihood receiver, the authors in [30] derived a selection criterion based on an upper bound of the error rate. The minimization of this upper bound is equivalent to the maximization of the minimum Euclidean distance of the receive constellation. Due to its high complexity computation, their proposed criterion is hard to be evaluated for larger constellations applied at the transmitter.

We propose an antenna selection criterion based on the accurate approximation of the conditional error probability given in (3.20).

4.2.1 Antenna selection for MIMO system

Figure 4.7 depicts a general model for multiple antennas system with antenna selection at one or both sides of the transmission. The antenna selection is performed at the receiver side. It needs the following blocks:

1. **Channel estimation** : Perfect CSI offers better performance. Imperfect CSI is treated in [70]. The authors show that the error probability performance of an adaptive MIMO system designed for perfect CSI is quite sensitive to the CSI imperfection.

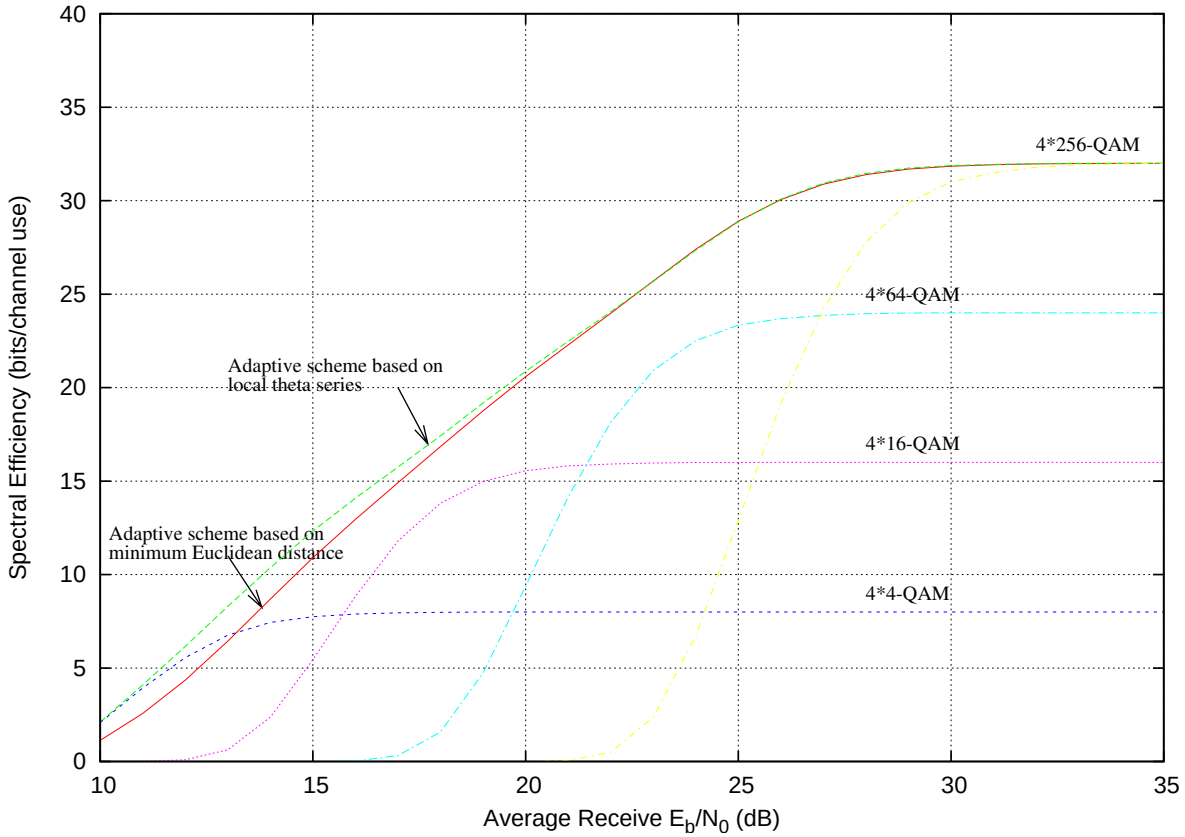

Figure 4.6: Average spectral efficiency of adaptive modulation versus non-adaptive scheme, 4×4 quasi-static MIMO channel.

2. **A selection block** : It is partitioned into two sub-blocks. The first one computes the chosen selection criterion for all possible combinations of antennas. Then, the second selects the best combination of antennas at the transmitter or/and the receiver, that optimizes the selection criterion.

3. **Feedback link** : It is required only for transmit selection in order to inform the transmitter about the selection to be perform. For both transmit/receive selections, the receiver should be notified about the selection to perform the detection.

Let n such that $1 \leq n \leq n_t$ (respectively m such that $1 \leq m \leq n_r$) be the number of active transmit (respectively receive) antennas after selection. For a given channel $\mathbf{H}$, the selection criterion is evaluated x times (x is the number of selection possibilities) according to the selection type :

- **Transmit selection**: all the available receive antennas are used for transmission, but only $n < n_t$ transmit antennas are activated. In this case, x is equal to $\begin{pmatrix} n_t \\ n \end{pmatrix}$.

- **Receive selection**: all the available transmit antennas are used for transmission, but only $m < n_r$ receive antennas are considered. In this case, x is equal to $\begin{pmatrix} n_r \\ m \end{pmatrix}$.

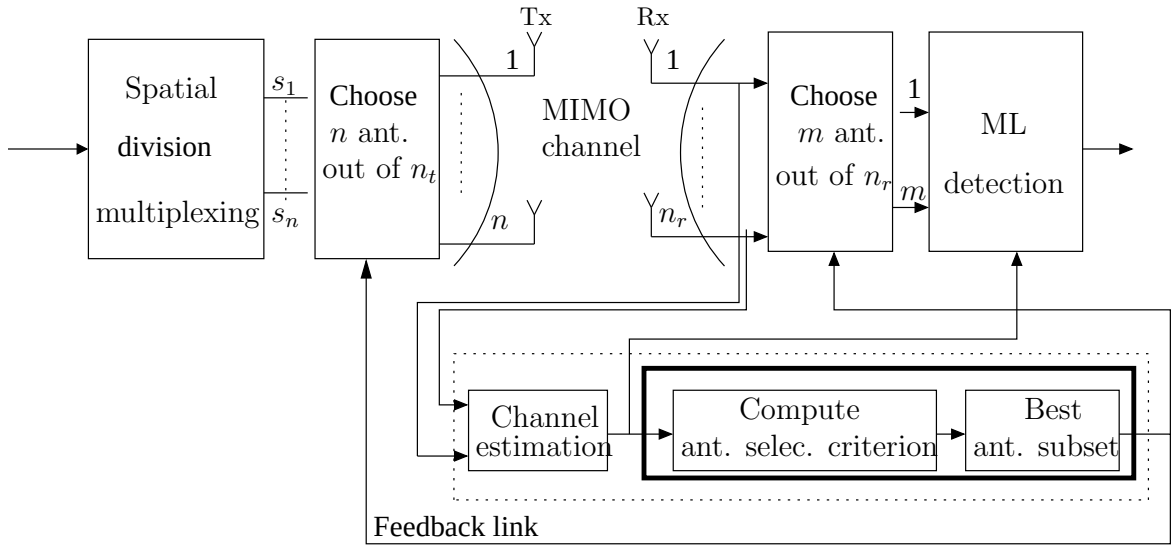

Figure 4.7: General model for MIMO system with antenna selection.

- **Transmit/Receive selection**: this is the case when selection is performed at both sides. Only $n < n_t$ and $m < n_r$ transmit and receive antennas are chosen for transmission. The number x is equal to the product of the above cases: $\begin{pmatrix} n_r \\ m \end{pmatrix} \times \begin{pmatrix} n_t \\ n \end{pmatrix}$. The computation complexity for this last case is more important.

In our study, we assume that perfect channel state information (perfect CSI) is available only at the receiver. CSI is not required at the transmitter side. The selection is performed for the general case, i.e. transmit/receive selection.

Let $\tilde{\mathbf{H}}$ be the $n \times m$ sub-matrix corresponding to the active transmit and receive antennas. A maximum-likelihood detector based on a sphere decoder is applied [63], [1], [8], [17] to accomplish a low complexity detection (as seen in chapter 2).

For one channel use, the received signal can be written as

$$\mathbf{r} = \mathbf{s}\tilde{\mathbf{H}} + \boldsymbol{\nu} \tag{4.1}$$

where $\mathbf{r}$ is the length m receive complex vector, $\mathbf{s}$ is the length n transmit vector and $\boldsymbol{\nu}$ is a length m additive white Gaussian noise vector with $2N_0$ variance per complex dimension. The transmitted symbol s_k belongs to a M_k-QAM modulation, $k = 1 \ldots n$. For the sake of simplicity, we assume that the same modulation M-QAM is applied on transmit antennas. The proposed selection criterion remains valid for the general case when distinct modulations are used at the transmitter as demonstrated in chapter 3.

The following section illustrates some results that outline the benefit of the antenna selection to improve system performance.

4.2.2 SIMO system performance with antenna selection

To emphasize the advantage of antenna selection regarding the system performance, we evaluate in this section the error probability obtained when selecting the antennas for transmission.

The performance is studied for the case of Single-Input Multiple-Output (SIMO) systems.

The selection criterion adopted in this section consists in choosing the set of receive antennas, which maximizes the instantaneous received SNR. For a given combination p, this SNR is equal to:

$$SNR_p = \frac{E_s \sum_{j=1}^{m} |h_j^{(p)}|^2}{2N_0} \tag{4.2}$$

where E_s is the transmit signal energy and $h_j^{(p)}$ correspond to the selected set of antennas. For a given channel realization, let $\tilde{\mathbf{H}} = [h_j]_{j=1,\ldots,m}$ be the sub-channel maximizing the received SNR. Assuming ML detection at the receiver, the error probability, $Pe^{(\tilde{\mathbf{H}})}$, conditioned on $\tilde{\mathbf{H}}$ is bounded by [48]:

$$Pe^{(\tilde{\mathbf{H}})} \leq N_e \mathrm{Q}\left(\sqrt{\frac{d_{\min}^2 ||\tilde{\mathbf{H}}||^2}{4N_0}}\right) \leq \frac{N_e}{2} \exp\left(-\frac{d_{\min}^2 ||\tilde{\mathbf{H}}||^2}{8N_0}\right) \tag{4.3}$$

where $d_{\min}$ is the minimum Euclidean distance of the transmit constellation, N_e is the maximum number of neighbors located at $d_{\min}$ and N_0 is the noise variance per real dimension.

To obtain the average error probability, we evaluate the expected value of the upper bound in (4.3) with respect to the distribution of the random vector $\mathbf{R} = (R_1, R_2, \ldots, R_m)$, where $R_i = |h_i|$ for $i = 1, \ldots, m$. That is

$$Pe_{\text{avg}} = E_{\mathbf{R}}(Pe^{(\tilde{\mathbf{H}})}) = \int_{\mathbf{R}} Pe^{(\tilde{\mathbf{H}})} p_{\mathbf{R}}(r) \prod dr_i \tag{4.4}$$

where $p_{\mathbf{R}}(r)$ is the probability density function (pdf) of $\mathbf{R}$.

In the following, we derive an upper bound for the average error probability after selection. We start with the simple case when $m = 1$. Then, we generalize the results for $m \geq 1$.

4.2.2.1 Antenna selection performance when $m = 1$

At the receiver, one antenna is selected for transmission. Substituting (4.3) in (4.4), we obtain

$$Pe_{\text{avg}} \leq \frac{N_e}{2} \int_{\mathbf{R}} \exp\left(-\frac{d_{\min}^2 r^2}{8N_0}\right) p_{\mathbf{R}}(r) dr \tag{4.5}$$

where $r = \max(r_1, r_2, \ldots, r_{n_r})$ for one channel realization.

The cumulative density function (cdf) of the variable $\mathbf{R}$ is given by

$$F_{\mathbf{R}}(r) = P(r_1 \leq r, \ldots, r_{n_r} \leq r) = \prod_{i=1}^{n_r} F_{R_i}(r), \;\; r \geq 0 \tag{4.6}$$

Knowing the statistics of the variables h_i, their norms R_i are then Rayleigh distributed[48], so

$$F_{\mathbf{R}}(r) = \left(1 - \exp(-r^2)\right)^{n_r}, \;\; r \geq 0 \tag{4.7}$$

The desired pdf of the selected channel is then equal to

$$p_{\mathbf{R}}(r) = 2n_r r. \exp(-r^2) \left(1 - \exp(-r^2)\right)^{n_r - 1} \tag{4.8}$$

Substituting (4.8) in (4.5), the upper bound follows as

$$Pe_{\text{avg}} \leq n_r N_e \int_0^{\infty} r.\exp\left(-\beta r^2\right)\left(1-\exp(-r^2)\right)^{n_r-1} dr \tag{4.9}$$

where $\beta = 1 + \frac{d^2_{\min}}{8N_0}$.

Assuming a square M-QAM modulation, the average transmit SNR E_b/N_0 and β are related by

$$\beta = \frac{3\log_2(M)}{2(M-1)}\frac{E_b}{N_0} + 1 \tag{4.10}$$

Applying the *binomial theorem*, equation (4.9) becomes

$$\begin{aligned} Pe_{\text{avg}} &\leq n_r N_e \sum_{k=0}^{n_r-1} \int_0^{\infty} r.\exp\left(-r^2\left(k+\beta\right)\right) dr \\ &\leq \frac{n_r N_e}{2} \sum_{k=0}^{n_r-1} \frac{\kappa_{k,n_r-1}}{k+\beta}, \end{aligned} \tag{4.11}$$

where

$$\kappa_{k,p} = (-1)^k \begin{pmatrix} p \\ k \end{pmatrix}$$

Since

$$\frac{1}{k+\beta} = \int_0^1 x^{k+\beta-1} dx,$$

inequality (4.11) can be written as

$$\begin{aligned} Pe_{\text{avg}} &\leq \frac{n_r N_e}{2} \sum_{k=0}^{n_r-1} \kappa_{k,n_r-1} \int_0^1 x^{k+\beta-1} dx \\ &\leq \frac{n_r N_e}{2} \int_0^1 (1-x)^{n_r-1} x^{\beta-1} dx \end{aligned} \tag{4.12}$$

In order to compute the upper bound in (4.12), we define

$$\Theta_{\alpha,\beta} = \alpha \int_0^1 (1-x)^{\alpha-1} x^{\beta-1} dx$$

By observing that

$$\Theta_{\alpha+1,\beta} = \frac{\alpha+1}{\beta}\Theta_{\alpha,\beta+1},$$

$\Theta_{\alpha,\beta}$ is simply

$$\Theta_{\alpha,\beta} = \frac{\alpha!}{\prod_{k=0}^{\alpha-1}(\beta+k)} \tag{4.13}$$

Substituting (4.13) in (4.12) for $\alpha = n_r$, Pe_{avg} is bounded by

$$Pe_{\text{avg}} \leq \frac{N_e}{2}\frac{n_r!}{\beta^{n_r}} \tag{4.14}$$

Thus, the diversity order is equal to that of the full system diversity[27],[25], and a loss in SNR of about $10\log_{10}(n_r!)^{1/n_r}$ is observed.

The generalization of this bound will be illustrated in the following section.

4.2.2.2 Antenna selection performance when $m \geq 1$

Rearranging in descending order the variables r_i^2 leads to

$$r_{k_1}^2 \geq r_{k_i}^2 \geq \ldots \geq r_{k_m}^2,\ k_1,\ldots,k_m \in \{1,\ldots,m\}$$

Let us denote $\gamma_i = r_{k_i}^2$, $1 \leq i \leq m$, and $\gamma_0 = +\infty$. Introducing γ_i in (4.4), the average error probability is bounded by

$$Pe_{\text{avg}} \leq \frac{N_e}{2} \int_0^{\gamma_0} \int_0^{\gamma_1} \ldots \int_0^{\gamma_{m-1}} e^{-(\beta-1)\sum_{i=1}^{m}\gamma_i} p_{\gamma_1\ldots\gamma_m} \prod d\gamma_i \tag{4.15}$$

The joint probability density function (pdf) for the m random variables γ_i maximizing the SNR, is given by [3]

$$p_{\gamma_1\ldots\gamma_m}(\gamma_1,\ldots,\gamma_m) = m!\begin{pmatrix} n_r \\ m \end{pmatrix}[F(\gamma_m)]^{n_r-m}\prod_{i=1}^{m} p(\gamma_i) \tag{4.16}$$

where $F(\gamma_i)$ (respectively $p(\gamma_i)$) denotes the cdf (respectively pdf) of the random variable γ_i.

Providing the statistics of the variables r_i, so the variables γ_i are distributed as

$$\begin{aligned} F(\gamma_i) &= 1 - e^{-\gamma_i} \\ &\text{and} \\ p(\gamma_i) &= e^{-\gamma_i} \end{aligned} \tag{4.17}$$

Let $\tau_i = \exp(-\beta\gamma_i)$. Substituting (4.16) and (4.17) in (4.15), the upper bound of Pe_{avg} becomes

$$Pe_{\text{avg}} \leq \frac{N_e A_{n_r}^m}{2} \int_0^{\gamma_0} \tau_1 \ldots \int_0^{\gamma_{m-1}} \tau_m \left(1 - e^{-\gamma_m}\right)^{n_r-m} \prod d\gamma_i \tag{4.18}$$

where $A_{n_r}^m = \frac{n_r!}{(n_r-m)!}$ is the arrangement number.

Using the binomial theorem for $(1 - e^{-\gamma_m})^{n_r-m}$, inequality (4.18) can be written as

$$Pe_{\text{avg}} \leq \frac{N_e A_{n_r}^m}{2} \sum_{k=0}^{n_r-m} \kappa_{k,n_r-m} \int_0^{\gamma_0} \tau_1 \ldots \int_0^{\gamma_{m-1}} \tau_m e^{-k\gamma_m} \prod d\gamma_i \tag{4.19}$$

In order to evaluate the Pe_{avg} upper bound, we define the variable $I_{t,k},\ t \geq 1$ as

$$I_{t,k} = \int_0^{\gamma_{m-t}} \tau_{m-t+1} \ldots \int_0^{\gamma_{m-1}} \tau_m e^{-k\gamma_m} \prod_{i=m-t+1}^{m} d\gamma_i \tag{4.20}$$

Thus,

$$Pe_{\text{avg}} \leq \frac{N_e A_{n_r}^m}{2} \sum_{k=0}^{n_r-m} \kappa_{k,n_r-m} I_{m,k} \tag{4.21}$$

Using the recurrence method, equation (4.20) becomes

$$I_{t,k} = \int_0^{\gamma_{m-t}} \left(\left(\sum_{j=1}^{t-1} \Psi_{t,j,k} \right) + \Phi_{t,k} \right) d\gamma_{m-t+1} \tag{4.22}$$

where

$$\Psi_{t,j,k} = \frac{(-1)^{j-1}\exp(-j\beta\gamma_{m-t+1})}{(t-1-j)!(j-1)!}\frac{1}{\beta^{t-2}\left((t-j)\beta+k\right)}$$

and

$$\Phi_{t,k} = \frac{(-1)^{t-1}\exp((t\beta+k)\gamma_{m-t+1})}{\prod_{j=1}^{t-1}(j\beta+k)}$$

Note that $I_{m,k}$ can be seen as the exponential factor of $\Psi_{m+1,1,k}$ (since $\gamma_0 = +\infty$), so

$$I_{m,k} = \frac{1}{(m-1)!\beta^{m-1}(m\beta+k)} \tag{4.23}$$

Substituting (4.23) in (4.21) leads to

$$Pe_{\text{avg}} \leq \frac{N_e A_{n_r}^m}{2(m-1)!\beta^{m-1}} \sum_{k=0}^{n_r-m} \frac{\kappa_{k,n_r-m}}{(m\beta+k)} \tag{4.24}$$

The sum

$$\sum_{k=0}^{n_r-m} \frac{\kappa_{k,n_r-m}}{(m\beta+k)}$$

can be computed similarly as in (4.12) and it corresponds to

$$\frac{\Theta_{n_r-m+1,m\beta}}{n_r-m+1}.$$

Hence, we can write

$$Pe_{\text{avg}} \leq \frac{N_e n_r!}{2(m-1)!\beta^{m-1}} \frac{1}{\prod_{i=0}^{n_r-m}(m\beta+i)} \leq \frac{N_e n_r!}{2m!m^{n_r-m}\beta^{n_r}} \tag{4.25}$$

The upper bound (4.25) is compared to another derived in [25] for the average pairwise error probability. The corresponding average error probability is obtained by applying the union bound and considering only the neighbors, N_e, located at $d_{\min}$. This leads to

$$Pe_{\text{avg}} \leq \frac{N_e}{2}(\beta-1)^{-n_r}\left(\frac{m}{n_r}\right)^{-n_r} \tag{4.26}$$

In the following, the bounds in (4.25) and (4.26) are respectively referred to KK bound and GD bound. Both (4.25) and (4.26) show that the selection maintains the full system diversity, equal to the number of receive antenna before selection : n_r.

Let denote $\Delta_{\text{SNR}}(N_i \to N_f)$ the loss in SNR when decreasing the number of active antennas from N_i to N_f. When selecting m receive antennas among n_r, the loss in SNR $\Delta_{\text{SNR}}(n_r \to m)$ given by (4.25) is equal to

$$\Delta_{\text{SNR}}^{(\text{KK})}(n_r \to m) = \frac{10}{n_r}\log_{10}\left(\frac{n_r!}{m!m^{n_r-m}}\right) \tag{4.27}$$

Notice that

$$\frac{n_r!}{m!m^{n_r-m}} = \frac{n_r(n_r-1)\ldots(m+1)}{m^{n_r-m}} \leq (\frac{n_r}{m})^{n_r-m},$$

therefore it is clear that $\Delta_{SNR}^{(KK)}$ is upper bounded by $\Delta_{SNR}(n_r \rightarrow m)$ shown in (4.26) which is defined by

$$\Delta_{SNR}^{(GD)}(n_r \rightarrow m) = 10\log_{10}(\frac{n_r}{m}) \tag{4.28}$$

It is obvious that decreasing the number of selected antennas leads to an SNR loss. Let N_{f_1} and N_{f_2} be the number of selected antennas for two different times, $N_{f_1}, N_{f_2} \leq N_i$. To evaluate the loss in SNR while choosing N_{f_1} instead of N_{f_2}, we define the following parameter

$$\Delta_{SNR}(N_i,N_{f_1},N_{f_2}) \stackrel{def}{=} \Delta_{SNR}(N_i \rightarrow N_{f_1}) - \Delta_{SNR}(N_i \rightarrow N_{f_2}) \tag{4.29}$$

It is clear that $\Delta_{SNR}(N_i,N_{f_1},N_{f_2}) \geq 0$ if $N_{f_1} \geq N_{f_2}$ and $\Delta_{SNR}(N_i,N_{f_1},N_{f_2}) \leq 0$ otherwise.

4.2.2.3 Simulations results

We consider a quasi-static SIMO channel with $n_r = 4$ receive antennas and QPSK modulation applied at the transmitter. The channel is kept unchanged during a frame of 100 QPSK symbols. For each channel realization, the best n receive antennas maximizing the instantaneous SNR are selected.

By comparing (4.25) and (4.26) to simulation results, it is shown in Fig. 4.8 that the KK bound is more accurate than the GD bound for $m = 3, 2$. The loss in SNR as defined in (4.29), $\Delta_{SNR}^{(Sim)}(4,3,2)$ given by simulations, is equal to $\Delta_{SNR}^{(KK)}(4,3,2)$, whereas it is upper bounded by $\Delta_{SNR}^{(GD)}(4,3,2)$.

To compare the SNR loss for different values of m, we illustrate in Fig. 4.9 the required average transmit SNR to achieve an error probability of 10^{-4} for $m = 1,2,3,4$. Let $SNR(m)$ be the required SNR for m active antennas obtained from simulations. The required SNR for (4.25) is equal to $SNR(m) + K$, where K remains constant equal to 2.4 dB for all m values, whereas it equals $SNR(m) + V(m)$ for (4.28), where $V(m)$ depends on m value (e.g. $V(1)$=5.3 dB, $V(4)$=2.7 dB). Hence, the exact SNR loss is almost equal to that derived from (4.28), but it is upper bounded by that indicated in [25].

4.2.3 Antenna selection under different criteria

In order to evaluate the system performance using the proposed criterion (error probability approximation (3.20)), it is interesting to compare the performance obtained with those achieved using other existing selection criteria. The different considered selection criteria are given in the following. They consist in choosing the best set of antennas among $\begin{pmatrix} n_t \\ n \end{pmatrix} \times \begin{pmatrix} n_r \\ m \end{pmatrix}$ possibilities. For every subset p of active transmit/receive antennas, we denote $\tilde{\mathbf{H}}_p$ the associated channel.

- **Error probability criterion:**

For every subset p of transmit or receive antennas, compute the conditional error probability given in (3.20) when $n \leq m$ and the generalized version if $n > m$. Then choose the subset that minimizes the conditional error probability.

- **Capacity criterion:**

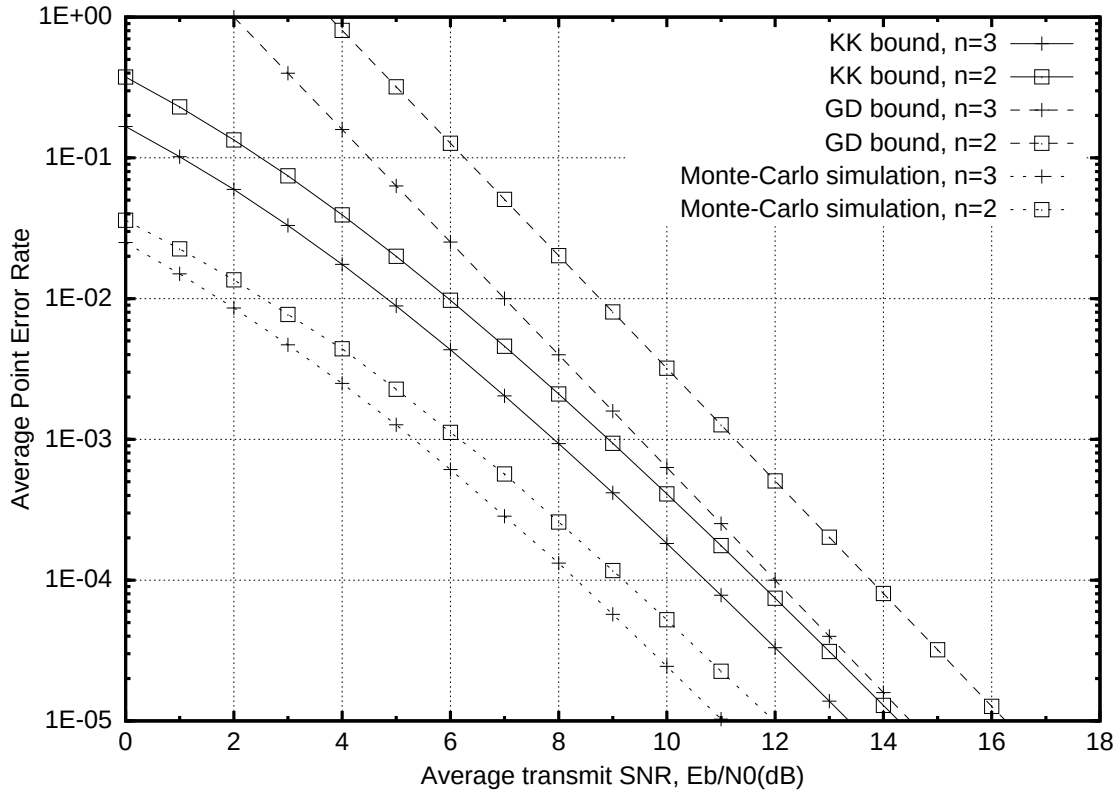

Figure 4.8: Average error probability for a 1×4 quasi-static system with receive selection.

For every subset p of transmit/receive antennas, compute the instantaneous capacity of the channel $\tilde{\mathbf{H}}_p$ assuming a Gaussian channel input

$$C_{\text{inst}}^{p} = \log \det \left(I_n + \frac{E_s}{2N_0 n} \tilde{\mathbf{H}}_p \tilde{\mathbf{H}}_p^{\dagger} \right)$$

where E_s denotes the total transmit energy, and then choose the subset with the largest C_{inst}^{p}.

During a frame transmission ($\tilde{\mathbf{H}}$ is fixed), the channel model given by equation (4.1) can be represented in the real space by

$$\mathbf{y} = \mathbf{x} + \boldsymbol{\nu} \tag{4.30}$$

where $\mathbf{x} \in \mathbb{R}^{2n}$ whose components are the real and imaginary parts of the complex vector $\mathbf{s}\tilde{\mathbf{H}}$, denotes the input of the scalar Gaussian channel (4.30).

For a scalar additive Gaussian channel, Shamai et al propose in [18] the following theorem.

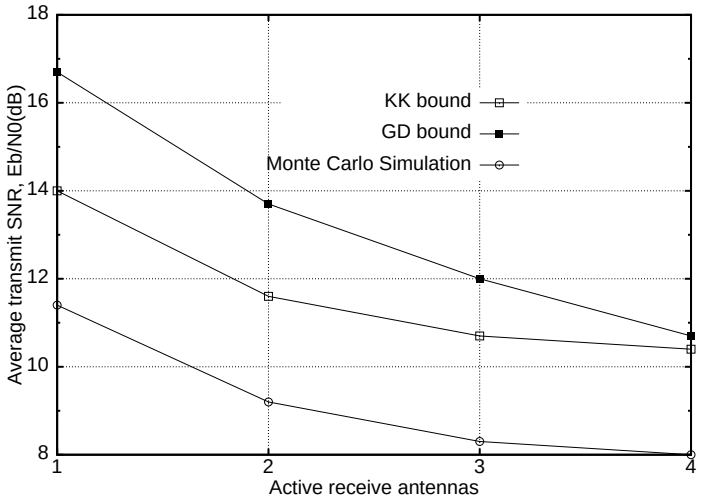

Figure 4.9: Variation of the required transmit SNR w.r.t the number of selected antennas at the receiver for an error probability = 10^{-4}.

Theorem 1 *For every input distribution $P_{\mathbf{x}}$ with $E(\mathbf{x}^2) < \infty$ and every snr,*

$$\frac{d}{dsnr} I(snr) = \frac{1}{2} mmse(snr) \tag{4.31}$$

where $mmse(snr) = E\left(\mathbf{x} - E\left(\mathbf{x}/\mathbf{y}; snr\right)\right)$ denotes the minimum mean-square-error in estimating the input given the output and $I(snr)$ represents the input-output mutual information of the channel given by (4.30).

Thus, the application of the capacity criterion leads to the maximization of the channel capacity which allows to minimize the mmse as indicated in (4.31). The validity of this conclusion will be verified in the following via simulation results.

- **Minimum Euclidean distance criterion:**

Heath et al proposed in [30] a selection criterion based on minimum error rate. The authors in [30] considered the error probability upper bound given in (4.32) by :

$$Pe \leq \left(2^{nb} - 1\right) Q\left(\frac{d^c_{min}}{2\sqrt{N_0}}\right) \tag{4.32}$$

where $b = \log_2 \mathrm{M}$, and derive a selection criterion that minimizes this bound. The criterion proposed in [30] consists in choosing the subset of antennas that maximizes the minimum Euclidean distance of the constellation $C^{\tilde{\mathbf{H}}_p}$ denoted d^c_{min}. The computation of d^c_{min} requires a search over $2^{nb-1}\left(2^{nb} - 1\right)$ distances which can be prohibitive for large constellations. For example, when 16-QAM modulation is applied, 32640 distances have to be computed when only 2 antennas are used at the transmitter. The comparison of the complexity computation between (3.20) and (4.32) shows that the latter is more complex when $M \geq 16$ and especially

when $n \geq 3$.
In [30], simulation results show that this criterion is better than capacity criterion for ML receiver.

- **Maximum post-processing SNR:**

This criterion is considered for ZF and MMSE receivers [29].
For a ZF receiver, compute the pseudo-inverse matrix $\mathbf{G}$ for every subset p,

$$\mathbf{G}_p^{(ZF)} = \tilde{\mathbf{H}}_p^{\dagger} \left(\tilde{\mathbf{H}}_p \tilde{\mathbf{H}}_p^{\dagger} \right)^{-1}$$

The post-processing SNR for a given stream k, denoted $SNR_p^{(k)}$, corresponding to the subset p is

$$SNR_p^{(k)} = \frac{E_s}{2N_0 n \left[\left(\tilde{\mathbf{H}}_p \tilde{\mathbf{H}}_p^{\dagger} \right)^{-1} \right]_{kk}}$$

where $\left[\left(\tilde{\mathbf{H}}_p \tilde{\mathbf{H}}_p^{\dagger} \right)^{-1} \right]_{kk}$ denotes the k^{th} diagonal element of the matrix $\left(\tilde{\mathbf{H}}_p \tilde{\mathbf{H}}_p^{\dagger} \right)^{-1}$. The best subset p is the one that corresponds to $\max_p \min_{1 \leq k \leq n} SNR_p^{(k)}$.

For an MMSE receiver, the pseudo-inverse matrix $\mathbf{G}$ for every subset p is given by

$$\mathbf{G}_p^{(MMSE)} = \tilde{\mathbf{H}}_p^{\dagger} \left(\tilde{\mathbf{H}}_p \tilde{\mathbf{H}}_p^{\dagger} + \frac{2N_0}{E_s} I_n \right)^{-1}$$

The corresponding post-processing SNR for the stream k is

$$SNR_p^{(k)} = \frac{E_s}{2N_0 n \left[\tilde{\mathbf{H}}_p \tilde{\mathbf{H}}_p^{\dagger} + \frac{2N_0}{E_s} I_n \right]_{kk}^{-1}} - 1$$

4.2.4 Simulation results

In this section, the selection criteria described above are compared using Monte Carlo simulations for transmit or receive selection. The case which combines both selection sides is not considered in this section. We assume that QPSK modulation is applied on all transmit antennas. System performance are illustrated in terms of average PER (Point Error Rate). The matrix $\mathbf{H}$ is selected at random and kept unchanged during one frame (i.e. $T_c = 100$ channel uses). The selection computation is achieved every T_c periods and selects the optimal sub-matrix $\tilde{\mathbf{H}}_p$ to be used during the frame transmission. The average PER is plotted versus the average transmit signal-to-noise ratio (SNR). Notice that the choice of transmit SNR instead of receive SNR is justified as follows. The antenna selection modifies the initial variance of the coefficients h_{ij}. Therefore, to find the average receive SNR, we need the evaluation of the channel coefficients variance when using the selection.
Note that the variation of the average PER in function of the received SNR needs the evaluation of the channel coefficients variance, since the selection modifies the initial variance of the coefficients h_{ij}.

The antenna selection based on different criteria is applied for different receiver schemes, namely ML, MMSE, and OSuIC receivers.
We consider the following pairs: (n_t,n_r) = (3 , 2) and (5 , 4). The transmit (respectively receive)

selection consists in choosing the $n_t - 1$ (respectively $n_r - 1$) best transmit (respectively receive) antennas for both cases.

To emphasize the advantage of antenna selection, we plot for each scenario the performance of uncoded MIMO system without selection, i.e. $(n_t - 1) \times n_r$ when transmit selection is performed, and $n_t \times (n_r - 1)$ when receive antenna selection is chosen.

4.2.4.1 ML receiver

Figures 4.10 and 4.11 illustrate the performance when selection is performed at transmit side and receive side respectively. Each figure depicts the performance of 2×2 and 4×4 quasi-static MIMO channel.

By comparing with the non selection case, it is noticed that the selection creates a new diversity order for all criteria. Indeed, one could notice that the diversity becomes 3 instead of 2 when choosing the 2 best antennas among 3, and equals 5 instead of 4 when 4 antennas are selected from 5. This additional diversity is independent from the selection side. An SNR improvement is achieved also over system without selection. For example, when transmit selection is chosen for (3,2) MIMO system, a gain greater than 7 dB is noticed.

While observing the performance with different selection criteria, it is noticed in Figs. 4.10 and 4.11 that our proposed criterion minimizes the error probability for all SNR range. The minimum Euclidean distance criterion achieves almost the same performance as the best one. This means that the first term of (3.20), for which d_i equals the minimum Euclidean distance of the constellation $C^{\tilde{\mathbf{H}}_p}$, is sufficient to achieve the antenna selection.

The capacity criterion is the worst. A loss of about 2 dB is noticed over the above criteria at PER = 10^{-5} when transmit selection is considered.

The comparison between transmit and receive selection simulation results in Figs. 4.10 and 4.11 shows that error probability and minimum Euclidean distance criteria give better performance when applying the selection at the transmitter, with a gain of 2 dB at PER=10^{-5}. Indeed, both criteria consist in minimizing the error probability by reducing the inter-channel interference (ICI) among the spatial channels.
Unlike the above criteria, performance with capacity criterion is almost independent from the selection side.

4.2.4.2 Linear MMSE receiver

Simulations have been carried out with a linear MMSE detector at the receiver. Figure 4.12 illustrates the performance of 4×4 quasi-static MIMO system for different antenna selection criteria at both sides.

By comparing the different selection criteria, it is noticed in Fig. 4.12 that the SNR and the capacity provide the best performance. However, a little gain is achieved by the former over the latter, for both transmit and receive selection. The selection introduces an additional diversity for both criteria, so that the system diversity order becomes 2 instead of 1. The criterion based on the minimization of the ML error probability is not adapted to the studied system with MMSE detection. That is why it presents the worst performance. The diversity remains lower

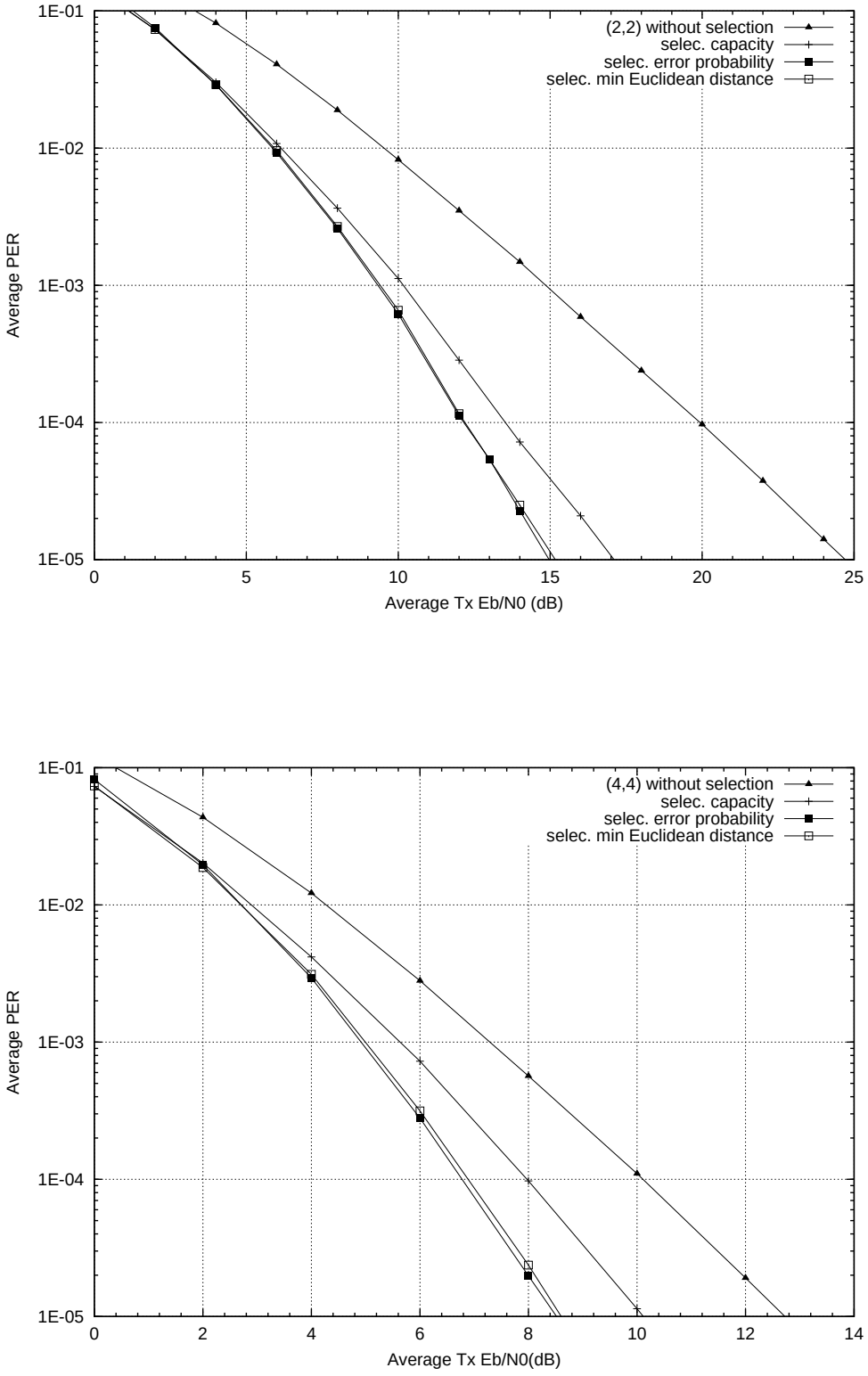

Figure 4.10: Average error probability with transmit selection and ML receiver. Select 2 antennas among 3 Tx antennas (on the top). Select 4 antennas among 5 Tx antennas (on the bottom).

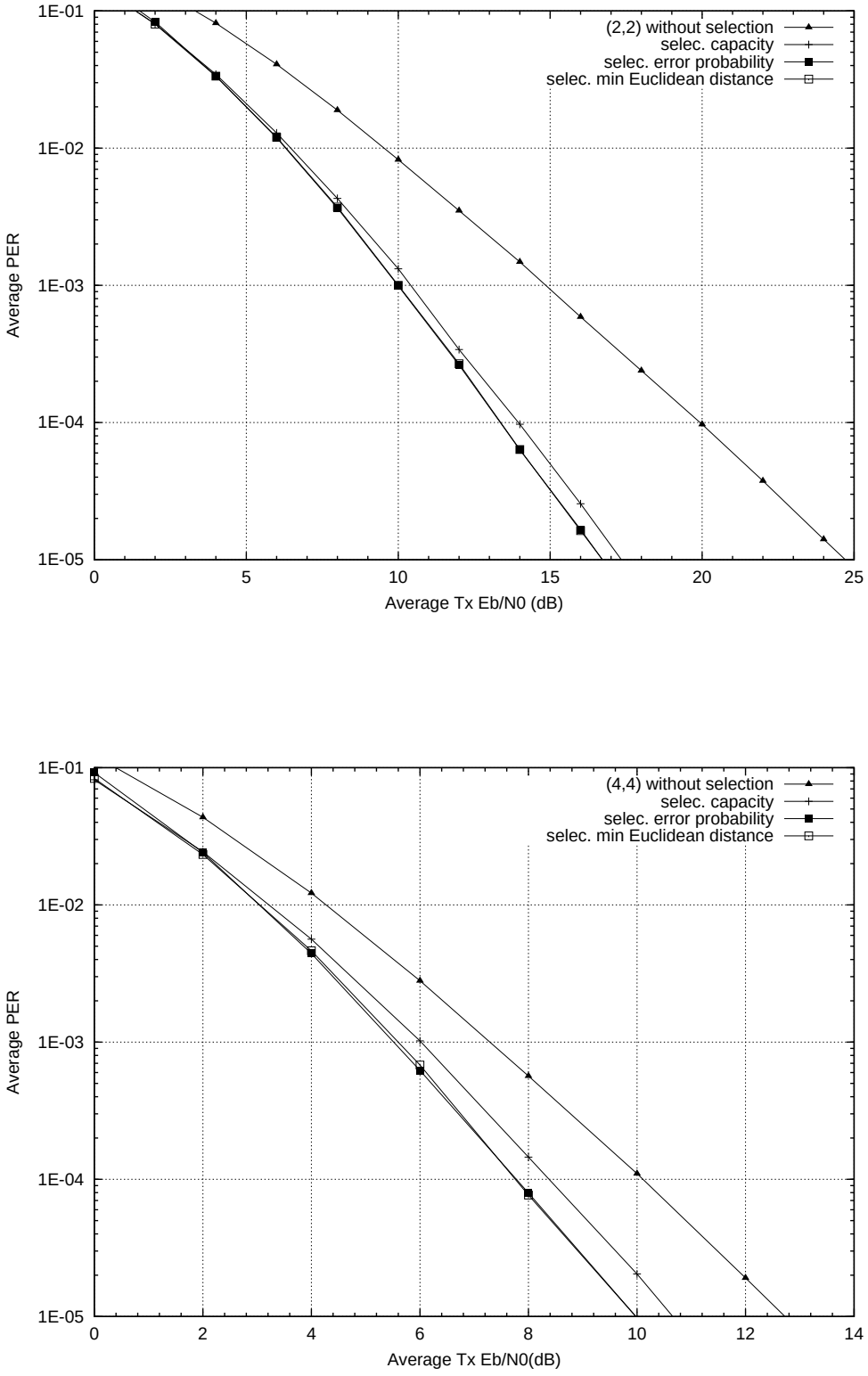

Figure 4.11: Average error probability with receive selection and ML receiver. Select 2 antennas among 3 Rx antennas (on the top). Select 4 antennas among 5 Rx antennas (on the bottom).

than 2 for this criterion, whereas a gain of 5 dB is noticed at PER = 10^{-3} over the no selection case for both transmit and receive selection.

4.2.4.3 MMSE-OSuIC receiver

In this section, we assume a MMSE-OSuIC detector at the receiver. Both transmit and receive selection choose the 2 best antennas among 3. Simulation results are plotted in Fig. 4.13 for 2×2 quasi-static MIMO system. The performance of 2×2 system with ML detection without selection is plotted too.

While comparing the two examined selection criteria, we notice that the proposed criterion based on error probability gives almost the same performance as the capacity at low SNR ($E_b/N_0 \leq 12\ dB$), whereas a loss over the capacity performance is observed at high SNR. The diversity order of no selection case is maintained below 2, when using the error probability, whereas it is improved to 2 when applying capacity criterion. Thus, the proposed criterion performs better with MMSE-OSuIC than with linear MMSE at low SNR. This fact can be explained when comparing the ML and MMSE-OSuIC receivers. For example, for a 2×2 system, Fig. 4.13 shows that the MMSE-OSuIC performance is close to that of the ML receiver at low SNR. Therefore, the ML error probability criterion can be used in this case. As for the linear MMSE receiver, the application of the selection at the receiver does not change significantly the performance comparing to the selection at the transmitter.
Based on simulation results given in the previous sections, it is noticed that the application of the capacity as a transmit or a receiver selection criterion provides a selection diversity gain for all the receiver schemes as shown in theorem (4.31).

Conclusions

In this chapter, we presented two applications of the error probability approximation derived in chapter 3 for uncoded MIMO systems, namely adaptive modulation and antenna selection. We started by proposing an efficient algorithm to adapt modulations while maximizing the total spectral efficiency and satisfying a constraint on error probability. This algorithm considers a short list of modulation combinations and uses the dichotomy method to go through the list. This leads to a reduced complexity. Finally, the designed adaptive modulation algorithm was compared to another algorithm using the simple bound (3.4) and to the non-adaptive scheme. In both comparisons, the gain of our adaptive scheme was noticed regarding the total spectral efficiency.
Then, the performance of SIMO systems with antenna selection were studied. We showed with analytical expressions that the diversity is kept while activating only some antennas and we proposed a bound for such systems. Then, we presented the antenna selection algorithm with our proposed selection criterion as well as with other existing criteria. This algorithm is based on an exhaustive search over all the antenna combinations. Next, the performance with antenna selection were compared to the non-adaptive scheme with the same number of active antennas. The benefit of the adaptive technique was observed in diversity order and in SNR gain. We noticed via simulation results that the proposed criterion to select the best set of antennas provides the best performance (compared to other existing selection criteria) when detection is based on ML criterion. However, the same criterion gives bad results while using sub-optimal receivers (ZF, MMSE, OSuIC) comparing to the other criteria. Indeed, the proposed selection criterion was derived assuming a ML detection. That's why, it performs better for the optimal receiver than for the sub-optimal receivers.

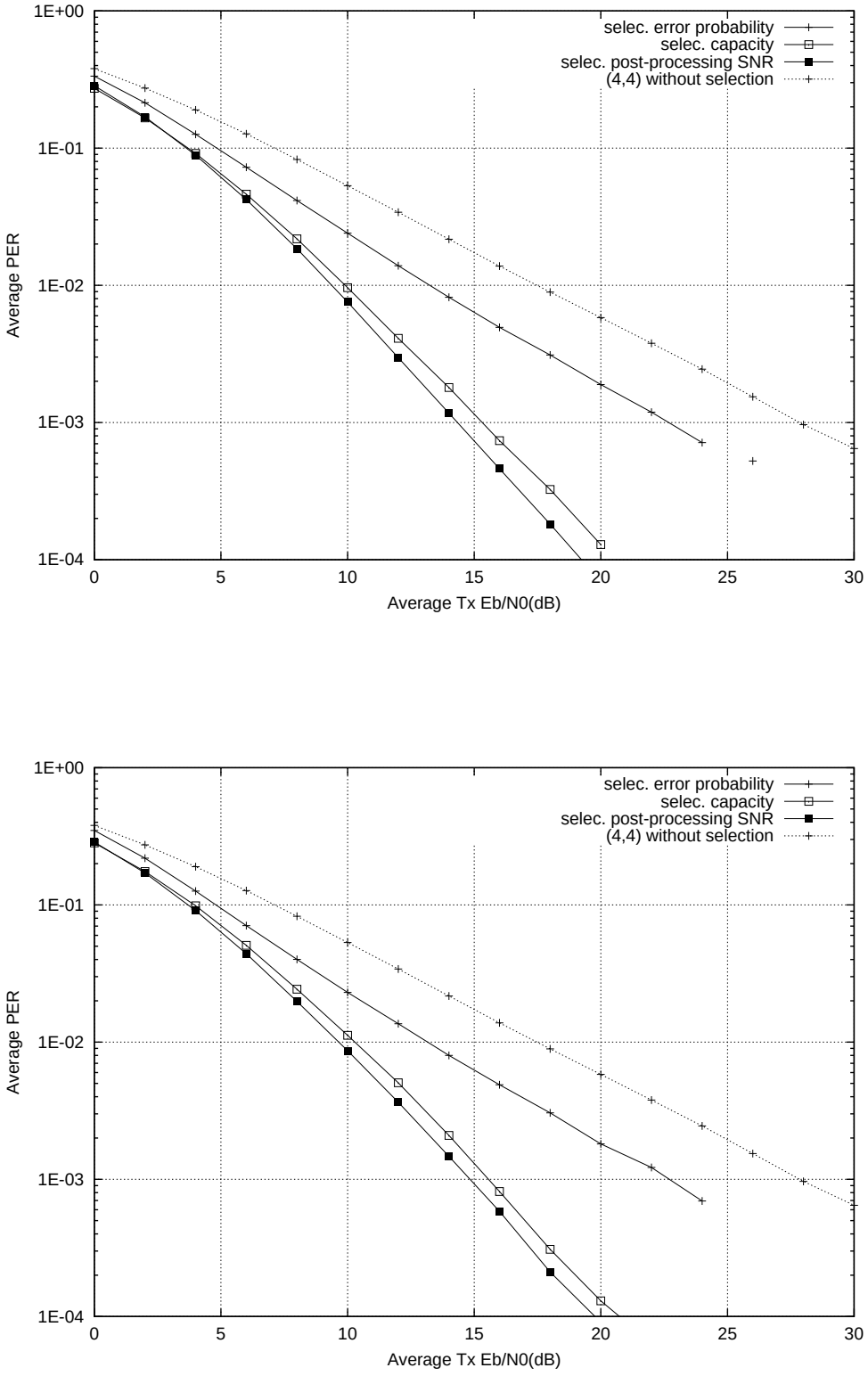

Figure 4.12: Average error probability with transmit/receive selection and MMSE receiver. Select 4 among 5 Tx antennas (on the top). Select 4 among 5 Rx antennas (on the bottom).

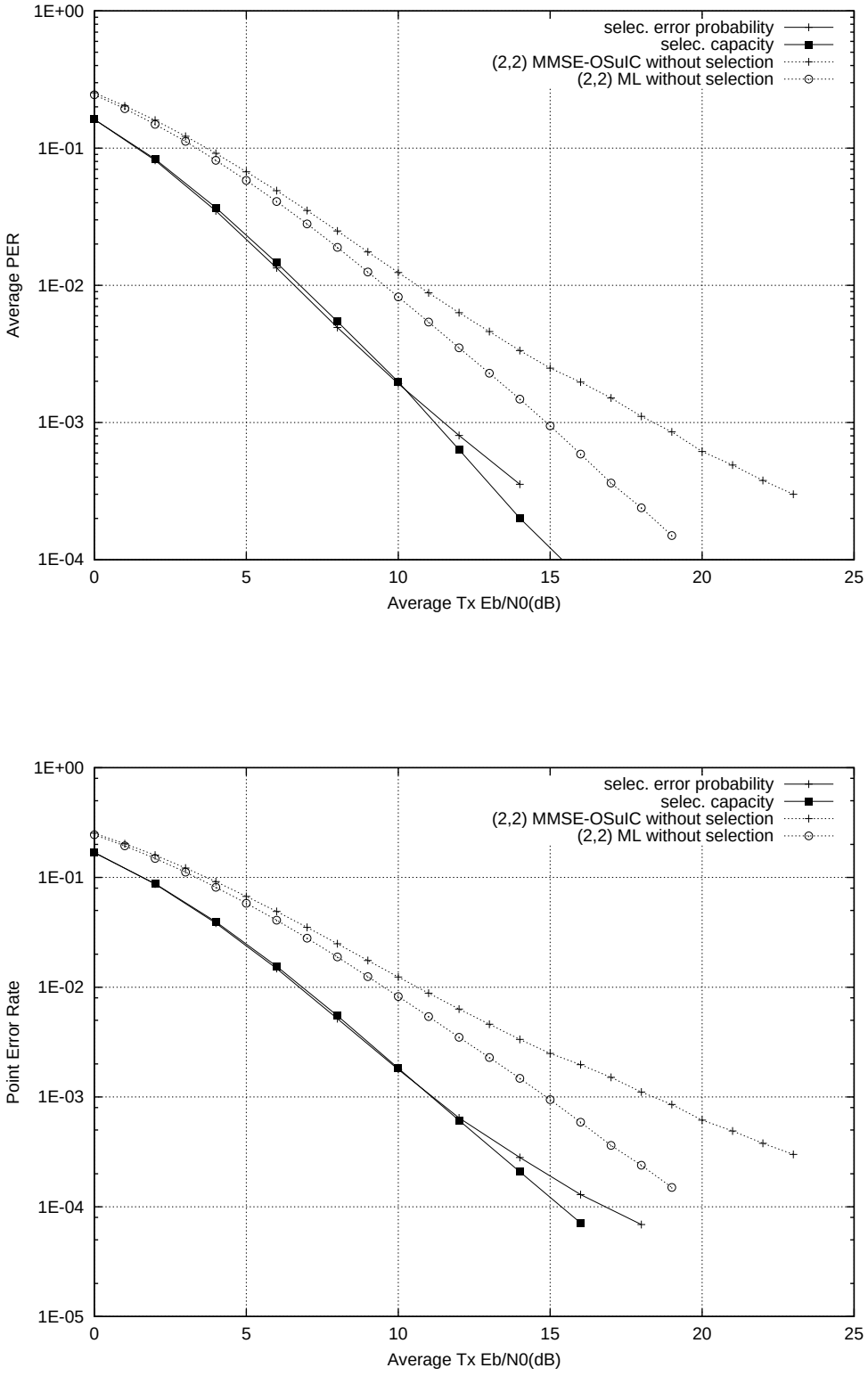

Figure 4.13: Average error probability with transmit/receive selection with MMSE-OSuIC. Select 2 antennas among 3 Tx antennas (on the top). Select 2 antennas among 3 Rx antennas (on the bottom).

It appears that both adaptive techniques improve the performance in MIMO systems but increase the complexity computation due to the search of the appropriate adaptive parameters, especially for high number of antennas. One approach to reduce this complexity will be proposed in the next chapter.

Chapter 5

Classification of multiple antenna channels

Introduction

The material described in this chapter can be applied to any problem that admits a lattice representation. The great interest of the research community and public in multiple antenna digital transmission [7] made us study the Hermitian forms classification and use it on that particular subject. The classification of multiple-input multiple-output (MIMO) frequency non-selective fading channels has a considerable importance in information and communication theory. It consists in associating to the continuous set of MIMO channels a discrete set of representatives (or centroids), called codebook. Each channel will be then represented by the nearest element of the designed codebook. The set of channels corresponding to the same centroid defines a class.
Some potential applications for the classification would be adaptive modulation and adaptive channel coding in wireless local area networks and in 3G-4G mobile radio data networks. In this case, the choice of the optimal adaptive parameters needs only the determination of the nearest centroid. Then, the selected parameters for this centroid could be applied. Additional applications may be also related to other closed-loop (which require a CSI at the transmitter) systems, e.g. beamforming [45], [34], water-filling [21], [59], etc.
The classification algorithm given in this chapter is valid for both correlated and uncorrelated frequency non-selective MIMO. No assumption on channel distribution is required.

This chapter is organized as follows. First, section 5.1 recalls the procedure of the quantization (in our terminology classification) as well as the related parameters (e.g. codebook, centroids, training data samples, class, metric, etc). It also illustrates the famous quantization algorithm: Lloyd algorithm that is used to design our MIMO classification algorithm. Second, section 5.2 focuses on the classification of MIMO channels. First, it introduces the MIMO system model on which the classification will be based. Then, it describes our classification scheme. This scheme considers the Hermitian forms corresponding to the MIMO channels. That is why, we introduce in section 5.3 some basic notions from algebra and differential geometry dealing with the space of Hermitian forms. These concepts are used in section 5.4 to describe our proposed MIMO classification algorithm and to derive a metric to compute the distance between Hermitian forms associated to MIMO channels. This algorithm is then extended to lattices in

section 5.5. Section 5.6 compares the derived metric to the natural one based on the Euclidean distance by illustrating some results about the generated centroids, the population of each class, etc. Simulation results are also given to validate the designed classification by measuring the resemblance between MIMO channels and their associated centroids based on Voronoi regions and error probabilities. Finally, we propose to apply the classification for beamforming, as an example of closed-loop MIMO systems, to estimate the channel at the transmitter. At the end, simulation results are exposed to compare the error probability when using the classification to that when assuming a perfect CSI.

In this chapter, we use some definitions and parameters from lattice theory and quadratic forms theory which are introduced in chapter 2.

5.1 Quantization

Quantization refers to the process of approximating the continuous set of values of an arbitrary source with a finite (preferably small) set of values [16]. This set is known as a codebook and its elements are called centroids.

The quantization process needs the definition of a relevant metric to find the distance between the input data and the different centroids. The representative of each data input is the one which minimizes the chosen metric. A good quantizer should represent the original data with minimum loss or distortion. This distortion is generally defined by the mean square distance

$$MSD = \frac{1}{card(\{\mathbf{X}\})} \sum_{\mathbf{X}} d^2(\mathbf{X},\hat{\mathbf{X}}) \tag{5.1}$$

where the set $\{\mathbf{X}\}$ denotes the input data set, $card(\{\mathbf{X}\})$ is its cardinality and $\hat{\mathbf{X}}$ is the representative of the element $\mathbf{X}$.
It is clear that the quantization distortion depends on the codebook size. Thus, the huger this codebook is, the smaller the distortion is. Therefore, the user should choose the codebook size according to the envisaged application and the related constraint on distortion.

The common way to design the codebook for quantization is to generate a large set of data samples, called training database, and update iteratively an initial codebook, in order to decrease the mean square distance, based on the database.
One of the best known methods for the codebook design is the Lloyd algorithm [19][42]. The Lloyd algorithm is iterative. It starts with an initial set of centroids (or codebook), that are chosen randomly, and modifies them through a sequence of iterations.
It works as follows: Given any set of N centroids, for each centroid $\hat{\mathbf{X}}$, let $C(\hat{\mathbf{X}})$ denote the set of data points for which $\hat{\mathbf{X}}$ is the nearest representative. In the next iteration of the algorithm, each old centroid $\hat{\mathbf{X}}$ is replaced (providing an update rule) by the new centroid of $C(\hat{\mathbf{X}})$ and then the set $C(\hat{\mathbf{X}})$ is updated by recomputing the distance from each point to its nearest centroid. These steps are repeated until convergence of the algorithm is achieved.

As long as successive iterations of the Lloyd algorithm continue to generate new centroids, the mean square error strictly decreases. Unfortunately, the Lloyd algorithm is sensitive to the choice of the initial codebook.

As an example we take a source that generates complex Gaussian random variables and we

intend to classify these variables by finding the best representative. The number of classes, or equivalently the size of the codebook, is equal to 8. By applying the Lloyd algorithm on that source, the classification results are depicted on Fig. 5.1. This figure shows 8 regions separated by continuous lines. To each region, a representative or centroid, denoted C_i, is associated. Given an input variable, the centroid that is chosen to represent it is the one in the same Voronoi region. The centroid C_x is determined to be the closest in Euclidean distance from the input variable x, that is

$$C_x = arg \min_{C_j} \|x - C_j\|$$

In the sequel, we focus on the quantization/classification of MIMO channels. Thus, we need a metric to compute the distance between each data sample and the different centroids. Also, a way to built the codebook is required.

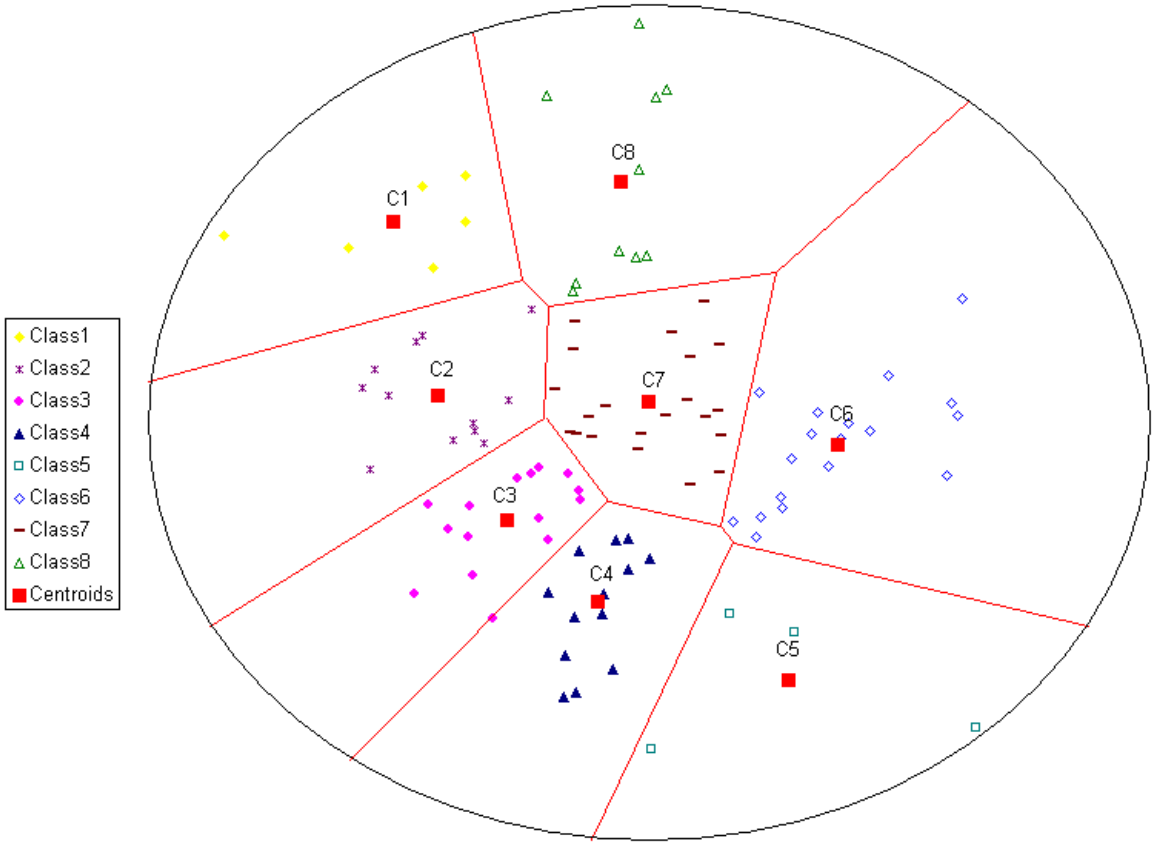

Figure 5.1: An example of quantization of complex Gaussian random variables.

5.2 MIMO channels classification

This section introduces first the system model which is used for the classification. Then, it presents the proposed classification scheme for MIMO channels.

5.2.1 System model

Let us briefly recall the mathematical model for a multiple antenna channel [7] and introduce some notations. We restrict our study to a square channel where the number n_t of transmit antennas is equal to the number n_r of receive antennas. Let $n = n_t = n_r$. Unlike chapters 3 and 4, matrices and vectors are in column convention. The input-output model is given by

$$\mathbf{r} = \mathbf{H}\mathbf{z} + \boldsymbol{\nu} \tag{5.2}$$

where:

- the transmitted vector $\mathbf{z}$ belongs to $\mathbb{Z}[i]^n$, $\mathbb{Z}[i]$ being the ring of Gaussian integers
- $\boldsymbol{\nu} \in \mathbb{C}^n$ is an additive white Gaussian noise
- $\mathbf{H} = [h_{ij}]$ is an $n \times n$ matrix defining the MIMO channel coefficients
- $\mathbf{r} \in \mathbb{C}^n$ is the received vector.

We suppose that $\mathbf{H}$ is perfectly known at the receiver side. No channel state information is assumed at the transmitter because, in most imaginable applications, the classification will be performed at the receiver side. A widely used model assumes that the coefficients h_{ij} are complex Gaussian distributed with zero mean and unit variance (as shown in chapter 1).

In the sequel, we assume that $\det(\mathbf{H}) = 1$. In fact, two channel matrices $\mathbf{H}_1$ and $\mathbf{H}_2$ related by $\mathbf{H}_1 = c\mathbf{H}_2$ generate two equivalent lattices (definition 10 in section 2.1.1). Then if $\det(\mathbf{H}_1) \neq 1$, we can consider $\mathbf{H}_2 = \frac{1}{\sqrt[n]{\det(\mathbf{H}_1)}}\mathbf{H}_1$ since $\det(\mathbf{H}_2) = 1$. Thus, it is necessary to normalize the fundamental volume of lattices in order to avoid the scaling factor. This corresponds to adding a multiplicative factor to the signal-to-noise ratio (a simple shift when expressed in dB). The probability distribution of $\det(\mathbf{H})$ can be further taken into account in potential applications of the proposed classification.

5.2.2 Classification scheme

The main procedure of the proposed algorithm is illustrated in Fig. 5.2. Given the number of transmit and receive antennas, given the number of classes to be distinguished, the classification algorithm runs in its training phase on a large number M of some training instances. Once a codebook of K centroids is built, any instance $\mathbf{H}$ can be quantized to the nearest class centroid. The classification needs a metric and an update rule as in the classical multidimensional Lloyd also known as k-Means clustering algorithm [19][42].

A matrix $\mathbf{H}$ such that $\det(\mathbf{H}) = 1$ generates a complex lattice $\Lambda(\mathbf{H})$ with a normalized fundamental volume [15]. The lattice $\Lambda(\mathbf{H})$ is associated to the Hermitian form $\mathbf{z}^\dagger\mathbf{H}^\dagger\mathbf{H}\mathbf{z}$, where $\mathbf{A}^\dagger$ denotes the transpose conjugate of $\mathbf{A}$. Therefore, our proposed classification algorithm will consider the Hermitian forms corresponding to the MIMO channels. As a consequence, we need some basic mathematical notions about the structure of the Hermitian forms space which are exposed in the next section.

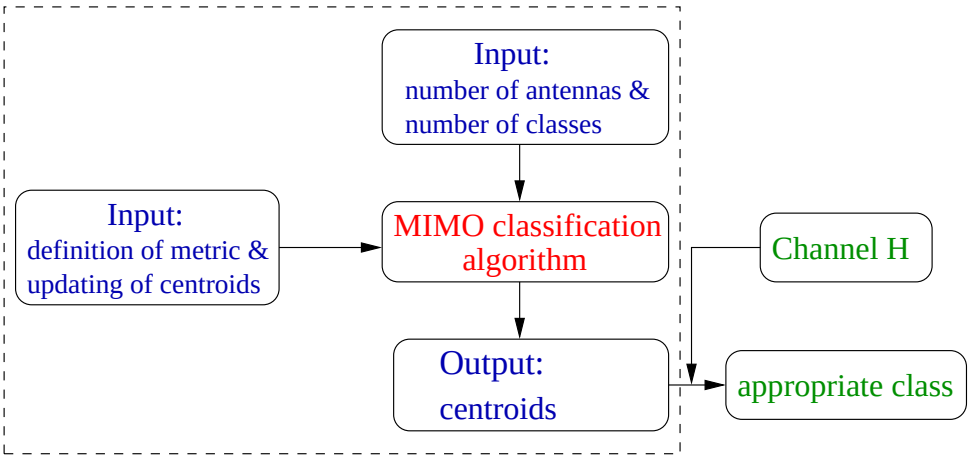

Figure 5.2: The procedure of MIMO classification.

5.3 Some basic mathematical notions

5.3.1 Some algebra concepts

This section recalls some algebra notions which are used later.

Let F be a field, mainly $F = \mathbb{R}$ or $\mathbb{C}$ and $M_n(F)$ be the set of $n \times n$ matrices in F. Some useful definitions from algebra are introduced in the following.

Definition 11 *(**Some groups of** $M_n(F)$)*

The General linear group *: $GL_n(F)$ of size n is the set of $n \times n$ invertible matrices. $GL_n(F)$ with the operation of ordinary matrix multiplication, $(GL_n(F),\times)$, is a group.*

The Special linear group *: $SL_n(F)$ is a subgroup of $GL_n(F)$ of all matrices with determinant +1.*

The Unitary group *: $U(n)$ is the subgroup of $GL_n(\mathbb{C})$ of unitary matrices $\mathbf{M}$ such that $\mathbf{M}\mathbf{M}^\dagger = \mathbf{I}_n$.*

The Special unitary group *: $SU(n)$ is the subgroup of $U(n)$ of matrices with unit determinant.*

Definition 12 *(**Equivalence relation and set partitions**):*

Equivalence relation *: An equivalence relation on a set X is a binary relation on X which is reflexive, symmetric, and transitive. That is, if the relation is denoted by the symbol "$\sim$",*
$\forall a, b, c \in X$

1. *$a \sim a$ (reflexivity)*
2. *if $a \sim b$ then $b \sim a$ (symmetry)*
3. *if $a \sim b$ and $b \sim c$ then $a \sim c$*

*A **partition** P_X of a set X is a set of subsets of X such that :*

1. *No element of P_X is empty : $\forall s \in P_X, s \neq \emptyset$.*

2. *The union of the elements of P_X is equal to X : $X = \bigcup_{s \in P_X}$.*

3. *The intersection of any two distinct elements of P_X is empty : $\forall s_1, s_2\ (s_1 \neq s_2) \in P_X, s_1 \cap s_2 = \emptyset$.*

Every equivalence relation on X defines a partition of X into subsets called ***equivalence classes****: all elements equivalent to each other are put into one class. Conversely, if the set X can be partitioned into subsets, then we can define an equivalence relation $\sim$ on X by the rule "$a \sim b$* if and only if *a* and *b* lie in the same subset".
The set of all equivalence classes in X for an equivalence relation $\sim$ is usually denoted as $X/\sim$ and called the quotient set *of X by $\sim$.*

If G is a group, H a subgroup of G, and x an element of G, then

1. *$xH = \{xh \mid h \in H\}$ is a* ***left coset*** *of H in G,*

2. *$Hx = \{hx \mid h \in H\}$ is a* ***right coset*** *of H in G.*

The left (respectively right) cosets of H in G are the equivalence classes under the equivalence relation on G given by $x \sim y$ if and only if $y \in xH$ (respectively $y \in Hx$).

Definition 13 ***(Group action)***

A group G is said ***to act on a set*** *X when there is a map ϕ from $G \times X$ to X such that :*

1. *$\forall x \in X, \phi(e,x) = x$ where e stands for the identity element of G*

2. *$\forall g_1, g_2 \in G, \phi(g_1,\phi(g_2,x)) = \phi(g_1.g_2,x)$*

In this case ϕ is called a ***left group action****.*

This action induces an equivalence relation $\sim$ such that

$$\forall x,y \in X, x \sim y \iff \exists g \in G, y = \phi(g,x)$$

In the special case when G is a subgroup of X, a ***natural action*** *of G on X could be given by*

$$\phi(g,x) = g.x,\ g \in G, x \in X$$

The corresponding quotient set $G\backslash X$ is the set of the right cosets of G in X.

The action G on X is called ***transitive*** *if for any two $x, y \in X$, there exists a $g \in G$ such that $gx = y$. In particular, when there exists precisely one $g \in G$ such that $gx = y$, the action G on X is then both transitive and free, and it is called* ***regular*** *or simply* ***transitive****. In this case, X is known as a principal* ***homogeneous space*** *for G.*

Consider a group G acting on a set X. The ***orbit*** *of a point $x \in X$ is the set of elements of X to which x can be moved by the elements of G. The orbit of x is denoted by Gx:*

$$Gx = \{g.x \mid g \in G\}$$

The defining properties of a group guarantee that the set of orbits of X under the action of G form a partition of X. For example, a transitive group action implies that there is only one group orbit equal to X. The associated equivalence relation is defined by saying $x \sim y$ iff there exists a $g \in G$ with $gx = y$.

The orbits are then the equivalence classes under this relation; two elements x and y are equivalent iff their orbits are the same, i.e. $Gx = Gy$.
The set of all orbits of X under the action of G is written as X/G or $G\backslash X$, and is called the ***quotient of the action****; in geometric situations it may be called the* ***orbit space****.*

Some elements of a group G acting on a space X may fix a point x. These group elements form a subgroup called isotropy group of x, defined by

$$G_x = \{g \in G \mid gx = x\}$$

For example, consider the group $SO(3)$ of all rotations of a sphere S^2. Let x be the north pole (0,0,1). Then, as illustrated in Fig. 5.3, a rotation which does not change x must turn around the usual axis, leaving the north pole and the south pole fixed. These rotations form the isotropy group for both north and south poles.

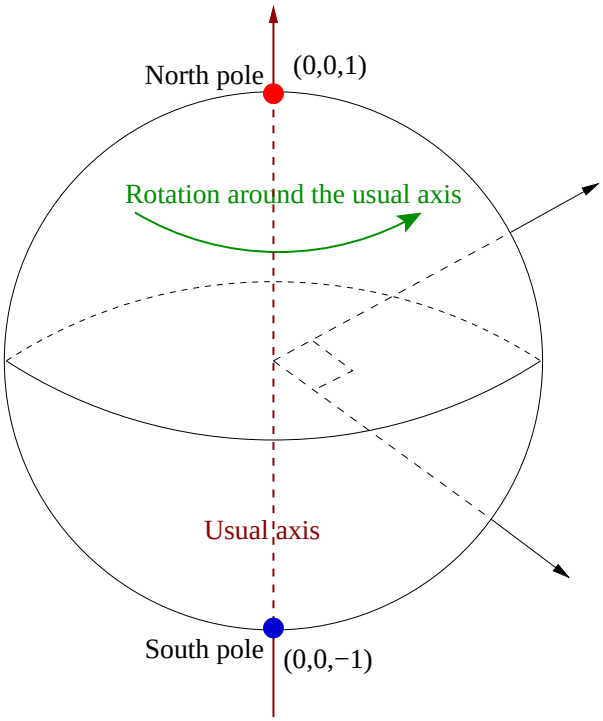

Figure 5.3: An example of isotropy group. $X = S^2$ and $G = SO(3)$.

When two points x and y are on the same group orbit, say $y = gx$, then the isotropy groups are conjugate subgroups. More precisely, $G_y = gG_xg^{-1}$. In fact, any subgroup conjugate to G_x occurs as an isotropy group G_y to some point y on the same orbit as x.

Let ϕ be the group action of a group G on a set X. The action ϕ is ***irreducible*** *if there are no nontrivial subspaces in X that are invariant by this action. The unique subspaces which are invariant by the action of ϕ are the entire space X and the null space.*

5.3.2 Some definitions from differential geometry

Some notions of differential geometry are also needed for MIMO classification study to design a new distance between Hermitian forms.

5.3.2.1 Differentiable manifolds

Definition 14 *(Manifold)*

*A **manifold** is a space that is locally like an Euclidean space $\mathbb{R}^n$, but globally its structure may be more complicated.*
To illustrate this idea, consider the surface S of a sphere. Locally, an open subset of S resembles to an open subset of $\mathbb{R}^2$, which is not true globally.

Definition 15 *(Topological manifold)*

*S is a **topological manifold** if*

1. *S is a Hausdorff topological space. This means that S is a topological space in which two different points can be separated by disjoint open sets.*

2. *$\forall p \in S$, $\exists$ an open subset U of S containing p, and an homeomorphism (a bijective continuous function whose inverse is also continuous) ϕ of S onto an open subset of $\mathbb{R}^n$.*

We say that n is the dimension of the manifold S, and the pair (U,ϕ) is an open chart, known also as a system of local coordinates, on S.

Definition 16 *(Differentiable manifold)*

*S is called a n-dimensional C^∞ **differentiable manifold** if*

1. *S is a topological manifold.*

2. *$\exists$ a collection of open charts $\{(U_\alpha,\phi_\alpha)\}_{\alpha\in A}$ of S ($S = \cup_{\alpha\in A} U_\alpha$), such that for each pair $\alpha, \beta \in A$, the mapping $\phi_\beta \circ \phi_\alpha^{-1}$ is a C^∞ differentiable mapping from $\phi_\alpha(U_\alpha \cap U_\beta)$ onto $\phi_\beta(U_\alpha \cap U_\beta)$.*

*A **complex manifold** is a manifold S whose coordinate charts are open subsets of $\mathbb{C}^n$ and the transition functions between charts, $\phi_\beta \circ \phi_\alpha^{-1}$, are holomorphic functions (i.e. have a derivative at every variable x_i, $(x_1,x_2,\ldots,x_n) \in \mathbb{C}^n$). Naturally, a complex manifold of dimension n also has the structure of a real differentiable manifold of dimension $2n$.*

*A **submanifold** is a subset of a manifold that is itself a manifold, but has smaller dimension.*

Definition 17 *(Symmetric space)*

*A differential manifold S is called a **symmetric space** if for each $x \in S$ there exists a diffeomorphism s_x which satisfies the following conditions :*

1. *x is an isolated fixed point of s_x,*

2. *s_x is involutive, that is, $s_x^2 = 1$,*

3. *$s_x(s_y(z)) = s_{s_x(y)}(s_x(z))$ for any y and z in S.*

5.3.2.2 Tangent vector and tangent space

In differential geometry, one can attach to every point p of a differentiable manifold a **tangent space**, a F vector space which intuitively contains the possible "directions" in which one can pass through p. The elements of the tangent space are called **tangent vectors** at p. All the tangent spaces have the same dimension, equal to the dimension of the manifold.

For example, if the given manifold is a sphere in $\mathbb{R}^2$, one can picture the tangent space at a point x as the plane which touches the sphere at x. It is also the plane which is perpendicular at x to the line joining the sphere center and x.

In particular, when $S \subset K^n$, $K = \mathbb{R}$, or $\mathbb{C}$ and S is defined by the equations

$$\begin{aligned} F_1(x_1,x_2,\ldots,x_n) &= 0 \\ &\vdots \\ F_r(x_1,x_2,\ldots,x_n) &= 0 \end{aligned}$$

where $\mathbf{x} = (x_1,x_2,\ldots,x_n) \in K^n$ and $F_i : K^n \to K$, the tangent space to S at the point $\mathbf{x}$ is the set of the tangent vectors whose coordinates $(t_1,t_2,\ldots,t_n)$, satisfy

$$\sum_{i=1}^{n} t_i \frac{\partial}{\partial x_i} F_j(x_1,x_2,\ldots,x_n) = 0, \ \forall j = 1,\ldots,r \tag{5.3}$$

As an example, we consider the space of invertible matrices with unit determinant, $S = SL_n(\mathbb{C}) \subset \mathbb{C}^{n\times n}$. Let us compute the tangent vector at the identity point I_n of this space.
Let $\mathbf{M} = [x_{i,j}] \in SL_n(\mathbb{C})$. The space $SL_n(\mathbb{C})$ can be defined by the unique equation of n^2 variables $x_{i,j}$

$$F(x_{11},x_{12},\ldots,x_{nn}) = \det \begin{bmatrix} x_{11} & x_{12} & \cdots & x_{1n} \\ x_{21} & x_{22} & \cdots & x_{2n} \\ \vdots & \vdots & \ddots & \vdots \\ x_{n1} & x_{n2} & \cdots & x_{nn} \end{bmatrix} - 1 = 0$$

Theorem 2 *The tangent space at the identity matrix $\mathbf{I}_n$ for the space $SL_n(\mathbb{C})$ is the set of matrices with trace equal to zero.*

Proof: According to (5.3), we have

$$\sum_{j,k=1}^{n} t_{jk} \frac{\partial}{\partial x_{jk}} F(x_{11},x_{12},\ldots,x_{nn}) = 0 \tag{5.4}$$

Let compute the partial derivatives.

$$\frac{\partial}{\partial x_{jk}} F(x_{11},\ldots,x_{nn})_{|\ \mathbf{M}=\mathbf{I}_n} = \frac{\partial}{\partial x_{jk}} \det(\mathbf{M})_{|\ \mathbf{M}=\mathbf{I}_n}$$

Since

$$\det(\mathbf{M}) = \sum_{\sigma\in S_n} sgn(\sigma) \prod x_{i\sigma(i)}$$

where S_n is the permutation group of the set $\{1,2,\ldots,n\}$ and $sgn(\sigma)$ denotes the signature of the permutation σ: $+1$ if σ is an even permutation and -1 if it is odd.

$$\begin{aligned}
\frac{\partial}{\partial x_{jk}} F(x_{11},\ldots,x_{nn})_{|\,\mathbf{M}=\mathbf{I}_n} &= \sum_{\sigma\in S_n} sgn(\sigma)\frac{\partial \prod_{i=1}^{n} x_{i\sigma(i)}}{\partial x_{jk}}\;{}_{|\,x_{jk}=\delta_{jk}} \\
&= \sum_{\sigma\in S_n} sgn(\sigma)\left(\prod_{i=1,i\neq j}^{n} x_{i\sigma(i)}\right)\frac{\partial x_{j\sigma(j)}}{\partial x_{jk}}\;{}_{|\,x_{jk}=\delta_{jk}} \\
&= \sum_{\sigma\in S_n,\sigma(j)=k} sgn(\sigma)\prod_{i=1,i\neq j}^{n} x_{i\sigma(i)\;|\,x_{jk}=\delta_{jk}} \\
&= \sum_{\sigma=I,\sigma(j)=k} sgn(I)\prod_{i=1,i\neq j}^{n} x_{ii\;|\,x_{jk}=\delta_{jk}} \quad (I \text{ is the identity element of } S_n) \\
&= \delta_{jk} \qquad (5.5)
\end{aligned}$$

Therefore, by replacing (5.5) in (5.4), the tangent vectors to $SL_n(\mathbb{C})$ at the identity $\mathbf{I}_n$ satisfy

$$\sum_{i=1}^{n} t_{ii} = 0 \qquad (5.6)$$

Thus, the tangent space at $\mathbf{I}_n$ is the set of matrices with trace zero. ■

5.3.2.3 Riemannian manifold

Definition 18 *(Riemannian manifold)*

*A **Riemannian manifold** (S,g), is a differentiable manifold S in which each tangent space is equipped with an inner product g in a manner which varies smoothly from point to point. In other words, for any tangent vectors D, D' at a point $p \in S$, $g(D,D') \in \mathbb{R}$ and g satisfies :*

1. *Linearity: $g(aD + bD',D'') = ag(D,D'') + b(D',D''), \forall a, b \in \mathbb{R}$*
2. *Symmetry: $g(D,D') = g(D',D)$*
3. *Positive-definiteness: If $D \neq 0$ then $g(D,D) > 0$*

This allows one to define various notions such as the length of curves, angles, areas (or volumes), curvature, gradients of functions and divergence of vector fields.

Definition 19 *(Geodesic on a Riemannian manifold)*
Let $\gamma : [a,b] \to S$ be a continuously differentiable curve in the Riemannian manifold S, $[a,b]$ is some interval of $\mathbb{R}$. We define its length $L(\gamma) = \|\gamma\|$ to be

$$L(\gamma) \overset{def}{=} \int_a^b \|\gamma'(t)\|\,\mathrm{d}t. \qquad (5.7)$$

where $\gamma'(t)$ is a tangent vector in the tangent space at the point $\gamma(t)$.

With the definition (5.7), every connected Riemannian manifold S becomes a metric space (and even

a length metric space) in a natural fashion: the distance $d(x,y)$ between the points x and y of S is defined as

$$d(x,y) = \inf_{\gamma}\{L(\gamma) \mid \gamma \text{ is a continuously differentiable curve joining } x \text{ and } y\}.$$

Even though Riemannian manifolds are usually "curved", there is still a notion of "straight line" on them: the ***geodesics****. These are curves which locally join their points along the shortest paths.*

5.3.2.4 Lie group

Definition 20 ***(Lie group)***

A ***Lie group*** *G is a differentiable manifold obeying the group properties and that satisfies the additional condition that the group operations (multiplication and inversion)*

$$\begin{array}{rcl} G \times G & \rightarrow & G \\ (g,h) & \mapsto & gh \end{array}$$

and

$$\begin{array}{rcl} G \times G & \rightarrow & G \\ g & \mapsto & g^{-1} \end{array}$$

are differentiable.

A ***complex Lie group*** *is defined in the same way using complex manifolds rather than real ones.*

Some examples of Lie groups :

1. The group $GL_n(F)$ of invertible matrices (under matrix multiplication) is a Lie group of real dimension n^2 if $F = \mathbb{R}$ and $2n^2$ if $F = \mathbb{C}$.
2. The subgroup $SL_n(F)$ of matrices of determinant 1 is also a Lie group of real dimension $n^2 - 1$ if $F = \mathbb{R}$ and $2n^2 - 2$ if $F = \mathbb{C}$.
3. The group of unitary matrices $U(n)$ is a real Lie group of dimension n^2.
4. The group of special unitary matrices $SU(n)$ is a real Lie group of dimension $n^2 - 1$.

There are several standard ways to form new Lie groups from old ones. For example:

1. The product of two Lie groups is a Lie group.
2. Any closed subgroup of a Lie group is a Lie group.
3. The quotient of a Lie group by a closed normal subgroup is a Lie group. Notice that the quotient of a Lie group by a closed subgroup is only a differentiable manifold

Definition 21 ***(Homogeneous space for Lie group)***

Let A be a topological group, in particular a Lie group, and F be a closed subgroup of A. The system of left cosets aF, $a \in A$ denoted A/F, is an ***homogeneous space****. Indeed, $X = A/F$ has a transitive group action for the group $G = A$. The group action could be defined by*

$$\begin{array}{rcl} \tau : G \times X & \rightarrow & X \\ (a, x = bF) & \mapsto & abF \end{array}$$

A homogeneous space S of a Lie group G is a space with a transitive group action by G. Because a transitive group action implies that there is only one group orbit, S is isomorphic having the same form to the quotient space G/H where H is the isotropy group G_x. The choice of x in S does not affect the isomorphism type of G/G_x because all of the isotropy groups are conjugate.

In the following section, we focus on the space of Hermitian matrices that can be seen as a Riemannian space. Consequently, all the above definitions can be applied for the classification of MIMO channels.

5.4 MIMO classification algorithm

As pointed out previously, our proposed classification algorithm will be used for Hermitian forms. This section defines how the normalized MIMO channels could be identified by their Hermitian forms (using an equivalence relation). Then, the section 5.4.2 describes the computation of the geodesic distance between Hermitian forms and how it could be used as a metric for the classification algorithm. Finally, section 5.4.3 introduces the Frobenius distance and shows the application of this distance for the classification. Frobenius distance will be compared in section 5.6 to the geodesic distance regarding the performance of the classification.

In the sequel, the complex cubic lattice $\mathbb{Z}[i]^n$ associated to the identity matrix will play the role of a reference Hermitian form.

5.4.1 Equivalence of MIMO channels

Let define an equivalence relation on the set $SL_n(\mathbb{C})$.

Definition 22 ***(Equivalence relation for MIMO channels)***
Two channels are equivalent in $SL_n(\mathbb{C})$ if there exist a unitary matrix $\mathbf{U}$ in $SU(n)$ such that $\mathbf{H}_2 = \mathbf{U}\mathbf{H}_1$.

First representation of MIMO channels equivalence

From a differential geometric point of view, the objects considered in this report can be described as follows. Elements of $\mathbb{C}^n$ will be considered as column vectors, so that a unimodular basis of $\mathbb{C}^n$ corresponds to an element of the special linear group $SL_n(\mathbb{C})$, and the natural action of the special unitary group $SU(n)$ on $\mathbb{C}^n$ induces an action of $SU(n)$ on $SL_n(\mathbb{C})$, given by left multiplication. Thus the equivalence class of such a basis under unitary transformations corresponds to an element of the quotient set

$$X = SU(n)\backslash SL_n(\mathbb{C}).$$

Elements of this quotient set are cosets of the form

$$[\mathbf{H}] = SU(n) \cdot \mathbf{H} \text{ for } \mathbf{H} \in SL_n(\mathbb{C}).$$

Note that if we had chosen row notation instead of column notation, then $SU(n)$ would have acted by right multiplication, and the quotient set to consider would have been $SL_n(\mathbb{C})/SU(n)$, whose elements are cosets of the form $\mathbf{H} \cdot SU(n)$.

The quotient set $SU(n)\backslash SL_n(\mathbb{C})$ is an example of homogeneous space, that is, the quotient of the Lie group $SL_n(\mathbb{C})$ by the closed subgroup $SU(n)$. As such, it carries a differential structure

and an action of $SL_n(\mathbb{C})$, given by right multiplication.

$$\begin{array}{rcl} \phi : X \times SL_n(\mathbb{C}) & \rightarrow & X \\ ([\mathbf{H}_1] = SU(n) \cdot \mathbf{H}_1, \mathbf{H}_2) & \mapsto & [\mathbf{H}_1 \cdot \mathbf{H}_2] = SU(n) \cdot \mathbf{H}_1 \cdot \mathbf{H}_2 \end{array} \tag{5.8}$$

Second representation of MIMO channels equivalence

There is another way to describe the space $SU(n)\backslash SL_n(\mathbb{C})$ that is quite useful in practice. Observe that two unimodular matrices $\mathbf{H}_1$ and $\mathbf{H}_2$ in $SL_n(\mathbb{C})$ have the same Gram matrix $\mathbf{G} = \mathbf{H}_1^\dagger \mathbf{H}_1 = \mathbf{H}_2^\dagger \mathbf{H}_2$ if and only if there is a unitary matrix $\mathbf{U} \in SU(n)$ such that $\mathbf{H}_2 = \mathbf{U}\mathbf{H}_1$, that is if and only if the classes of $\mathbf{H}_1$ and $\mathbf{H}_2$ in $SU(n)\backslash SL_n(\mathbb{C})$ coincide. Conversely, any positive definite Hermitian matrix $\mathbf{G}$ of determinant 1 can be written in the form $\mathbf{G} = \mathbf{H}^\dagger \mathbf{H}$ for $\mathbf{H} \in SL_n(\mathbb{C})$ uniquely determined up to left multiplication by a unitary matrix. In fact one can mention two specific choices of $\mathbf{H}$ that are of particular interest: the first one is to take $\mathbf{H}$ upper triangular, given by Cholesky decomposition, while the second is to take $\mathbf{H}$ Hermitian, by extracting the square root of $\mathbf{G}$ as

$$\mathbf{H} = \sqrt{\mathbf{G}} = \mathbf{U}\mathbf{D}\mathbf{U}^\dagger \tag{5.9}$$

where $\mathbf{D} = diag(\sqrt{\lambda_1}, \ldots, \sqrt{\lambda_n})$ and $\lambda_1, \ldots, \lambda_n$ are the eigenvalues of $\mathbf{G}$ and $\mathbf{U}$ the normalized vectors.

These considerations allow to identify $SU(n)\backslash SL_n(\mathbb{C})$ with the space of positive definite Hermitian matrices of determinant 1, by identifying the coset $SU(n) \cdot \mathbf{H}$ with the Gram matrix $\mathbf{G} = \mathbf{H}^\dagger \mathbf{H}$. The differential structure on $SU(n)\backslash SL_n(\mathbb{C})$ can be retrieved as the natural differential structure on this space of Hermitian matrices seen as a real submanifold of $\mathbb{C}^{n \times n}$.

The right action of $SL_n(\mathbb{C})$ on the quotient set $SU(n)\backslash SL_n(\mathbb{C})$ sends the matrix $\mathbf{H} \in SL_n(\mathbb{C})$ to $SU(n) \cdot \mathbf{H} \cdot \mathbf{P}$, where $\mathbf{P} \in SL_n(\mathbb{C})$. Thus, using the identification of the coset $SU(n) \cdot \mathbf{H}$ with the Gram matrix $\mathbf{G} = \mathbf{H}^\dagger \mathbf{H}$, we can define the right action of $SL_n(\mathbb{C})$ on the space of positive definite Hermitian matrices of determinant 1 as follows:

if $\mathbf{G}$ *is an Hermitian matrix and* $\mathbf{P} \in SL_n(\mathbb{C})$*, then* $\mathbf{P}$ *acts on* $\mathbf{G}$ *by sending it to* $\mathbf{P}^\dagger \mathbf{G} \mathbf{P}$.

In the sequel, we denote Γ the space of positive definite Hermitian matrices of determinant 1. So the classification is applied on the space Γ instead of the space of MIMO channels in $SL_n(\mathbb{C})$.

The next subsection focuses on the computation of the geodesic distance between Hermitian matrices, and on its application as a metric in the classification algorithm.

5.4.2 Geodesic distance for MIMO Classification

- **Geodesic distance for Hermitian matrices**

It appears that $SU(n)\backslash SL_n(\mathbb{C})$ is a special type of homogeneous space, called a symmetric space, and thus carries a natural Riemannian structure. We will refer to [31] which is the classical reference on this topic (along with E. Cartan's original works). More precisely, following the classification given in [31], §IX.6.1, $SU(n)\backslash SL_n(\mathbb{C})$ is the Riemannian global symmetric space of type IV associated with the Lie algebra of type $\mathfrak{a}_{n-1}$.

Therefore, we can define a geodesic in the Riemannian space $SU(n)\backslash SL_n(\mathbb{C})$ (or equivalently the space of Hermitian forms Γ) to compute the shortest distance between two elements of the space Γ providing the Riemannian metric (or inner products) on this space (definition 19 in section 5.3.2.3).

The aim of the following proposition is to describe the geodesics and the distance associated to the Riemannian structure $SU(n)\backslash SL_n(\mathbb{C})$.

Proposition 1 *Let $\mathbf{G}_1$ and $\mathbf{G}_2$ be two positive definite Hermitian matrices of size n with determinant 1. Let $\mathbf{P}_1$ be any element of $SL_n(\mathbb{C})$ such that $\mathbf{G}_1 = {\mathbf{P}_1}^\dagger \mathbf{P}_1$, and put $\mathbf{G} = ({\mathbf{P}_1}^\dagger)^{-1}\mathbf{G}_2{\mathbf{P}_1}^{-1}$ and $\mathbf{L} = \log(\mathbf{G})$. Then:*

1. *There is a unique geodesic segment γ joining $\mathbf{G}_1$ to $\mathbf{G}_2$, given by the parametrization $\gamma(t) = {\mathbf{P}_1}^\dagger \exp(t\mathbf{L})\mathbf{P}_1$ for $t \in [0,1]$.*
2. *Up to multiplication by a constant, the geodesic distance between $\mathbf{G}_1$ and $\mathbf{G}_2$ is*

$$d_{\text{geod}}(\mathbf{G}_1,\mathbf{G}_2) = \left(\sum_{1\leq i\leq n} |\log \lambda_i|^2 \right)^{1/2}, \tag{5.10}$$

where $\lambda_1,...,\lambda_n$ are the eigenvalues of $\mathbf{G}$.

Recall that if $\mathbf{A}$ is an Hermitian matrix, and F a real analytic function (i.e. it possesses derivatives of all orders) that is well defined on the eigenvalues of $\mathbf{A}$, then $F(\mathbf{A})$ can be defined as follows:

if $\mathbf{A} = \mathbf{V}^\dagger \text{diag}(\mu_1,...,\mu_n)\mathbf{V}$ is the diagonalization of $\mathbf{A}$, then $F(\mathbf{A}) = \mathbf{V}^\dagger \text{diag}(F(\mu_1),...,F(\mu_n))\mathbf{V}$

where $\mathbf{V}$ is unitary matrix and $\mu_1,...,\mu_n$ are real eigenvalues of $\mathbf{A}$.

In particular, with the notations of the proposition, if one writes $\mathbf{G} = \mathbf{U}^\dagger \text{diag}(\lambda_1,...,\lambda_n)\mathbf{U}$ with $\mathbf{U}$ unitary, then

$$\begin{cases} \mathbf{L} = \log(\mathbf{G}) = \mathbf{U}^\dagger \text{diag}(\log(\lambda_1),..., \log(\lambda_n))\mathbf{U} \\ \\ \gamma(t) = {\mathbf{P}_1}^\dagger \exp(t\mathbf{L})\mathbf{P}_1 = {\mathbf{P}_1}^\dagger \mathbf{U}^\dagger \text{diag}(\lambda_1^t,...,\lambda_n^t)\mathbf{U}\mathbf{P}_1 \end{cases}$$

Proof: Since the right action of $SL_n(\mathbb{C})$ must send geodesics to geodesics and preserve the distance, one can suppose that $\mathbf{G}_1 = \mathbf{I}_n$, $\mathbf{P}_1 = \mathbf{I}_n$, and $\mathbf{G}_2 = \mathbf{G}$.
This observation is depicted in Fig. 5.4. This figure illustrates the space of Hermitian matrices Γ. The geodesic relating two elements of Γ, $\mathbf{G}_1$ and $\mathbf{G}_2$ is denoted by γ_2. The length of γ_2 is equal to that of γ_1, which is the geodesic between the identity element $\mathbf{I}_n$ and the matrix $\mathbf{G}$ obtained by right action of $SL_n(\mathbb{C})$ on $\mathbf{G}_1$ and $\mathbf{G}_2$ respectively.

Since $SU(n)$ is the set of fixed points of the analytic involution $\sigma : \mathbf{H} \mapsto (\mathbf{H}^\dagger)^{-1}$ of $SL_n(\mathbb{C})$, one can apply [31], Proposition IV.3.4, to retrieve the fact that $SU(n)\backslash SL_n(\mathbb{C})$ is a Riemannian globally symmetric space. The tangent space to $SL_n(\mathbb{C})$ at $\mathbf{I}_n$ is the space of matrices with trace zero (Theorem 2). From [31], Proposition IV.3.3(iii), it follows that the tangent space $\mathcal{T}$ to $SU(n)\backslash SL_n(\mathbb{C})$ at $\mathbf{I}_n$ can be identified with its subspace of anti-invariants under $d\sigma$. That is for $\mathbf{M} \in \mathcal{T}$, $d\sigma$ satisfies $d\sigma(\mathbf{M}) = -\mathbf{M}^\dagger$. Since $d\sigma$ sends a matrix $\mathbf{M}$ to $-\mathbf{M}^\dagger$, one sees that this tangent space $\mathcal{T}$ is the space of Hermitian matrices with trace zero. Since $\mathbf{G} = \mathbf{U}^\dagger \text{diag}(\lambda_1,...,\lambda_n)\mathbf{U}$ is

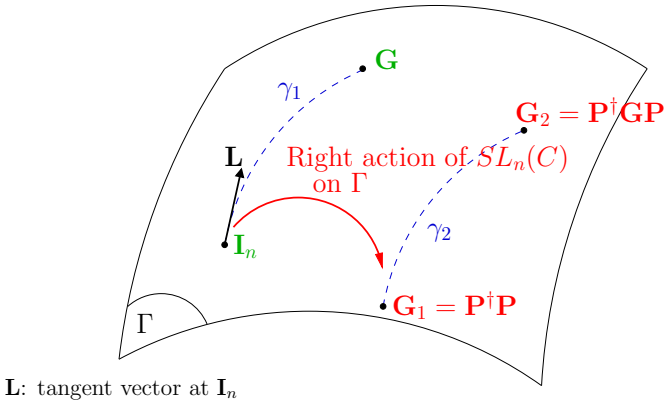

Figure 5.4: Action of $SL_n(\mathbb{C})$ on the space of Hermitian matrices Γ.

of determinant 1, one checks that $\mathbf{L} = \mathbf{U}^\dagger \mathrm{diag}(\log(\lambda_1),...,\log(\lambda_n))\mathbf{U}$ indeed is an element of $\mathcal{T}$. Now it follows again from [31], Proposition IV.3.3(iii) that any geodesic segment starting at $\mathbf{I}_n$ is of the form $\gamma_{\mathbf{L}'} : t \mapsto \exp(t\mathbf{L}')$ for some $\mathbf{L}' \in \mathcal{T}$, and the condition $\gamma_{\mathbf{L}'}(1) = \mathbf{G}$ forces $\mathbf{L}' = \mathbf{L}$. This proves the first part of the proposition.
Now since $\gamma_{\mathbf{L}}$ is a geodesic segment, its tangent vector has constant norm equal to $\|\mathbf{L}\|$, where $\|.\|$ is the norm on $\mathcal{T}$ given by the Riemannian structure. This norm must be invariant under the action of $SU(n)$ on $\mathcal{T}$, and since this action is irreducible, $\|.\|$ is unique up to multiplication by a constant. One can check indeed that the so-called Frobenius norm defined by

$$\|\mathbf{L}\| = \left(\sum_{1 \le i,j \le n} |L_{ij}|^2 \right)^{1/2}$$

is invariant.

Using this invariance property, this can also written as:

$$\begin{aligned} d_{\mathrm{geod}}(\mathbf{I}_n,\mathbf{G}) &= \mathrm{length}(\gamma) \\ &= \int_0^1 \|\mathbf{L}\| dt = \|\mathbf{L}\| \\ &= \|\mathbf{U}^\dagger \mathrm{diag}(\log(\lambda_1),...,\log(\lambda_n))\mathbf{U}\| \\ &= \|\mathrm{diag}(\log(\lambda_1),...,\log(\lambda_n))\| \\ &= \left(\sum_{1 \le i \le n} |\log \lambda_i|^2 \right)^{1/2}, \end{aligned}$$

which proves the second part of the proposition. ■

- **Centroid update in generalized Lloyd for Hermitian forms**

The generalized Lloyd algorithm iterates between two steps. The first step determines the borders of Voronoi regions. A Voronoi region is also called a class in our terminology. This Lloyd first step utilizes the geodesic metric given by proposition (1) in the previous section.

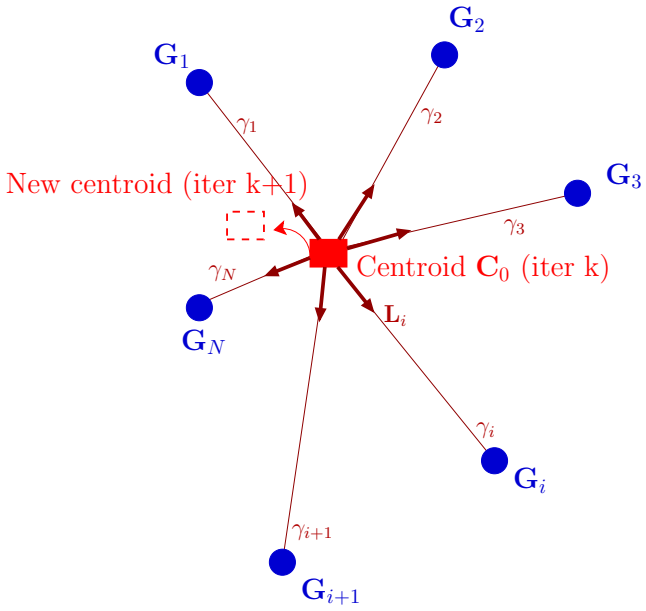

Figure 5.5: Centroid update rule after k Lloyd iterations.

The second step updates the centroid of each class.
In the second step of Lloyd algorithm applied to the space $SU(n)\backslash SL_n(\mathbb{C})$, given some positive definite Hermitian matrices $\mathbf{G}_1$,...,$\mathbf{G}_N$ with determinant 1, one needs to find the centroid $\mathbf{C}$ of this class of cardinality N that minimizes the sum of the squared distances $d_{\text{geod}}(\mathbf{C},\mathbf{G}_1)^2 + ... + d_{\text{geod}}(\mathbf{C},\mathbf{G}_N)^2$, that is

$$\mathbf{C} = \arg\min_{\tilde{\mathbf{C}}} \left\{ d_{\text{geod}}(\tilde{\mathbf{C}},\mathbf{G}_1)^2 + ... + d_{\text{geod}}(\mathbf{C}',\mathbf{G}_N)^2 \right\}$$

To our knowledge, there is no exact way to perform this minimization, however, proposition (1) suggests a way to find at least a good approximation of this centroid, based on a gradient heuristic.
Indeed, suppose we know that $\mathbf{G}_1$,...,$\mathbf{G}_N$ already are not too far from an "old" centroid $\mathbf{C}_0$. Using the invariance of the geodesic distance under the action of $SL_n(\mathbb{C})$, one can reduce to the case $\mathbf{C}_0 = \mathbf{I}_n$. Then if $\mathbf{L}_i$ is the tangent vector at $\mathbf{I}_n$ to the geodesic segment ending at $\mathbf{G}_i$, so that $\mathbf{L}_i = \log(\mathbf{G}_i)$, the gradient at $\mathbf{I}_n$ of the function $\mathbf{C} \mapsto d_{\text{geod}}(\mathbf{C},\mathbf{G}_1)^2 + ... + d_{\text{geod}}(\mathbf{C},\mathbf{G}_N)^2$ is proportional to $\mathbf{L} = \mathbf{L}_1 + ... + \mathbf{L}_N$. It is thus natural to take for $\mathbf{C}$ the endpoint of the geodesic with tangent vector $\frac{1}{N}\mathbf{L}$, that is

$$\mathbf{C} = \exp\left(\frac{1}{N}\left(\log \mathbf{G}_1 + ... + \log \mathbf{G}_N\right)\right) \tag{5.11}$$

Figure 5.5 illustrates an example to update the old centroid $\mathbf{C}_0$ knowing the different elements $\mathbf{G}_1$,...,$\mathbf{G}_N$ that are associated to $\mathbf{C}_0$.
One can check easily that if $N = 1$, or if $N = 2$ and $\mathbf{C}_0$ already lies on the unique geodesic passing through $\mathbf{G}_1$ and $\mathbf{G}_2$, then this approximate $\mathbf{C}$ is the exact $\mathbf{C}$ that minimizes the sum of the squared distances.

The next subsection presents the Euclidean distance (or Frobenius distance) which could be used as a metric for MIMO classification.

5.4.3 Frobenius distance for MIMO classification

- **Frobenius distance for Hermitian matrices**

From a computational point of view, a drawback with the mathematical constructions used for geodesic distance, is that they require to diagonalize some of the matrices involved, which can be heavily time-consuming. A computationally lighter alternative is then to consider the space of positive definite Hermitian matrices with determinant 1 as a subset of the affine space of all Hermitian matrices, and to use the distance and the averaging process coming from this affine structure. More precisely, this amounts to replacing the geodesic distance d_{geod} with the Frobenius distance

$$d_{\text{Frob}}(\mathbf{G}_1,\mathbf{G}_2) = \left(\sum_{1\leq i,j\leq n} |(\mathbf{G}_1 - \mathbf{G}_2)_{ij}|^2 \right)^{1/2} \tag{5.12}$$

- **Centroid update in generalized Lloyd for Hermitian forms**

When Frobenius distance is considered for the classification algorithm, we proceed as follows to update the centroids at the end of each Lloyd algorithm step. We define the linear average of $\mathbf{G}_1$,...,$\mathbf{G}_N$ as

$$\tilde{\mathbf{C}} = \frac{1}{N}(\mathbf{G}_1 + ... + \mathbf{G}_N),$$

and then we construct the new centroid as by applying the normalization

$$\mathbf{C} = \left(\det(\tilde{\mathbf{C}})\right)^{-1/n} \tilde{\mathbf{C}} \tag{5.13}$$

5.4.4 Summary

The algorithm 3 illustrates the different steps of MIMO channels classification to generate the centroids $\mathbf{C}_1$,$\mathbf{C}_2$,...,$\mathbf{C}_K$ of the different K classes. This algorithm is valid for any selected metric to compute the distance between two Hermitian forms. The Lloyd algorithm mentioned in algorithm 3 is described in algorithm 4.
In our study, we choose two metrics, namely geodesic and Frobenius distances. Thus, the distance, $dist(\mathbf{C}_k^{iter},\mathbf{G}_i)$, in the algorithm 4 is computed as (5.12) if Frobenius distance is selected and as (5.10) if geodesic distance is the chosen metric. Also, the centroid update after k Lloyd iterations in algorithm 4 is determined as given in (5.13) if Frobenius distance, otherwise as (5.11) if geodesic distance is considered. Notice that the normalization of the centroid $\mathbf{C}_k^{iter+1}$ in algorithm 4 is required only when selecting Frobenius distance. It is easy to check that the centroid update rule proposed for geodesic distance keeps $\det(\mathbf{C}_k^{iter+1}) = 1$.

The design of a quantizer for $SU(n)\backslash SL_n(\mathbb{C})$ via the different distances (e.g. geodesic or Frobenius) and these different centroids averaging processes should be tuned to the specific target application.

5.5 Lattice classification

In the previous section, we classified MIMO channels which correspond to finite subsets of lattices. In this section, we will extend this classification to lattices.

input : Data samples $\{\mathbf{H}_1,\mathbf{H}_2,\ldots,\mathbf{H}_M\}$, where $M \gg 1$ and $\mathbf{H}_i \in \mathbb{C}^{n\times n}$
output: Centroids defined by their Hermitian forms $\{\mathbf{C}_1,\mathbf{C}_2,\ldots,\mathbf{C}_K\}$, where $\det(\mathbf{C}_i) = 1$

3.1 **for** $i = 1$ **to** M **do**
3.2 | *compute normalized Hermitian form* $\mathbf{G}_i = \frac{1}{\sqrt[n]{\det(\mathbf{H}_i^\dagger \mathbf{H}_i)}} \mathbf{H}_i^\dagger \mathbf{H}_i$;
3.3 **end**
3.4 *Build an initial codebook of Hermitian forms* $\{\mathbf{C}_1^0,\mathbf{C}_2^0,\ldots,\mathbf{C}_K^0\}$, *where* $\det(\mathbf{C}_i^0) = 1$;
3.5 *Apply Generalized Lloyd Algorithm procedure GEN_LLOYD()*;
3.6 *return*;

Algorithm 3: Classification algorithm for $n \times n$ MIMO channels.

input : $(\mathbf{G}_i)$, $(\mathbf{C}_i^0)$, *maxIter* , K , M , *dist*() , *updateCentroid*()
output: $(\mathbf{C}_i)$

4.1 **for** *iter* $= 1$ **to** *maxIter* **do**
4.2 | $MSE_{iter} = 0$;
4.3 | **for** $i = 1$ **to** M **do**
4.4 | | $d = MAXDBL$;
4.5 | | **for** $k = 1$ **to** K **do**
4.6 | | | *Compute* $d_k = dist(\mathbf{C}_k^{iter},\mathbf{G}_i)$;
4.7 | | | **if** $d \geq d_k$ **then**
4.8 | | | | $d = d_k$;
4.9 | | | | $k_{min} = k$;
4.10 | | | **end**
4.11 | | **end**
4.12 | | *Assign* $\mathbf{G}_i$ *to the centroid* $\mathbf{C}_{k_{min}}^{iter}$;
4.13 | | $MSE_{iter} += d_{k_{min}}$;
4.14 | **end**
4.15 | **if** $MSE_{iter} == MSE_{iter-1}$ **then**
4.16 | | *return*;
4.17 | **end**
4.18 | **else**
4.19 | | **for** $k = 1$ **to** K **do**
4.20 | | | $\mathbf{C}_k^{iter+1} = updateCentroid(\mathbf{G}_{i_k})$, *where* $\mathbf{G}_{i_k} \in Class(\mathbf{C}_k^{iter+1})$;
4.21 | | | *Normalize* $\mathbf{C}_k^{iter+1}$ *so that* $\det(\mathbf{C}_k^{iter+1}) = 1$;
4.22 | | **end**
4.23 | **end**
4.24 **end**

Algorithm 4: Procedure GEN_LLOYD().

5.5.1 Lattice classification algorithm

Recall that a n-dimensional complex lattice Λ over $\mathbb{Z}[i]$ is defined by

$$\Lambda = \{\mathbf{x} = \mathbf{H}\mathbf{z} \in \mathbb{C}^n; \mathbf{z} \in \mathbb{Z}[i]^n\}$$

The columns $\mathbf{h}_i, i = 1, \ldots, n$ of the matrix $\mathbf{H}$ form a complex basis for Λ. In contrast to the last chapters dealing with lattices, the above definition assumes a column notation for matrices and vectors. Therefore, the reader should adapt the definitions given especially in chapter 2 to the current notation.

In chapter 2, section 2.1.1, it has been defined that two matrices in $SL_n(\mathbb{C})$ span the same lattice Λ over $\mathbb{Z}[i]$ if and only if they differ by a right multiplication of an element in $SL_n(\mathbb{Z}[i])$. In other words, let $\mathbf{H}_1$ and $\mathbf{H}_2$ be two bases for Λ; they are related by

$$\mathbf{H}_2 = \mathbf{H}_1\mathbf{P}$$

where $\mathbf{P} \in SL_n(\mathbb{Z}[i])$ denotes an unimodular matrix.

Thus the set of equivalence classes of unimodular lattices, defined in chapter 2 section 2.1.1), over the ring of Gaussian integers is represented by the quotient set

$$SL_n(\mathbb{C})/SL_n(\mathbb{Z}[i])$$

Using the action of $SU(n)$ on the quotient set $SL_n(\mathbb{C})/SL_n(\mathbb{Z}[i])$ given by a left multiplication leads to the double quotient space

$$SU(n)\backslash SL_n(\mathbb{C})/SL_n(\mathbb{Z}[i]),$$

whose elements are double cosets of the form

$$[\mathbf{H}] = SU(n) \cdot \mathbf{H} \cdot SL_n(\mathbb{Z}[i])$$

Notice that if row notation is chosen, then $SL_n(\mathbb{Z}[i])$ would have acted by a left multiplication and $SU(n)$ by a right multiplication, and the quotient set becomes $SL_n(\mathbb{Z}[i])\backslash SL_n(\mathbb{C})/SU(n)$.

The classification problem that was treated in section 5.4.1 for $SU(n)\backslash SL_n(\mathbb{C})$ could also be carried out for $SU(n)\backslash SL_n(\mathbb{C})/SL_n(\mathbb{Z}[i])$ with the same techniques, although some additional tools are needed.

Remember that a lattice Λ has many bases. The most common of them are the reduced bases that are used for many applications thanks to their 'nice' properties (section 2.1.3). Any matrix $\mathbf{H} \in SL_n(\mathbb{C})$ generating a lattice Λ is related to a reduced basis $\mathbf{H}_{red}$ by

$$\mathbf{H} = \mathbf{H}_{red}\mathbf{P}_{red}$$

Since the basis change does not alter the lattice, a lattice Λ could be identified by its reduced basis. Therefore, the classification of lattices is equivalent to classify the MIMO channels with their reduced form. Then, we can apply the techniques described in the previous section to classify lattices.
It is clear that the action of $SL_n(\mathbb{Z}[i])$ on $SU(n)\backslash SL_n(\mathbb{C})$ reduces the number of MIMO channel

representatives.

To find the reduced basis associated to a given lattice basis, several reduction algorithms were proposed (see section 2.1.3). In this work, we choose the lowest complexity algorithm to determine $\mathbf{H}_{red}$: the LLL algorithm [14]. As indicated in section 2.1.3.3, the LLL algorithm does not guarantee to find the shortest lattice vector satisfying the Minkowski criteria that are given in section 2.1.3.1. However, it guarantees in polynomial time to find a vector within a factor of the shortest vector.
The classification algorithm for lattices is similar for MIMO channels (algorithm 3) with small change to obtain the reduced bases. This leads to algorithm 5.

input : Data samples $\{\mathbf{H}_1,\mathbf{H}_2,\ldots,\mathbf{H}_M\}$, where $M \gg 1$ and $\mathbf{H}_i \in \mathbb{C}^{n\times n}$
output: Centroids defined by their Hermitian forms $\{\mathbf{C}_1,\mathbf{C}_2,\ldots,\mathbf{C}_K\}$, where $\det(\mathbf{C}_i) = 1$

5.1 **for** $i = 1$ **to** M **do**
5.2 *Apply the chosen reduction algorithm on the bases* $\mathbf{H}_1,\mathbf{H}_2,\ldots,\mathbf{H}_M$ *to produce a reduced basis* $\mathbf{H}_1^{red},\mathbf{H}_2^{red},\ldots,\mathbf{H}_M^{red}$;
5.3 *compute normalized Hermitian form* $\mathbf{G}_i = \frac{1}{\sqrt[n]{\det(\mathbf{H}_i^{red^\dagger}\mathbf{H}_i^{red})}}\mathbf{H}_i^{red^\dagger}\mathbf{H}_i^{red}$;
5.4 **end**
5.5 *Build an initial codebook of Hermitian forms* $\{\mathbf{C}_1^0,\mathbf{C}_2^0,\ldots,\mathbf{C}_K^0\}$, *where* $\det(\mathbf{C}_i^0) = 1$ *and* $\mathbf{C}_i^0$ *is the Gram matrix of a reduced basis*;
5.6 *Apply Generalized Lloyd Algorithm procedure GEN_LLOYD_LATTICE()*;
5.7 *return*;

Algorithm 5: Classification algorithm for n-dimensional complex lattices.

The LLL algorithm applied for complex lattices will be given in the next subsection.

5.5.2 LLL algorithm for complex bases

As outlined previously, the n-dimensional complex lattice Λ associated to the channel matrix $\mathbf{H}$ is defined by

$$\Lambda = \{\mathbf{x} = \mathbf{H}\mathbf{z} \in \mathbb{C}^n; \mathbf{z} \in \mathbb{Z}[i]^n\}$$

where the columns $\mathbf{h}_i, i = 1,\ldots,n$ of the matrix $\mathbf{H}$ form a complex basis for Λ. The complex basis $(\mathbf{h}_i)_{1\le i\le n}$ is LLL-reduced if [23]

$$\begin{cases} \Re(\mu_{i,j}) \le 0.5, \ 1 \le j < i \le n \\ \Re(\mu_{i,j}) \le 0.5, \ 1 \le j < i \le n \\ \left(\delta - |\mu_{i+1,i}|^2\right)\|\mathbf{h}_i^*\|^2 \le \|\mathbf{h}_{i+1}^*\|^2, \ 1 \le i < n \text{ and } 1/2 \le \delta \le 1 \end{cases} \tag{5.14}$$

The set of orthogonal vectors $\{\mathbf{h}_i^*\}_{1\le i\le n}$ span the same space as $\{\mathbf{h}_i\}_{1\le i\le n}$. They are generated using the Gram-Schmidt orthogonalization procedure as (see section 2.1.3.3)

$$\mathbf{h}_i^* = \mathbf{h}_i - \sum_{j=1}^{i-1}\mu_{ij}\mathbf{h}_j^*, \ 1 \le i \le n \tag{5.15}$$

input : $(\mathbf{G}_i)$, $(\mathbf{C}_i^0)$, *maxIter* , K , M , *dist*() , *updateCentroid*()
output: $(\mathbf{C}_i)$

6.1 **for** *iter* = 1 **to** *maxIter* **do**
6.2 $MSE_{iter} = 0$;
6.3 **for** $i = 1$ **to** M **do**
6.4 $d = MAXDBL$;
6.5 **for** $k = 1$ **to** K **do**
6.6 Compute $d_k = dist(\mathbf{C}_k^{iter}, \mathbf{G}_i)$;
6.7 **if** $d \geq d_k$ **then**
6.8 $d = d_k$;
6.9 $k_{min} = k$;
6.10 **end**
6.11 **end**
6.12 Assign $\mathbf{G}_i$ to the centroid $\mathbf{C}_{k_{min}}^{iter}$;
6.13 $MSE_{iter} += d_{k_{min}}$;
6.14 **end**
6.15 **if** $MSE_{iter} == MSE_{iter-1}$ **then**
6.16 *return*;
6.17 **end**
6.18 **else**
6.19 **for** $k = 1$ **to** K **do**
6.20 $\mathbf{C}_k^{iter+1} = updateCentroid(\mathbf{G}_{i_k})$, *where* $\mathbf{G}_{i_k} \in Class(\mathbf{C}_k^{iter+1})$;
6.21 *Construct the reduced Hermitian form associated to* $\mathbf{C}_k^{iter+1}$ *by evaluating an associated basis. This can be achieved by extracting the square root of* $\mathbf{C}_k^{iter+1}$ *as in (5.9) or by applying the Cholesky decomposition. Then, apply the reduced algorithm on the computed basis* $\mathbf{H}^{red}$;
6.22 *Compute the Hermitian form* $\mathbf{G}^{red} = \mathbf{H}^{red^\dagger}\mathbf{H}^{red}$ *and normalize* $\mathbf{G}^{red}$ $(\det(\mathbf{G}^{red}) = 1)$, *the new centroid is then* $\mathbf{C}_k^{iter+1} \leftarrow \mathbf{G}^{red}$;
6.23 **end**
6.24 **end**
6.25 **end**

Algorithm 6: Procedure GEN_LLOYD_LATTICE().

The Gram-Schmidt coefficient μ_{ij} is equal to

$$\mu_{ij} = \frac{\langle \mathbf{b}_i, \mathbf{b}_j^* \rangle}{|\mathbf{b}_j^*|^2}$$

where $\langle x, y \rangle$ stands for the Hermitian inner product between x and y.

In algorithm 7, we present the LLL algorithm to reduce the bases of complex vectors. When the rank of the channel is equal to 2 and $\delta = 1$, the LLL algorithm reduces to the optimal reduction algorithm, i.e. the Minkowski reduction. More orthogonal reduced bases can be obtained by increasing δ to one. However, this may increase the number of iterations required.

The evaluation of the proposed classification performance is achieved based on numerical results. The next section illustrates some simulation results to validate the classification algorithm.

5.6 Numerical results

The reader could notice that the described classification algorithm does not depend on the channel model (e.g. PDF of the channel matrix coefficients, channel correlation, etc). For numerical results, we consider both cases:

- The first one corresponds to the simple case where channel coefficients are uncorrelated.
- The second one focuses on channels whose coefficients present a spatial correlation due to the proximity of transmit or/and receive antennas. The correlation model that is adopted in our simulations is given by[41]

$$\mathbf{H} = \mathbf{R}_r \cdot \mathbf{H}_w \cdot \mathbf{R}_t \tag{5.16}$$

  where $\mathbf{H}_w$ is an $n_r \times n_t$ matrix of iid complex Gaussian random variables with zero mean and unit variance. The matrices $\mathbf{R}_r \in \mathbb{C}^{n_r \times n_r}$ and $\mathbf{R}_t \in \mathbb{C}^{n_t \times n_t}$ are the correlation matrices at the receiver and the transmitter, respectively. Both $\mathbf{R}_r$ and $\mathbf{R}_t$ are positive semi-definite Hermitian matrices. Generally, the coefficients $\{r_{ij}\}_{i,j}$ of both correlation matrices satisfy [41]

$$r_{ij} = \begin{cases} \gamma^{j-i} & i \leq j \\ \overline{r_{ji}} & i > j \end{cases}$$

  where $\gamma = \gamma_0 e^{j\theta}$ with $|\gamma| \leq 1$, and $\overline{x}$ denotes the conjugate of x. In our study, we consider the simple case where $\theta = 0$. The matrices $\mathbf{R}_r$ and $\mathbf{R}_t$ are equal to

$$\mathbf{R}_r = \begin{bmatrix} 1 & \alpha & \cdots & \alpha^{n-1} \\ \alpha & 1 & \cdots & \alpha^{n-2} \\ \vdots & \vdots & \ddots & \vdots \\ \alpha^{n-1} & \cdots & \alpha & 1 \end{bmatrix} \quad \mathbf{R}_t = \begin{bmatrix} 1 & \beta & \cdots & \beta^{n-1} \\ \beta & 1 & \cdots & \beta^{n-2} \\ \vdots & \vdots & \ddots & \vdots \\ \beta^{n-1} & \cdots & \beta & 1 \end{bmatrix}$$

input : a basis $\{\mathbf{h}_1,\mathbf{h}_2,\ldots,\mathbf{h}_n\}$ for a lattice Λ in C^n
output: a reduced basis for Λ

7.1 $\mathbf{h}_1^* \leftarrow \mathbf{h}_1$, $B_1 = \langle \mathbf{h}_1,\mathbf{h}_1 \rangle$;
7.2 **for** $i = 2$ **to** n **do**
7.3 $\quad \mathbf{h}_i^* \leftarrow \mathbf{h}_i$;
7.4 $\quad$ **for** $j = 1$ **to** $i - 1$ **do**
7.5 $\quad\quad \mu_{ij} \leftarrow \langle \mathbf{h}_i,\mathbf{h}_j^* \rangle / B_j$ *and* $\mathbf{h}_i^* \leftarrow \mathbf{h}_i^* - \mu_{ij}\mathbf{h}_j^*$;
7.6 $\quad$ **end**
7.7 $\quad B_i = \langle \mathbf{h}_i^*,\mathbf{h}_i^* \rangle$;
7.8 **end**
7.9 $k \leftarrow 2$;
7.10 **while** $k \leq n$ **do**
7.11 $\quad$ **for** $l = k - 1$ **to** 1 **do**
7.12 $\quad\quad$ *RED(k,l)*;
7.13 $\quad$ **end**
7.14 $\quad B \leftarrow \langle \mathbf{h}_k,\mathbf{h}_k \rangle$, $i \leftarrow 1$;
7.15 $\quad$ **while** $i \leq k - 1$ **do**
7.16 $\quad\quad$ **if** $\delta B_i \leq B$ **then**
7.17 $\quad\quad\quad B \leftarrow B - \mu_{k,i}^2 B_i$, $i \leftarrow i + 1$;
7.18 $\quad\quad$ **end**
7.19 $\quad\quad$ **else**
7.20 $\quad\quad\quad$ *INSERT(k,i)*;
7.21 $\quad\quad\quad$ **if** $i \leq 2$ **then**
7.22 $\quad\quad\quad\quad k \leftarrow i - 1$, $B \leftarrow \langle \mathbf{h}_k,\mathbf{h}_k \rangle$, $i \leftarrow 1$;
7.23 $\quad\quad\quad$ **end**
7.24 $\quad\quad\quad$ **else**
7.25 $\quad\quad\quad\quad k \leftarrow 1$;
7.26 $\quad\quad\quad$ **end**
7.27 $\quad\quad$ **end**
7.28 $\quad$ **end**
7.29 $\quad k \leftarrow k + 1$;
7.30 **end**
7.31 *return* $\{\mathbf{h}_1,\mathbf{h}_2,\ldots,\mathbf{h}_n\}$;

Algorithm 7: LLL lattice basis reduction algorithm.

8.1 **if** $\Re(\mu_{k,l}) \geq 1/2$ *or* $\Im(\mu_{k,l}) \geq 1/2$ **then**
8.2 $\quad \mathbf{h}_k \leftarrow \mathbf{h}_k - \lfloor \mu_{k,l} \mathbf{h}_l \rceil$;
8.3 $\quad$ **for** $j = 1$ *to* $l - 1$ **do**
8.4 $\quad\quad \mu_{k,j} \leftarrow \mu_{k,j} - \lfloor \mu_{k,l} \rceil \mu_{l,j}$;
8.5 $\quad$ **end**
8.6 $\quad \mu_{k,l} \leftarrow \mu_{k,l} - \lfloor \mu_{k,l} \rceil$;
8.7 **end**

Algorithm 8: Procedure RED(*k*,l).

```
9.1 h ← h_k;
9.2 for j = k − 1 downto i + 1 do
9.3 |  h_j ← h_{j−1};
9.4 end
9.5 h_i ← h;
```

Algorithm 9: Procedure INSERT(k,i).

Note that $\mathbf{H}_w$ is a full rank matrix. In the presence of receive or transmit correlation, the rank of the channel matrix $\mathbf{H}$ is constrained by $\min(rank(\mathbf{R}_r), rank(\mathbf{R}_t))$.

We consider both channel models: with uncorrelated/correlated coefficients before doing the determinant normalization. Our numerical results on MIMO classification are obtained via a generalized Lloyd similar to the one-dimensional Lloyd [36]:

1. Build an initial codebook with K elements chosen randomly.
2. Assign each data sample to its nearest centroid (according to the chosen metric or distance).
3. Update the centroid of class i based on the N_i data samples belonging to this class, for $i = 1, \ldots, K$. These are the new K centroids.
4. Go back to step 2 during n_L iterations.

We distinguish two scenarios. The first one chooses one channel model (correlated or uncorrelated) for all channel samples. The second considers both models (correlated and uncorrelated) for channel samples with equal proportions, i.e. half of them satisfy the uncorrelated model and the others satisfy the correlated model.

As mentioned in section 5.1, any quantization process introduces a distortion for the original data. This distortion depends essentially on the adopted metric and also on the codebook size. For the MIMO classification, that consists in quantizing Hermitian forms given by their associated matrices, the codebook size should depend on the dimension of the Hermitian forms space. That is, a good quantization which represents the original data requires a codebook size of order $\exp(c \cdot n^2)$, where n is the dimension of the Hermitian forms space and $c > 0$ is a non zero positive integer. For example, if $n = 2$ (i.e. 2×2 MIMO systems), an acceptable quantization could be achieved with a codebook equal at least to $K = 16$. Therefore, one octet could be sufficient to quantize the 2-dimensional space. When $n = 4$ (i.e. 4×4 MIMO systems), at least $K = 65536$ centroids are needed, which is a high number. Two octets at least are necessary to quantize the 4-dimensional space.
For simulations, we apply the Lloyd algorithm (algorithm 3 or 5) for $K = 32$ and $K = 256, 1024$ when $n = 2$ and $n = 4$ respectively.
Another parameter that could impact the codebook size is the channel coefficients distribution. Indeed, for uncorrelated channel matrix, the degree of freedom (i.e. the number of values which are freely available) is higher than the one for the correlated model case. Therefore, the uncorrelated model requires more centroids than the correlated one to represent the MIMO channels.

The following subsections illustrate some numerical results to evaluate the classification algorithm for MIMO channels. First, we focus on the generated centroids and their associated classes. Second, we outline the resemblance between any channel and its corresponding centroid by using Voronoi regions and error rates.

5.6.1 Centroid orbits

To observe the repartition of the centroids in the space of Hermitian forms, $SU(n)\backslash SL_n(\mathbb{C})$, we evaluate the distance between each centroid and the identity element of this space, i.e. the identity matrix $\mathbf{I}_n$. This distance is computed using equation (5.10) when geodesic metric is adopted and (5.12) when Frobenius metric is chosen.

The set of centroids lying at the same distance from the identity matrix is called orbit. Figures 5.6- 5.14 show the geodesic and Frobenius orbits of centroids after n_L Lloyd iterations on $M = 10^6$ Hermitian form samples for different scenarios. Each figure illustrates:

1. The origin that represents the identity matrix, $\mathbf{I}_n$.
2. A square symbol that represents a centroid $\mathbf{G}_c$ placed on a circle of radius equal to its distance from the identity

$$d_{geo}(\mathbf{I}_n,\mathbf{G}_c) = \sqrt{\sum_{i=1}^{n} \log(\lambda_i)^2}\ \text{, in case of geodesic distance}$$

$$d_{lin}(\mathbf{I}_n,\mathbf{G}_c) = \sqrt{\sum_{i=1}^{n} (\lambda_i - 1)^2}\ \text{, in case of Frobenius distance}$$

   where λ_i, $i = 1,\ldots,n$ are the eigenvalues of the centroid $\mathbf{G_c}$.
3. The angles, $\alpha(\mathbf{G}_c)$, that surround the different centroids and are proportional to the size of their classes, that is

$$\alpha(\mathbf{G}_c) = 2\pi \frac{card(\mathbf{G}_c)}{\sum_{1\leq i\leq K} card(\mathbf{G}_{c_i})}, \text{ where } \{\mathbf{G}_{c_i}\}_{1\leq i\leq K} \text{ are the centroids.}$$

For some values of K considered as small, the codebook is spherical in the geodesic representation and classes are equiprobable if Lloyd reaches a steady state at large n_L. Clearly, when K is high, the codebook includes many orbits. Some singular orbits may correspond to rare Hermitian forms or to a non convergence state of Lloyd algorithm.

The analysis of the different scenarios depicted on Figs. 5.6-5.14 is illustrated in the following sections for MIMO channels and lattices.

5.6.1.1 Case of MIMO channels

- 2-dimensional case

For uncorrelated model, both geodesic and Frobenius metrics in Fig. 5.6 lead essentially to two orbits around the origin. For $K = 32$, the repartition of centroids in both orbits is less balanced for geodesic than Frobenius distance. For correlated model in Fig. 5.7, there are more orbits for both distances. The size of different classes is almost equal for geodesic distance, whereas a large class contains almost half of data samples for Frobenius distance. Comparing both models, one can deduce that more centroids are required for the uncorrelated model than for the correlated model as expected previously.

- 4-dimensional case

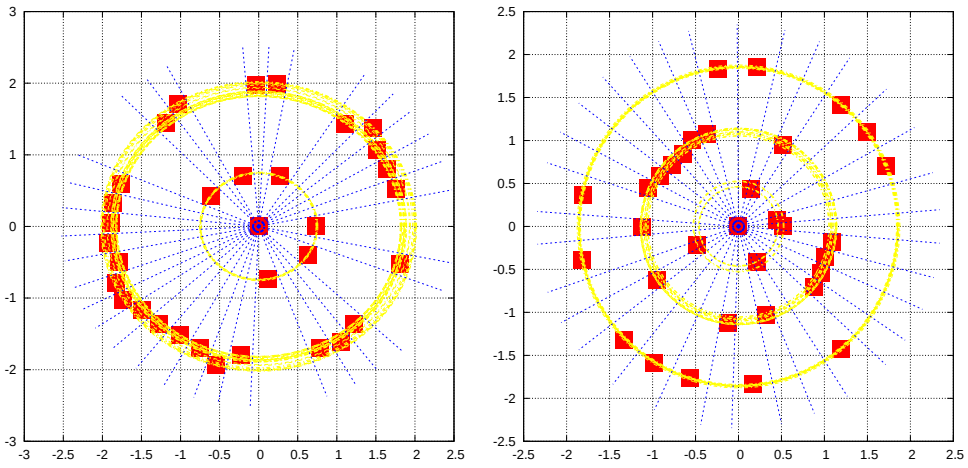

Figure 5.6: MIMO classification : Geodesic (on the left) and Frobenius (on the right) orbits for $n = 2$ antennas, uncorrelated model, $K = 32$ classes, $n_L = 120$ Lloyd iterations.

For $K = 256$ and uncorrelated channels, the application of Lloyd algorithm using the geodesic metric generates K centroids with almost equal eigenvalues, since all centroids belong to the same orbit in Fig. 5.8. A second orbit appears when increasing the codebook size, $K = 1024$, with a few number of centroids. For the second metric, Fig. 5.9 illustrates two distinct orbits for $K = 256$ and more for $K = 1024$. One can believe that $K = 1024$ is insufficient to quantize the Hermitian forms in the 4-dimensional space.

For correlated model, more orbits are obtained for $K = 256$ in Fig. 5.10 for both metrics. As for $n = 2$, we can deduce that more centroids are needed for uncorrelated model. For Frobenius distance, it is noticed that the difference between the classes size is more significant for $n = 4$. While the distribution of classes size is almost uniform for the geodesic distance.

To go further in the comparison of both metrics, we consider the classification of mixed channel models. We generate correlated and uncorrelated data samples with equal proportions, and we apply the classification algorithm to a small codebook, $K = 32$, to generate the centroids for both metrics. Figure 5.11 illustrates simulation results for both geodesic and Frobenius distances. We distinguish essentially two orbits for both metrics but with different centroid distributions. The nearest orbit to the origin contains the centroids associated to the uncorrelated model channels, whereas the second orbit consists of centroids which correspond to correlated model channels. Frobenius distance generates only one centroid for correlated channels with the highest class size comparing to the uncorrelated centroids. However, geodesic distance shares out almost fairly (in class size) the codebook between correlated and uncorrelated models.

- Conclusions

As conclusions, it seems that geodesic distance is less sensitive to channel distribution than Frobenius distance. Indeed, the above results focusing on centroid orbits show that the distribution of classes population with geodesic metric is quasi uniform for both cases: correlated and uncorrelated models. However, the classification with Frobenius distance leads to a dise-

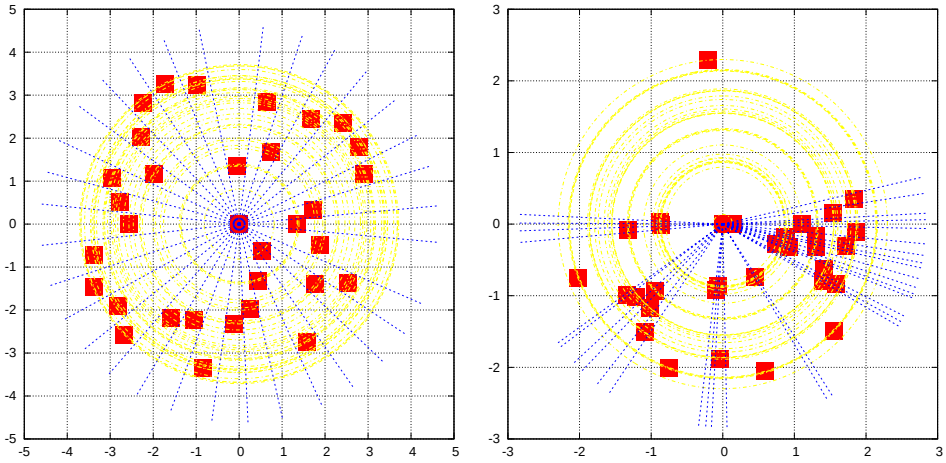

Figure 5.7: MIMO classification : Geodesic (on the left) and Frobenius (on the right) orbits for $n = 2$ antennas, correlated model, $K = 32$ classes, $n_L = 120$ Lloyd iterations.

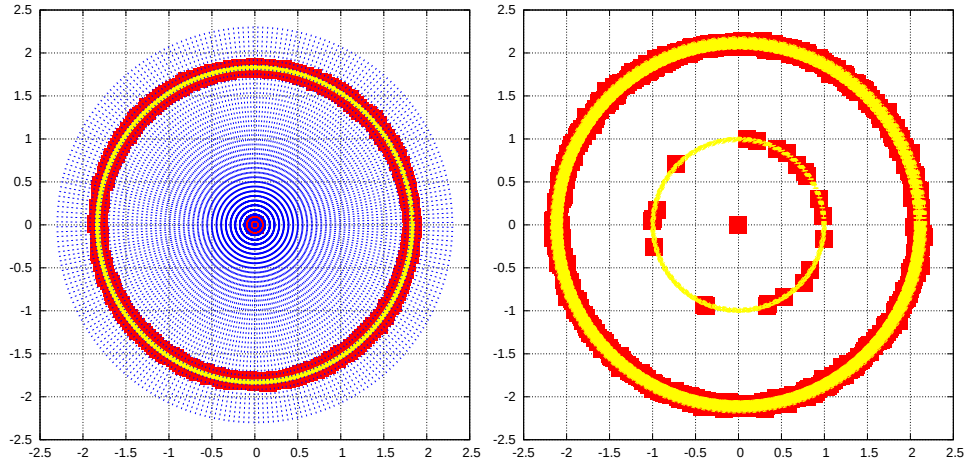

Figure 5.8: MIMO classification : Geodesic orbits for $n = 4$ antennas, uncorrelated model, $K = 256$ (on the left), $K = 1024$ (on the right) classes, $n_L = 120$ Lloyd iterations.

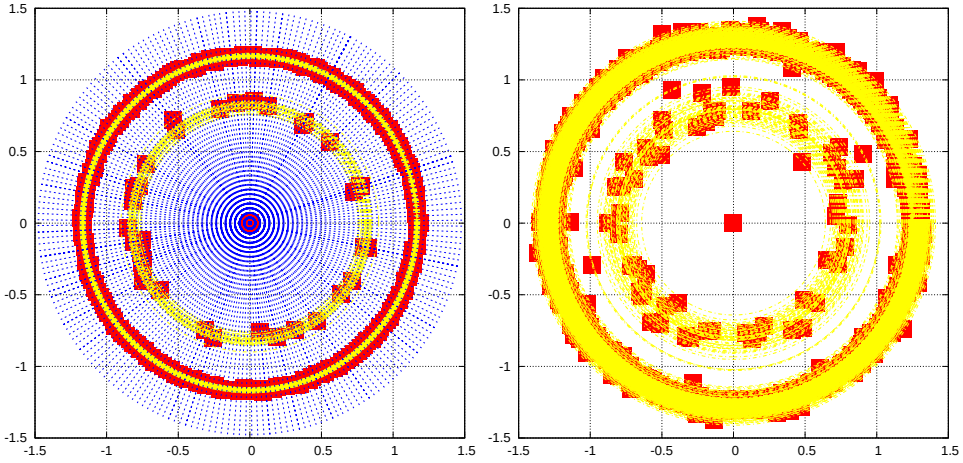

Figure 5.9: MIMO classification : Frobenius orbits for $n = 4$ antennas, uncorrelated model, $K = 256$ (on the left), $K = 1024$ (on the right) classes, $n_L = 120$ Lloyd iterations.

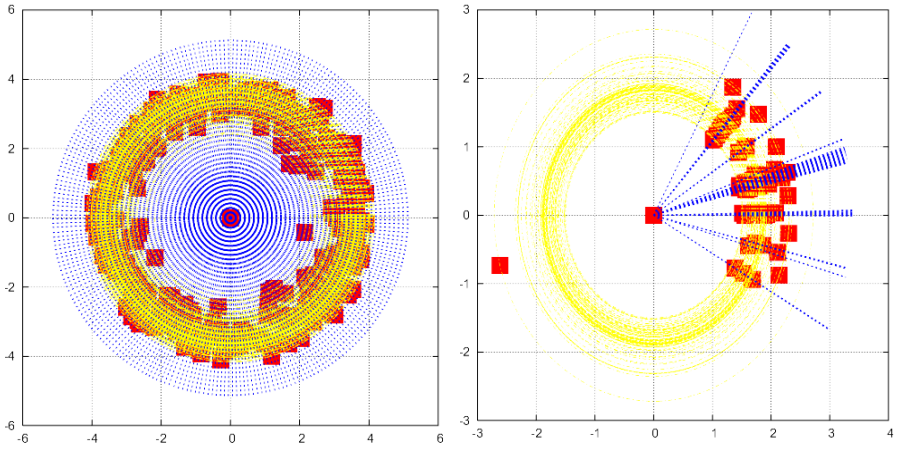

Figure 5.10: MIMO classification : Geodesic (on the left) and Frobenius (on the right) orbits for $n = 4$ antennas, correlated model, $K = 256$ classes, $n_L = 120$ Lloyd iterations.

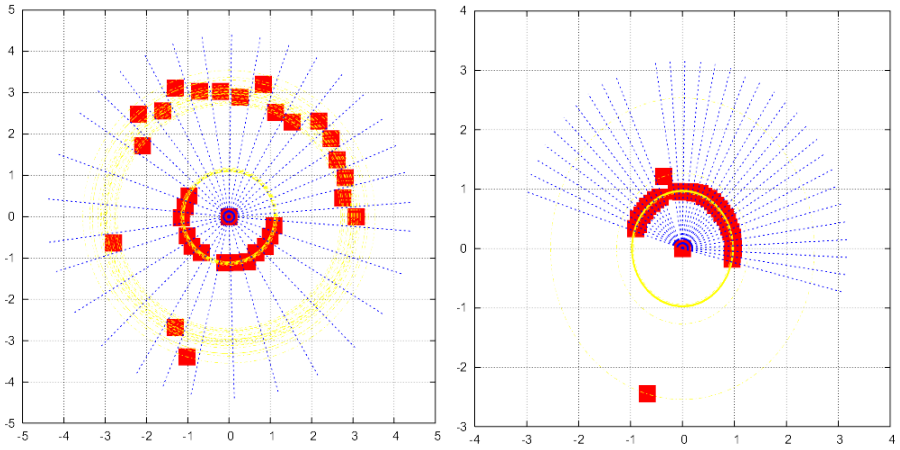

Figure 5.11: MIMO classification : Geodesic (on the left) and Frobenius (on the right) orbits for $n = 4$ antennas, correlated & uncorrelated models, $K = 32$ classes, $n_L = 120$ Lloyd iterations.

quilibrium between classes size for correlated model; whereas a uniform distribution is shown for uncorrelated model.

By considering the diagonalization of the centroid $\mathbf{G}_c = \mathbf{U}\mathbf{D}\mathbf{U}^\dagger$, where $\mathbf{D} = diag(\lambda_1, \ldots, \lambda_n)$ and $\mathbf{U} \in SU(n)$, and the fact that all centroids have almost the same eigenvalues λ_i for the geodesic distance and $n = 4$, one can deduce that this metric starts by quantizing the unitary matrix $\mathbf{U}$. When K is high, the quantization of both $\mathbf{U}$ and $\mathbf{D}$ should be noticed by distinguishing the different orbits. In this work, we limit K to $1024 = 2^{10}$ since most of wireless applications require a few number of bits to quantize channels.

5.6.1.2 Case of lattices

We apply the classification algorithm extended to lattices (algorithm 5) and we expose in this section the simulation results for three scenarios: ($n = 2$, $K = 32$), ($n = 4$, $K = 256$), and ($n = 4$, $K = 1024$). Figures 5.12, 5.13, and 5.14 illustrate the centroid orbits for in case of lattices associated to uncorrelated model for geodesic and Frobenius metrics. It is clear that there are more orbits in this case than for the previous case of MIMO channels. Therefore, we can deduce that lattices classification requires less centroids as representatives. This result can be observed intuitively since the degrees of freedom for lattices is lower comparing to MIMO channels: two distinct channels could represent the same lattice and the reciprocal is not correct.

5.6.2 Classification validation

In this section, we focus only on the proposed geodesic metric to validate our classification algorithm. Using this metric, we compare some channel parameters to those of their associated centroids. These parameters are: Voronoi regions and error rate.

5.6.2.1 Validation based on Voronoi regions

Let $\Lambda_\mathbf{Q}$ and $\Lambda_\mathbf{G}$ be two lattices. This criterion consists in comparing the shape of the Voronoi regions $\mathcal{V}_\mathbf{Q}$ and $\mathcal{V}_\mathbf{G}$ associated to $\Lambda_\mathbf{Q}$ and $\Lambda_\mathbf{G}$, respectively. To do this, we proceed as follows:

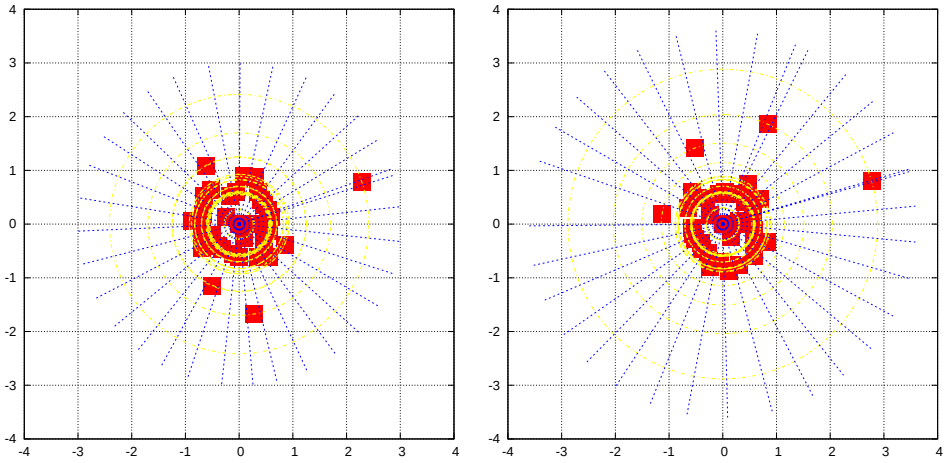

Figure 5.12: Lattices classification : Geodesic (on the left) and Frobenius (on the right) orbits for $n = 2$ antennas, uncorrelated model, $K = 32$ classes, $n_L = 120$ Lloyd iterations.

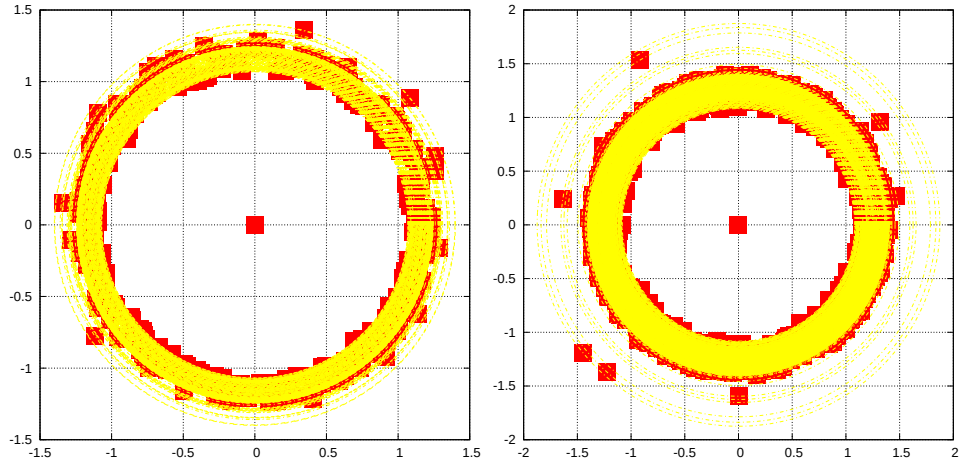

Figure 5.13: Lattices classification : Geodesic orbits for $n = 4$ antennas, uncorrelated model, $K = 256$ (on the left) , $K = 1024$ (on the right) classes, $n_L = 120$ Lloyd iterations.

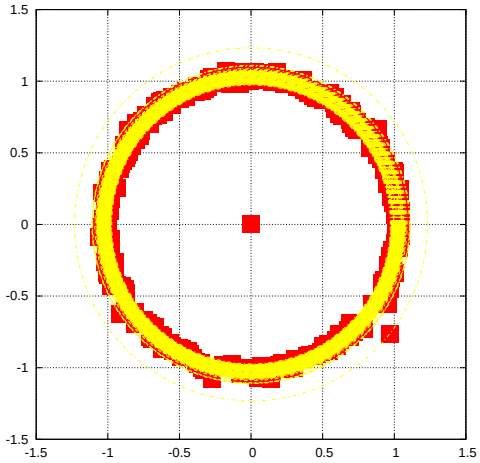

Figure 5.14: Lattices classification : Frobenius orbits for $n = 4$ antennas, uncorrelated model, $K = 256$ classes, $n_L = 120$ Lloyd iterations.

1. Step 1: Normalize the fundamental volume of $\Lambda_{\mathbf{Q}}$ and $\Lambda_{\mathbf{G}}$ to avoid the scaling factor as assumed in section 5.2.1. This implies $Vol(\mathcal{V}_{\mathbf{Q}}) = Vol(\mathcal{V}_{\mathbf{G}}) = 1$.
2. Step 2: Evaluate the intersection between $\mathcal{V}_{\mathbf{Q}}$ and $\mathcal{V}_{\mathbf{G}}$.

To perform Step 2, we define the function $I_{\mathcal{V}}$, associated to the Voronoi region $\mathcal{V}$, as follows:

$$\begin{aligned} I_{\mathcal{V}} : \mathbb{R}^{2n} &\rightarrow \mathbb{R} \\ \mathbf{x} &\rightarrow 1 \text{ if } \mathbf{x} \in \mathcal{V} \text{ and } 0 \text{ otherwise} \end{aligned} \tag{5.17}$$

Therefore, Step 1 leads to

$$\int_{\mathbb{R}^{2n}} I_{\mathcal{V}_{\mathbf{Q}}}(\mathbf{x})d\mathbf{x} = \int_{\mathbb{R}^{2n}} I_{\mathcal{V}_{\mathbf{G}}}(\mathbf{x})d\mathbf{x} = 1$$

The figure of merit defined by

$$\mu(\mathbf{Q},\mathbf{G}) = \int_{\mathbb{R}^{2n}} I_{\mathcal{V}_{\mathbf{Q}}}(\mathbf{x}) I_{\mathcal{V}_{\mathbf{G}}}(\mathbf{x})d\mathbf{x} \tag{5.18}$$

gives the intersection between $\mathcal{V}_{\mathbf{Q}}$ and $\mathcal{V}_{\mathbf{G}}$. Given the definition (5.17), it is clear that $\mu(\mathbf{Q},\mathbf{G}) \in [0,1]$ (providing that $\forall\ \mathbf{x} \in \mathbb{R}^{2n}$, $0 \leq I_{\mathcal{V}_{\mathbf{Q}}}(\mathbf{x}) I_{\mathcal{V}_{\mathbf{G}}}(\mathbf{x}) \leq I_{\mathcal{V}_{\mathbf{Q}}}(\mathbf{x})$). The Voronoi regions $\mathcal{V}_{\mathbf{Q}}$ and $\mathcal{V}_{\mathbf{G}}$ are geometrically close if their associated $\mu(\mathbf{Q},\mathbf{G})$ is near to 1.

The evaluation of $\mu(\mathbf{Q},\mathbf{G})$ requires the knowledge of $\mathcal{V}(\mathbf{Q})$ and $\mathcal{V}(\mathbf{G})$. Several solutions are proposed in the literature to define the Voronoi regions of particular lattices [15], [62]. Nevertheless, the determination of Voronoi regions for random lattices is still an open problem.

Recall that the goal of this section is to compare the MIMO channel $\mathbf{H}$ to its associated centroid via their Voronoi regions. This comparison consists in evaluating the figure of merit (5.18) between the Hermitian form $\mathbf{Q} = \mathbf{H}^{\dagger}\mathbf{H}$ and its nearest centroid $\mathbf{G}_c$.
We propose a numerical approach to evaluate the figure of merit. A high number of points $\mathbf{x}$ are generated uniformly within a cube centered at the origin with edge length equals $2d_{\min}$,

where $d_{\min}$ is the minimal Euclidean distance of the lattice $\Lambda_{\mathbf{Q}}$ associated to $\mathbf{H}$. To determine both $I_{\mathcal{V}_{\mathbf{Q}}}(\mathbf{x})$ and $I_{\mathcal{V}_{\mathbf{G}_c}}(\mathbf{x})$, we apply the sphere decoder [1], [63] around the origin. For example, when the decoder is applied for the lattice associated to $\mathbf{Q}$, $I_{\mathcal{V}_{\mathbf{Q}}}(\mathbf{x}) = 1$ if the point $\mathbf{x}$ is decoded as $\mathbf{0}$ and $I_{\mathcal{V}_{\mathbf{Q}}}(\mathbf{x}) = 0$ otherwise.

Figure 5.15 illustrates the figure of merit $\mu(\mathbf{Q},\mathbf{G}_c)$ for different scenarios, where $\mathbf{G}_c$ denotes the centroid associated to the Hermitian form $\mathbf{Q}$. In Fig. 5.15, the notation (n,K) means that the dimension of the Hermitian form is n and K is the size of the codebook. We plot the figure of merit of 10 different Hermitian forms for (2,20), (2,512) and (4,1024). It seems that the scenario (2,512) achieves almost the best performance with respect to (2,20). In average, $\mu(\mathbf{Q},\mathbf{G}_c)$ is close to 0.9 for the best one and it is less than 0.8 for (2,20). The case (4,1024) oscillates between 0.5 and 0.7, which means that 50% to 70% of generated points belong to both $\mathcal{V}_{\mathbf{Q}}$ and $\mathcal{V}_{\mathbf{G}_c}$.

Therefore, given the results depicted on Fig. 5.15, one could deduce that the resemblance between one channel and its associated centroid is more tight in case of $n = 2$, even with a small codebook size than in case of $n = 4$. This observation will be noticed also in the following sections.

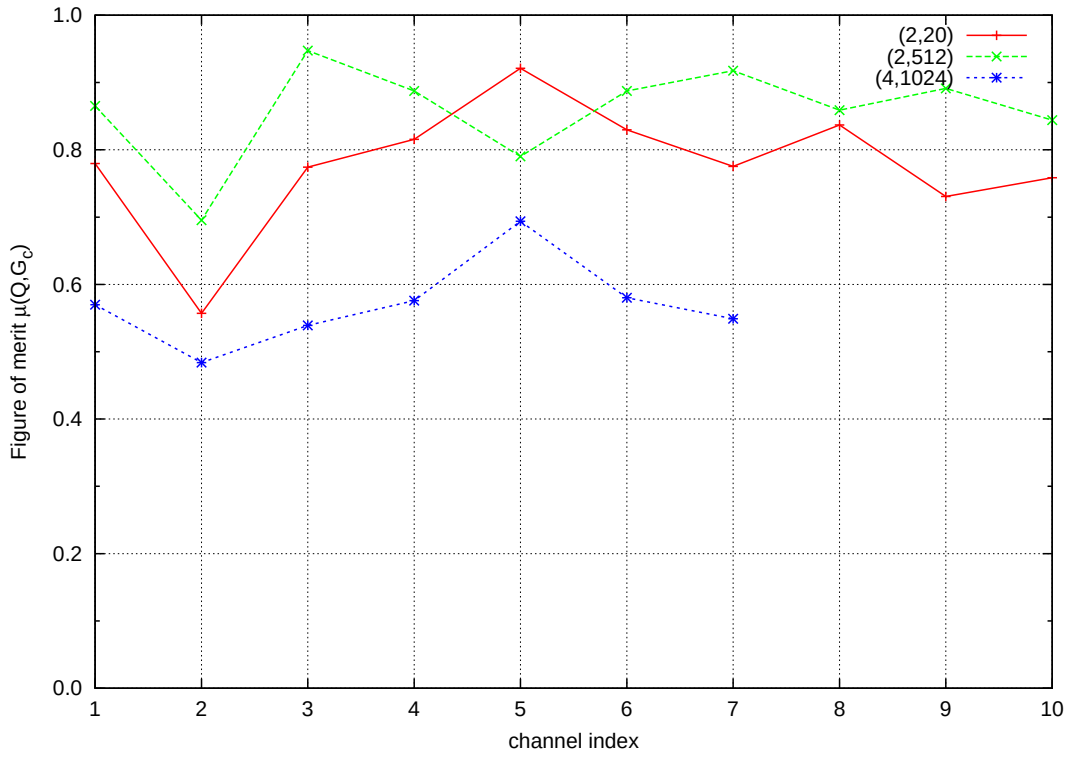

Figure 5.15: Classification is based on geodesic distance. Figure of merit for ($n = 2$,$K = 20$), ($n = 2$,$K = 256$), ($n = 4$,$K = 1024$) cases.

5.6.2.2 Validation based on error rate

Another characterization for the geometrical resemblance between a MIMO channel and its associated centroid is considered in this section.

Principle

This criterion consists in comparing the channel to its centroid by detecting the transmit signal while having the centroid as an estimate for the channel.

Let $\mathbf{H}$ be a $n \times n$ MIMO channel matrix with Gram matrix $\mathbf{G} = \mathbf{H}^{\dagger}\mathbf{H}$. Rewriting the MIMO channel model (5.2) leads to

$$\mathbf{r} = \mathbf{H}\mathbf{z} + \boldsymbol{\nu},$$

where $\mathbf{r}$ denotes the received vector, $\mathbf{z} \in (\text{M-QAM})^n$ is the transmit signal, and $\boldsymbol{\nu}$ is an AWGN vector with variance $2N_0$ per complex dimension.

The current validation aims at decoding the transmit signal $\mathbf{z}$ using the Gram matrix of the centroid $\mathbf{G}_c$ instead of the channel Gram matrix $\mathbf{G}$. This is equivalent to minimize the following metric over $\mathbf{z} \in (\text{M-QAM})^n$

$$\hat{\mathbf{z}} = \arg \min_{\mathbf{z} \in (\text{M-QAM})^n} \|\mathbf{y} - \mathbf{R}_c\mathbf{s}\|^2 \tag{5.19}$$

where $\mathbf{R}_c = \sqrt{\mathbf{G}_c}$, $\mathbf{G}_c$ is the centroid associated to the Hermitian form $\mathbf{G}$, and $\hat{\mathbf{z}}$ is an estimate for $\mathbf{z}$.

One could notice that this criterion is close to the one based on the Voronoi region comparison. However, the previous criterion considers the lattice Voronoi region which is not necessary equal to that of the lattice constellation associated to the MIMO channel (section 2.1.4). The evaluation of the error probability using the channel centroid $\mathbf{R}_c$ is equivalent to comparing the Voronoi regions of lattice constellations associated to $\mathbf{R}_c$ and $\mathbf{H}$.

Simulation results

To use this criterion, we classify first 4 different channels, generated at random, to determine their associated centroids. Then, we decode the signal $\mathbf{z}$ as given in (5.19). To reduce the complexity of the detector, a sphere decoder [1], [63] could be applied. Simulation results are plotted in Figs. 5.16, 5.17, and 5.18 in terms of point error probability wrt the transmit SNR per bit. The notation (*index*,*K*) means that the index of the channel is *index* and the size of the codebook used for the classification is K, e.g. (2,20) denotes the performance of the channel 2 using a codebook whose size is equal to 20. Notice that $K = \infty$ (optimal case) means that the detection is based on a perfect estimation of the channel $\mathbf{H}$.
For this criterion, the classification will be validated by evaluating the gap between two cases for the detection:

1. the optimal case where the channel is perfectly known at the receiver, i.e. $K = \infty$.
2. the sub-optimal case where the channel is estimated with its associated centroid.

Notice that the choice of K in simulations is done randomly. We believe that there may be a more intelligent way to find the optimal codebook size regarding the dimension n and the quantization metric.
The two first figures, 5.16 and 5.17, illustrate the performance for 2-dimensional Hermitian forms when applying 4-QAM and 16-QAM on transmit antennas. We consider, for instance, the channel indexed by 1, 2, 4, 5 in Fig. 5.15. It is clear in both figures that increasing the size of the codebook improves the performance. For example, in Fig. 5.16, for the channels of index 1 and 5, the loss in SNR is negligible (< 0.1 dB) for $K = 512$ and ≥ 0.6 dB for $K = 20$, at error

probability close to 10^{-3}, with respect to the optimal case. Also in Fig. 5.16, the loss in SNR for the channel of index 4 is divided by two when moving from 20 to 512 in codebook size. In addition, both figures 5.16 and 5.17 show that the distance between the channel of index 2 and its centroid is the highest and the loss in SNR is more significant for $K = 20$ than for $K = 512$. In this case, the detection with the centroid leads to a significant loss for the all codebook and constellation sizes. This conclusion could be made provided the simulation results plotted in Fig. 5.15 which shows a low figure of merit for this channel.
In Fig. 5.17, the loss in SNR due to the estimation error (using $\mathbf{R}_c$ instead of $\mathbf{H}$) is more significant when using bigger constellation size, i.e. 16-QAM. It is more important for $K = 20$ than for $K = 512$. Indeed, for the same channel ($index = 1$), the loss is equal to 2 dB for $K = 512$ and much higher for $K = 20$, at error probability equal to 10^{-3}.

The last figure 5.18 corresponding to $n = 4$ and 4-QAM applied on transmit antennas, shows that a codebook of 1024 is insufficient to well represent 4×4 MIMO channels. The lowest SNR loss is given by the channel of index 5. At error probability equal to 10^{-3}, this loss is about 4.3 dB. This result could be deduced also when observing Fig. 5.15.

Conslusions

To conclude, the estimation of MIMO channel with its associated centroid leads to a loss over a perfect channel estimation in terms of error probability. This loss increases wrt the dimension of the channel matrices and on the modulation size. Therefore, a high codebook size is recommended for high n and M. The adjustment of this size depends on the application constraints. It should be noticed that the introduction of channel coding in the considered transmission scheme should reduce the required codebook size. Indeed, to determine this size for coded system, lower error probability should be considered($\leq 10^{-2}$). In this case, the loss in SNR is reduced even for $n = 4$ wrt PER=10^{-3}. Hence, we can use a codebook with acceptable size.

After evaluating the accuracy of our classification by comparing MIMO channels to their associated centroids using Voronoi regions and error rates, we propose in the following section an application of this classification to closed-loop MIMO systems e.g. beamforming.

5.7 Application of the classification algorithm to closed-loop MIMO systems

The closed-loop MIMO systems are the wireless systems where CSI is assumed at the transmitter (e.g. beamforming). The CSI could be a full knowledge about the channel matrix or a partial knowledge of this matrix. In this study, we focus on systems that converts the MIMO systems into a bank of scalar channels. This operation requires the knowledge of the precoder matrix $\mathbf{U}$ at the transmitter. The matrix $\mathbf{U}$ is obtained by applying the singular value decomposition (SVD) on the MIMO channel matrix $\mathbf{H}$:

$$\mathbf{H} = \mathbf{V}\sqrt{\mathbf{D}}\mathbf{U}^{\dagger} \tag{5.20}$$

where $\sqrt{\mathbf{D}} = diag(\sqrt{\lambda_1}, \ldots, \sqrt{\lambda_m}, 0, \ldots, 0)$ is a diagonal matrix, $\mathbf{V}$ and $\mathbf{U}$ are unitary matrices and m is the channel rank.
By applying the basis change matrices $\mathbf{V}^{\dagger}$ and $\mathbf{U}$ on the model (5.2) at the receiver and the

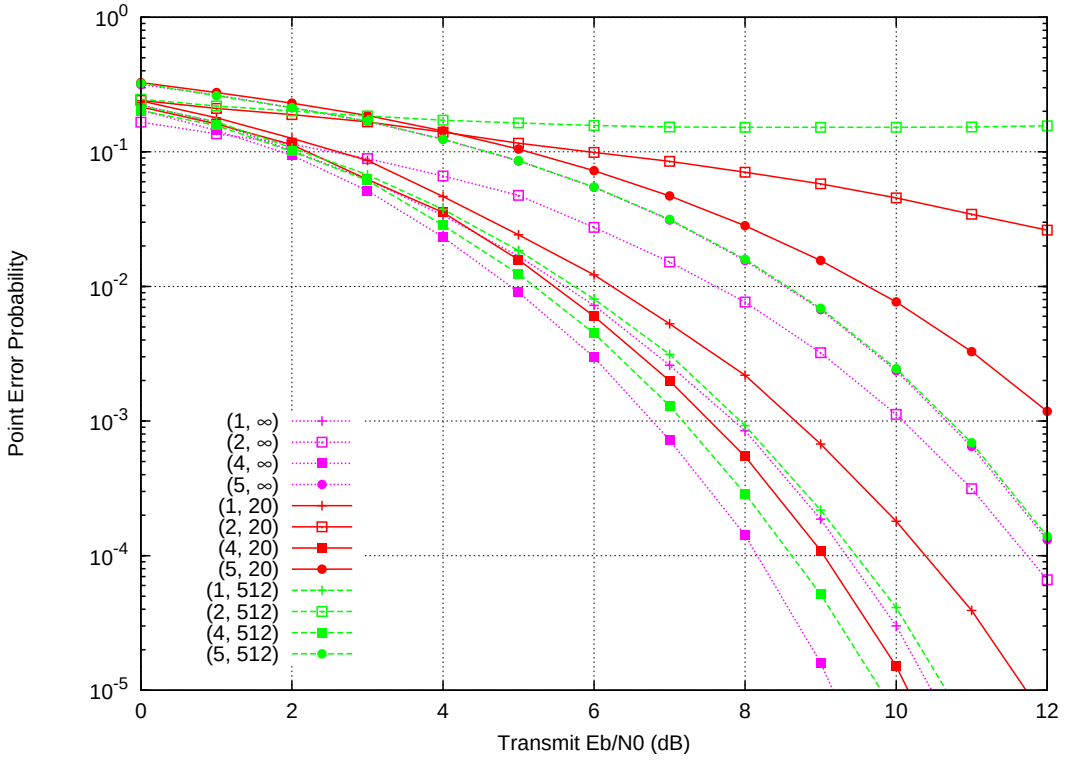

Figure 5.16: Point error rate performance for $n = 2$ antennas using centroids for detection. Classification using geodesic metric. Components of $\mathbf{z}$ are Gaussian integers taken from a 4-QAM constellation (uncoded).

transmitter respectively, the MIMO channel is transformed into m parallel and independent SISO channels:

$$\mathbf{V}^\dagger \mathbf{r} = \sqrt{\mathbf{D}}\mathbf{z} + \mathbf{V}^\dagger \boldsymbol{\nu} \tag{5.21}$$

For these systems, the SVD operation is often performed by the receiver which could have an estimate for the channel matrix, for example through a training sequence. Then, a feedback link is required to inform the transmitter about the precoder matrix $\mathbf{U}$. In practice, a limited-rate feedback is provided, which entails the quantization of the matrix $\mathbf{U}$. Unfortunately, a quantizer in MIMO systems generally needs a codebook size that grows exponentially with the product of the transmit and the receive antennas, $2n_t \times n_r$ [39]. For example, when $n = n_t = n_r = 4$, the matrix $\mathbf{U}$ has 32 parameters that should be quantized every T_c channel use. This means that the number of bits necessary to quantize the precoder matrix is exponential in 32, which exceeds the capacity of practical wireless systems. Therefore, it is important to design intelligent algorithms to quantize complex matrices (e.g. $\mathbf{U}$) under the constraint of a limited-rate feedback.

Several approaches were proposed in the literature to quantize the matrix $\mathbf{U}$ with a few bits. Most of them were designed to optimize a given criterion, e.g. maximize capacity or minimize error rate [39], [38], [43], [40]. In [38] and [43], the authors focused on beamforming technique and proposed to quantize only a column vector of the matrix $\mathbf{U}$ which corresponds to the highest mode. Their quantization strategies are then limited to applications consisting in the transmission of a single data stream (e.g. beamforming), although capacity in MIMO systems can increase with the transmission of multiple data streams simultaneously [59], [21].

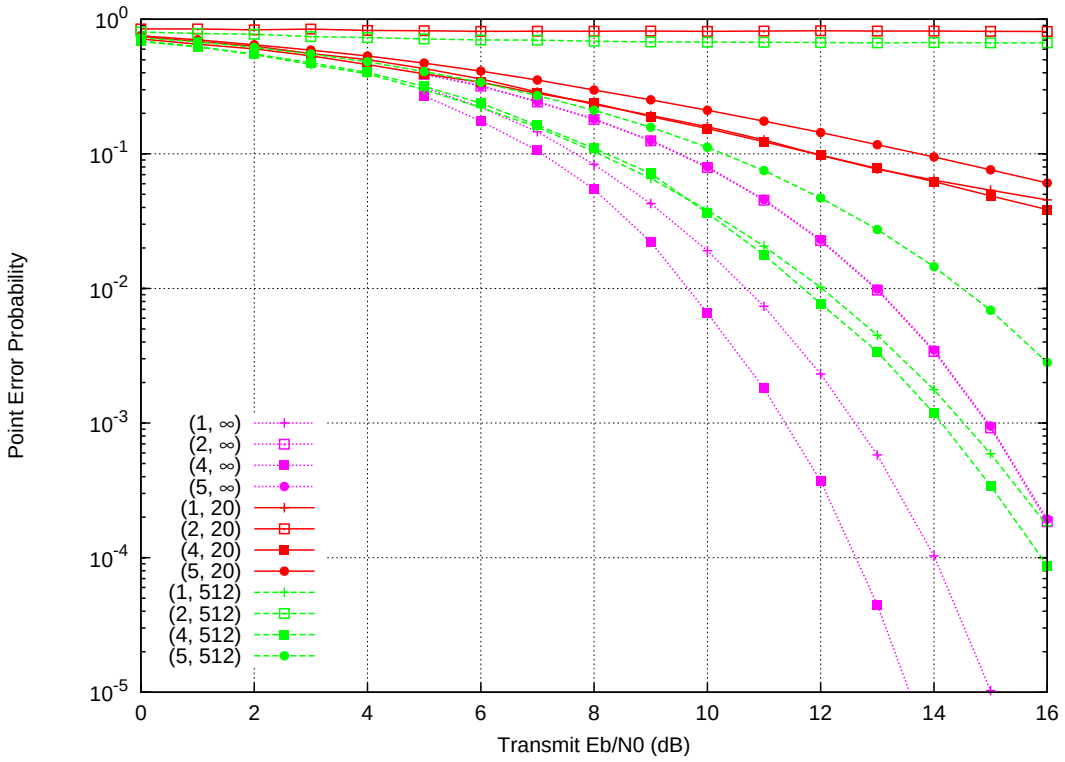

Figure 5.17: Point error rate performance for $n = 2$ antennas using centroids for detection. Classification using geodesic metric. Components of $\mathbf{z}$ are Gaussian integers taken from a 16-QAM constellation (uncoded).

We propose in the next section to apply our classification algorithm to quantize the overall precoder matrix $\mathbf{U}$.

5.7.1 Evaluation of the classification quantization

Quantization using the classification

The quantization is performed at the receiver side and it is composed of two steps. The first step consists in finding the nearest centroid $\mathbf{G}_c$ to the Hermitian form $\mathbf{G} = \mathbf{H}^\dagger\mathbf{H}$. The second step applies the diagonalization on $\mathbf{G}_c$ as

$$\mathbf{G}_c = \mathbf{U}_c \cdot \mathbf{D}_c \cdot \mathbf{U}_c^\dagger \tag{5.22}$$

Finally, the obtained matrix $\mathbf{U}_c$ is considered as an estimate for $\mathbf{U}$. The next section evaluates the performance of the quantization using the classification algorithm.

In the following, we examine the performance of the proposed approach to quantize the matrix $\mathbf{U}$. This consists in evaluating the diagonalization operation using the matrix $\mathbf{U}_c$ at the transmitter and $\mathbf{V}_c$ at the receiver.
To do this, we check the coefficients of the obtained matrix

$$\sqrt{D'} = \mathbf{V}_c \cdot \mathbf{H} \cdot \mathbf{U}_c = \mathbf{U}_c^\dagger \cdot \mathbf{U} \cdot \sqrt{\mathbf{D}} \cdot \mathbf{U}^\dagger \cdot \mathbf{U}_c$$

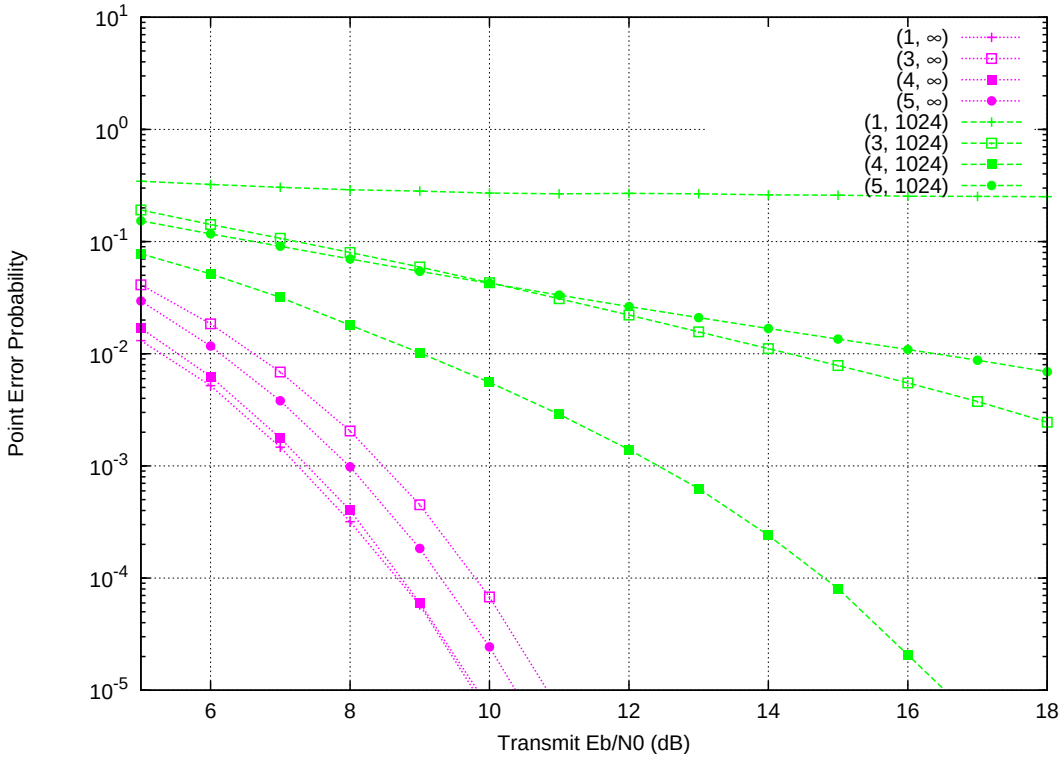

Figure 5.18: Point error rate performance for $n = 4$ antennas using centroids for detection. Classification using geodesic metric. Components of $\mathbf{z}$ are Gaussian integers taken from a 4-QAM constellation (uncoded).

We compute the ratio, $\rho_{i=1,\ldots,n}$, between a diagonal element and all the elements lying in the same row of the matrix $\sqrt{D'} = [d'_{ij}]$, that is

$$\rho_i = \frac{|d'_{ii}|^2}{\sum_{j=1}^{n} |d'_{ij}|^2} \tag{5.23}$$

When ρ_i approaches 1 for all i between 1 and n, the matrix $\sqrt{D'}$ could be considered as a diagonal matrix. Therefore, the classification is said to well quantize the matrix $\mathbf{U}$.

Figures 5.19 and 5.20 illustrate the distribution of the parameter $\rho_{i=1,\ldots,n}$, assuming an increasing order ($\rho_1 \leq \rho_2 \leq \cdots \leq \rho_n$), for the geodesic and Frobenius metrics. It is noticed that for 2-dimensional Hermitian space, a codebook of 512 well quantizes the matrix $\mathbf{U}$, whereas the quantization with a small codebook of 20 centroids is worse. For this case, it seems that the geodesic distance diagonalizes better the matrix $\mathbf{D}'$ than the Frobenius distance, for both codebook sizes. In 4-dimensional space, the classification performance for the diagonalization degrade, and the matrix $\sqrt{D'}$ couldn't be considered as a diagonal matrix for a codebook size equal to 256 with both metrics. Indeed, the majority of matrices $\sqrt{D'}$ have the parameter $\rho_{i=1,\ldots,n}$ lower than 1, which means that the estimation error due to quantization is not negligible and could lead to inter-symbol interference. Therefore, to have better performance for $n = 4$, a bigger codebook is required. Notice that ρ_1 and ρ_4 are closer to 1 for the Frobenius metric than for the geodesic one, and the inverse is observed for ρ_2 and ρ_3.

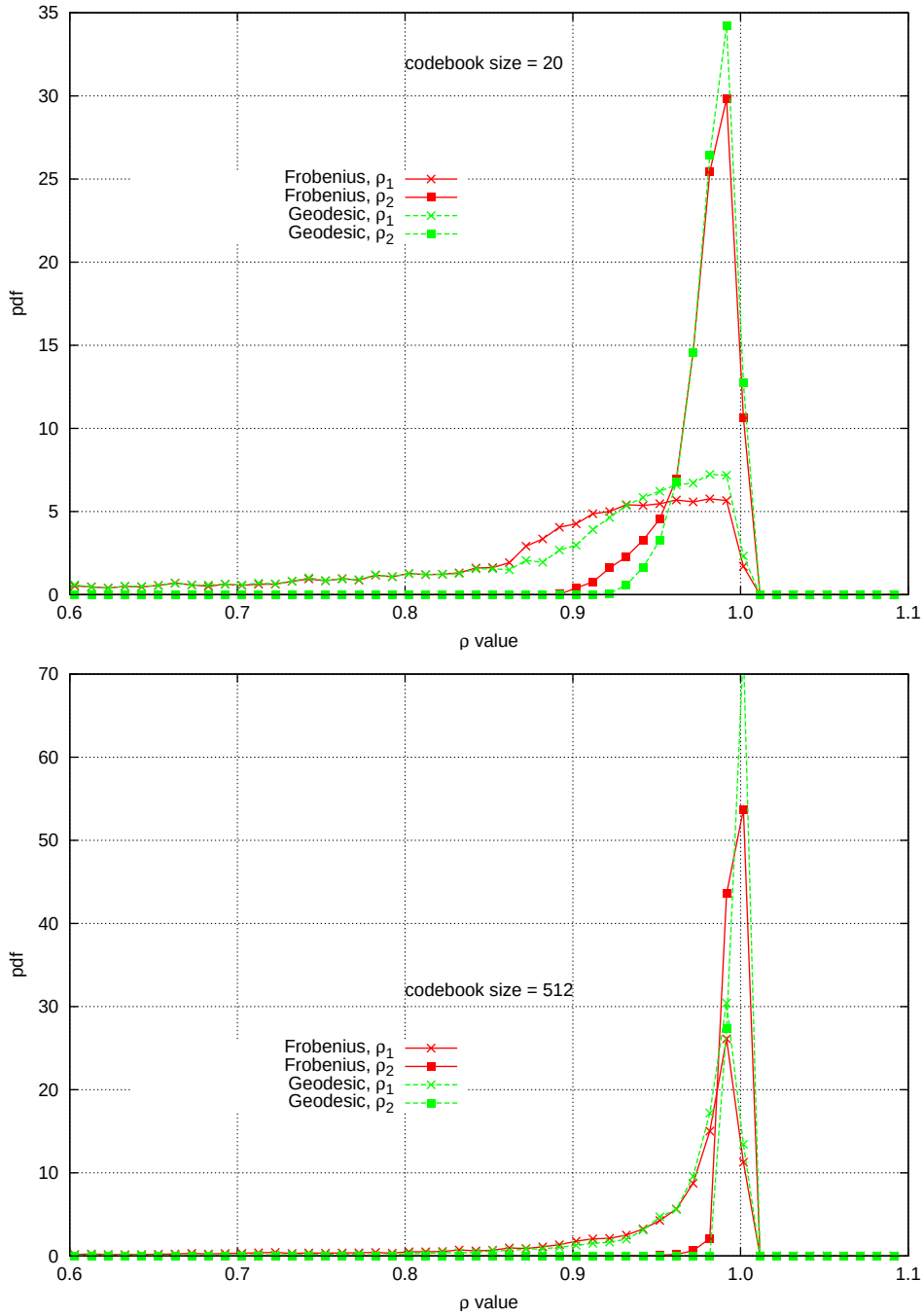

Figure 5.19: Distribution of the parameters ρ_1, ρ_2 given in (5.23). Classification with geodesic and Frobenius metrics when ($n = 2$,$K = 20$) (on the top) and ($n = 2$,$K = 512$) (on the bottom).

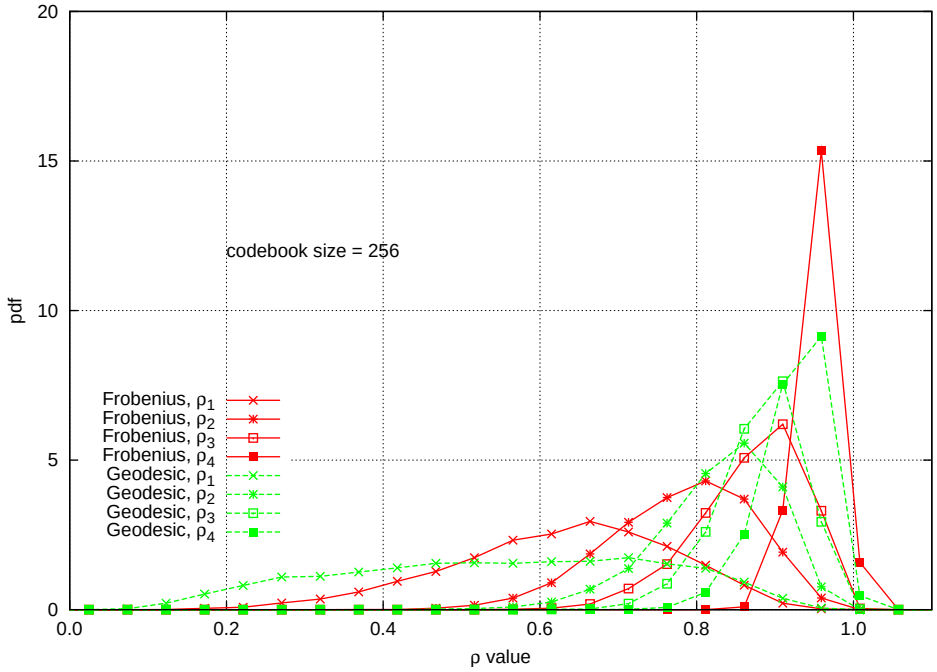

Figure 5.20: Distribution of the parameters ρ_1, ρ_2, ρ_3, ρ_4 given in (5.23). Classification with geodesic and Frobenius metrics when ($n = 4$,$K = 256$).

As an application for this quantization, we study in the sequel the beamforming technique.

5.7.2 Application of the classification to beamforming

Now, after focusing on the performance of the proposed approach to quantize the precoder matrix $\mathbf{U}$, we use it in the sequel for the beamforming technique. This section presents first the proposed beamforming scheme using the classification algorithm. Then, the performance (in terms of error rate) of the designed scheme for MIMO-beamforming systems are compared to the optimal case where a perfect estimation of the matrix $\mathbf{U}$ is assumed at the transmitter (i.e. $MSD = 0$).

5.7.2.1 Beamforming scheme

Beamforming [2] in MIMO systems works in two steps. The first step transforms the MIMO system into a finite number of SISO systems (or channel modes). The second step activates only the strongest mode and send the signal accordingly. Thanks to the combination of received signals from the multiple antennas, such systems can attain full diversity order in flat-fading Rayleigh channels [37], [24], [45], [34]. Regarding the benefits of this technique, MIMO beamforming is proposed for high data rates wireless LANs (IEEE 802.11) and for broadband wireless MANs (IEEE802.16).

Figure 5.21 illustrates our designed scheme for transmit beamforming. Given a perfect channel estimation and using the classification procedure described in algorithm 3, the receiver searches the centroid associated to the current channel. Then, it sends the index of the corresponding class to the transmitter via a feedback which is assumed error free. After that, the transmitter

applies the matrix $\mathbf{U}_c$ (eq. (5.22)) as an estimate for $\mathbf{U}$. Only the strongest mode, corresponding to the highest eigenvalue, is selected for the transmission. Notice that the feedback necessitates only $\log_2(K)$ bits where K is the codebook size. For example, if $K = 256$, 8 bits are only needed to quantize the matrix $\mathbf{U}$. The matrices $\mathbf{U}_c$ corresponding to the different centroids are stored in a lookup table. Having the centroid index, the transmitter finds the appropriate matrix $\mathbf{U}_c$ in this table.

The receiver applies the matrix $\mathbf{V}_c$ on the received signal $\mathbf{r}$, where

$$\mathbf{V}_c = \mathbf{U}_c^{\dagger} \cdot \sqrt{\mathbf{G}} \cdot \mathbf{H}^{-1}$$

and $\mathbf{G} = \mathbf{H}^{\dagger}\mathbf{H}$.

It is noticed that the receiver can use the matrix $\mathbf{V}$ given in (5.20) instead of the above matrix $\mathbf{V}_c$ since it has a perfect channel estimation. Nevertheless, we find via simulations that the diagonalization performance with $\mathbf{V}$ are worse than with $\mathbf{V}_c$.

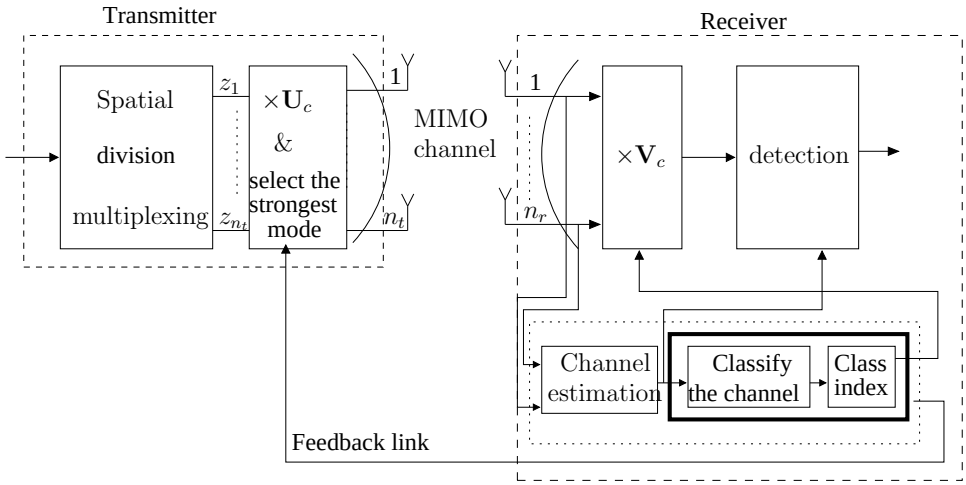

Figure 5.21: System model with the proposed beamforming scheme using the MIMO classification.

5.7.2.2 Simulation results

Applying the uncoded transmission scheme depicted in Fig. 5.21 to different scenarios leads to the simulation results plotted in Figs. 5.22 and 5.23. In both figures, the notation (*dist_type*,*K*) means that the distance between Hermitian forms is measured based on *dist_type* (geodesic or Frobenius) for a codebook size equal to K. *Perfect estimation* corresponds to the optimal case where the precoder matrix $\mathbf{U}$ is estimated without error (i.e. $K = \infty$).

Figures 5.22 and 5.23 illustrate the error rate per bit as a function of the transmit SNR for $n = 2$ and $n = 4$, respectively. As expected, the quantization provides good performance for $n = 2$, a low codebook size ($K = 20$) and a 4-QAM modulation with both geodesic and Frobenius. However, increasing the modulation size (16-QAM) degrades the performance, especially for $K = 20$. This impact is negligible for the geodesic distance with $K = 512$. For all cases, it is noticed that the geodesic distance performs better than the Frobenius distance in terms of error

rate. This result could be observed in Fig. 5.19 where the parameter ρ_2 is close to 1 for $K = 20$ and $K = 512$. Moreover, Fig. 5.22 shows the improvement of the diversity order from 2 to 4 when applying the mode selection.
Besides, in Figs. 5.22 and 5.23, the antenna selection, introduced in chapter 4, is compared to the beamforming (called also mode selection). The selection is achieved by activating only the transmit antenna that maximizes the received SNR. In both figures, the performance with the mode selection are better than with the antenna selection. Indeed, a gain of about 1dB in SNR is noticed at error rate equal to 10^{-5}.

When $n = 4$, the selected mode corresponds to the parameter ρ_4 in Fig. 5.20. This figure showed that the classification does not well perform the diagonalization for both metrics, which could lead to interference-inter symbol that impacts badly the decoding procedure. Indeed, this impact is observed in Fig. 5.23 where performance are degraded with $K = 256$.

As conclusions, based on simulation results, it appears that the performance (in terms of error rate) of the beamforming scheme using the classification comparing to the optimal one (perfect estimation of the precoder matrix) depend on the chosen metric, the channel dimension, the codebook size, and the modulation size on the transmitter. For low dimension $n = 2$, we noticed that the classification with the geodesic distance performs closer to the optimal one than the Frobenius distance for $n = 2$, $K = 512$ and different modulation sizes.
When $n = 4$ and $K = 1024$, the loss in performance using the classification approach are very important with both distances.

5.7.3 Potential application for the classification

Recall that the use of the precoder matrices $\mathbf{U}$ and $\mathbf{V}$ (5.20) at the transmitter and the receiver conveys the MIMO system into a parallel and independent SISO systems. In the previous section, we showed how the classification could be used to quantize the matrix $\mathbf{U}$.
We propose a second application to the classification for coded MIMO systems. It is known that applying some channel coding algorithms (e.g. LDPC codes, turbo codes, convolutional codes, etc) in MIMO systems increases the computation complexity due to the likelihoods [10], which are exponential in n, $2^{n \log_2(M)}$, where M is the modulation size and $n = n_t = n_r$. With the diagonal model (5.21), the likelihoods are computed for each SISO channel and not for the whole MIMO channel. This fact decreases the complexity from exponential in n to linear in n. Therefore, the proposed approach to diagonalize the MIMO channel could be used in this context to decrease the complexity of the decoding process.
This section gives some initial results for this application. The performance of the proposed approach in coded MIMO systems will be illustrated later.
We present, in the following, the performance of the diagonal model (5.21) while using all the modes. This allows to predict these performance while introducing the channel coding. Figures 5.24 and 5.25 illustrate the error rate per bit wrt the transmit SNR. The notations used in Figs. 5.22 and 5.23 remain valid in the current figures. For $n = 2$, it is noticed in Fig. 5.24 that geodesic distance performs better than Frobenius distance for $K = 20, 512$ and modulation size $M = 4, 16$, as expected from Fig. 5.19. It is clear that the quantization performance depends on the codebook size for both distances. The impact of the quantization is observed at high SNR. For the different cases, the error probability approaches a limit that depends on the codebook size and the selected distance. This behavior is conditioned essentially by the lowest mode which has the highest contribution in the inter-symbol interference.

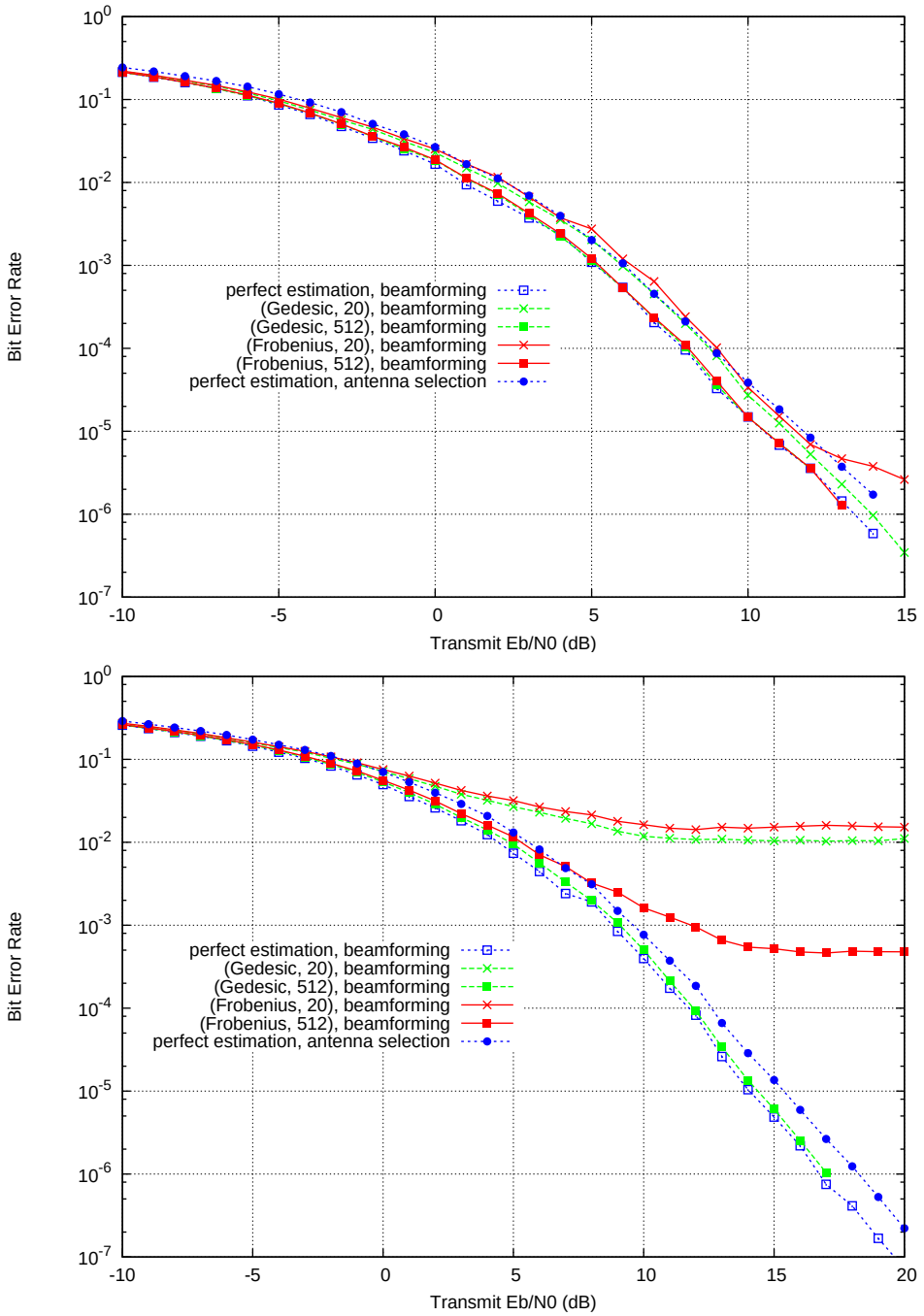

Figure 5.22: Bit error rate for the best eigen mode SISO channel resulting from the SVD of 2×2 static MIMO channel using the proposed quantization approach for beamforming. 4-QAM modulation (on the top) and 16-QAM modulation (on the bottom) applied on Tx antennas.

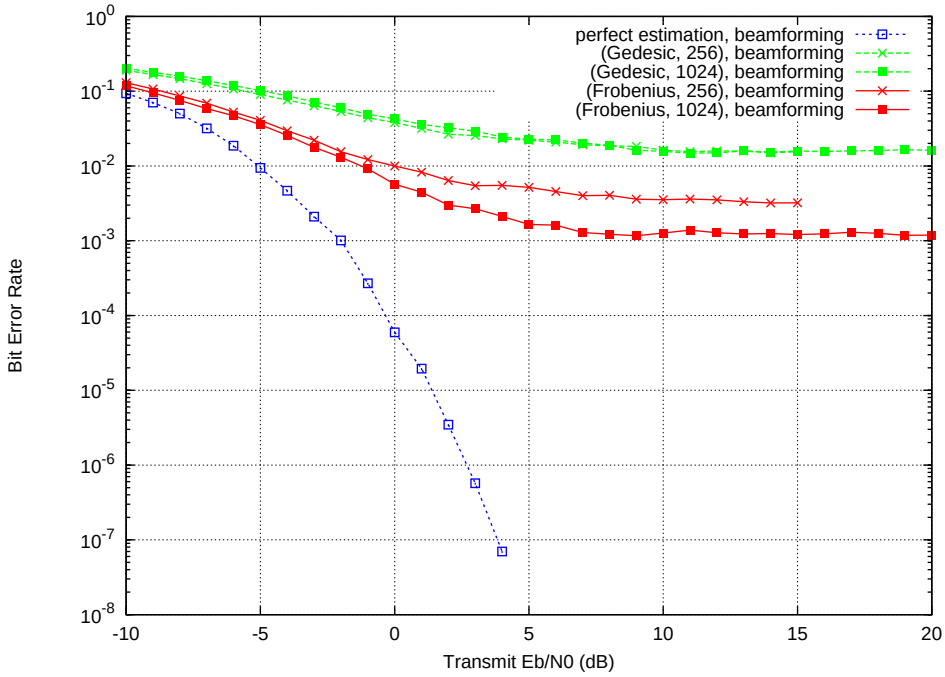

Figure 5.23: Bit error rate for the best eigen mode SISO channel resulting from the SVD of 4×4 static MIMO channel using the proposed quantization approach for beamforming. 4-QAM modulation applied on Tx antennas.

When introducing the channel coding, the performance should be improved with respect to the uncoded case. Therefore, it may be sufficient to focus on the classification performance at low error probability ($\leq 10^{-2}$) for uncoded system. In this case, the geodesic distance with $K = 512$ could be a good quantizer for both 4-QAM and 16-QAM.

For $n = 4$, the quantization of the precoder matrix $\mathbf{U}$ with $K = 256, 1024$ in Fig. 5.25 does not provide good performance in terms of error probability per bit. The impact of the quantization error is significant in this case. This is expected from Fig. 5.20 where the matrix $\sqrt{D'}$ couldn't be considered as diagonal for the majority of channels. A higher number of centroids is suggested.

Conclusions

This chapter described our proposed classification algorithm of Hermitian forms in multi-dimensional space. The classification procedure aims to quantize any Hermitian form by finding an appropriate representative (or centroid) which belongs to a given codebook. To design this algorithm, we derived a new metric, called geodesic, which measures the distance between Hermitian forms. We defined also a way to build a codebook using Lloyd algorithm. The classification algorithm was proposed first for MIMO channels by considering their associated Hermitian forms. Then, it was extended to lattices.

In the second part of this chapter, we evaluated the performance of the MIMO classification algorithm. First, we focused on the distribution of the MIMO channels between classes as well

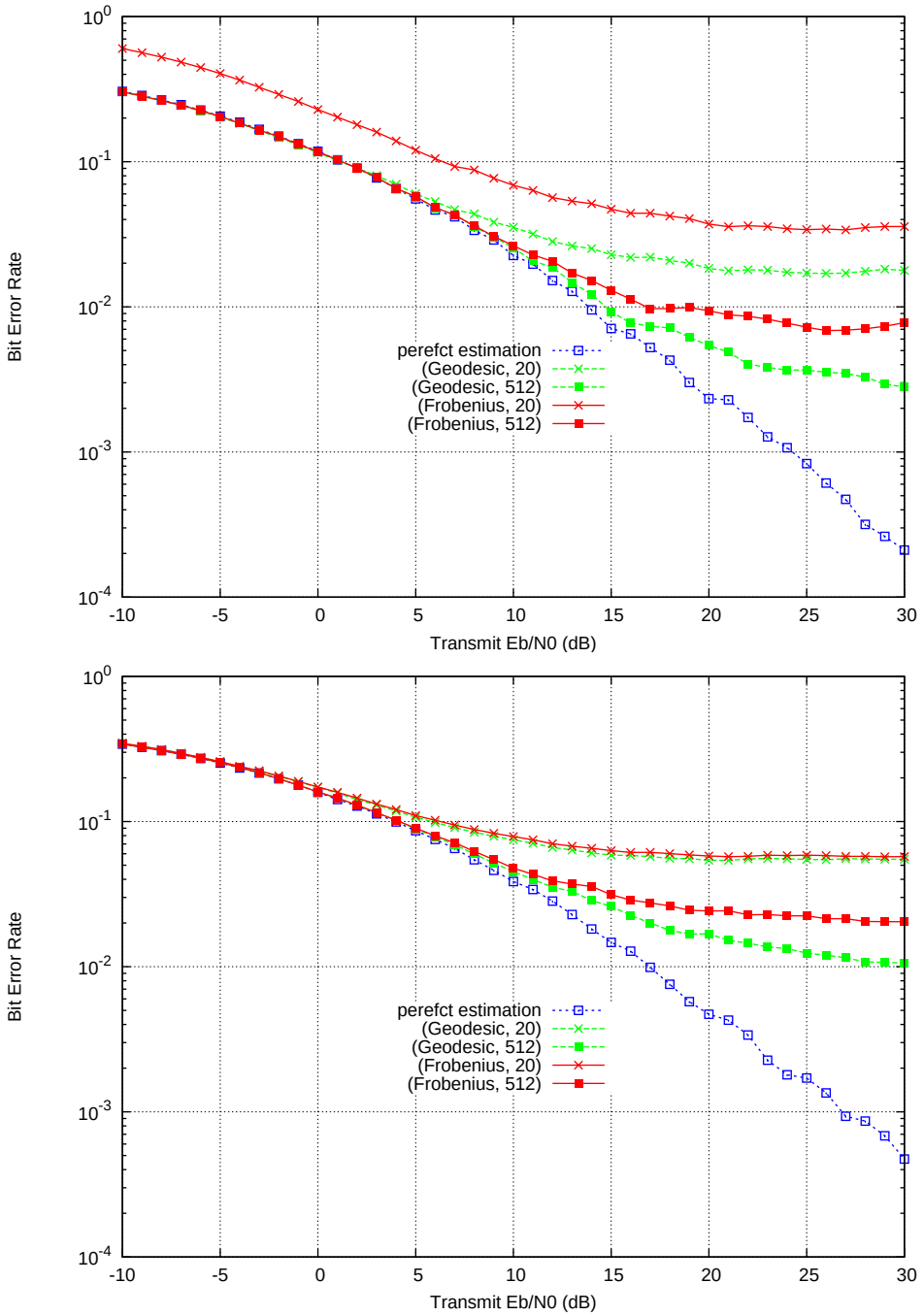

Figure 5.24: Bit error rate performance for 2 SISO channels resulting from the SVD of 2×2 static MIMO channel using the proposed quantization approach. 4-QAM modulation (on the top) and 16-QAM modulation (on the bottom) applied on Tx antennas.

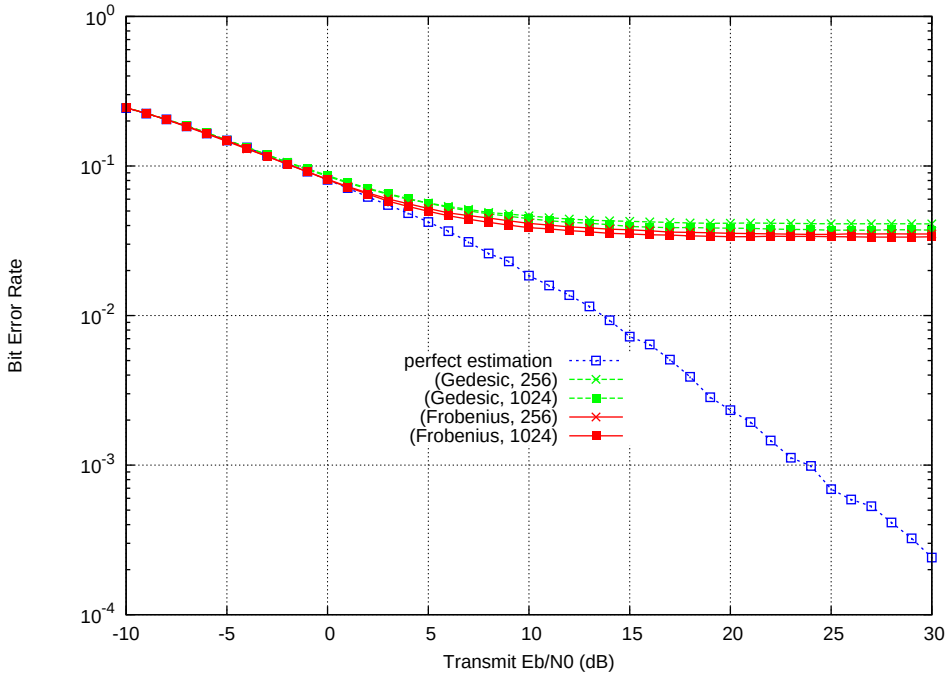

Figure 5.25: Bit error rate performance for 4 SISO channels resulting from the SVD of 4×4 static MIMO channel using the proposed quantization approach. 4-QAM modulation applied on Tx antennas.

as the distribution of the centroids wrt the Hermitian form space origin, $\mathbf{I}_n$. Two channel models were used for simulations: correlated and uncorrelated models. We noticed that the classification distributes the channels uniformly between classes for both models when using geodesic distance. However, this distribution depends on the selected model when Frobenius distance is adopted as the classification metric. When n is high ($n = 4$), simulation results showed that almost all the centroids lie in the same orbit wrt the origin, for a codebook size of 256 or 1024 and both metrics (geodesic and Frobenius). Thus, one could deduce that a bigger codebook size is required for $n = 4$. Second, we considered two criteria, Voronoi regions and error probabilities, to measure the resemblance between a MIMO channel and its associated centroid. Simulations were carried out only with geodesic distance. We found that the classification provides a good representative for 2×2 MIMO channels, with an acceptable codebook size. However, for higher dimension, $n_t = n_r \geq 3$, the performance degrade and a large codebook size may be necessary to well represent a MIMO channel with its nearest centroid.

Finally, we proposed to apply the classification to closed-loop MIMO systems, e.g. beamforming. Our algorithm is used at the receiver side to find the nearest centroid to the MIMO channel. Then, the transmitter is informed about the centroid index to select its corresponding precoder matrix (stored in look-up table). We compared the performance, in terms of error probability, of our approach to those with the optimal case (without estimation error due to classification). It appears that the performance for both cases are close with small constellation size (4-QAM) even for low codebook size with geodesic and Frobenius metrics. Nevertheless, the impact of the interference due to the estimation error increases with higher constellation size (16-QAM). This impact is still negligible with geodesic distance when using a large codebook size of 512. When $n_t = n_r = 4$, as noticed for the above criteria, a bigger codebook size is needed to get rid of

the interference even when only the best mode is used. At the end of this chapter, we outlined a potential application for the classification in coded MIMO systems. The classification can be used to diagonalize the MIMO channel into a finite SISO channels. Then, the decoding process could be achieved more easily for each SISO channel instead of processing the whole MIMO channel. This decreases the complexity of the decoding process in MIMO channels.

Conclusions and perspectives

Conclusions

In this report, we focused on uncoded MIMO systems with spatial multiplexing scheme at the transmitter. Wireless channels were assumed to be frequency non-selective and quasi-static, and a perfect CSI was supposed only at the receiver.

First, we studied the performance of such systems in terms of error probability when one or distinct modulations are applied on the transmit antennas. Considering the lattice constellation associated to the MIMO channel and using lattice theory, we derived an accurate approximation for the conditional error probability. This approximation was computed at first for the case when more antennas are available at the receiver side. Then, we generalized this approximation without any constraint on the number of antennas. Monte-Carlo simulation results for both cases showed the accuracy of our analytical approximation for different antenna and modulation configurations. The derived approximation was also compared to a simple bound for the lattice associated to the MIMO channel. Simulations showed a loss in SNR of about 2dB with the simple bound over the one proposed for 4×4 MIMO system and 4-QAM on transmit antennas. Finally, The complexity of our approximation was outlined.

Two applications were suggested for the derived error probability approximation: adaptive modulation and antenna selection. We proposed an efficient algorithm to adapt modulations while maximizing the total spectral efficiency and satisfying a constraint on error probability. This algorithm considers a short list of modulation combinations and uses the dichotomy method to go through the list. This leads to a reduced complexity. The proposed adaptive modulation scheme was compared to another one using the simple bound that is indicated in the previous paragraph. It was also compared to the non-adaptive scheme with different modulation configurations. For both cases, 4×4 quasi-static MIMO system and distinct modulations on transmit antennas case were assumed. It was shown that the proposed adaptive algorithm achieves the highest performance in terms of spectral efficiency while keeping the error rate close to the target one.
For antenna selection, we outlined at first the benefit of this technique in maintaining the diversity order even with a reduced number of active antennas for SIMO systems. We derived an error probability bound for such systems with antenna selection. Then, we illustrated our algorithm using the derived approximation as a selection criterion. Finally, we presented the performance achieved with antenna selection assuming different selection criteria and different receiver schemes. For each scheme, we noticed that with the same number of active antennas, the selection improves the performance comparing to the non selection case for different cri-

teria. The selection introduces an additional diversity order and an SNR gain for most of the selection criteria. We noted that the proposed selection criterion provides the best performance for ML detectors. Nevertheless, for sub-optimal receivers, it achieves the worst performance. This could be justified by the fact that the proposed approximation was derived assuming a ML detection at the receiver.

At the end of this thesis report, we proposed a classification algorithm for MIMO channels by considering their associated Hermitian forms. This algorithm could be used for adaptive modulation and adaptive channel coding. To apply this algorithm in MIMO channels, we derived a new metric, geodesic distance, that can be used for the corresponding Hermitian forms. Then, we adapted it to lattices. Our proposed metric was compared to the natural distance, known as Frobenius metric. Simulation results showed the performance of the proposed classification to quantize MIMO channels, with both geodesic and Frobenius metrics. We noted that the classification with geodesic distance leads to a uniform distribution of MIMO channels between classes for correlated and uncorrelated models. However, with Frobenius distance, the distribution between classes is different, according to the chosen model. The validation of the classification was achieved by comparing some properties of the classified channels to those of the associated centroids, such as Voronoi regions and error probabilities. For both criteria, we noticed that the classification provides good representatives for 2×2 MIMO channels, with an acceptable codebook size. Unfortunately, for high dimension ($n_t = n_r \geq 3$), a bigger codebook size is necessary for both metrics to well represent a MIMO channel with its nearest centroid. As an application for the classification, we illustrated the closed-loop systems, e.g. beamforming. The transmitter uses the centroid as an estimate for the channel to evaluate its precoder matrix. Then the highest eigen mode is selected for the transmission. For both distances, we noticed that the estimation error impact is negligible for 2×2 MIMO systems and 4-QAM even with the small codebook size. For 4×4 MIMO systems, a large codebook size is required to get rid of the interference even when only the best mode is used. A potential application of the classification for coded MIMO was also outlined. The proposed algorithm could be used to diagonalize MIMO channels to obtain a finite SISO channels. Then, the decoding process performs on each SISO channel instead of working on the whole MIMO system. This method leads to a significant complexity decrease for the decoding process in MIMO channels.

Perspectives

The current classification algorithm requires a large codebook size to well quantize MIMO channels in high dimension ($n_t = n_r \geq 4$). This is impractical for real wireless systems that are designed with a limited-rate feedback. We are studying some approaches to improve this algorithm and use it for high dimensional MIMO channels with an acceptable codebook size.

Another improvement for the proposed classification algorithm aims to determine the optimal codebook size or equivalently the number of classes with respect to different parameters: e.g. the selected quantization metric, the dimension of the Hermitian space and the target quantization distortion (i.e. target QoS). One possible approach from information theory point of view consists in deriving the distortion-rate function associated to a given metric. The distortion represents the distance between a MIMO channel and its appropriate centroid and the rate is equal to $\log_2(K)$, where K denotes the codebook size. Therefore, according to the allowed distortion, a minimum codebook size could be determined.

Finally, for MIMO systems with a fixed total power, adapting the transmit power to channel conditions over the different antennas could improve the performance. The water-filling algorithm is a good approach to increase the capacity in MIMO systems comparing to the uniform power allocation approach [21], [59]. Unfortunately, this technique requires some knowledge about the channel at the transmitter. The proposed classification algorithm could be used for such applications to give an estimate for MIMO channel under the constraint of a limited-rate feedback.

Bibliography

[1] E. Agrell, T. Eriksson, A. Vardy, and K. Zeger, "Closest point search in lattices," *IEEE Transactions on Information Theory*, vol. 48, no. 8, pp. 2201-2214, August 2002.

[2] E. Akay, E. Sengul, E. Ayanoglu, "Performance analysis of beamforming for MIMO OFDM with BICM," *in Proceedings of International Conference on Communications*, vol. 1, pp. 613-617, May 2005.

[3] A. Annamalai and C. Tellambura, "A new approach to performance evaluation of generalized selection diversity receivers in wireless channels," *in Proceedings of Vehicular Technology Conference*, vol. 4, pp. 2309-2313, October 2001.

[4] E. Biglieri, J. Proakis, and S. Shamai, "Fading channels: Information-Theoretic and Communication Aspects," *IEEE Transactions on Information Theory*, vol. 44, pp. 2619-2692, October 1998.

[5] E. Biglieri, G. Taricco, and A. Tulino, "Decoding space-time codes with BLAST architecture," *IEEE Transactions on Signal Processing*, vol. 50, no. 10, pp. 2547-2552, October 2002.

[6] E. Biglieri, G. Taricco, "How far away is infinity? Using asymtotic analyses in multiple-antenna capacity calculations," *JWCC Barolo, Itay*, November 2002.

[7] E. Biglieri and G. Taricco, *Transmission and reception with multiple antennas: Theoretical foundations*, now Publishers Inc., 2004.

[8] J. Boutros, N. Gresset, L. Brunel, and M. Fossorier, "Soft-input soft-output lattice sphere decoder for linear channels," *in Proceedings of IEEE Global Communications Conference*, vol. 3, pp. 1583-1587, December 2003.

[9] J. Boutros, E. Viterbo, C. Rastello, and J.C. Belfiore, "Good lattice constellations for both Rayleigh fading and Gaussian channels," *IEEE Transactions on Information Theory*, vol. 42, no. 2, pp. 502-518, March 1996.

[10] J. Boutros: *A tutorial on iterative probabilistic decoding and channel estimation*, downalable at http://www.comelec.enst.fr/ boutros/publications/, January 2005.

[11] C.N. Chuah, J.M. Khan, and D. Tse, "Capacity of indoor multiantenna array systems in indoor wireless environment," *in Proceedings of IEEE Global Communications Conference*, vol. 4, pp. 1894-1899, November 1998.

[12] C.N. Chuah, D. Tse, J.M. Khan, and R. Valenzuela, "Capacity scaling in MIMO wireless systems under correlated fading," *IEEE Transactions on Information Theory*, vol. 48, pp. 637-650, March 2002.

[13] S.T. Chung and A.J. Goldsmith, "Degrees of freedom in adaptive modulation: a unified view," *IEEE Transactions on Communications*, vol. 49 , no. 9, pp. 1561-1571, September 2001.

[14] H. Cohen: *Computational algebraic number theory*, Springer Verlag, 1993.

[15] J. H. Conway and N. J. Sloane: *Sphere packings, lattices and groups*, 3rd edition, Springer-Verlag, New York, 1998.

[16] T.M Cover, J.A. Thomas: *Elements of Information theory*, John Wiley & Sons, 1991.

[17] T. Cui and C. Tellambura, "An efficient generalized sphere decoder for rank-deficient MIMO systems," *IEEE Communications Letters*, vol. 9, no. 5, pp. 423-425, May 2005.

[18] G. Dongning, S. Shamai, and S. Verdu, "Mutual information and MMSE in gaussian channels," *in Proceedings of International Symposium on Information Theory*, pp. 349-349, June 2004.

[19] E. Forgey, "Cluster Analysis of Multivariate Data: Efficiency vs. Interpretability of Classification," Biometrics, vol. 21, pp. 768, 1965.

[20] G. D. Forney, "Coset codes I: introduction and geometrical classification,", *IEEE Transactions on Information Theory*, vol. 34, no. 5, pp. 1123-1151, September 1988.

[21] G.J. Foschini and M.J. Gans,"On limits of wireless communication in a fading environment when using multiple antennas," *Wireless Personal Communications*, vol. 6, no. 3, pp. 311-335, March 1998.

[22] G.J. Foschini, G.D. Golden, R.A. Valenzuela, and P.W. Wolniansky, "Simplified processing for high spectral efficiency wireless communication employing multi-element arrays", *IEEE Journal on Selected Areas in Communications*, Vol. 17, no. 11, pp. 1841-1852, November 1999.

[23] Y.H. Gan and W.H. Mow, "Complex lattice reduction algorithms for low-complexity MIMO detection," *in Proceedings of Global Communications Conference*, vol. 5, pp. , November 2005.

[24] D. Gesbert, M. Shafi, D.-S. Shiu, P. J. Smith, and A. Naguib "From theory to practice: An overview of MIMO space-time coded wireless systems," *IEEE Journal Selection Areas in Commununications*, vol. 21, no. 3, pp. 281-302, April 2003.

[25] A. Ghrayeb and T. M. Duman, "Performance analysis of MIMO systems with antenna selection over quasi-static fading channels," *IEEE Transactions on vehicular technology*, vol. 52, no. 2, pp. 281-288, March 2003.

[26] A.J. Goldsmith and S.-G. Chua, "Variable-rate variable-power M-QAM for fading channels," *IEEE Transactions on Communications*, vol. 45 , no. 10, pp. 1218-1230, October 1997.

[27] A. Gorokov, D. A. Gore, and A. Paulraj, "Receive antenna selection for MIMO spacial multiplexing : theory and algorithms," *IEEE Transactions on signal processing*, vol. 51, no. 11, pp. 2796-2807, November 2003.

[28] B. Hassibi and H. Vikalo, "On the expected complexity of sphere decoding," *in Proceedings of Asilomar Conference on Signals, Systems and Computers*, vol. 2, pp. 1051-1055, November 2001.

[29] R.W. Heath, S. Sandhu, and A. Paulraj, "Antenna selection for spatial multiplexing systems with linear receivers," *IEEE Communications Letters*, vol. 5, no. 4, pp. 142-144, April 2001.

[30] R.W. Heath and A. Paulraj, "Antenna selection for spatial multiplexing systems based on minimum error rate," *in Proceedings of IEEE International Conference on Communications*, vol. 7, pp. 2276-2280, June 2001.

[31] S. Helgason: *Differential Geometry, Lie Groups, and Symmetric Spaces.* Graduate Studies in Mathematics, vol. 34, American Mathematical Society, 2001.

[32] R. Horn and C. Johnson: *Matrix Analysis*, NewYork: Cambridge University Press, 1985.

[33] R. Kannan, "Improved algorithmsfor integer programmingon related lattice problems," *in Proceedings of the ACM Symposium on Theory of computing*, pp. 193-206, April 1983.

[34] E. G. Larsson and P. Stoica: *Space-Time Block Coding for Wireless Communications*, Cambridge University Press, New York, 2003.

[35] A. Leon-Garcia: *Probability and Random Processes for Electrical Engineering*, Addison Wesley, New York, NY, 2nd edition, 1994.

[36] S.P. Lloyd, "Least squares quantization in PCM," *IEEE Transactions on Information Theory*, vol. 28 no. 2, pp. 129-137, March 1982.

[37] T. K. Y. Lo "Maximum ratio transmission," *IEEE Transactions on Commununications*, vol. 47, no. 10, pp. 1458-1461, October 1999.

[38] D.J. Love, R.W. Heath, and S. Thomas, "Grassmannian beamforming for multiple-input multiple-output wireless systems," *IEEE Transactions on Information Theory*, vol. 49, no. 10, pp. 27335-2747, October 2003.

[39] D.J. Love, R.W. Heath, W. Santipach, and M.L. Honig, "What is the value of limited feedback for MIMO channels?," *IEEE Communications Magazine*, vol. 42, no. 10, pp. 54-59, October 2004.

[40] D.J. Love and R.W. Heath, "Limited feedback unitary precoding for orthogonal space-time block codes," *IEEE Transactions on Signal Processing*, vol. 53, no. 1, pp. 64-73, January 2005.

[41] S.L. Loyka, "Channel capacity of MIMO architecture using the exponential correlation matrix," *IEEE Communications Letters*, vol. 5, no. 9, pp. 369-371, September 2001.

[42] J. MacQueen, "Some Methods for Classification and Analysis of Multivariate Observations," *in Proceedings of the Fifth Berkeley Symposium Mathematical Statistics and Probability*, vol. 1, pp. 281-296, 1967.

[43] K.K. Mukkavilli, A. Sabharwal, E. Erkip, and B. Aazhang, "On beamforming with finite rate feedback in multiple-antenna systems," *IEEE Transactions on Information Theory*, vol. 49, no. 10, pp. 2562-2579, October 2003.

[44] A. Papoulis: *Probability, Random Variables, and Stochastic Processes*, McGrawHill, New York, NY, 1984.

[45] A. Paulraj, R. Nabar, and D. Gore: *Introduction to Space-Time Wireless Communications*, Cambridge University Press, New York, 2003.

[46] M. Pohst, "On the computation of lattice vectors of minimal length, successive minima and reduced bases with applications," *in the ACM SIGSAM Bulletin*, vol. 15, no. 1, pp.37-44, February 1981.

[47] M. Pohst and H. Zassenhaus: *Algorithmic algebraic number theory*, Encyclopedia of Mathematics and its Applications, Cambridge University Press, 1989.

[48] J. Proakis: *Digital Communications*, 4th edition, McGrawHill, New York, 2000.

[49] G. Rekaya and J.C. Belfiore, "On the complexity of ML lattice decoders for decoding linear full-rate space time codes," *in Proceedings of IEEE International Symposium on Information Theory*, pp. 206-206, July 2003.

[50] C. Roh and B.D. Rao, "Adaptive modulation for multiple antenna channels," *in Proceedings of the Thirty-Sixth Asilomar Conference on Signals, Systems and Computers*, vol. 1, pp. 526-530, November 2002.

[51] C.P. Schnorr and M. Euchner, "Lattice basis reduction: Improved practical algorithms and solving subset sum problems,"*Mathematical Programming*, vol. 66, pp. 181-191, August 1994.

[52] P. Sebastian, H. Sampath, and A. Paulraj, "Adaptive modulation for multiple antenna systems," *in Proceedings of Asilomar Conference on Signals, Systems and Computers*, vol. 1, pp. 506-510, October 2000.

[53] C.E. Shannon, "A Mathematical Theory of Communication," Bell Systems Technical Journal, vol. 27, July and October 1948.

[54] P.J. Smith and M. Shafi, "On a Gaussian approximation to the capacity of a wireless MIMO systems," *in Proceedings of IEEE International Conference on Communications*, vol. 1, pp. 406-410, April 2002.

[55] G. Taricco and E. Biglieri, "Exact pairwise error probability of space-time codes," *IEEE Transactions on Information Theory*, vol. 48, no. 2, pp. 510-513, February 2002.

[56] G. Taricco and E. Biglieri, "Correction to ëxact pairwise error probability of space-time codes," *IEEE Transactions on Information Theory*, vol. 49, no. 3, pp. 766-766, March 2003.

[57] V. Tarokh, N. Seshadri, and A.R. Calderbank, "Space-time codes for high data rate wireless communication: performance criterion and code construction," *IEEE Transactions on Information Theory*, vol. 44, no. 2, pp. 744-765, March 1998.

[58] V. Tarokh, Alexander Vardy, and Kenneth Zeger, "Universal Bound on the Performance of Lattice Codes," *IEEE Transactions on Information Theory*, vol. 45, no. 2, pp. 670-681, March 1999.

[59] I.E. Telatar, "Capacity of multi-antenna Gaussian Channels," *European Transactions on Telecommunications*, vol. 10, no. 6, pp. 585-595, November-December 1999.

[60] S. Verdu: *Multiuser detectection*, 2nd edition, Cambridge U.K: Cambridge University Press, 1998.

[61] E. Viterbo and E. Biglieri, "A univeral lattice decoder," in Gretsi 14eme *colloque*, (Juan les Pins), September 1993.

[62] E. Viterbo and E. Biglieri, "Computing the Voronoi cell of a lattice: the diamond-cutting algorithm," *IEEE Transactions on Information Theory*, vol. 42, no. 1, pp. 161-171, January 1996.

[63] E. Viterbo and J. Boutros, "A universal lattice code decoder for fading channels," *IEEE Transactions on Information Theory*, vol. 45, no. 5, pp. 1639-1642, July 1999.

[64] Z.Y. Wang and C. HE, "Adaptive modulation MIMO system based on minimizing transmission power," *Journal of Zhejiang University SCIENCE A*, pp. 1046-1050, 2006.

[65] J.H. Winters, J. Slaz, and R.D. Gitlin, "The impact of antenna diversity on the capacity of wireless communication systems," *IEEE transactions on Communications*, vol. 42, no. 234, pp. 1740-1751, February/March/April 1994.

[66] P.W. Wolniansky, G.J. Foschini, G.D. Golden, and R.A. Valenzuela "V-BLAST: an architecture for realizing very high data rates over the rich-scattering wireless channel," *in Proceedings of URSI International Symposium on Signals, Systems, and Elecetronics*, vol. x, no. 98, pp. 295-300, September 1998.

[67] C. Windpassinger and R.F.H. Fischer, "Low-complexity near-maximum-likelihood detection and precoding for MIMO systems using lattice reduction," *in Proceedings of Information Theory Workshop*, vol. x, no. x, pp. 345-348, March 2003.

[68] H. Yao and G.W. Wornell "Lattice-Reduction-Aided Detectors for MIMO Communication Systems," *in Proceedings of IEEE Global Telecommunications Conference*, vol. 1, pp. 424-428, November 2002.

[69] S. Zhou and G.B. Giannakis "Adaptive modulation for multi-antenna transmissions with channel mean feedback," *IEEE transactions on Wireless Communications*, vol. 3, no. 5, pp. 1626-1636, September 2004.

[70] Z. Zhou, B. Vucetic, M. Dohler, and Y. Li "MIMO systems with adaptive modulation," *IEEE transactions on Vehicular Technology*, vol. 54, no. 5, pp. 1828-1842, September 2005.

Publications

[1] Antenna selection for MIMO systems based on an accurate approximation of QAM error probability, by F. Kharrat-Kammoun, S. Fontenelle, S. Rouquette, and J.J. Boutros, IEEE Vehicular Technology Conference, Stockholm, May 2005.

[2] A classification of multiple antenna channels, by J.J. Boutros, F. Kharrat-Kammoun, and H. Randriambololona, IEEE International Zurich Seminar on Communications, ETHZ, Zurich, February 2006.

[3] Accurate Approximation of Error Probability on MIMO Channels and its Application to Adaptive Modulation and Antenna Selection, by F. Kharrat-Kammoun, S. Fontenelle, and J.J. Boutros, IEEE International Conference on Acoustics, Speech, and Signal Processing, Toulouse, May 2006.

[4] Accurate approximation of QAM error probability on quasi-static MIMO channels and its application to adaptive modulation, by F. Kharrat, S. Fontenelle and J.J. Boutros, accepted for publication in the IEEE Transactions on Information Theory, submitted November 2004, to appear in 2006.

[5] Disclosure published at IP.com (2004): Adaptive modulations for MIMO systems.

[6] Disclosure published at IP.com (2006): A reduced complexity Adaptive Modulation for MIMO Systems.